Geomorphological Dating of Scarps

in Temperate Climate Using a Modified Diffusion Model

Dissertation

zur

Erlangung des Doktorgrades (Dr. rer. nat.)

der

Mathematisch-Naturwissenschaftlichen Fakultät

der

Rheinischen Friedrich-Wilhelms-Universität Bonn

vorgelegt von

Mamke Oemisch

aus

Aschaffenburg

Bonn 2004

Angefertigt mit Genehmigung der Mathematisch-Naturwissenschaftlichen Fakultät der Rheinischen Friedrich-Wilhelms-Universität Bonn.

1. Referent: Prof. Dr. St. Hergarten
2. Referent: Prof. Dr. R. Dikau

Tag der Promotion: 17. Dezember 2004

Diese Dissertation ist auf dem Hochschulschriftenserver der ULB Bonn http://hss.ulb.uni-bonn.de/diss_online elektronisch publiziert.

Abstract

Geomorphological dating of a certain landform or geomorphological structure is based on the evolution of the landscape itself. In this context it is difficult to use common absolute dating techniques because they require datable material which is often not available. Additionally, these methods do not always date the time since the formation of these structures. For these reasons the application of geomorphological dating seems one possibility to date certain geomorphological features.

The aim of this study was to relate present-day shapes of terrace risers to their ages. The time span since scarp formation ceased is reflected by the stage of degradation along with the rounding of the profile edges due to erosive processes. It is assumed that the average rate of downslope soil movement depends on the local slope and can be described by a diffusion equation. Furthermore, present-day scarps are often asymmetric and suggest a higher diffusivity at the base than at the toe of a slope. The diffusion equation has been modified and a linear approach with increasing diffusivity in downslope direction is suggested and assimilated in a model to obtain a better fit between observed and simulated profiles.

In order to date the scarps, the model had to be calibrated. For this purpose, published diffusivities taken from literature were used as well as estimated diffusivities by fitting modelled profiles to observed ones of known age. Field data were collected in the area around Bonn, Germany, and in Valais, Switzerland. In addition, profiles from literature which have already been dated were digitized. For the general use of geomorphological dating, a Java tool was developed where, e. g., different initial profiles and diffusivities can be chosen. Results show a better match between simulated and observed profiles in comparison to models using a constant diffusivity. But a reliable calibration of the model finally failed which brings up the question whether the diffusion equation and the presented modification are really an adequate description of the geomorphological processes degrading a slope.

Zusammenfassung

Die geomorphologische Datierung einer bestimmten Geländeform oder geomorphologischen Struktur basiert auf der Entwicklung der Landschaft selber. In diesem Zusammenhang ist es schwierig herkömmliche Datierungsmethoden anzuwenden, da diese in der Regel datierbares Material benötigen was oft nicht zur Verfügung steht. Außerdem datieren diese Methoden nicht immer die vergangene Zeit seit Entstehung der Strukturen. Aus diesen Gründen scheint die Anwendung der geomorphologischen Datierung eine Möglichkeit zu sein, bestimmte geomorphologische Merkmale zu datieren.

Das Ziel dieser Arbeit war es, die heutige Form von Geländekanten in Form von Terrassenstufen und deren Alter in Bezug zu setzen. Der Degradationsgrad sowie die Abrundung der Profilober- und -unterkanten durch erosive Prozesse reflektieren dabei die Zeitspanne seit Beendigung der Terrassenformation. Es wird weiterhin angenommen, dass die durchschnittliche Erosionsrate hangabwärts von der lokalen Hangneigung abhängt und somit durch eine Diffusionsgleichung beschrieben werden kann. Außerdem sind rezente Kanten oft asymmetrisch und deuten eine höhere Diffusivität an der Unterkante als an der Oberkante an. Die Diffusionsgleichung wurde modifiziert und ein linearer Ansatz mit hangabwärts zunehmender Diffusivität angenommen. Dieser wurde in ein Modell integriert um eine bessere Anpassung zwischen natürlichen und simulierten Profilen zu erreichen.

Zur Datierung von Geländekanten musste das Model kalibriert werden. Dazu wurden neben Daten aus der Literatur auch Diffusivitäten abgeschätzt indem simulierte Profile an natürliche Profile bekannten Alters angepasst wurden. Felddaten wurden in Gebieten rund um Bonn in Deutschland sowie im Wallis in der Schweiz erhoben. Zusätzlich wurden bereits datierte Profile aus der Literatur digitalisiert. Zur einfacheren Handhabung dieser Datierungsmethode wurde ein Java Tool entwickelt in dem z.B. das Initialprofil sowie die Diffusivität verändert werden kann. Die Ergebnisse zeigen eine bessere Übereinstimmung von simulierten und natürlichen Profilen als bei der Anwendung von Modellen mit konstanter Diffusivität. Aber eine verlässliche Kalibrierung des Modells konnte letztendlich nicht erreicht werden, so dass in Frage gestellt wird, ob die geomorphologischen Erosionsprozesse wirklich adäquat durch die hier vorgestellte modifizierte Diffusionsgleichung beschrieben werden.

Contents

List of Tables

List of Figures

Abbreviations

ΔH_m	height difference (measured)
a_d	angle of direction
a_r	angle of refraction
HA	horizontal angle
HD	horizontal distance
IH	instrument/total station height
OD	oblique distance
PH	prism height
VA	vertical angle
a	year
a.s.l.	above sea-level
BC	before Christ
BP	before the present
GUI	graphical user interface
ka	10^3 years
Ma	10^6 years
NRW	North Rhine-Westphalia
RMS	root mean square
SD	standard deviation
$\mathrm{SD}_{\mathrm{min}}$	minimum standard deviation

Chapter 1

Introduction

1.1 What is geomorphological dating?

The idea of geomorphological dating is simple: It is based on the general assumption that variation in scarp morphology is related to time-dependent degradational processes and that the extent to which the scarp's initial morphology has been degraded, reflects the date of scarp abandonment for a terrace riser or of scarp formation for a fault scarp. Studying properties of slope materials and the processes acting on them under transport-limiting conditions reveals that with time scarps mostly evolve from initially sharp-edged forms to more rounded ones in the upper and lower part. The main assumptions of geomorphological dating are that (1) the material transport rate is proportional only to local slope and that (2) the degradation can be described in terms of a diffusion equation. Knowing the initial shape of the scarp and predicting its degradation through time by such a diffusive slope evolution model results in a set of simulated profiles. In order to calibrate the model, the local diffusivity must be determined; at the best from scarps of known age. Comparing these synthetic profiles to the present shape of an observed slope, enables one to estimate the age of it.

Geomorphological dating has been applied successfully in various arid and semi-arid regions; only few studies employed this dating technique to scarps in temperate climates. It seems to be a rapid and inexpensive method for dating particular landforms, such as terraces or fault scarps, that are not amenable to dating by other means mostly either due to a lack of datable material or because the applied dating technique yields the age of the scarp's material and not of its formation. Especially Quaternary deposits are often fragmentary and only in individual cases direct dating is possible (Schreiner, 1992). The determination of ages of terrace risers is important to improve the study of river flow evolution. The application to Pleistocene fault scarps which were mostly formed by prehistoric high energy seismic events obtains information about the past history of earthquakes and helps to assess the regional seismic risks.

Most former studies on this topic investigated individual cases of dating single terraces or fault scarps. This study analyses the application of geomorphological dating involving a modified diffusion equation to different scarps in a temperate climate. The analysis is

limited to the investigation of two-dimensional profiles emphasizing the development of soil-mantled scarps mostly at the tens meter scale.

1.2 Other Dating Methods

A wide range of methods can be used to date deposits and events. This section shall just list some of them to give an overview. For an extended discussion of geological dating techniques, see e. g., Rey (1991), Schreiner (1992), Thome (1998), Noller et al. (2000) or Burbank and Anderson (2001). If not quoted differently, all information is collected from above mentioned authors.

Dating methods are in general classified into relative and absolute dating methods. The former yield a correlation with a relational information, while the later provide an age determination with year dates. Amongst the absolute dating methods, the most important ones are radiometric dating techniques based on radioactive decay and with a margin of error ranging from ±5 to ±20 per cent. The ability to date especially geological young deposits has improved greatly in the past few decades and dozens of dating techniques have either been developed or greatly refined. With regard to geomorphology some of those techniques are more directly relevant to landform analysis than others. Tables 1.1 and 1.2 present, respectively, the most common relative and absolute dating techniques.

Table 1.1. Relative dating methods with age range and materials needed. Modified after Burbank and Anderson (2001).

Relative Dating Methods		
Method	**Useful Range**	**Materials Needed**
Stratigraphic relationships	unlimited	sediment strata
Clast seismic velocity	1–100 ka	Boulders
Weathering rinds	1–10 ka	Clasts
Obsidian hydration rinds	1–500 ka	Obsidian lavas
Soil development	10–500 ka	Soils
Mineral weathering (carbonate coatings and other pedogenic indicators)	10 ka–1 Ma	Boulders
Landform modification	10 ka–1 Ma	–
Lichenometry	1–500 a	Lichens on rocks

Table 1.2. Absolute dating methods with age range and materials needed. Modified after Burbank and Anderson (2001).

Absolute Dating Methods		
Method	**Useful Range**	**Materials Needed**
Radioisotopic		
Radiocarbon (^{14}C)	< 40 ka	wood, charcoal, peat, bone, animal tissue, shells, speleothems, ground water, ocean water, glacier ice
U/Th	10–350 ka	organic carbonate
K/Ar	> 100 ka	Muscovite, biotite, hornblende, whole volcanic rock
Thermoluminescence (TL)	30–300 ka	quartz silt
Optically stimulated luminescence (OSL)	0–300 ka	quartz siltx
Fission track	very broad time span (> 10 Ma)	Zircon, uraninite (esp. volcanic rocks)
Cosmogenic		
In situ ^{10}Be,^{26} Al	3–4 Ma	quartz
He, Ne	Unlimited	olivene, quartz
Chemical		
Tephrochronology	0–several Ma	volcanic ash
Amino acid racemization	0–300 ka; range temperature dependent	carbonate shell
Palaeomagnetic		
Identification of reversals	> 700 ka	fine sediments, volcanic flows
Secular variations	0–700 ka	fine sediments

continued on next page

continued from previous page

Absolute Dating Methods

Method	Useful Range	Materials Needed
Biological		
Dendrochronology	10 ka, depending upon existence of a local master chronology	wood
Depositional		
Varve dating	several ka	annually deposited layers of sediment (mainly glacier varves)

Especially for Quaternary geology, several examination methods from different research fields exist (e. g., Schreiner, 1992):

- Geomorphology: geomorphological characteristics of Pleistocene formations;
- Investigations in the field and the lab: rounding of pebbles and boulders, debris composition, grain size distribution, heavy-mineral analysis, quartz grain surfaces;
- Drillings: hand-drilled wells and wells made by bigger drilling tackles;
- Seismic reflection;
- Quaternary paleontology: mammals, molluscans, micro fauna, insects, plant remains;
- Physical and chemical age determination.

Pierce (1986) summarized about 26 dating techniques which can be applied to date deposits and events of late Cenozoic age grouped as numerical methods, relative-dating methods, and correlation methods. Numerical techniques are based on processes that do not require any further calibration, but often datable material is lacking. Relative-dating techniques are nearly always applicable but are not precise. They require calibration by numerical methods and an understanding of the process being measured and its relevant history (e. g., temperature, precipitation) to estimate numerical ages. Nevertheless, such methods are important in the context of this study as they are applied to a local sequence of deposits that differ in age but are similar in other characteristics. In this category, Pierce (1986) includes complex processes such as soil development, rock and mineral weathering, progressive landform modification, deposition and deformation rates, and geomorphic position and incision rates. Rigorous evaluation of these complex methods would require modelling of each process and quantification of their relative effects. Nevertheless, empirical quantification has been done and following Pierce (1986), some age estimates based on these methods may be more reliable than, if not so precise as, some carbon-14

ages. Amongst above listed complex processes, progressive landform modification resembles geomorphological dating most. In addition to time, this method depends on factors such as climate, lithology, and vegetation that need to be held constant or accounted for otherwise. The technique is based on the reconstruction of original landform and on the understanding of processes resulting in a change of landform, including creep and erosion. The optimum resolution ranges between 10^2–10^6 years and the method is nearly always applicable. Correlation techniques are locally useful and depend on recognition of an event whose age is known, such as a volcanic eruption or a palaeomagnetic reversal.

Which of all above mentioned methods should be chosen depends on the availability of the proper material, the details of the geomorphic setting, and, of course, the cost. The surfaces of geomorphic markers, such a fluvial terraces, that exceed the range of radiocarbon dating are for instance difficult or impossible to date.

1.3 Scope

The next Chapter 2 describes the slope system as the main working area including the most relevant items reaching from the slope material over geomorphic processes to the form of slopes. Because of the multitude of hillslope evolution models, an overview of the most common models is given in Chapter 3 where they are subdivided into descriptive models and dynamic models. Chapter 4 describes the geomorphological dating technique in detail. Previous work in this research field with a distinction between empiric and analytic models is described in Chapter 5. The modification of the diffusion equation and the nonlinear numerical model as well as the software description of the developed Java tool are drawn in Chapter 6. To evaluate the method, field data were collected from local areas around Bonn, Germany. Additionally, three profiles were levelled in the Turtmann valley in Valais, Switzerland. This is also a research area within the Research Training Group (GRK) 437 "Landform – a structured and variable boundary surface" at the University of Bonn of which the presented study is project C 5. Chapter 7 describes all field data. The calibration of the model as well as the age determinations of the investigated scarps are presented in Chapter 8. Finally, the results and the applicability of the presented dating tool are discussed (Chapter 9). Conclusions and an outlook are deduced in Chapter 10.

Chapter 2

The slope system

Among the numerous and varied landforms, this work pays particular attention to **hillslopes** defined as curved, sloping surfaces, which are mostly formed when rivers cut valleys and which are largely shaped by geomorphic processes. The main emphasis lies on relatively small, soil-mantled **slopes** in form of terrace risers which may also be termed scarps. Strictly speaking, a **scarp** (short form of "escarpment") is any steep, abrupt slope or cliff along the margin of a plateau, terrace, or other topographic bench which may be formed by either tectonic, erosional, or depositional geological causes (Bloom, 1991). For simplicity, the terms hillslope, slope and scarp are equated in this study.

The properties and behaviour of the slope materials, i. e., the strength, or resistance to deformation, are very important in understanding the form and mode of the development of slopes. Furthermore, the slope form is dependent on the nature, frequency and intensity of the geomorphic processes acting upon the landscape. These processes are again strongly influenced by climate and relief. As slopes are transitional both in process and in form, they are exceptionally difficult to study (Bloom, 1991).

2.1 Climate, erosion and topography

The climate of a region is characterized by average weather conditions together with their variability (Summerfield, 1996). Climate varies at all time scales from decades to tens of millions of years and influences erosivity and indirectly also the erodibility of slope materials especially because it affects vegetation and moisture content. **Erosivity** describes the potential of slope processes to cause erosion, whereas **erodibility** is the resistance of slope materials to entrainment and transport. But whether a climatic change affects the nature and rate of geomorphic processes depends on its magnitude and duration, and on the properties of the landform concerned. Principal approaches to reconstructing recent climatic changes include the analysis of pollen (palynology) and landforms themselves, and as the most important technique oxygen isotope analysis ($\delta^{18}O/\delta^{16}O$ ratio). For an outline of the local Quaternary record of climatic changes and present climate see Section 7.4.

There is a clear relation between climate and erosion which is a function of erosivity and erodibility. Important factors in weathering as freezing, thermal expansion, and the

solvent action of water are related to temperature and rainfall. Warm, humid climates speed up chemical weathering which preludes mechanical weathering. Frost action and extreme daily variations in temperature directly cause rock disintegration. But one of the most important impacts of climate is its control on vegetation which in turn often influences chemical weathering and the shaping of the relief in general. In a dry climate, the growth of much vegetation is prevented and the decay by the solvent action of water is slowed which both gives rise to physical weathering taking place more often than chemical weathering.

Erosion shapes topography, and therefore topography is also affected by climate. In turn, topography strongly controls climate and influences the nature of erosion. High altitude and relief enhance the rate of mechanical weathering due to freezing and thawing and due to fragmented debris quickly moving downhill which results in thin soils. In comparison, chemical weathering is predominant in low-lying plains where detritus is not removed so quickly causing thick soil layers. Topographic effects and their control on weathering are in the end fundamentally connected with deep-seated tectonic movements pushing up mountains and creating associated kinds of climate. According to Burbank and Anderson (2001), topography influences climate much more strongly and directly than climate does topography. Tectonic uplift causes an increase in erosion rate which in turn lowers the surface elevation and increases the sedimentation rate. The evolution of landscape is thus a balance between tectonic uplift and erosion rate (see also Section 2.6). But finally, the small-scale slope form itself is still much more influenced by climate and lithology than by tectonic (Carson and Kirkby, 1972; Young, 1975).

The shaping of landforms in response to various climatic conditions and the association of climate with characteristic landscape types in morpho-climatic zones as suggested by some geomorphologists is the essential assumption of **climatic geomorphology** (or morphogenesis) (Bloom, 1991). The areas with the investigated profiles of this study are part of the humid mid-latitude morpho-climatic zone with a mean annual temperature of 0–20°C and a mean annual precipitation of 400–1800 mm (Tricart and Cailleux, 1972). Chemical weathering rates in this zone are moderate but increasing to high at lower latitude. The mechanical weathering activity is moderate too. Frost action is important at higher latitude. Fluvial process rates are moderate; mass movement activity is moderate to high. Wind action is confined to the coasts.

Many geomorphologists have challenged the validity of the assumptions behind climatic geomorphology. They see evidence of a precise relationship between climate and landform genesis only under the most extreme climatic conditions and most processes operate in most environments at least to some degree. However, there are major contrasts in the kind and intensity of geomorphic processes active under certain climatic regimes. Summerfield (1996) states that most landforms are likely to be out of equilibrium with prevailing climatic conditions because of the rapid and drastic global climatic changes especially over the past 2–3 Ma. Although variations in both degree of humidity and of temperature can be sensitively reflected in geomorphic processes, other factors related to tectonics and lithology often predominate. Two further major problems in climatic geomorphology are (1) the diversity of conditions under which apparently similar forms can develop and (2) the unambiguous linking of a particular landform with specific climatic conditions.

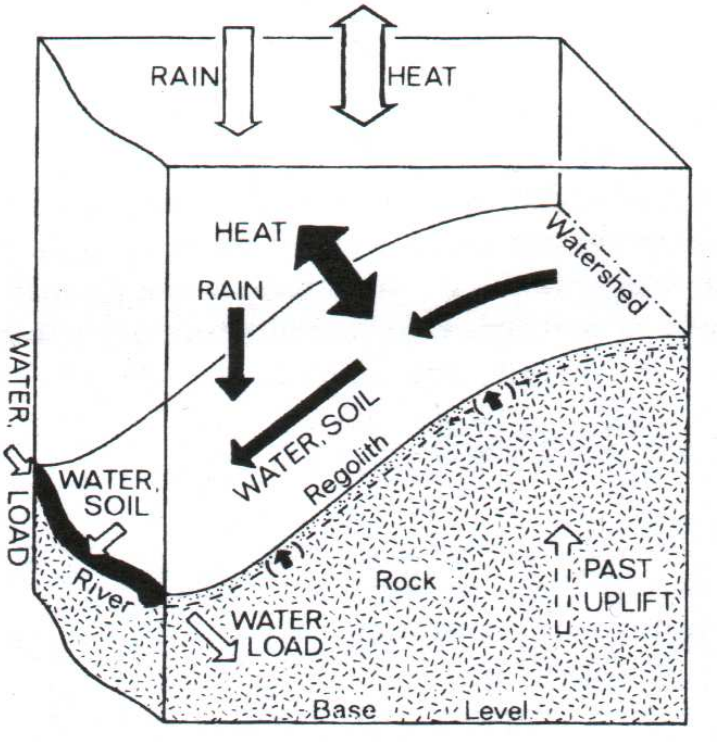

Figure 2.1. A slope as an example of an open physical system with arrows showing flows of energy and material. Solid and open arrows show, respectively, intra-system flows and flows across the boundaries of the system (Fig. 6, p. 21 from Young, 1975).

Important terms related with topography are furthermore dynamic **equilibrium state** and **steady state** which have been given a variety of imprecise, overlapping, and sometimes contradictory definitions (Howard, 1988). Some geomorphic processes are fast enough to respond nearly instantaneously to some overwhelming stress. Although most processes act much more slowly. In this sense, dynamic equilibrium refers to the process rates and their causes (Ahnert, 1996). Hence, dynamic equilibrium conditions describe the balance between uplift and erosion, or more generally, spatially and temporally uniform erosion rates. It is a major topic of geomorphic study whether all landforms are always graded, i. e., dynamically stable or fully adjusted to the erosional processes that are actively shaping them, or whether the graded condition develops slowly and progressively. The interaction of surface processes with geological structures does not give a complete explanation of landforms unless including the length of time during which the processes have been operating or the degree of equilibrium (stage) that has been reached. A graded slope is an example of an open physical system through which both energy and matter move. Figure 2.1 shows the boundaries of such an open physical system and some of the flows of energy and material. Two vertical boundaries are marked through the watershed and the river bank and two perpendicular vertical planes are arbitrarily placed. The base level and a horizontal plane at an arbitrary distance above the highest point on the watershed correspond to the lower and upper boundary, respectively. Such a system tends to maintain itself in the most efficient possible configuration by self-regulating processes. Slopes constantly change but always tend toward some central graded state appropriate to the environment of the movement.

Steady state describes the geomorphic evolution of landscape as a balance of forces resulting in a topography unchanging with time, i. e., a steady state system is time-independent. According to Ahnert (1996), steady state includes the permanent properties of shape and material associated with the dynamic equilibrium of the process rates. Depending on the state of balance between structural uplift and erosion, different topographies evolve: Mature landscapes with high relief, steep to moderate slopes and sharp divides, and old-age topography with low relief, wide valleys and gentle slopes. This progression from youth to old age occurs only after the main tectonic activity dies down following different paths in different regions. The concept of steady state seems to make it more difficult to reconstruct the geomorphic history of a region, for it says that what a region is like is the product of currently active events and processes, not what went before.

2.2 Slope material

Soil and rock are the two fundamental types of slope materials. This report deals only with soil-mantled slopes. **Soil** is defined as a weak, unconsolidated deposit, not held together by a cement or a strong interlocking crystal structure, between the topographic surface and the soil-/bedrock-interface. It is a complex material containing voids filled with air or water and solid particles of various sizes and is produced by the slow decay and fragmentation of chemical and mechanical weathering (Summerfield, 1996). Unconsolidated residual or transported material that overlies the solid rock on the earth is also termed regolith. According to Young and Saunders (1986) most humid-temperate landscapes are mantled by 0.3–3 m thick regolith. On one hand this might simply be a measure of the time since periglaciation, multiplied by the weathering rate, and thus the regolith is becoming thicker. On the other hand a steady state might have been attained in which the weathering would speed up if the regolith became thinner, and transport or solution removal would become faster if it became thicker. Especially slopes below 35° frequently possess a continuous regolith cover. Following Selby (2000), the general pattern of a soil in its vertical profile is a simple A-B-C scheme:

A horizon: The top section is usually the darkest, for it contains most of the organic matter (humus) and is a zone of intense biological activity. In a thick, old soil, most minerals are clays and residual insoluble minerals like quartz while soluble minerals are absent. Its formation takes many hundreds to several thousands of years.

B horizon: An intermediate layer with little organic matter and where soluble minerals and iron oxides are present. It takes 10,000 to 100,000 years to evolve.

C horizon: The lowest part which is slightly altered broken and decayed bedrock mixed with clay and merging into solid bedrock at its base.

Above scheme assumes a downward water movement as it usually occurs in humid climate. Essentially A/C- and A/B/C-soils can be distinguished depending on the age and the stage of development.

Soil formation is affected by climate, source rock, landform and relief, erosion and uplift rates, vegetation, water, soil organisms and burrowing animals, human influence, and duration affect soil formation (Ahnert, 1996). Heimsath et al. (1997) presented an empirical soil production function showing that in regions with soil production primarily due to biogenic disruption of weathered bedrock, the production rate additionally varies inversely with soil depth. Climate, particularly rainfall and temperature, is an important factor and there is a fair correspondence between soil type, thickness, and climatic regions. Soils are permeable, and rainwater running through them reacts with the minerals. The extent of mineral alteration depends on (1) the saturation of the water: undersaturated, i. e., fresh, water reacts more, (2) the time the water runs through a soil: the longer the time, the more minerals are altered, and (3) the temperature: the higher it is, the faster the reactions (Selby, 2000). Temperature also increases the rate of soil formation due to more growth of vegetation and bacteria. All effects together explain the thickness of tropical soils and why they are devoid of most unstable minerals whereas arid soils are thin and rich in unstable minerals. In other words, the more a soil is preceded by prolonged and intense chemical weathering, i. e., an older soil receiving warmth and moisture, the thicker it is. If a soil is very slowly eroded from the top, it is gradually deepened by chemical reactions. But if the erosion is rapid, chemical decay cannot keep up, and the soil is thinned. Generally, a thick soil together with dense vegetation hinders runoff and erosion while thin soils and a sparse vegetation cover intensifies runoff and erosion.

Based on the above mentioned soil-forming factors, soils have been classified into many soil types with typical successions of soil horizons in the vertical profile (Ahnert, 1996). Additionally, soils are divided into soil types according to their granulometric composition (AG Boden, 1994). Selby (2000) describes the properties and formation of soils in detail. The book by Miayzaki (1993) provides a very detailed review about the effect of water in soils.

2.3 Slope stability

The strength of slope materials can generally be defined as the ability to resist deformation and fracture without significant failure (Summerfield, 1996). Regarding slopes and their experienced stresses generated by gravity, it is shear strength that is most important, i. e., strength in relation to shear stress. Shear strength is controlled (1) by the frictional resistance between the constituent particles of a material (inherent frictional properties + normal stress), and (2) by cohesive surface forces which are determined by electrostatic grain surfaces that immobilize the water films between them (Bloom, 1991). Changes in shear strength over time for both densely packed and loosely packed soils differing in their initial behaviour, ultimately attain the same residual value. Following Selby (2000), it depends on the proportions of the components and the water content whether a soil behaves as an elastic, plastic or viscous material under stress. Due to the varying abilities of different clay minerals to absorb water, the strength of the majority of soils is most of all influenced by the clay content.

Slope stability generally describes the relationship between those stresses tending to disturb the slope material and cause it to move and those factors tending to resist these

driving stresses. Among other things, this relationship can be represented as the safety factor for a slope which is expressed as the ratio between shear strength and shear stress. Following Summerfield (1996), three states of slopes exist:

state of slope	**safety factor**	**movement**
stable	> 1.3	none
conditionally stable	$1 - 1.3$	occasional
actively unstable	< 1	continuous or intermittent

Conditionally stable slopes fail on occasion in response to transient changes in shear strength especially due to changes in the water content of slope materials. Several further approaches to analyse the stability of a slope exist and are discussed by, e. g., Brunsden and Prior (1984), Nash (1987a) or Ahnert (1996). Carson and Kirkby (1972) present an extended review about several derivations of slope stability formulae in the appendix of their book "Hillslope form and process" from page 425 on. At this point it is worth mentioning that their pioneering book generally remains a valuable guide to the broad field of slope studies.

Table 2.1. Typical angles of repose for various types of slope material. Based on Carson and Kirkby (1972).

Slope Angle (°)	**Slope Material**
43 – 45	Jointed and fractured rock that is virtually cohesionsless but with a high packing density
33 – 38	Same material as above but with looser packing
25 – 28	Taluvial slopes in which high pore-water pressures can be attained
19 – 21	Sandy material
8 – 11	Clays

The stability of slopes as well as the velocity of movements are determined by two important factors (Summerfield, 1996). First in importance is oversteepening of slopes when they exceed the **angle of repose** which is alternatively termed threshold or limiting angle of stability. According to, e. g., Freeze (1987), the angle of internal friction, the cohesion (controlled by cementation, roots, etc.), and the pore pressure contribute to that critical slope. For cohesionless material, this angle of repose at which slope failure occurs will be nearly equal to the angle of internal friction of that material. The latter is a function of parameters such as grain size, shape, sorting, packing, secondary cementation, mode of deposition and surface roughness of the particles, and is mainly related to the shear strength of the slope materials (Carson, 1977). Therefore also slope stability is strongly influenced by the above mentioned surface material (Sect. 2.2): Larger, flatter, and more angular pieces of loose material remain stable on steeper slopes. Pierce and Colman (1986) state that angles of repose become steeper if coarse alluvial deposits are combined with fine-grained sediments such as loess which decreases porosity. Roots of a vegetation cover might also stabilize a slope such that the angle of repose increases. According to Bloom (1991), the flow of rainwater runoff in the surface soil on a slope reduces the stable angle of repose to less than half of the dry value. Some gradients at which failure occurs are rather more frequent than others in the landscape; they are listed in Table 2.1.

Table 2.2. Collection of values of angles of repose in different materials. Sources in literature are given.

Approx. angle of repose (°)	**Material**	**Source**
25 – 35	unconsolidated deposits	Colman and Watson (1983)
30	well-sorted sand (porosity = 40 %)	Pierce and Colman (1986)
30	unconsolidated material	Carretier et al. (2002a)
30 – 35	all kinds	e. g., Carson and Kirkby (1972), Nash (1986), Pierce and Colman (1986)
33	sand and gravel pits	Pierce and Colman (1986)
33 – 35	no details	Colman (1987)
≈ 35	material with no cohesion between grains	Hanks et al. (1984) Andrews and Hanks (1985); Andrews and Bucknam (1987)
35	unconsolidated fanglomerates	Tapponnier et al. (1990)
35.5	sand and gravel	Wallace (1977)
35 – 36	sand-gravel-mixtures (porosity = 20 %)	Pierce and Colman (1986)
35±4	sandy to cobbly loose alluvium	Avouac (1993)
35 – 40	angular, poorly sorted material	Terzaghi (1950)
41±2	cobble alluvium	Nivière and Marquis (2000)

To emphasize the range of values for the angle of repose, a collection of values taken from literature is given in Table 2.2. For a rather comprehensive review of characteristic and limiting slope angles as well as angle classification, see also Young (1975).

Next in importance is the effect of lubricant, usually water, with its complex effect on the sliding friction between surfaces of rock-forming minerals: The grains slide past each other with little friction if filling the pores of permeable material (Selby, 2000). In other materials the effects on slope and lubricant become more complex, depending on the nature of the mixture, the irregularities of slopes, the structurally stabilizing role of vegetation roots, and the amounts of water required to saturate the materials. There are of course several additional preparatory and triggering factors that contribute to the occurrence of mass movements which are described by, e. g., Ahnert (1996).

2.4 Slope formation

This study deals mainly with **terrace risers** as one type among the existing multitude of hillslope types and of which the formation shall be described briefly. A terrace is a relatively flat bench in a slope limited by upper and lower escarpments. River terraces are remnants of former valley floors as the river incises into its floodplain and according to Burbank and Anderson (2001), they are common examples of preserved, sloping geomorphic features. The original floodplain is thereby abandoned and corresponds to the river terrace which is separated from the new floodplain below by a steep slope. These narrow ramps between alluvial surfaces are termed terrace risers or terrace scarps. Aggradational (or constructional or fill) terraces are the result of alternating vertical erosion and aggradation of river-transported alluvium along a river's course during valley formation

(Ahnert, 1996). In between, lateral erosion may occur too. The upper terrace level marks the final level of fluvial aggradation while the terrace base reflects the ending of fluvial erosion which is followed by a new period of aggradation (Thome, 1998). Terraces cut into bedrock covered only by a thin sediment veneer form when predominant vertical and lateral erosion alternate. This type is termed degradational (or erosional or cut or strath) terrace and is mostly caused by tectonic uplift. The term of river terraces must not be mixed up with denudation terraces which are formed due to different resistant rocks within a slope and where more resistant layers develop steep slopes while less resistant layers are flattened terrace-like (Ahnert, 1996).

Generally, the longitudinal profile of river terraces is smoothly inclined downstream with the same slope as the incised former valley bottom (Burbank and Anderson, 2001) but mostly at a different inclination as the active floodplain (Ahnert, 1996). If a valley side contains a vertical sequence of terraces, the lowest is the youngest, while the highest is the oldest usually partly degraded one. If rivers flow from uplift to subsidence areas, the position of the terraces is reversed and older terraces are situated lower than younger ones. Such an intersection of terraces occurs for instance in the area north of Bonn in the transition zone of terraces of the middle Rhine valley (uplift area) to terraces of the lower Rhine valley (subsidence area) (Thome, 1998). Summerfield (1996), Burbank and Anderson (2001) and others additionally distinguish paired and unpaired terraces. The former evolve when vertical incision is stronger than the lateral migration of the river channel, whereas the latter forms where lateral shifting of the river is more rapid. Ahnert (1996) states this to be an mistake: A certain terrace level ist often only preserved on that valley side where erosion is less active. Terrace flights with identical levels on both valley sides (as in many schematic diagrams) imply an narrowing valley bottom which seldom develops naturally. A terrace must therefore occur along the valley at several places in comparable heights and with similar deposits to reconstruct a former valley bottom.

According to Ahnert (1996), four essential reasons for terrace formation exist: (1) crustal movement, especially tectonic and isostatic uplift, (2) eustatic sea level changes, (3) fluctuations in climate, and (4) capture. All of them cause either alterations in base level and channel gradient, in discharge or sediment load; they are nearly always combined with each other. Near-shore areas are mainly affected by (2), whereas (1) and (3) are predominant causes inside continents. Thome (1998) states that terraces even develop with steady discharge and constant incision because of the formation and displacement of meanders. Terraces also develop at the bank of former glacial lakes but up to now none have been found in German low mountain ranges. Many paired aggradational terraces are assumed to form in response to climatic cycles (Burbank and Anderson, 2001). For instance, Penck and Brückner (1909) state that fluvial terraces in areas of alpine glaciation correlate with moraines associated with glacial advance or standstill. But the development of terraces has both direct and indirect climate controls: Even if climatic conditions encourage terrace building, aggradation will not occur if sediment supply is not sufficient for transport within the upstream drainage. Both changes in sea level and climate have been frequent and rapid over the past 3 Ma which supported terrace formation. And as the material of terraces often contains glacial indications it is assumed that most fluvial terraces in Central Europe developed during glacial periods: In each glacial the river incised into a lower level (Thome, 1998). Therefore, the lowest terrace above the contemporary river

bed (= Lower terrace) mostly reflects the river bed during the last glacial, i. e., the age of the Lower terraces mostly corresponds to the Würm or Weichsel glacial (see Section 7.4).

The age of a terrace is often important and worth knowing if, e. g., tectonic rates are to be determined. From the height and age difference of two terraces it is possible to infer the rate of valley deepening or crustal uplift. Eustatic terraces give information about sea level changes. But dating terraces is often not that easy and requires persistence, familiarity with available techniques, innovation, and some luck (Burbank and Anderson, 2001): The former longitudinal profile of the river must be reconstructed independently from the recent profile, redeposition of terrace material must be taken into account, and often datable material (like fossils) is difficult to find for an absolute dating. Hence, if possible superficial layers or relict soils must be dated relatively. Such methods of establishing terrace stratigraphy include degree of soil development, weathering rinds, or morphostratigraphy (preservation and texture of a geomorphic surface) (Mayer, 1984). The complex nature of alluvial terrace formation in coupled systems includes erosion, transport, and deposition of sediments. According to Humphrey and Heller (1995), the response of such systems to changes in controlling parameters as discharge, sediment supply, rock uplift rate, or base-level lowering is not instantaneous or uniform. It is therefore not reliable to assume that the upper terrace surface is essentially isochronous along its length, even where the physical downstream continuity of a terrace is clear (Burbank and Anderson, 2001). Bremer (1989) states that this is especially valid for periglacial regions where lateral erosion often disposes older terraces. Finally, the vertical distance of different terrace levels does not always allow an unambiguous subdivision in individual stages of river incision either caused by climatic or by tectonic conditions. For instance, some Pleistocene terrace levels in Central Europe conceal more than one glacial (Thome, 1998). Larger variabilities in age-determination at the scale of a few thousand years must be excluded especially when dating postglacial and Holocene terraces.

2.5 Geomorphic processes on slopes

The most widespread geomorphic processes are erosion, transport and redeposition or deposition of rock material (Ahnert, 1996). Bloom (1991) uses the collective term of mass wasting for all gravitational or downslope movements of weathered rock debris and describes the two classification schemes which are in common use. Both schemes categorize geomorphic processes depending on (1) the type of material which is transported (e. g., adopted by Ahnert (1996), and (2) the type of transport. For the most part, this section follows Summerfield (1996) who uses the latter scheme and who subdivides geomorphic processes on slopes into mass movement processes and wash processes. According to Rohdenburg (1989), mass movements as non-selective, continuous transport mechanisms of all occurring grain sizes are mainly important on relatively steep slopes of 25° to 35° depending on the moisture content of the soil and the vegetation cover. And continuous processes generally tend to smooth out the surface (Young and Saunders, 1986).

This section covers only the most widespread and frequent geomorphic processes of which a majority is slope-dependent. Scheidegger (1991) as well as Selby (2000) describe the physical background in detail. For an extended discussion of below mentioned and further processes, see, e. g., Parsons (1988), Ahnert (1996) or Selby (2000).

2.5.1 Mass movement processes

In a broader sense, mass movements can be defined as slow to rapid downhill movements of debris of erosion under the influence of the gravitational force of the material itself and without the assistance of moving water, ice or air. Mass movements are clearly related to the stability of a slope described in Section 2.3. The transport rates cover a great range and are given in numbers if reasonable.

Summerfield (1996) categorizes six fundamental types of mass movement: creep, flow, slide, and heave all with a predominant lateral component, and fall and subsidence both with a predominant vertical component. Each of these types can be subdivided into more specific forms of movement varying in moisture content and velocity. Observations showed that most movements involve a combination of processes.

Creep is the plastic deformation of rock or soil and the entire downslope transfer of material which reduces its effect on slope retreat. Subtypes are rock creep and continuous soil creep. Bloom (1991) describes creep as an imperceptible and non-accelerating downslope movement, slow enough to span significant intervals of Quaternary climate change. It is a very slow to extremely slow motion with rates rarely above 1–2 cm/a (Ahnert, 1996). Following Young and Saunders (1986), the rate of soil creep in western Europe with its temperate maritime climate ranges from 0.5 to 2.0 mm/a. The rate increases when the regolith gets unusually wet although the moisture content is low in most cases. Creep is generated by the weight of overburden and is therefore especially active where weakly competent materials, such as clays, are overlain by more competent beds. According to Nash (1986) and others, creep as the slow, steady downslope transportation of material on transport-limited hillslopes (see Chapter 3) is the result of alternate expansion and contraction within the material due to heating and cooling, hydration and dehydration, or freezing and thawing of pore water. Creep produces a variety of forms, e. g., cambering, valley bulging, outcrop of bedding curvature. The major function of creep is a smoothing one by removing soil from local mounds and filling and erasing gullies and hollows (Tucker, 1998). Selby (2000) states that creep processes produce an expanding upper convexity on a slope. The downslope soil movement due to creep can be regarded as a diffusive transport process depending on the local slope. Moeyersons (1975), for instance, demonstrated in experimental studies that the creep rate increases nonlinearly with increasing gradient for a given rainfall rate. The material moving downslope is called colluvium (Bloom, 1991).

Flow includes dry flow, solifluction, gelifluction, mud flow, slow and rapid earthflow, debris flow, debris (rock) avalanche (sturzstrom), snow and slush avalanche. Following Bloom (1991), the subdivision can be based either on the kind of material, the degree of saturation, or the speed of advance. It is an extremely slow to extremely rapid motion. Solifluction, for instance, spans a wide range but shows a majority cluster in the 10–100 mm/a range (Young and Saunders, 1986). Internal turbulence and either discrete boundaries or narrow marginal zones of shear are the criteria for defining flow (Bloom, 1991). Summerfield (1996) states that in a pure flow, shear occurs throughout the moving mass without a well-defined shear plane. Flow is often initiated by falls or slides becoming flows when the moving soil or rock mass breaks up showing various natures of movement (e. g., funnelled, widespread, or confined elongated flow, rapid collapse and lateral spreading of soil, catastrophic low friction movement). The moisture content is usually

high.

Slides can be subdivided into translational types as rock slides, rock block slides, debris/earth slides, debris/earth block sides and rotational types as rock slumps and debris/earth slumps. Generally a slide is the downslope movement of material involving fall and flow along discrete shear surfaces (Bloom, 1991). Rates of slides cover a great range and vary from extremely low to extremely high. In a pure slide failure occurs along a well-defined shear plane. Translational slides show predominantly planar shear surfaces. Rotational slides have concave-up shear planes and are common where slopes consist of thick, homogeneous materials, such as clays. Both kinds are precipitated by a temporary excess of shear stress over shear strength within the slope. The length-width ratio is typically 10:1 but most slides are small and shallow with depths of 2–3 m. Shallow slides affecting the regolith can occur only on slopes above a certain limiting angle of approx. 25° on most kinds of rocks whereas gentler angles are required for deeper movements (Young and Saunders, 1986). Selby (2000) reports that shallow landslides produce parallel retreat of the affected slope unit and a lower concavity where the material is deposited. The moisture content is low to moderate.

Heave is the widespread incremental downslope movement of soil or rock particles. Subtypes are frost creep and, based on the particle size, soil creep and talus creep. Heave is an extremely slow motion depending on soil type, steepness of slope, rainfall, and vegetation cover. It ranges from 1–2 mm/a in humid temperate regions up to 5–10 mm/a in semiarid regions with cold winters (Parsons, 1988). Pure heave results from minute movements caused by expansion (normal to the sloping ground surface) and contraction (tends to be more nearly vertical under gravity) of slope material due to, e. g., wetting and drying, freezing and thawing, thermal expansion, activities of burrowing organisms, root movements of growing and decaying plants, and soil heave. The rate of creep becomes greater with increasing slope angle and in soils rich in clay or in silt-sized material, whereas it decreases with depth below the slope surface. The moisture content is low. There is an upper limit for soil creep above an angle of around 25° where soil cover is thin or absent.

Fall describes the downward motion of rock or, more rarely, soil through the air as an extremely to very rapid motion and is subdivided into rock fall and debris/earth fall (topple). Free fall can only occur from very high, steep slopes of cliff faces often with only very little soil cover. Topples additionally rotate the block of material as it falls away. Dislodged fragments can be an active erosive agent and large rock falls are often transformed into debris avalanches. The moisture content is low.

Subsidence is subdivided into cavity collapse and settlement. It occurs either as the collapse of rock or soil into underground cavities (very rapid motion) or as a progressive lowering of the ground surface due to ground compaction usually resulting from withdrawal of ground water (slow motion). The moisture content is low.

2.5.2 Wash processes

Wash processes on slopes describe the transport of slope material by water. According to Summerfield (1996) rainsplash erosion, slope wash and solute transport are involved. While the first two processes are often summarized as surface wash which are effective

only on soil-covered slopes (Young and Saunders, 1986), the latter one may take place on both soil and rock slopes.

The required water is mostly rainwater which either runs off the surface, is held in surface depressions or infiltrates through the slope surface. The latter either percolates down to the water table and contributes to groundwater storage, or is diverted laterally through the slope more or less parallel to the surface (Selby, 2000). The water amount flowing down the slope surface rather than infiltrating depends on the intensity and duration of precipitation, on the density of vegetation cover, and on the properties of the slope surface that determines its infiltration capacity. This rate at which a surface can absorb water is measured in millimeters per hour and depends on the pore volume and the properties of the pores. Consequently the infiltration capacity is influenced by the particle size, the plentifulness of organic matter and the intensity of faunal activity, and decreases, e. g., with increasing loamification. According to Summerfield (1996), low infiltration capacities are most likely in arid and semi-arid regions due to soils with a low organic content. But they are also common in all environments influenced by human activities where the vegetation cover is artificially removed or where the surface is compacted.

If the infiltration capacity of a surface is exceeded although the soil is not water-saturated, a proportion of the precipitation falling on a slope will flow over the surface as **infiltration-excess overland flow** (or Hortonian overland flow) (Ahnert, 1996). Following Horton (1945), overland flow must reach a critical depth at which the eroding stress of the flow exceeds the shear resistance of the soil surface before erosion by overland flow can occur on a hillslope (Fig. 2.2). Hortonian overland flow is mostly valid for arid catchments and/or catchments with impermeable soils. In comparison, **saturation overland flow** is predominant in humid and semi-humid environments where sufficient intense and long precipitation locally saturates the soil and raises the water table to the surface without exceeding the infiltration capacity. Such conditions are most likely reached in areas with perched ground water, as for instance close to stream channels, and in lower parts of a slope with water supply from above. Hence, runoff varies as a function of soil thickness Dunne (1978). Overland flow is additionally also influenced by topography and below listed wash processes.

Rainsplash erosion describes the dislodgement of particles on the soil surface by the impact of raindrops. This erosion is possible wherever the ground is not entirely overgrown with vegetation and it is influenced by slope gradient and surface characteristics. The steeper the slope, the more particles dislodged by raindrops move downslope. It is more effective on coarser surfaces, e. g., sand, because finer particles contribute to cohesion. A high erosion rate is achieved when combined with slope wash because raindrop impacts (1) continuously make available particles, (2) increase the turbulence of the water flow which both enhances water to entrain and transport sediment, and (3) displace fine particles which infill near-surface voids which in turn lowers infiltration capacity and raises overland flow due to crusting (Ahnert, 1996). Generally, rainsplash erosion tends to even out the surface.

Slope wash is the unchanneled entrainment and transport of sediment by a thin sheet of water flowing across a slope surface and operating over the whole area. Alternatively it is termed soil, surface or sheet wash or flow. True sheet flow can only move very fine

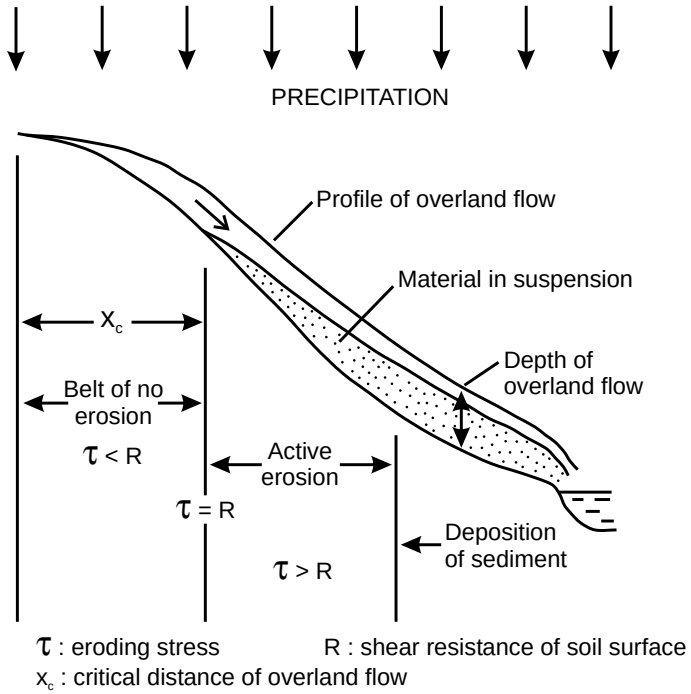

Figure 2.2. Horton's model of surface erosion by infiltration-excess overland flow. Modified after Horton (1945).

particles and is controlled by particle size, degree of particle cohesion, extent and nature of vegetation cover, and slope gradient. Local climatic conditions often induce a continuous vegetation cover that avoids excessive erosion by slope wash due to reduced runoff on the surface. But as stated by Selby (2000), runoff generally increases with slope length, height, and steepness. Crusting due to flowing water moving silt and clay particles in open pores reduces infiltration and raises overland flow. Microtopography tends to disturb sheet flow which then can grade into channelled fluvial (or concentrated) flow: The water movement progressively concentrates into particular downslope routes which allows the transport of larger material. Concentrated flow is influenced by the depth and velocity of flow, and it tends to carve channels and rills and enlarge them into gullies. According to Tucker (1998), the mechanisms for channel initiation vary depending on the setting (climate, hydrology, geology, relief, vegetation, etc.). In humid areas rills usually develop only on surfaces where the vegetation cover is artificially disturbed, whereas they can occur naturally in arid and semi-arid regions. Convex contour curvature disperses sheet flow downslope and minimizes erosion, whereas concave contour curvature achieves the opposite effect. According to Selby (2000), wash processes produce an increasing lower concavity. The rates of surface wash vary widely from 1 mm/ka in temperate, well-vegetated woodlands up to 10,000 mm/ka on badlands with a majority cluster in the 2–200 mm/ka range (Young and Saunders, 1986). This diversity is due to variations in rainfall intensity, vegetation cover, soil erodibility, slope angle, and slope length. Surface wash is the primarily denudational process in semiarid and tropical subhumid environments.

Solute transport describes soil materials taken into solution during weathering reactions and transported downslope as solutes. The removal of dissolved substances takes place in the groundwater, by lateral throughflow or deeper groundwater movement and leads to rearrangement and settling of the remaining particles. But it is difficult to calculate this effect on the slope form itself. The rate of solute transport can be estimated by measuring the discharge of subsurface flow on a slope and relating this to its solute concentration. Following Young and Saunders (1986), the rates are never very high, all in all ranging from 2 to 100 mm/a. Limestones have a higher range (10–100 mm/ka) than siliceous rock (2–60 mm/ka). Generally, denser vegetation increases the weathering and in turn the transport of solutes through seepage water (Rohdenburg, 1989). Selby (2000) states that uniform solution produces a parallel downwearing. The initial phase of percolation leads to most rapid rates of solute release that decrease as the soil solutions move towards equilibrium with the minerals present within the slope materials. Generally, solution is faster when excess water leaches solutes away, bringing less saturated water in contact with the rock and so increasing chemical reaction rates (Young and Saunders, 1986). The solute transport is greatest where subsurface flow is at maximum, i. e., at the base of slopes and slopes with concave contour curvature. Because solution operates by what may be called direct removal, already a very low rate of solution produces more slope retreat than the fastest reasonable assumptions about creep and surface wash: Solution at a rate of 10 mm/ka means a slope retreat at 10 mm/ka for a slope of any length and any angle, including erosion surfaces (Young and Saunders, 1986).

2.6 Rates of denudation

Denudation describes areal degradation resulting in the general lowering of the earth's surface by removal of sediment (solid and dissolved) due to water, ice, wind, and also gravity. No specific slope processes need to be identified. The term **erosion** is more used in the context of slopes and the locally restricted degradation. In German terminology, denudation comprises all processes of areal degradation, while erosion describes line-like degradation, for instance, along rivers or glaciers (Ahnert, 1996). This work follows the former definition.

The rate of denudation is averaged over regions and measured in units of millimeters per 1,000 years. Often also the Bubnoff unit B is employed where 1 B = 1.0 mm/ka (Young and Saunders, 1986). Table 2.3 lists some denudation rates showing the obvious effects of climate and relief but also the enormous variability due to the wide range of processes and structures. Vegetation cover as well as soil and rock type are excluded as independent variables. Human influences generally accelerate denudation by up to 20 times or might even exceed this value, depending on the intensity of land use (Young and Saunders, 1986). Recent studies presented by Burbank and Anderson (2001) show that mechanical erosion alone can already proceed at rates as high as 5-10 mm/a.

There are several techniques to estimate the effects of slope processes and the rate of slope denudation: (1) from the direct measurement of ground lowering, (2) from the mass or volume of sediment transport, or (3) from the velocity of the transported material, depending on the type of denudation (Ahnert, 1996). But all measurements are for a limited

Table 2.3. Rates of denudation (mm/ka). Gentle relief covers slopes <25°; steep relief covers slopes >25°. Modified after Young and Saunders (1986).

Climate	Relief	Typical range for rate of denudation [mm/ka]
temperate continental	gentle	10 – 100
	steep	100 – 200
temperate maritim	mostly gentle	5 – 100
Mediterranean	variable	10 – ?
subtropical humid	variable	10 – 1000
tropical subhumid	variable	100 – 500
tropical humid	gentle	10 – 100
	steep	100 – 1000
arid	variable	10 – ?
semiarid	gentle	100 – 1000
polar/mountainous	mostly steep	10 – 1000
glacial	gentle (ice sheets)	50 – 200
	steep (valley glaciers)	1000 – 5000
any climate	badlands	1000 – 1,000,000

time (few months to few years) and therefore unreliable to represent average rates over the long term. The problem remains the assessment of the true long-term significance of geomorphic events with long recurrence intervals. Nevertheless there is a considerable variation in the activity of particular processes under different morpho-climatic regimes (see Sect. 2.1). Burbank and Anderson (2001) state that in some mountainous regions erosion by glaciers, rivers, or landslides is rapid enough to accommodate nearly all of the documented rates of unloading. Rates of individual geomorphic processes are mentioned in above Section 2.5.1. Further problems in the determination of process rates include sediment transfer paths, the spatial and temporal sampling frames, magnitude and frequency, climatic changes, relict landforms, slope retreat, equilibrium and steady state, and the relations between processes and landform evolution.

According to Figure 2.3, larger landforms will generally be more durable in contrast to progressively smaller landforms which can be both created and destroyed relatively more rapidly (Dikau, 1989). In addition, smaller landforms are more frequent and on top of older and bigger landforms with which they are functionally connected. Consequently, the net change of a landscape seems to occur at a decreasing rate when viewed over progressively larger area or over longer periods of time (Ahnert, 1996). The intensity of change for any finite time interval or the rate of change for any finite area typically seem excessive when applied to a longer time scale or larger area. In other words, rates and intensities are time- and area-dependent.

Surface uplift as well as crustal uplift are of secondary importance in the context of this work. Following Summerfield (1996), surface uplift describes an upward movement of the landsurface with respect to a specific datum (normally sea level) and is mostly associated with active tectonic processes. In areas of active uplift, denudation is generally less than the rate of surface uplift (Burbank and Anderson, 2001). The upward movement of the rock column with respect to a specific datum (such as the geoid) is termed crustal or bedrock uplift. This type can occur simply due to the removal of material through

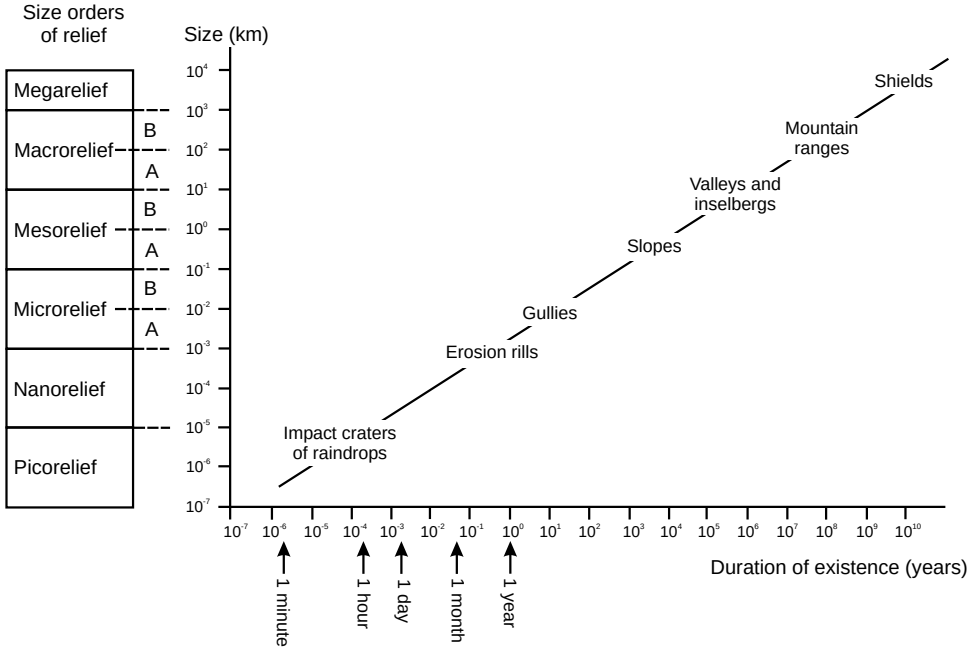

Figure 2.3. Relationship between size and duration of landforms. Modified after Dikau (1989).

denudation which reduces the load on the crust which in turn moves upward to restore isostatic equilibrium. According to Summerfield (1996), such crustal uplift generally does not exceed the rate of denudation so there is no net surface uplift. For details, reference can be made to Burbank and Anderson (2001) where this topic is better discussed.

Soil erosion occurs on the one hand by natural processes, on the other hand considerably by plowing and tilling. Following Summerfield (1996), the rate of soil erosion is a function of both erodibility and erosivity. The **Universal Soil Loss Equation** (USLE) was introduced as the most comprehensive index of soil erosion to express the rate of soil erosion and to predict soil loss especially in croplands (Wischmeier and Smith, 1962; Wischmeier, 1978). Following factors are included: soil loss, rainfall erosivity, soil erodibility, slope length and gradient, the proportion of the ground surface that is covered by crops, and the presence or absence of soil conservation measures such as contour ploughing (Selby, 2000). The USLE was devised for practical conservation purposes and in order to apply its concepts in other parts of the world, modified versions have been developed and applied. But despite the extensive use of the USLE in soil erosion studies in croplands with Hortonian overland flow, it has not been generally applied to areas completely covered with grass or tree and it does not apply to soils being eroded by mass wasting.

2.7 Slope form

Slopes can be simply subdivided into individual convex, concave or straight components according to their form which is most often represented in terms of two-dimensional profiles (Ahnert, 1996). On the whole, many slopes show an upper convex segment, a straight

main segment, and a lower concave segment. A overview of slope classification gives, e. g., Young (1975). Figure 2.4 illustrates the hypothetical nine-unit slope model discussed by Dalrymple et al. (1968) who additionally shows how different slope processes tend to predominate on different slope units. If slopes are regarded as three-dimensional components of the landscape, their rectilinear, convex or concave plan form is important too because of the effect of contour curvature on the routes taken by water, sediment and solutes moving downslope. Parsons (1988) shows and discusses the resulting nine possible three-dimensional shapes for hillslope units. A general survey of relief classification models is represented by Dikau and Schmidt (1999).

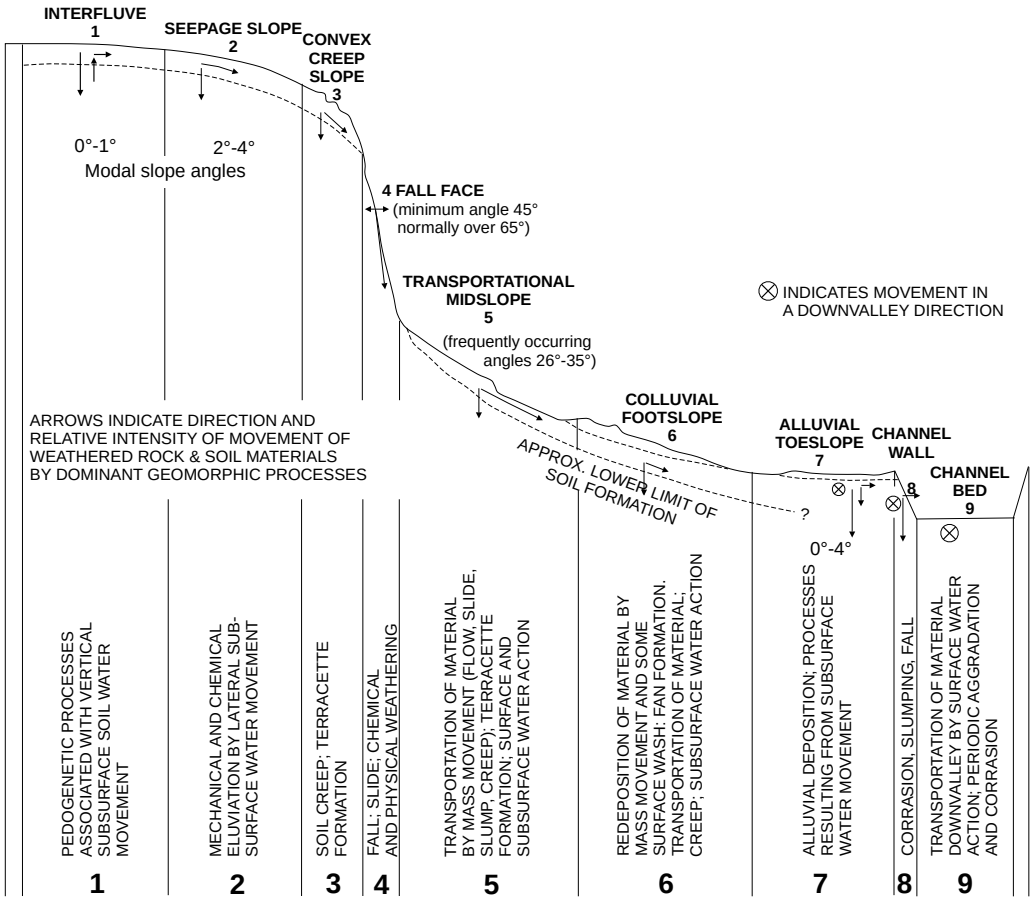

Figure 2.4. Hypothetical slope units and corresponding processes after Dalrymple et al. (1968) (Fig. 10.2, p. 190 from Selby, 2000).

Soil-mantled slopes in humid temperate climate are typically convex–rectilinear–concave, many of the convex and concave slope units being smoothly curved (Young, 1975). According to Jyotsna and Haff (1997), a convex-concave profile is also the characteristic shape of diffusion-dominated terrain. The upper convex slope segments often form half or more of the total profile and result probably mainly due to soil creep. First qualitative explanations of hillslope profile convexity were given by Gilbert (1909) who assumed that the amount of material that creeps past any point is proportional to the distance of the point from the summit, i. e., larger quantities must move through cross sections progres-

sively farther downhill. Or in other words, the lowering of the surface is accompanied by an increasing rate of transport of material. As creep is primarily a gravitational process, the rate of soil creep increases with gradient. This in turn implies a downslope increase in slope angle in order to move the progressively greater amount of material, thereby giving rise to slope convexity (Bloom, 1991). The same holds for rainsplash erosion and solifluction in semi-arid and periglacial regions, respectively.

Rectilinear main slopes develop where mass movements transport debris downslope to a relatively constant depth. Active stream incision evolves extensive straight main slopes while basal undercutting steepens a slope until a shallow debris or earth slide restores the slope to the angle of repose (see Sect. 2.3). According to Wallace (1977), scarps that are about 12 ka old have maximum slope angles of 20° to 25°. Much older scarps have principal slopes as low as 8° to 9°.

The lower part of a slope mostly corresponds to concave slope segments which are normally associated with either slope wash or the deposition of talus. Generally, on lower slopes transportation by flowing water assumes dominance over creep (Bloom, 1991). With slope wash the depth of the downslope flow increases due to the increase of the contributing area away from the slope crest. Therefore the velocity of flow can be kept up at progressively lower gradients. Simultaneously there is a decrease in the average grain size away from the drainage divide. As finer material needs less power to transport than coarser, even lower slope angles can maintain the rate of sediment transport. Consequently, slopes dominated by wash processes, including seepage and rill wash, develop basal concavity since the slopes become progressively less steep in downslope direction (Ahnert, 1996). The basal concavity is replaced by a straight slope around the angle of repose if active stream incision removes material from the slope base as quickly as it is supplied. Missing basal undercutting often leads to slopes with convexo-concave profile: Predominant rainsplash or soil creep in the upper part give way at some point downslope to the prevalence of slope wash. For a rather comprehensive review of slope concavity, see Carson and Kirkby (1972).

Simplified and summarized, soil creep near the top of a slope increases the gradient downhill until water begins to flow over the surface instead of penetrating and saturating the creeping soil, and sheet wash and slope concavity begin. Generally, the transport capacity of geomorphic processes on hillslopes determines the ability of these processes to shape the slope form. But fashioning of the slope form by slope processes can always additionally be affected by external or internal conditions, such as climatic factors or changes within the slope material.

Chapter 3

Slope evolution models

Earth scientists develop and use slope evolution models in order to describe, analyse, simplify, and display their understanding of hillslope systems. More recent, complex landform evolution models try to incorporate all kinds of operating variables as tectonics, rock type, extent of rock weathering, drainage in relation to climate and vegetation, together with the possibility of some randomness in the course of events, often resulting in a low degree of predictability. This Chapter gives an overview of some of the most widely known hillslope evolution models. Several subdivisions exist but are most often inconsistent; one possible classification is shown in Figure 3.1.

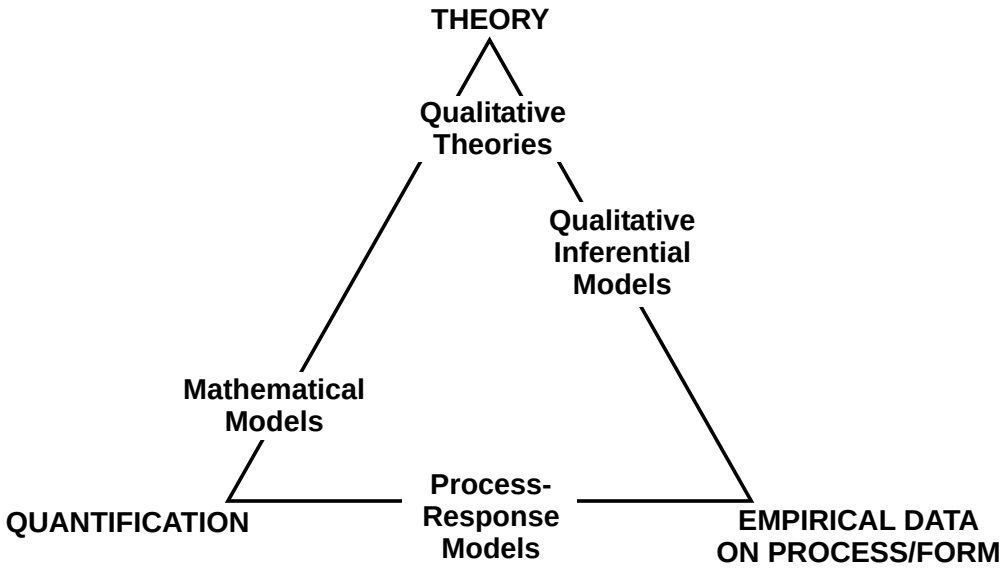

Figure 3.1. Classification of studies of hillslope evolution through time. Based on Parsons (1988).

Studies based on theoretical input seek to provide a general, qualitative model for hillslope evolution. They are not based on detailed empirical observations, and additionally they do not yield specific quantitative predictions about the change of slope form over time. Hillslope evolution in a particular locality or under a closely defined set of conditions may be better explained in studies emphasizing empirical data on slope processes and form (qualitative inferential models). Both types of models account for observed slope forms in terms of a particular sequence of events and are described as descriptive models in Section 3.1. Deductive mathematical models and process-response models are the result of quantified studies and are summarized together with composite, numerical models as dynamic models in Section 3.2. The model presented in this study belongs to the latter category.

Before describing the most common models it is important to distinguish two general kinds of situations concerning the degradation of hillslopes which can occur in all climates: weathering-limited slopes and transport-limited slopes. This distinction was first indicated by Gilbert (1877). Subsequent hillslope researchers had largely overlooked this basic dichotomy until it was noted by Schumm (1956). Finally, Carson and Kirkby (1972) introduced the above terms of weathering- and transport-limited slopes.

Weathering-limited slopes : Weathering-limited degradation of slopes depends on the rate at which material is made available through weathering, i. e., more material can be transported than provided by weathering (Ahnert, 1996). Such scarps are generally not covered by soil but expose solid bedrock and are common in arid to semiarid regions with insufficient moisture to support a continuous vegetation cover. The form of such slopes is mainly determined by the type of weathering. According to Nash (1980b), the removal of a uniform thickness of loosened material from the scarp face without accumulation at the base of the scarp results in parallel retreat without rounding of the crestal convexity or basal concavity (e. g., active fluvial cut-banks and wave-cut bluffs). Such scarps retreat with little or no decrease in gradient and are generally stripped bare of debris. If the undercutting ceases and the loosened material accumulates at the base of the scarp, an apron of debris inclined at the characteristic angle of repose will progressively grow which in the end buries the retreating scarp face. In subsequent works, Nash (1986) described this degradation pattern as loosening-limited due to the fact that debris is carried away as rapidly as it is loosened from the surface.

Transport-limited slopes: Transport-limited slopes represent temperate, humid regions with rapid weathering and continuous vegetation and soil cover. However, such slopes are found in any climatic region where surfaces are underlain by weakly consolidated or unconsolidated material. These scarps are generally covered with soil or loosened debris and produce more loosened material than the transport processes are capable of removing (Nash, 1986). While reclining, the scarps become more rounded with time. As described by Colman and Watson (1983), changes in the morphology of transport-limited scarps are primarily controlled by processes like soil creep, raindrop impact, and slope wash. Generally, these slopes tend to reach a dynamic equilibrium and to develop a characteristic morphology according to the involved processes (Ahnert, 1996). Kirkby (1971) described this as a "characteristic form" which may be attained while 50–75 percent of the initial relief remains (see Sect. 3.2). Following Carson and Kirkby (1972), characteristic forms are shown to be convex for predominant slow mass movements (e. g., soil creep) as occurring

in middle and higher latitudes. Wash processes (e. g., soil wash with gullying) prevailing in tropic and sub-tropic climate form regressively concave slopes if overland flow increases continuously towards base. A simultaneous combination of slow mass movements and wash processes or ungullied soil wash forms a convexo-concave slope due to increasing downslope runoff supporting wash processes. This S-shaped profile with a convex upper part and a concave lower part is frequent in middle latitudes. But according to Ahnert (1996), this sigmoidal slope form can also evolve if upslope loosened material is deposited downslope as hill or slope wash (see Sect. 2.7). Nash (1980b) remarks that the degradation of these slopes is complex and particularly influenced by the debris cascade across them.

Summerfield (1996) states that above dichotomy implies (1) that on slopes with sufficient erodible particles transport processes will always operate on capacity, (2) that it neglects the contribution of mass movement processes in determining slope form, and (3) that it overemphasizes the role of water erosion on slopes. Instead, Ellison (1947) introduced **detachment control** as a basis for understanding the relationship between slope processes and slope form (see also Parsons, 1988; Summerfield, 1996). The surface materials of hillslopes can be regarded as lying along a continuum of detachability with respect to particular hillslope processes. At one end of this range, surface materials have no detachability and removal is limited by the rate of weathering of particles which are detachable by this particular process. At the other end, surface materials are infinitely detachable so that hillslope erosion is limited by the transportation capacity of that particular process. Detachability between these two endpoints is influenced by soil aggregate stability, surface crusting, pore pressure and other factors (Parsons, 1988). Regarding particular processes, detachability varies both in space and with time, for instance due to downslope differences in soil composition or sporadically operating processes.

For an extended discussion for the most of below mentioned models, see, e. g., Brunsden (1971), Carson and Kirkby (1972), Young (1975), Parsons (1988) or Selby (2000).

3.1 Descriptive models

Until the 1950s, geomorphic research laid the emphasis upon landscape history and the long-term evolution of slopes proposing a couple of classic models of slope development mainly based on qualitative theories. Much of that discussion concentrated upon the problems of the origin of the convexity and the concavity, and the evolution of the steepest (or any straight) part of the slope. Most theoretical models postulate a continuous and uniform development and are based on gravity as the main controlling factor (Bremer, 1989).

In 1899, W.M. Davis suggested a model of long-term progressive decline in gradient with an increasing rounding of hillslopes within his wider concept of the "geographical cycle" (Davis, 1899). In the Davisian sense, ungraded (dynamically unstable) slopes retreat fast and mostly by mass movements. In contrast, on graded (dynamically stable) slopes with a continuous soil and vegetation cover, slow and continuously acting processes take over (Young and Saunders, 1986). Bryan (1922) introduced the idea of parallel retreat of hillslopes retaining a steep gradient. W. Penck presented his concept of slope evolution through replacement from below of steeper gradients by gentler ones in 1924 (Penck, 1924).

He resumed some of Davis' ideas in 1953 (Penck, 1953). In the same year, L.C. King (1953) resumed Bryan's suggestion and proposed his model of parallel retreat additionally incorporating an earlier model developed by Wood (1942) which is in turn includes ideas by Lawson (1915). Noteworthy studies which also observed the pattern of scarp degradation with parallel retreat were also presented by Hamblin (1976), Anderson (1977) and Wallace (1980).

The observation of degrading natural hillslopes by comparing the morphology of a series of different aged hillslopes assumed to have had the same initial morphology was probably first used by Savigear (1952). This might be considered as the introduction of qualitative inferential models. Since the 1960s at the latest, studies of slope evolution have revealed that the evolution of most hillslopes is far more complex than suggested in most previously mentioned classic models. Especially from the seventies on there has been made great progress in the understanding of hillslopes resulting from careful studies of the degradation patterns and processes active on hillslopes. Studies that documented the change of spatial sets of hillslope profiles with time were presented by Carter and Chorley (1961), Welch (1970), Brunsden and Kesel (1973), Dunkerley (1980) and others.

Fair (1947) and Hack (1960) presented models where the relationship of hillslope profiles to underlying geological structure has been used to infer a temporal sequence of hillslope profile form. Hack additionally elaborated the concept of dynamic equilibrium in landform evolution. Later studies with similar approaches include, e. g., Ollier and Tuddenham (1962), Mills (1978), Pain (1986) and Pavich et al. (1989).

3.2 Dynamic models

The above mentioned hypotheses and concepts and the increasing knowledge about geomorphic processes enabled analytical and numerical modelling of scarp degradation where the change of hillslope form through time is a function of the present state of a slope.

Mathematical models in a narrower sense are deduced theoretically and predict approximate hillslope forms which a profile will tend to approach over time if specific slope processes operated in a manner described by particular equations. They need not specify the physical processes intrinsically or a particular sequence of events and their results must be verified in nature (Parsons, 1988). The first model in a mathematical sense may be dated back to the work of Fisher (1866) who described the parallel retreat of coastal chalk cliffs with accumulation of a basal debris apron. Lawson (1915) and Lehmann (1933) extended this simple model and incorporated different stages of weathering. Fisher's model was furthermore modified by Bakker and Le Heux (1946), van Dijk and Le Heux (1952) and Looman (1956). To permit the treatment of scarps with nonhorizontal crests and bases, the model was further modified by Nash (1981a).

Since 1960, significant progress has been made in mathematical modelling of processes, especially of short-term processes. Culling presented his studies and proposed a linear diffusivity-type equation applicable to the evolution of transport-limited hillslopes with a rate of removal of weathered material being proportional to the slope gradient (Culling, 1960). Although Gilbert was the first one who considered in his field notes of 1876 the

application of diffusion equation concepts to hillslope erosion (Johnson and Pollard, 1977). Culling (1963, 1965) based his analysis of the basic processes underlying the diffusion equation on the argument that soil creep is a stochastic process which is produced by random movements of individual particles that is similar to Brownian motion on a macroscopic level, a concept involving the use of the mathematics of molecular diffusion. Most scarp degradation models which are used to date scarps as also the one presented in this study are based on this diffusion equation which is better discussed in Chapter 4.

Scheidegger (1961) presented a variety of assumptions about the relationship of the rate of denudation to the shape of the hillslope with a distinction in linear and non-linear theory where degradation acts vertically and normal to the slope surface, respectively. Another extension of Fisher's basic ideas was presented by Ahnert (1964). He based his models of hillslope evolution on the assumption that the rate of weathering is a function of the thickness of the overlying waste mantle and that the waste mantle moves slowly downslope at a velocity proportional to the sine of hillslope gradient.

The diffusivity-type model of hillslope degradation introduced by Culling has been proposed by many following researchers. Based on the relationship of velocity of downslope movement to tangential and critical shear stress and viscosity, Souchez (1963, 1966) developed a model under the influence of transport-limited mass movements. He assumed that downslope movement is by plastic flow and that soil creep plays only a minor role in denudation. Hirano (1968, 1972, 1975) combined cases of Scheidegger's linear theory with the diffusion model of Culling and demonstrated that a broad variety of convex-concave profiles may be developed. Hirano (1976) and Ohmori (1983, 1984) extended the diffusivity equation to three dimensions. Varying erodibility (e. g., lithology) of the slope material was incorporated in models using a modified diffusion equation which were proposed by Tödten (1976a) and Pierce and Colman (1986). Tödten (1976b) suggested that hillslope erosion and deposition by overland flow (esp. by sheet wash and rill erosion) may also be described by a similar diffusion equation. Gossmann (1976) first observed slopes in nature and then described them in reverse order in mathematical equations combining different processes that are defined by the climatological conditions and that are representative for specific cases. Noteworthy are also the studies of Pollack (1968), Luke (1972, 1976), and Carter and Nobes (1980).

A process-response model in the widest sense is any model that applies an operator (usually expressed as a mathematical function of x and y) to an initial form (usually defined by its coordinates x and y). The simplest models assume only one process operating on a slope and link it to the slope form (Bremer, 1989). Most process-response models adopt simulation techniques, some apply analytical methods, but generally the **continuity equation** is the necessary basis for any process-response model (Selby, 2000). The continuity equation for unconsolidated material was first obtained by Exner (1922). Kirkby (1971) presented one widely applied approach using the continuity equation in differential form for a theoretical analysis of slope development under transport-limited processes, i. e., there is no limitation on the supply of material.

Assuming that there is (1) no transport of sediment into or out of individual profile lines, i. e., conservation of mass in cross section, and that there is (2) no change in density of the surficial material, the change in elevation of a point must therefore be equal to the

difference between the amount of material transported to the point and the amount of material transported away from it. This can be expressed by a **continuity equation** of the differential form, for the one-dimensional case,

$$\frac{\partial H}{\partial t} = -\frac{\partial q}{\partial x} = -\nabla q. \tag{3.1}$$

The continuity equation is specified by the volume flux, q, in terms of morphological factors. Kirkby (1971) applied a simple type where q is simply proportional to the local slope and that is appropriate for most slow mass movements, surface wash and stream transport:

$$q = f(x)^m \left(-\frac{\partial H}{\partial x}\right)^n \tag{3.2}$$

where H is the elevation of a point, and x is the horizontal distance of a point from the crest. q is also defined as the rate of downslope transport or transport capacity and is given in meters^3 per meter of contour per year, or meters^2/year. m and n are constants where n describes the influence of increasing gradient and which is usually considered to be zero or positive. $f(x)^m$ represents a positive function which describes the influence of increasing area or distance from the divide, i. e., a function proportional to distance from the watershed (roughly the distance over which overland flow is ineffective). $(\partial H/\partial x)^n$ represents processes in which sediment transport is proportional to hillslope inclination. The volume flux q depends on x, possibly to some power, and may include slope to some power (e. g., Carson and Kirkby, 1972). Hence, if $f(x)^m = kx^m$, where k is a proportionality constant reflecting the transport efficiency, the transport rate q is a power function of the distance from the divide x to the power m multiplied by the local slope to the power n, and scaled by a rate constant k:

$$q = kx^m \left(-\frac{\partial H}{\partial x}\right)^n. \tag{3.3}$$

(3.3) may adequately describe processes involving overland flow (e. g., wash, rills, gullies, and rivers) as well as those processes that depend only on slope and not on distance from the divide (e. g., soil creep, rainsplash, frost heave, and animal induced disturbance). If q is defined as above, equation (3.1) is also termed mass conservation equation and expresses the transporting capacity of the slope as a function of slope gradient and distance from the drainage divide where t is the elapsed time. If the gradient in mass flux is positive (more mass leaving than arriving), the surface will decline in elevation (erosion), and vice versa. Hence, the variation of the transport rate largely controls the slope form and the rate of change. The continuity equation is a very general and broadly applicable statement and is valid for hillslopes, riverbeds, and seafloors (Burbank and Anderson, 2001). Following Nash (1980b), the effects of contour curvature are ignored.

For a satisfactory statement of the solution of (3.1), it is required to specify the initial form of the profile, the conditions at the crest which are usually regarded as fixed, and at the base of the slope where constant removal of material is the simplest condition. If divide and base level are fixed horizontally through time, an analytical solution of the continuity equation exists which describes the resulting equilibrium profile, i. e., the characteristic form to which the profile tends as time passes, and to which it approximates closely by the time the initial relief has been reduced to half (Kirkby, 1971; Carson and Kirkby, 1972). This form depends on lithology, climate, vegetation and on the processes operating but not on the initial slope geometry. If $m > 1$, the slope will be concave-upward; if $m < 1$, the slope will be convex-upward. In addition, the effects of variation in m are more significant than those for variations in n. Characteristic long-term slope forms for different processes are illustrated in Figure 3.2. For slope wash without and with gullying, Kirkby (1971) suggested, $m = 1$, $n = 1 - 2$ and $m = 2$, $n = 2$, respectively. In the case of diffusive processes such as soil creep and rainsplash, it is generally accepted that $m = 0$ and $n = 1$ (Pierce and Colman, 1986). This is not valid for cohesion-limited (nonlinear) creep where $m = 0$ and $n > 1$ due to the efficiency of creep processes as a function of the surface gradient. However, empiric observations also carried out by Pierce and Colman (1986) suggest that n is not > 1. Although there is considerable variation in m and n for slope wash, slope wash on relatively short, steep slopes of scarps seems as well likely to conform $m = 0$ and $n = 1$. In both cases where $m = 0$ and $n = 1$, the downslope transport rate is directly proportional to the local slope curvature. According to Pierce and Colman (1986), solifluction may also be simply proportional to the surface gradient for sites which are moist throughout the year although this process is generally more dependent on moisture than on slope.

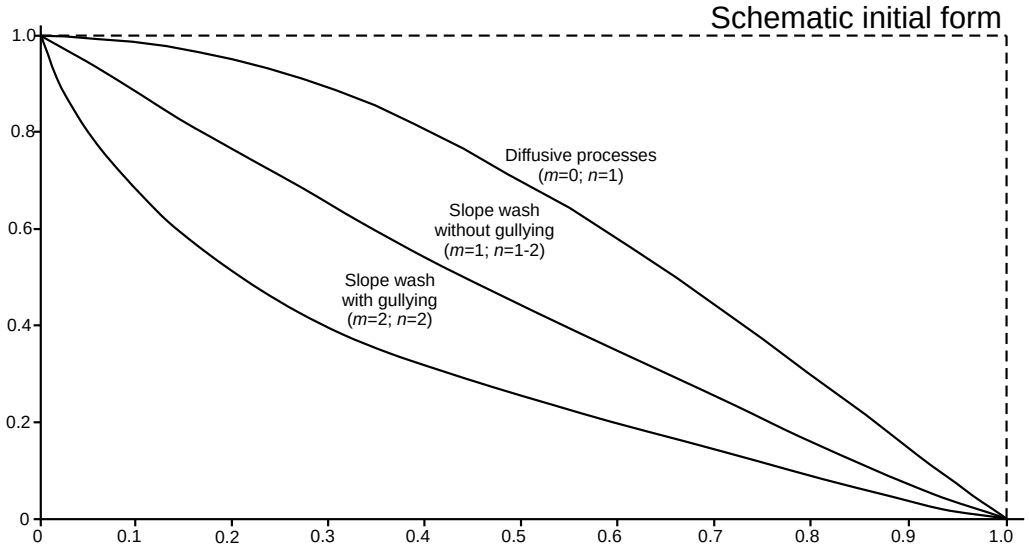

Figure 3.2. Dimensionless graph showing approximate characteristic slope forms for different geomorphic processes with transport-limited conditions, no tectonic displacements, constant elevation boundary conditions, and reduction of the initial relief by $\sim 50\%$. Modified after Kirkby (1971).

Above described process-response models can only predict a single hillslope form resulting from continuously operating processes. But in reality all hillslope processes are discontinuous, e. g., soil creep with many individual heave movements depending among other things on weather conditions. Furthermore, as understanding of geomorphic processes has become more detailed, the expression of these processes in equations and their solutions are more difficult. Numerical models of hillslope evolution can cope better with such more complex process equations and with the long-term morphologic consequences of such short-term processes. Most of these models are based on the same continuity equation described previously. Instead of seeking analytical solutions to it, they predict the changes of specific points on a hillslope through time by a repeated calculation of the new coordinates of these points which then form the input hillslope for the next iteration step. Almost identical models but based on different assumptions were developed by Young (1963) and Ahnert (1966, 1970b,a, 1971, 1973) to which reference can be made for details. Especially Ahnert (1971) and Ahnert (1973) performed the pioneering work in computer simulation of hillslope degradation. Several following authors have applied the approach of numerical simulation to model hillslope evolution, e. g., Parsons (1976), Kirkby (1976, 1984, 1985), Trofimov and Moskovkin (1984), and Band (1985).

Extended three-dimensional simulation of hillslope evolution, i. e., evolution of hillslopes rather than hillslope profiles, emerged from the 1970s on. In such numerical models, a continuous topographic surface is approximated as a discrete lattice of cells. Ahnert (1976) modelled the effects of weathering, overland flow and surface wash, viscous flow, plastic flow and debris slides on an initial surface of any configuration (regarding structural effects) and with basal conditions that could be varied during the simulation (regarding base-level change). A model presented by Armstrong (1976) allowed the simulation of weathering, soil creep and wash processes on an initial surface incised by streams which remained fixed throughout the simulation. Kirkby (1986) considered the process of lateral migration of stream channels by defining the initial topography as a pseudofractal surface and allowing stream channels to form and be destroyed during simulation in response to the operation of hillslope processes. A model for hillslope development by landsliding and the recognition of threshold slopes was developed by Kirkby (1987). Ahnert (1987) presented a landform development model program (SLOP3D), also based on the mass balance concept, which can be applied to geomorphological problems at different spatial and temporal scales.

Since the 1990s, the development of quantitative computer models that simulate long-term, 3-D basin-scale and larger-scale topography was reinforced by various groups. As such models go beyond the scope of this study, only some authors shall be mentioned at this point without paying detailed attention to the individual models: e. g., Beaumont et al. (1992), Chase (1992), Howard et al. (1994), Moglen and Bras (1994), Rigon et al. (1994), Willgoose (1994a,b), and Tucker and Bras (1998). For large-scale landform evolution models especially applying the diffusion equation see also Section 5.3.

Chapter 4

Dating technique

4.1 Introductory words

Following several authors (e. g., Young, 1975; Wallace, 1977; Hanks et al., 1984; Andrews and Hanks, 1985), the general evolution of simple scarps only a few meters high and formed in erodible, unconsolidated material, such as those terrace riser investigated in this study, proceeds in two phases:

(1) During formation of a scarp or shortly after it, an initial phase of rapid morphological change occurs if a free face is formed, i. e., if the slope is oversteepened and the angle of repose is exceeded. This might occur either by faulting or, in the case of terrace risers, by entrenching due to lateral undercutting of terrace gravels by a stream (Pierce and Colman, 1986). The fast but mostly piecemeal process of gravitational degradation is characterized by slumping, spalling, and other processes with large random variations. The abandoned scarp collapses back as masses of sediment from the upper part of the slope break loose and fall or slide to its base (Bloom, 1991). Loosened material accumulates directly below the free face and buries the base of a slope with the debris apron. The scarp is modified until the slope reaches a rectilinear shape at approximately the angle of repose of the material in which the scarp is developed (usually about 25° to 35°, see Sect. 2.3) and within a relative short period a straight, long-term stable slope is established.

(2) The slope morphology is altered through time by much slower erosional and diffusive slope processes during the second phase. Concerning fault scarps, the original fault plane is replaced by one controlled by erosional processes and a scarp profile identical to that of fluvial terraces forms (Nash, 1984). Associated with a decrease in the maximum slope angle, the scarp evolves in a way consisting of a progressive rounding of the basal concavity and the crestal convexity. Concerning the slope above and below a scarp, Enzel et al. (1994) state that the far-field slope of a faulted alluvial fan always exceeds 0° in the downstream direction whereas the upper and lower far-field slopes of a terrace riser are very close to 0° due to the topographic profile being perpendicular to the flow direction.

Stüwe (2000) states that many morphogenetic processes can be described through diffusion or advection, but also production, because transport of material on a surface often follows the same principles as the transport of heat. As slopes generally tend to degrade through

time, one widely applied approach which was first introduced by Culling (1960) uses the one-dimensional, linear **diffusion equation** in second-order partial differential form for a theoretical analysis of slope development through time.

Such a model does not attempt to determine the time period required to degrade a free face to the angle of repose by weathering-limited processes as it is not appropriate for this purpose. Although rounding of the crest often follows a diffusion model, the deposition of the loosened material from the free face at the base of a scarp follows a simple wedge model (Nash, 1981a). The duration of the rapid ravelling period is assumed to be short compared with the age of the scarps considered. Hanks and Andrews (1989) claim that this interval lasts on time scales of hundreds of years to perhaps 1,000 years; Colman and Watson (1983) and Avouac (1993) shorten this interval to only 10 to 100 years. And Pierce and Colman (1986) describe it to be even only several years. In fact, the time required to reduce the free face to the angle of repose needs to be found empirically, and, strictly speaking, it must be added to the time interval in which the diffusive analysis does apply. Following Pierce and Colman (1986), the resulting scarp shape at that certain time when the scarp reaches a slope at or slightly below the coefficient of friction and when the slower transport-limited processes begin, might be termed as the "starting form" at the "starting time" in the context of the presented study.

4.2 The diffusion equation

According to Nash (1986), a slope profile can be regarded as a series of linear segments each receiving material from above at its upslope end and loosening material at its downslope end. The first assumption underlying this study is that conservation of mass holds on a local scale which requires that the material within such a segment must increase if more material enters the segment than leaves it. This results in an increase in the height of the segment. Conversely, the elevation decreases if more material leaves the segment than enters it. This change in height is therefore determined by the downslope change in the volumetric material flow per unit width q. If q decreases in downslope direction, material will accumulate and the elevation will increase and vice versa. The downslope divergence of the volume flux q is equal to the change in height H, with time t, in horizontal spatial dimension x and is expressed by the **continuity equation**, recalled from Section 3.2,

$$\frac{\partial H}{\partial t} = -\frac{1}{\rho}\frac{\partial q}{\partial x} \tag{4.1}$$

where ρ is the mass density in grams per square centimeter per centimeter along strike. Unlike equation (3.1), above equation does not initially assume a constant density of the surficial material. The slope distance ds over which the volume flux q changes is approximated by the horizontal distance dx. As $dx \leq ds$ except for zero slopes, this slightly overpredicts the geomorphic displacement rate. But Arrowsmith (1995) showed that the approximation is justified because the difference is small for low slopes $<45°$.

What is now needed to close the system, is a process rule controlling the hillslope flux q. Two statements can be confirmed unambiguous: (1) all hillslope processes depend on some

degree on the local slope, and (2) the type of process how material is moved downslope and its rate are dictated by the local climate and slope material. Therefore, erosion processes are often expressed in terms of a proportional relationship between erosion rate and local slope curvature (Culling, 1960; Ahnert, 1970c; Andrews and Bucknam, 1987). In the simplest case, many mass movements may be regarded on a single hillslope, of which a scarp is an example. If (1) the transport capacity equals the material transport rate and is uniform along the profile, and (2) the transport of particles downslope past any point x is assumed to be a function only of the local slope S, equation (3.3) can be simplified (i. e., $m = 0$ and $n = 1$), resulting in a linear **transport equation** with respect to one spatial dimension x,

$$q = -kf(S) = -k\frac{\partial H}{\partial x} = -k\nabla H \tag{4.2}$$

where k is a constant of proportionality which allows $f(S)$ to be a dimensionless function of the dimensionless variable slope S. H is the height, x is the horizontal distance along the profile, and hence, $S = \partial H/\partial x$ and expresses the topographic gradient in two dimensions normal to the elevation contour, i. e., the change of height H with distance x. $f(S)$ is required to be positive for positive S and negative for negative S. Consequently, the leading minus sign ensures that the net volume flux is in downslope direction, i. e., a positive transport rate down a negative slope. In general, the flux q expresses the volume transported in a cross-strike direction per unit length along strike. But in geomorphology q is often referred to the width and not to the cross-section of a profile. The hillslope flux q is therefore the volume rate of sediment transport per unit width in the x direction and is given in meters^3 per meter of contour per year, or meters^2/year. The transported material was eroded at any time from any point on a scarp profile, q is in this context thus also termed rate of erosion.

Equation (4.2) is based on theoretical, experimental, and empirical analyses of downslope transport by creep, raindrop impact, overland flow, and channel flow processes (Sterr, 1985). But according to Culling (1963) and Carson and Kirkby (1972), (4.2) is only appropriate for the transport-limited conditions of slow continuous movement of particles at the surface over moderate to low slope (e. g., soil creep over a slope <30° as loosened material will seldom remain on steeper slopes). The equation also adequately describes the downslope rate of material by raindrop impact alone on gentle slopes where significant surface runoff is negligible as on slopes of highly permeable material (Nash, 1980b). Slow hillslope processes also include the effects of bioturbation and burrowing animals as this may cause surficial downslope creep of the sediment which should be diffusive too (e. g., Imeson and Kwaad, 1976; Black and Montgomery, 1991; Rosenbloom, 1992) and which is believed to be especially widespread in pelagic sediments (e. g., Stow, 1986). Assuming that bioturbation may smooth the topography in a similar way to hillslope creep on land, produces movement which can be modelled using the diffusion equation. Arrowsmith et al. (1996) states that bioturbation additionally seems to provide adequate supply of material for transport. Further disturbances mobilizing sediment on soil-mantled slopes include tree throw, animal burrowing, and wet/dry cycles (Roering, 1999). Concerning creep, Figure 4.1a shows that the net downslope displacement of material at a point is

proportional to the sine of the slope angle ψ at that point if expansion occurs by heaving perpendicular to the slope surface and contraction by vertical dropping of the surface (Kirkby, 1967). For a single expansion-contraction episode generating soil creep, p. 16), the actual displacement of soil decreases linearly with depth, but at maximum till the depth of penetration if the amount of expansion and contradiction of the debris mantle is uniform throughout its thickness (Fig. 4.1b). The frequency with which an expansion-contraction cycle penetrates into the ground also decreases with depth. The combination of both observations produces a concave-downslope displacement and is shown in Figure 4.1c. Such a displacement profile has also verified by several field studies (Carson and Kirkby, 1972).

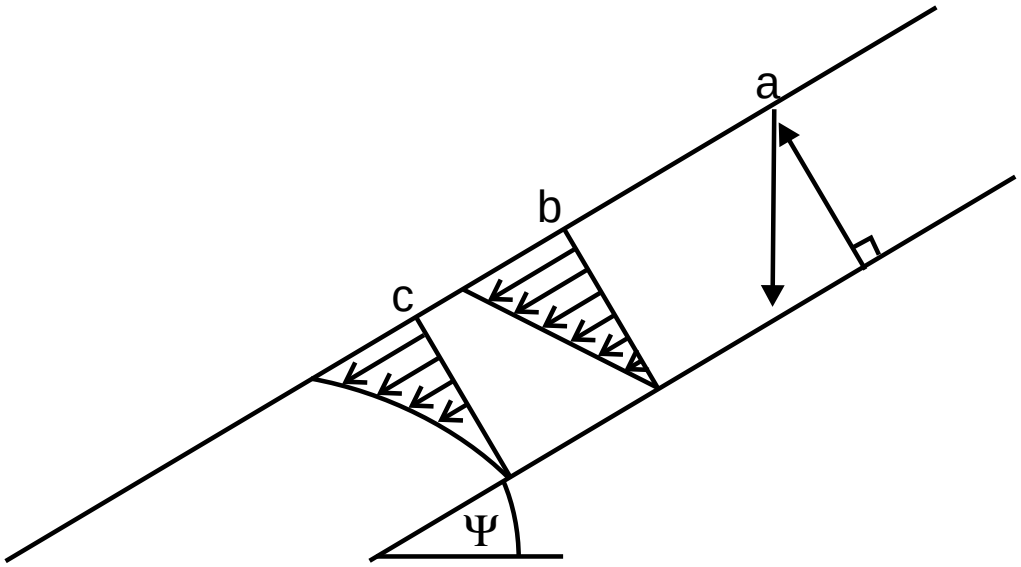

Figure 4.1. Displacement of soil due to downslope creep caused by expansion and contradiction; for explanation see text (from Nash, 1986).

All above mentioned disturbance-driven processes have been termed diffusive because the resulting sediment flux is thought to be primarily slope-dependent. Equation (4.2) is not valid for slope-length dependent processes (where q is proportional to x), such as overland flow (Carson and Kirkby, 1972). Nash (1987b) states that a convincing theoretical argument can be made that q should be proportional to the force of gravity acting tangentially to the surface, i. e., proportional the sine of ψ, if the material is rheologically similar to a Bingham model or to an alternate expansion-contraction creep model; but there is little experimental data. For slopes not steeper than 30°, q is also proportional to the tangent of the slope angle ψ,

$$q = -k \sin \psi \approx -k \tan \psi. \tag{4.3}$$

Above first-order approximation also includes and describes the fact that shear strain is proportional to shear stress for the low stresses on nearsurface materials on slopes and that in turn shear stress in a slope is proportional to the sine of the slope angle. This was shown by Mitchell (1976) and co-workers who have conducted extensive theoretical

and experimental investigations of creep on small slopes for a wide variety of soils in the laboratory under conditions of constant shear stress. Schumm (1967) showed that the creep velocity of fragments can also be fit fairly closely with a linear function of gradient although this velocity is not the same as q. His observation supports equation (4.2) if it is assumed that the thickness of the creeping debris mantle is independent of gradient. But according to Nash (1987b) this should not be assumed a priori, and field studies of regolith flux are still badly needed.

Next, the continuity equation (4.1) is combined with the dependence of downslope transport on surface gradient, and q is eliminated from (4.1) and (4.2), yielding

$$\frac{\partial H}{\partial t} = \frac{1}{\rho}\frac{\partial}{\partial x}\left(k\frac{\partial H}{\partial x}\right). \tag{4.4}$$

The proportionality constant k is taken as an independent material property, i. e., k is constant, which is reasonable without any a priori information about what the functional form of k might be. The density ρ is taken to be constant too, i. e., the density of the material prior to removal is the same as its density after deposition. Thus,

$$D = k/\rho \tag{4.5}$$

where D is the erosional diffusivity (see Sect. 6.3) that expresses the volume of material that can move per unit time. D is numerically equivalent to the volumetric transport rate at unit gradient. Finally, this results in the 1-D, homogeneous and linear **diffusion equation** with constant coefficients:

$$\frac{\partial H}{\partial t} = \frac{\partial}{\partial x}\left(D\frac{\partial H}{\partial x}\right). \tag{4.6}$$

Hence, the erosion or deposition rate depends only upon the local curvature of the surface. Assuming D to be constant with time, the elevation H is a function of horizontal distance x and time t, (4.6) can also be written as

$$\frac{\partial H(x,t)}{\partial t} = \frac{\partial}{\partial x}\left(D\frac{\partial H(x,t)}{\partial x}\right). \tag{4.7}$$

Finally, if the diffusivity D is considered independent of gradient or position x, (4.6) becomes

$$\frac{\partial H}{\partial t} = D\frac{\partial^2 H}{\partial x^2} = D\nabla^2 H. \tag{4.8}$$

The diffusion equation expresses that at any point on the initial slope, the rate at which the elevation H changes with horizontal distance x and elapsed time t is the product of the diffusivity D and the local slope.

Summarized, following assumptions are included in the model (e. g., Hanks et al., 1984; Andrews and Hanks, 1985; Arrowsmith et al., 1996):

(1) the transported volume is assumed to be conserved on a local scale, thereby eliminating dissecting erosional processes and terranes from consideration;

(2) the rate of downslope movement of material at a point on the hillslope is proportional to the gradient of the hillslope profile at that point;

(3) the specific, partly discontinuous, erosion processes on the short-term scale are averaged on the long-term scale, i. e., the evolution of the landscape surface and the flow of material along it are continuous;

(4) the hillslope is formed in weakly consolidated material, it remains covered by loose debris and the bedrock-/soil-ratio exceeds a given level as the model ignores that the production of regolith is required before it can be transported, i. e., the slope is transport-limited;

(5) the scarp is one-dimensional, i. e., the elevation H depends on only one space coordinate x but also on time t;

(6) particles move down the surface slowly on the time scale in which slope is changing, i. e., the erosional processes are slow and diffusive;

(7) particles moving down the slope remain within the extent of the scarp profile (porosity changes are ignored);

(8) no water is lost due to evaporation or infiltration;

(9) loss of material, e. g., through wind and water, is ignored and the effects of solution are negligible;

(10) no tectonic displacement or transport of the surface material;

(11) the slopes must not exceed the frictional angle of the material;

(12) the far-field slope is the same above and below the scarp.

The diffusion equation is a simple and believable first-order approximation to the erosional evolution of nondissecting landforms regarded as closed systems, i. e., no outlet. Hence, under certain conditions also the erosional evolution of gully profiles and alluvial channels that were affected by base level lowering can be modelled using the diffusion equation suggesting that such processes are also diffusive (e. g., Begin et al., 1981; Begin, 1987, 1988; Schumm et al., 1987). The resulting synthetic channel profiles fit the observed ones reasonably well but the diffusivities are 4 to 5 orders of magnitude greater than those determined for scarps. According to Arrowsmith et al. (1996), such large diffusivities may

indicate a failure of the assumptions regarding the behaviour of the processes, rather than large variations in the rates of a given process, and consequently, such profiles should not be considered in the diffusion equation. But equation (4.6) still applies if the root-mean-square distance jumped by surface particles is small compared to the length of the scarp profile (Andrews and Hanks, 1985). As the conditions are assumed to be transport-limited, the conversion of bedrock to soil is not explicitly considered but it is assumed that either it occurs at a rate exceeding the erosion rate or that the material was never lithified.

In physics, unstable systems in which changes occur slowly to establish equilibrium and always in the same direction represent stochastically fluctuating systems: under non-equilibrium conditions, a fluctuating quantity is subject to a diffusivity equation with a symmetric diffusivity tensor (Scheidegger, 1991). Above diffusion equation (4.6) is identical in form to the diffusion equation used to describe many known processes in conductive heat flow. Thus, the former introduced diffusion constant D is the topographic equivalent to the thermal diffusivity. But the application of the diffusion equation in geomorphology proceeds on less sure physical basics than it does in heat conduction where it is directly verifiable. This is not the case in non-steady scarp evolution where it is simply assumed that there are mechanisms by which mass transport takes place and which lead to landform modification if a topographic gradient is given and which can all be parameterized with the mass diffusivity D. The diffusion equation is also employed in chemical dispersion and viscous or fluid flow through porous or permeable media, respectively; in mineralogy and geochemistry it is known as Fick's law of diffusion in which fluxes are proportional to chemical gradients. The diffusion equation thus also represents the tendency of a closed system towards attaining a state with maximum entropy. For a rather detailed review of diffusion mathematics, see Crank (1979). A brief but comprehensive explanation of the basics of heat conduction is given in Stüwe (2000).

4.3 Physical description

Geomorphological dating is based on the general assumption that variation in scarp morphology is related to time-dependent degradational processes. Applying the diffusion equation to scarps results in reduced curvatures of the crestal convexity and the basal concavity, i. e., upper and lower edge become more rounded, while their lateral extents increase, thereby lowering the midslope angle with time. The maximum scarp angle occurs at the inflection point between positive and negative curvature. The midslope gradient decreases at a rate which is related to the diffusivity D (still assumed to be independent of x and t), to the height H and to the midsection slope of the initial profile. For the same value of D, sharp features degrade faster than smooth ones. By the simplest assumptions of the diffusion equation, the midpoint of the slope does not change position and the initial scarp height does not decrease. Hence, the mathematical treatment of creep as a simple diffusion phenomenon is consistent: The diffusion curve is symmetrical around the center point on the profile with a lower half simply recording the accumulation of an equivalent cross section of material removed from the upper half: Erosion occurs on the convex-upward portion (negative curvature or downslope decrease in gradient) of the scarp; no ground loss takes place on the rectilinear slope; the concave-upward portion (positive cur-

vature or downslope increase in gradient) results in accumulation and deposition, more soil being brought in from upslope than is removed downslope. The difference in elevation between the horizontal plane above and below the scarp remains unchanged if measured sufficiently far from the upper and lower edge, respectively. The downslope transport rate is simply a linear function of slope, so with the decrease of the local curvature, also the further rate of change decreases. As the convexity progressively decreases, an equal amount of ground loss requires significant longer periods of time in the later stages with low curvature than in the earlier stages with relatively high curvature. Other geomorphic processes remove some of the accumulated material from the lower half of the profile on slopes higher than a few meters (Bloom, 1991). In this case the midpoint of the curve migrates with the retreating slope and the simple diffusion curve becomes asymmetric. But still the fundamental relationship between the rate of creep and the convexity of the local upper slope is retained.

Assuming that the state of degradation reflects the time of scarp formation, Wallace (1977) demonstrated that strictly geometric measures of scarp morphology, e. g., the scarp slope or the rounding of the corners, at any time could yield information on its relative age. Hence, knowing the diffusion constant D, the diffusion equation (4.7) can be used to predict the age of an unknown scarp by its shape, and thus, D can be seen as the "clock" of scarp erosion as it determines the rate of degradation.

To calibrate the model, for a given initial scarp (usually at the specific angle of repose) a family of synthetic profiles is generated by the diffusive model depending upon the passage of time t and the value of the diffusivity D. Each profile is compared with and fitted to naturally occurring profiles, at best of known age, to determine the smallest deviation between both. With a constant diffusivity, the model calculations with the best match yield the product of the elapsed time t and the rate constant D which is defined as the **morphological age** or **diffusion age** Dt of a scarp having the dimension [length^2]. The value of Dt actually uniquely defines the resulting scarp form. Dt is also termed **degradation coefficient** τ (see Sect. 5.2) which consequently depends on the age of a scarp and the erosion rate of alluvium materials in a given climatic environment (Avouac and Peltzer, 1993). Small t and large D result in the same form as large t and small D. From the morphologic age τ and a known absolut age t, the diffusivity D for the specific material and conditions can be determined:

$$D = \tau/t. \tag{4.9}$$

Absolut, chronological ages t in units of [a] or [ka] are finally calculated by dividing the morphologic age Dt by the calibrated regional diffusion constant D. As the time required for the previously described first gravitational process is relatively short the calculated age is generally assumed to be equal to the total age of the scarp. The age t is thus defined as the elapsed time since a scarp was left to erode without the influence of a stream undercutting it.

The diffusion equation (4.6) includes the diffusive (such as creep and rainsplash) as well as the advective (such as slope wash) aspects of hillslope evolution. In fact, hillslope topography results from the competition between such diffusion-dominated hillslope transport and

runoff-dominated erosion (Tucker and Bras, 1998). According to, e. g., Howard (1997), for a one-dimensional slope profile, the point of transition from creep-type to flow-driven erosion can be analytically defined as the point at which both processes are equally effective in transporting sediment. Insights into the mechanics and rates of individual degrading processes are not provided by the diffusive approach, but it yields a reliable picture of the morphologic changes through which the degrading hillslopes has evolved. Hence, the diffusive-advective model is valid for the evolution of a source area depending on erosion rate, mean effective runoff rate, fluvial transport efficiency, and hillslope diffusivity.

The resulting artificial profiles predicted by the properly calibrated model match the shape of naturally occurring profiles quite exactly. But comparing younger and older scarps in the field shows that the latter ones are characterized by lower slope angles if both types have the same height, consist of similar material and are influenced by similar climatic conditions (Enzel et al., 1994). Nash (1980b) also describes this observation for normal fault scarps produced by earthquakes. If scarps are of same age and underlain by the same material, they tend to be less steep when less high, i. e., the gradient of the midsection of a low scarp decreases faster than that of a higher scarp (Bucknam and Anderson, 1979). Although according to Colman (1987), the assumption of q being proportional to the local slope which is applied in the linear diffusion-equation model reveals that scarp height (or length) should have no effect on the diffusivity.

The pattern of the predicted scarp degradation as well as the calibration effort will additionally be strongly influenced by the specification of boundary conditions, including the initial configuration of the scarp. Three boundary condition are conceivable: (1) constant elevation, (2) variable elevation, and (3) constant material flux. If a scarp is treated as an open system, the upper slope boundary (at the crest) is continuous, material will be added constantly to the system and the boundary elevation remains unchanged without any overall lowering of the landscape. If the scarp is treated as a closed system, this boundary is reflective with zero sediment flux which could correspond to a hillslope divide with no material input, the boundary elevation will decrease with time. Similarly, if the lower boundary (at the base) is made continuous, debris will be removed from the system. Such a constant elevation could correspond to the middle of a valley where a stream channel determines base level. With a lower reflective boundary with zero sediment flux, the loosened material will accumulate against the boundary. This could correspond to the filling of a valley if no stream removes material. Constant elevation boundary conditions are easy to imagine but are probably rare in nature (Arrowsmith et al., 1998). Although both conditions are reasonable approximations for most scarps which change much more rapidly than the general landscape. Lowering or raising profile boundaries due to tectonic or geomorphic processes operating beyond the landform of interest are thus more likely. To reduce the influence of model boundary conditions on the pattern of scarp degradation and to exclude that the results are adversely affected, the scarp should be given a long crest and base. Carretier et al. (2002a), for instance, solved the diffusion equation on a 300 m wide profile, so that the scarp evolution does not depend on the boundary conditions (constant elevation at the base, fixed elevation at the crest). However, the presented model applies constant elevations at both the crest and the base. The influence of boundary conditions on scarps with long and short crests and toes was investigated in Section 8.3.

Chapter 5

Previous work in geomorphological dating of scarps

5.1 Empirical approaches

The geomorphological development of riverside bluffs through time was investigated by Brunsden and Kesel (1973). The author performed a space-time calibration to, among other things, relate changes in slope form to certain processes and to estimate the rate of such changes.

Wallace (1977) described useful geomorphic characteristics of fault-scarp profiles younger than a few thousand years such as maximum angles and angularity or curvature of the break in slope at the crest to determine their relative ages and the ages of fault displacement. The author showed that the rate of slope degradation is not linear. Hence, a $>35°$ slope gradient reflects events of ≤ 100 years. Scarps younger than a few thousand years have a steep free face, a debris apron with a slope of about 35°, and a sharp break in slope at the crest. Older scarps decline with age resulting in maximum slope angles of 20° to 25° for scarps that are approx. 12 ka old. Much older scarps with ages of more than 100,000 years show angles as low as 8° to 9°. Additionally, the crestal break in slope broadens with age. Wallace (1977) also describes the relationship between material in the scarp face and the rate of scarp degradation.

Bucknam and Anderson (1979) studied numerous fault scarps of late Quaternary age in unconsolidated gravels of alluvial fans located in the semiarid eastern part of the Basin and Range province, USA, where the valleys are typically covered up to 20 percent with low shrubs. The authors investigated the relationship between scarp height, scarp-slope angle, and geomorphic age to provide a quantitative age evaluation and to estimate the rates of regional seismic activity averaged over periods of thousands of years. They formalized their considerations graphically with plots of scarp height versus scarp-slope angle allowing to estimate the stage of degradation. The authors state that (1) for a given fault-scarp age (estimated by using shoreline datums), the maximum slope angle of the scarp is proportional to the logarithm of the scarp height, i. e., a regular increase in mid-slope gradient with increasing height, and that (2) the maximum slope angle decreases

with estimated age for scarps of a given height. Bucknam and Anderson also observed that the midsection gradient of a low scarp decreases faster than that of a higher scarp. Additionally, variations in the initial slope angle seem to have little effect on the observed relationships.

Both last two approaches are the most widely known empirically based studies in geomorphological dating. Several following investigators applied similar empirical approaches, e. g., Machette (1982), Mayer (1982), Colman (1983), Sterr (1985), Crittenden and Muhs (1986), Pearthree and Calvo (1987), and Matmon et al. (2000). But as a detailed description of such studies goes beyond the point it shall just be referred to, e. g., Machette (1989) where summarized details can be read up on.

5.2 Analytical approaches

Such approaches try to mathematically model the evolution of hillslopes. Most of them involve matching of a measured profile with a scarp morphology predicted by a model which follows the diffusion equation. This application of the linear diffusion equation (4.7) to date landforms has motivated a couple of studies since the 1980's. Only several years later, also nonlinear diffusion models were developed. Different diffusivity coefficients have been estimated by fitting simulated profiles to naturally occurring ones of known age, for instance, marine and fluvial terraces, fault scarps, and ancient lake shore scarps. Table 5.1 shows the very wide range of D values published in literature; it is followed by detailed descriptions of several analytical approaches.

Table 5.1. Estimates of the diffusivity coefficient D.

D [$\mathrm{m^2/ka}$]	**Location**	**Climate**	**Source**
> 0.1	Terrace risers and alluvial fault scarps, Negev Desert, Israel	arid	Begin (1993)
0.2–0.3	Fault scarps and terrace risers, Arava Valley, Negev Desert, Israel	hyperarid	Enzel et al. (1994, 1996)
0.31–0.45	Late-glacial terrace scarps, Idaho, USA (2–5 m scarp offset, N-facing)	semiarid	Pierce and Colman (1986)
0.37	Lake Lisan beach terraces, Dead Sea area, Israel	arid	Bowman and Gerson (1986)
0.44	Normal fault scarps (Drum Mountains), Utah, USA	arid to semiarid	Nash (1980b)
0.46	Lake Bonneville shoreline scarps, Utah, USA	arid to semiarid	Andrews and Bucknam (1987)
0.52–1.1	Lake Bonneville and Lake Lahontan shoreline scarps, Utah and Nevada, USA	arid to semiarid	Hanks and Andrews (1989)

continued on next page

continued from previous page

D [m^2/ka]	Location	Climate	Source
0.54–1.62	Late-glacial terrace scarps, Idaho, USA (2–5 m scarp offset, S-facing)	semiarid	Pierce and Colman (1986)
0.57	Lake Bonneville shoreline scarps and single-event fault scarps (Drum Mountains), Utah, USA (2 m scarp offset)	arid to semiarid	Pierce and Colman (1986)
0.68–0.92	Late-glacial terrace scarps, Idaho, USA (10–15 m scarp offset, N-facing)	semiarid	Pierce and Colman (1986)
0.9	Lake Bonneville shoreline scarps and single-event fault scarps (Drum Mountains), Utah, USA	arid to semiarid	Colman and Watson (1983)
0.9	Lake Lahontan shoreline scarps, Nevada, USA	arid to semiarid	Andrews and Bucknam (1987)
0.9–1.0	Faults and antecedent scarps, Idaho, USA	semiarid	Hanks (1999)
0.98	Lake Bonneville shoreline scarps and single-event fault scarps (Drum Mountains), Utah, USA (5 m scarp offset)	arid to semiarid	Pierce and Colman (1986)
1.1	Lake Lahontan shoreline and Beachfront fault scarps, Nevada, USA	arid to semiarid	Hanks and Wallace (1985)
1.1	Lake Bonneville shoreline scarps and single-event fault scarps (Drum Mountains), Utah, USA	arid to semiarid	Hanks et al. (1984)
1.2	Late-glacial terrace scarps, Idaho, USA (∼20 m scarp offset, N-facing)	semiarid	Pierce and Colman (1986)
1.4	Fluvial terrace risers, Upper Rhine valley, Germany	semi-continental (temperate)	Nivière et al. (1998); Nivière and Marquis (2000)
2.0±0.4	Fault and fluvial terrace scarps, West Yellowstone, Montana, USA	intermediate between humid and semiarid	Nash (1984)
2.8±1.1	Lake Bonneville shoreline scarps and fault scarps, Utah, USA	arid to semiarid	Mattson and Bruhn (2001)
3.3±1.4	Abandoned terrace risers, Hotan region, Xinjiang province, China	arid	Avouac and Peltzer (1993)
3.3±1.7	Fault scarps, Gansu province, China	arid	Tapponnier et al. (1990)
3.3±1.7	Cumulative reverse fault scarps, Mongolia	arid	Carretier et al. (2002b)

continued on next page

continued from previous page

D [m^2/ka]	Location	Climate	Source
3.4–5.2	Late-glacial terrace scarps, Idaho, USA (10–15 m scarp offset, S-facing)	semiarid	Pierce and Colman (1986)
5.5±2	Terrace edges, Tien Shan, Xinjiang province, China	semiarid	Avouac (1993); Avouac and Peltzer (1993)
7.0	Late-glacial terrace scarps, Idaho, USA (∼20 m scarp offset, S-facing)	semiarid	Pierce and Colman (1986)
7.0	Marine fault scarps	–	Mitchell (1996)
8.5	Fault scarps along the San Andreas Fault, California, USA	Mediterranean	Arrowsmith (2001b)
8.5±1.8	Fault scarps along the San Andreas Fault, California, USA	Mediterranean	Arrowsmith et al. (1995)
8.6±0.8	Fault scarps along the San Andreas Fault, California, USA	Mediterranean	Arrowsmith et al. (1998)
11.0	Abandoned sea cliffs, Santa Cruz, California, USA	Mediterranean	Hanks et al. (1984)
12.0	Shoreline wave-cut bluffs, Michigan, USA	humid	Nash (1980a)
16.0	Fault scarp, San Gabriel Mountains, California, USA	Mediterranean	Hanks et al. (1984)

Nash (1980b) proposed the first technique for morphologic dating using the relationship between scarp height and rate of degradation and studied the transport-limited evolution of normal fault scarps in cohesionless deposits. The author applied a simple quantitative diffusive model to approximate the erosional evolution of nondissecting (i. e., no overland flow) scarps using a finite difference solution to the diffusion equation. Hence, the time t in which the maximum midsection slope decreases from α to β is proportional to the square of the initial height or offset of a scarp H, i. e., the smaller the initial height, the more rapid is the degradation for scarps with equal initial slope angles and equal transport rates. This also implies that lower scarps will have smaller slope angles than higher scarps at any subsequent time after their simultaneous formation with the same slope angle but with different heights. The basis of morphologic dating of normal fault scarps is therefore supplied by the determinate relationship between initial hillslope height and the rate of decrease of the maximum slope angle which thus is considered to be the key geometric parameter. The product of the numerical age by the diffusivity can be estimated directly from one scarp measuring its regional slope, its half offset, and its maximum scarp angle. But the use of this model is limited as it requires a wide range of heights for each scarp to be dated.

Nash (1980a) levelled three sets of age-related wave-cut bluffs (one modern, devoid of vegetation and two abandoned, heavily vegetated) along the eastern coast of Lake Michigan, USA, which are composed of homogeneous, weakly consolidated, sandy morainic material. The author modelled the profiles using the diffusion equation: By using the known age differences between sets of profiles, Nash was able to derive a value for the diffusivity D and

to predict the degradation of hillslopes. In addition, statistically significant morphologic differences were found among the three groups of profiles. But the presented technique required that all scarps were underlain by the same material and showed a continuous range of heights along their length.

A more flexible method than the one from Nash (1980b) was proposed by Nash (1981b). The author showed that any combination of values for the diffusivity D, the scarp offset H, the time t, and the initial angle α that yields the same value for $(tD/H^2)\tan^2(\alpha)$ necessarily results in identical values of $\tan(\beta)/\tan(\alpha)$ with β as the decreased midslope angle. Nash presented *FAULT* which is a FORTRAN program for modelling the erosional degradation of active normal fault scarps to estimate times and amounts of vertical displacement of such faults. This program was able to model the parallel scarp retreat of weathering- or loosening-limited scarps as well as the rounding of the upper and lower edge in the case of transport-limited slopes. The latter was achieved in the way described above in Nash (1980a) and Nash (1980b) applying the diffusion equation. The mathematical model of parallel retreat corresponds to a further-modified version of Fisher's model (see Sect. 3.2).

Colman and Watson (1983) presented a degradation model with an explicitly solved diffusion equation for scarp boundary conditions using analytical methods. A solution of the diffusion equation is described where for each scarp profile the product of the diffusivity and the scarp age can be calculated from the initial and final configurations of the scarp. The authors pointed out that the time for which the diffusion equation applies to scarp degradation is after the removal of the free face of a scarp. As an example, Colman and Watson (1983) demonstrated how the solution can be used to estimate ages of single-event fault scarps and wide-spread wave-cut scarps in the western United States. The authors conclude finally, that the diffusion equation model is most seriously limited by the difficult estimate of the diffusivity.

Hanks et al. (1984) applied morphologic dating techniques to nondissecting alluvial scarp-like landforms which developed under different tectonic and climatic conditions, and which are therefore comprised of varying deposits. The authors analysed and compared morphologic observations in the form of cross-strike elevations profiles or in the form of slope-offset plots which are point plots of maximum scarp slope versus scarp offset. Their study demonstrated that elementary analytical model solutions to the linear diffusion equation can reproduce the actual topography of wave-cut and faulting-controlled landforms with remarkable accuracy, even with a constant diffusion coefficient (representing linear, diffusionlike processes). Hanks et al. determined the age from the midpoint slope of a scarp and applied analytical solutions (1) to a vertical initial-value scarp in the case of abandoned sea cliffs, (2) to a vertical continuous offset scarp in terms of the repeated faulting problem (without an initial scarp), and (3) to a finite-slope initial-value scarp in the case of Lake Bonneville shoreline scarps. The latter was applied to treat landforms suggestive of being formed by nonlinear erosional processes which in turn is indicated by a dependence of the morphologic age Dt on the scarp height. In addition, Hanks et al. (1984) proposed that the limit of scarp recognition is assumed to be a slope segment 3° steeper than the segments below and above it.

In his study, Nash (1984) applied the simple analytical diffusion equation model to fault and fluvial terrace scarps along the Madison River near West Yellowstone, Montana, USA, and presented the BASIC program SLOPEAGE. The author took the definite relationship realised by Nash (1981b) and plots $(tD/H^2)\tan^2(\alpha)$ against $\tan(\beta)/\tan(\alpha)$ which yields the morphologic age. This technique can be applied to scarps with crest and bases inclining less than 10° and where the total of the initial midslope angle is less than 35°. But the relationship breaks down for slopes with crests and bases that incline more than 20° or where the angle of the crest and of the base differ by more than a few degrees. Scarps with significantly differing curvatures of the crestal convexity and of the basal concavity are also inappropriate to be dated with this method as the simple diffusion equation cannot model asymmetric hillslope rounding. Likewise, multiple scarps, i. e., scarps consisting of two or more smaller scarps either due to undercutting of higher terraces by lateral migration of a cutbank without complete removal of the higher terrace or due to a splitting fault, cannot be dated by this technique because the stepped scarps are rapidly smoothed out as they degrade, and will resemble a degraded unstepped scarp after a relatively short time. Hence, morphologic dating will yield erroneous ages. Composite scarps produced by repeated faulting events should be avoided too. In contrast to the previously described model by Nash (1980a), this model does not require a wide range of height and degraded slope angle values. In addition, it needs no curve fitting, it is easy applicable, and the results are amenable to descriptive and testing statistics. Nash suggested that differences in degradation rates among different areas were partly due to differences in grain size. The author also indicated a possible correlation between hillslope aspect (compass orientation) and diffusion constant. Hence, the diffusivity reaches a minimum on scarps with a northerly aspect. This would be consistent with studies of valley asymmetry summarized by Young (1975) which indicate that for east-west-striking valleys in the northern hemisphere, the north-facing valley walls are generally steeper than the south-facing ones. Above relationship was later recovered by Nash (1986) who also described the two different patterns of transport- and loosening-(=weathering-)limited degradation and discussed the two fundamentally different required models.

Mayer (1984) showed that diffusion model ages depend on material, climate, and scarp height, and pointed out that large variations in diffusion or morphologic ages Dt may already result from different levelling techniques or site selections. The author also stated that the maximum scarp angle decreases with age and increases with scarp height.

Hanks and Wallace (1985) fit the pattern of degradation observed on the Lake Lahontan shoreline (Nevada, USA) with the pattern predicted by the diffusion equation. In their study the authors used the same value of diffusivity D as Hanks et al. (1984) determined for Lake Bonneville shoreline scarps which are of comparable ages in a comparable climate. The authors found both sets of shoreline scarps to be indistinguishable from one another if the effects of surface offset and far-field or fan slope are accounted for according to the rules of linear diffusion except for a slightly smaller positive curvature on the lower slope of the observed profiles compared to the model calculations which were attributed to wash processes.

Andrews and Hanks (1985) applied the linear diffusion equation to develop a technique to invert an observed scarp profile to find its diffusion age Dt by allowing an objective fit of model to profile data. The inverse determination of the diffusion age is based on

the second moment of scarp slope which grows linearly with diffusion age together with an assumed initial scarp shape and whose computation leads to a direct estimate of the diffusion age. Thus, the diffusion age takes into account the width of the scarp slope distribution and the global shape of the scarp profile, and not only, as previously, the maximum slope angle. Furthermore, the apparent age is defined as the second moment of a profile divided by its zeroth moment (= scarp offset) and is equal to the diffusion age if a vertical initial scarp is assumed. The initial apparent age is nonzero for any non-vertical initial scarp and differs from true diffusion age by a constant amount as age increases. The authors specifically applied the previously mentioned finite-slope initial-value scarp model by Hanks et al. (1984) yielding the so-called inferred age and compared this with the simpler vertical initial-value scarp model yielding the apparent age. Finally, the authors applied their technique to synthetic data and described a number of conclusions especially concerning different initial scarp shapes (nonsymmetric, multiple-fault trace and repeated-event profiles), and an arbitrary nonlinear flux. The apparent ages were converted to chronological ages using a nominal diffusivity of 1 m^2/ka.

The effects of height and compass orientation (microclimate) of terrace scarps on geomorphic degradation rates and processes by keeping constant variables such as age, lithology, and regional climate was studied by Pierce and Colman (1986). Thus, the diffusion equation model predicts a relation between maximum scarp angle and scarp height for a group of scarps of same age and known starting angle. For latest Pleistocene terrace scarps in Idaho, USA, the authors observed that, (1) maximum slope-angle increases linearly with log of height, and (2) as the scarps height increases, the slope angle is more degraded than modelled by the diffusion equation with a constant degradation rate. Consequently, the terrace scarps show a strong, linear relation between the diffusivity and the height such that the diffusivity increases with height. In other words: Assuming a scarp is of the same age along its strike, there is a strong positive correlation between age calculated by morphologic age (Dt) based on the simple diffusion model and scarp offset. Additionally, gentler starting angles reduce the dependence whereas steeper angles emphasize it. Pierce and Colman (1986) inferred that the greater degradation (diffusivity increases tenfold with scarp height) probably results from increased soil wash which transports mass at a rate depending on slope size or height. Soil wash is modelled as being linear in slope with a coefficient increasing linearly with distance from the scarp crest resulting in a highly asymmetric model, i. e., the flux is dependent on position on the slope x. Pierce and Colman (1986) state additionally that the efficiency of creep may increase with surface gradient, and that infiltration is less and runoff is greater on steeper slopes which both also contributes to the dependance of the diffusivity on height. All such height attributes probably affecting the diffusion coefficient cannot be modelled by the linear diffusion equation with a constant rate coefficient but with one increasing linearly with distance from the scarp crest, i. e., the transport rate is proportional to more than the first power of the slope expressed as a tangent. Such an assumption is necessary to get average diffusivity proportional to scarp size, and it implies that the overland flow of water arises from the rain falling only on the scarp itself. The scarp profile predicted by such a model is highly asymmetric. Moreover, the diffusion constants of south-facing scarps are higher than those of north-facing scarps which is mainly due to the interrelated effects of solar radiation on soil moisture, vegetation, and freeze-thaw and wet-dry cycles. The authors proposed to

normalize the diffusivity for W-facing scarps of the same height to remove their observed dependence. Finally, ages of fault scarps were estimated using the scarp morphology and analytical solutions for the diffusion equation.

Bowman and Gerson (1986) estimated the age of fault scarps on the basis of the extent of dissection, the amount of rounding of the scarp crest, the scarp gradient, the stage of clast weathering, the intensity of the micro-relief, and the stage of soil and desert pavement development. The authors analysed their field data from the Gulf of Elat region, eastern Sinai, and applied the approaches of Wallace (1977), Bucknam and Anderson (1979), and Nash (1981b). It was proved that the trend of slope angles of lower scarps being smaller although being coeval is statistically significant. The diffusivity was obtained by applying the technique presented by Nash (1981b, 1984).

Wave-cut shoreline scarps of late Pleistocene Lakes Bonneville and Lahontan, Utah, USA, were examined by Andrews and Bucknam (1987). A plot of the so-called *apparent diffusion age* (equals the morphologic age Dt for linear diffusion) versus scarp offset again showed that the apparent age increases nearly linearly with offset. The increase is only partly explicable by non-vertical initial slope, and thus the material transport rate downslope must be significantly nonlinear through the midrange of investigated slopes. The authors therefore presented a model with an adopted **nonlinear transport law** with a coefficient independent of position and predicting symmetric profiles. Each examined profile was fit individually to a number of different models incorporating (1) linear transport, (2) a cubic transport law, (3) a frictional sliding transport law, and (4) a linear plus cubic transport law. The data fits presented in Andrews and Bucknam (1987) suggested that at small slopes ($<10°$) the transport law should be linear, while in the midrange of slopes it should increase faster than either the cubic or the frictional sliding law. At larger slopes it should not increase as rapidly to account for the duration of the free face. A correlation between D and scarp height for scarps 1–12 m high was not found and it was shown that the model ages correlate inversely with the fan slope above the slope for all the models considered. The inverse correlation between the diffusivity D and fan slope suggests that particle size is larger where an alluvial fan is steeper and that material with larger particles degrades slower. Finally, the presented model can easily be applied to simple shaped scarps (initial angle of 31° and scarp slope angles ranging from 10° to 24°) without computer calculation using the included table. Here one may find the dimensionless age of a scarp predicted by the linear plus cubic model and depending on scarp slope angle as well as on slope above and below the scarp. The diffusion age is determined by multiplying the above dimensionless age by offset squared.

In 1987, proceedings of conference XXXIX "Directions in Paleoseismology" (U.S. Geol. Surv. Open-File Rep., 87-673) were published with several articles concerning morphologic dating including amongst others Mayer (1987), Colman (1987), Pierce and Colman (1987), Nash (1987b), and Hanks and Andrews (1987). A couple of sources of errors in morphologic dating were described by Mayer (1987) who also noted the importance of the determination of precision or confidence in the age estimate. Errors referred to as non-age-related variations in model-derived ages either occur as a bias in the age estimates for a scarp of a given age or as scatter around a model age (equivalent to uncertainty in a statistical sense). Such errors include the effects of geologic processes (e. g., lithology, weathering and geotechnical characteristics of the scarp material, climate, etc.), measure-

ment error, and model error (e. g., systematic or random departures from a linear diffusion model, different methods of fitting a model to the data, etc.). Colman (1987) illustrated limits and constraints in diffusive scarp degradation modelling depending among other things on the chosen initial assumptions, processes, and boundary conditions. The author pointed out that assuming a linear mass-transport rate is not valid in all cases, and that additional difficulties arise due to various processes operating in different relative proportions on different scarps. The effect of height and microclimate on scarp degradation was described by Pierce and Colman (1987) with equal conclusion as those by Pierce and Colman (1986) (see above). A reevaluation of the simple linear-diffusion model was made by Nash (1987b). In his study, the author determined the influence of various factors on the calibration of that model, such as underlying geology, vegetation cover, and climate. Additionally, Nash (1987b) again found a strong positive correlation between the estimated morphologic age Dt and the height of a scarp. The author listed four possible explanations for that increase of Dt with offset: (1) D increases linearly with offset, e. g., because higher scarps are commonly more heavily vegetated and disturbed by grazing animals, (2) higher scarps were more probably initially stepped consisting of two or more smaller scarps, (3) higher scarps have a lower initial angle than lower scarps, and (4) the simple diffusion model is invalid. Concerning (2), it appears unlikely that the number of steps increases linearly to give the mentioned relationship between Dt and offset. Item (3) would mean too low initial scarps to account for that relationship. (4) is discussed in more detail, and Nash briefly described the model proposed by Andrews and Bucknam (1987) incorporating a cubic transport law (see above). But although such a model reduces the differences between observed and synthetic profiles (especially at the crestal convexity and the basal concavity), the Dt value still increases with increasing scarp height. Finally, Nash mentioned models in which the flux q is a function of distance x and of gradient which produce asymmetric profiles from initially symmetric ones. But with his data, the author could not demonstrate statistically that the volume of removed material differed from the volume of deposited material, and hence he concluded that such models based on q being some function of x are inappropriate. Hanks and Andrews (1987) published in principle preliminary results of their investigations about the effect of the far-field slope on model age determination. Those results were later published in Hanks and Andrews (1989) and are described below.

Hanks and Schwartz (1987) investigated a fault scarp in Custer County, Idaho, USA, with only very little variation in scarp height. The authors applied the simple analytical solution to the diffusion equation with constant diffusivity for the vertical initial-value scarp as presented by Hanks et al. (1984). Hanks et al. (1984) and Hanks and Wallace (1985) determined a value for the diffusivity $D = 1.1$ m^2/ka which was also used to calculate the age of the Custer County fault scarp and which is finally consistent with several further observations. Additionally, the authors analysed that less steep scarps have lost memory of their initial shape.

Sherman (1987) applied the computer program SLOPEAGE developed by Nash (1984) to analyse a set of terrace scarps of which about the half were found to be asymmetric. Sites with a large variation in scarp height also again showed a significant correlation between the morphologic age Dt and scarp height. A theoretical analysis of the diffusion equation derived for very simple conditions led to a more nearly complete one-dimensional diffusion

model with an equation predicting an asymmetric degradation under certain conditions. The equation additionally shows that the diffusivity D is actually kH, a constant times the height, which supports that D is a function of scarp height. But Sherman's study did not assess the theoretical analysis properly due to a lack of key field and experimental observations.

The effect of far-field slope on model age determination of scarplike landforms in weakly consolidated deposits was examined by Hanks and Andrews (1989). The authors considered linear and nonlinear diffusion models together with a mathematical transformation of the empirical approach by Bucknam and Anderson (1979). In the case of the linear diffusion model, they confirmed the increase of the diffusivity with increasing height which surly proves nonlinear diffusive processes. For the nonlinear model for scarps 1–12 m high, no correlation between D and scarp height was found (compare Andrews and Bucknam, 1987). By reducing the maximum scarp angle by the far-field or fan slope (= reduced scarp slope), it was demonstrated that the effect of far-field slope on model age is of first-order. The applied method of morphologic dating is thus based on the plot of that reduced scarp slope as a function of scarp half offset. If the far-field slope is taken into account correctly, the age determination is the same no matter which of above models is used; or conversely, the age determination is surely wrong, if the effect of far-field slope is not accounted properly. The authors additionally pointed out that the method of morphologic dating is quite sensitive to unrecognized sources of error as, for instance, small variations in the measurement of the regional slope, maximum slope angles or scarp height which can all result in large variations of the inferred value of the morphologic age Dt.

Tapponnier et al. (1990) investigated a large thrust scarp and analysed its morphology mathematically based on the diffusion model. The authors assumed a two-dimensional geometry and modelled the morphologic evolution of the scarp as the convolution of the initial scarp shape with a Gaussian degradation function whose variance increases with time. This approach is valid for scarps a few meters high, independent of the degradation process (rainsplash, slope wash, solifluction, gelifluction, or any other kind of surface creep proportional to slope), and without any remnant free face. For a detailed description of this method, see next paragraph where it is better discussed. Searching for the best match between synthetic and observed profiles revealed that there are misfits between both profiles near the crest and the base of the scarp. This induced Tapponnier et al. to assume more than one seismic event that formed the scarp. Finally, local uplift rates were determined which reveal the recent tectonic evolution of the region.

A Gaussian erosion model being more general than the diffusion model of scarp degradation was proposed by Avouac (1993). The slope is regarded as a distribution function which can thus be treated as a topographical impulse becoming subsequently reduced by geomorphic degradation processes. Hence, the morphologic evolution of scarps can be described as the convolution of the initial shape with an erosion (or degradation) function whose width increases with time and which is, for a linear diffusion, a good approximation of a Gaussian bell with a variance measuring the rounding degree of initial shape. It was shown in a synthetic experiment that the variance can be obtained by least square fitting of synthetic profiles to measured ones. Once the erosion function is known, the degradation coefficient τ can be considered as a geometric measure of the scarp width, i. e., of its degradation state defined as half the variance $\tau = \sigma^2/2$ and equating the diffusion age introduced by

Andrews and Bucknam (1987). The degradation coefficient is sensitive to regional slope and 3-dimensional processes, and to determine its value reliably and correctly, several long profiles perpendicular to the same scarp must be measured. Avouac (1993) compared the Gaussian erosion model with the diffusion model in which the degradation coefficient is proportional to numerical age and only the diffusivity D must be determined for absolute dating. But the author pointed out that there actually is no indication for the degradation coefficient being constant and thus proportional to numerical age, even under constant climatic conditions. If now D depends on time t, it appears that the diffusion model implies a Gaussian erosion function. However, assuming a constant D, the variance is proportional to numerical age of a scarp: $\tau = Dt = \sigma^2/2$ with τ being equal to the diffusion age. The quantitative morphologic analysis of scarp profiles by best fitting to synthetic profiles allowed quantification of uncertainties and revealed that it is important to work with long profiles in order to tightly constrain the far-field slope. In addition, profiles with a high density of levelled points at the crest and base where the main curvatures occur are required as these points define the scarp's "width" from which in turn the variance σ^2 and hence the degradation coefficient τ is deduced. In addition, Avouac (1993) introduced confidence intervals for τ which are within the smallest deviation between observed and modelled profile +5 cm. This choice is justified because the minimum standard deviation is generally in the order of 10 cm which may hence be regarded as the typical misfit between observed and modelled profiles. Finally, the presented model includes a test of feasibility as profiles whose slope distribution plots are too far from synthetic profiles are rejected. The same Gaussian model of erosion was applied by Avouac and Peltzer (1993) who levelled profiles across fault scarps and transverse abandoned terrace risers to determine their state of degradation. Furthermore, a set of cumulative fault scarp profiles was analysed using synthetic profiles generated with a simple incremental fault scarp model to estimate the amount and rate of vertical movement. Finally, a local minimum rate for subsidence of the Tarim basin (China) was determined. Avouac and Peltzer (1993) studied geometries and rates of late Cenozoic thrust faulting and folding in the same region. The degradation of terrace edges that are offset by an active thrust was analysed quantitative morphologically and confirmed a rate of vertical throw determined by dividing scarp offsets by the ages of the ruptured surfaces. Applying the slope-offset analysis to shorelines in western Tibet, Avouac et al. (1994) determined diffusivities ranging between 0.2 and 1.4 m^2/ka.

Begin (1993) applied the method of quantitative morphologic dating and studied alluvial fault scarps to define parameters of paleoseismicity in the Negev desert in Israel, i. e., to assess the smallest reasonable value of the diffusivity D. Introductory, difficulties and limitations of the diffusion model to date scarps are explained. Next, values of the morphologic age Dt were determined; these were not correlated to scarp offset. A fault scarp was examined and the value of a minimum D was used to date the time of scarp formation through the diffusion model. Finally, the author described the limitation of detectable paleoseismicity in the Negev due to scarps being to old with regard to their height to be recognized.

Fault scarps and terrace risers in Israel were studied and dated morphologically by Enzel et al. (1994). Due to the lack of numerical ages in the study area, it was almost impossible to determine a specific regional diffusivity; the authors thus initially used the entire range of published diffusion constant estimates for the area. The results showed that the

variability of the morphologic age Dt is relatively small with varying initial scarp angles. In addition, the results of the diffusion model were compared with the age estimates based on other age-dating techniques which helped to improve the estimation of a regional diffusivity. Finally, the authors assessed the recurrence interval of faulting and the intensity of the long-term seismic activity in the region. Enzel et al. (1996) analysed additional recent fault scarps in the same region using the same values for the diffusivity and drew equal conclusions.

Arrowsmith presented several works applying morphologic dating to fault scarps along the San Andreas fault, Carizzo Plain, California, USA (e. g., Arrowsmith et al., 1995, Arrowsmith et al., 1996, Arrowsmith et al., 1998). In 1996, Arrowsmith et al. presented an extended model of existing morphologic diffusion erosion analysis to simulate tectonic and geomorphic displacements and to find out more about their interaction in the formation of a landscape. Geomorphic processes were modelled by solving the diffusion equation numerically using a transient finite difference approach (Arrowsmith, 1995). The extended morphologic dating model considers additional geomorphic conditions and processes (transport- or weathering-limited conditions, material flux boundary conditions, and the development of gullies and knickpoints) and includes more heterogeneous spatial and temporal distributions of tectonic displacement. For changing model parameters, the model returns the final topography and soil-/bedrock-interface indicating which parameters and processes are important. Finally, the difference between instantaneously formed fault scarps (earthquake events) and continuously formed ones (aseismic creep) was examined. The experiments were carried out with a value for the diffusivity of 1 m^2/ka. Arrowsmith et al. (1998) applied morphologic dating to determine the normal fault slip rates for two graben-bounding faults. Both are in the vicinity of the scarps used to calibrate the model. Forward modelling of scarp development yielded the local diffusivity D. The authors showed (1) that the uncertainty in the estimate of D increases with increasing morphologic age, (2) that D also increases with inferred profile age, and (3) that D does not depend on scarp height. The forward modelling procedure also revealed that, in general, the best fitting profiles were eroded too much in the upper parts of the scarps, and too little in the lower parts. But Arrowsmith et al. (1998) stated that this is probably due to secondary deformation adjacent to the San Andreas fault rather than due to variations in the transport capacity rule (i. e., nonlinear diffusion) because of the observed profiles having relatively sharp variations that contribute the misfits. With the determined value of D, the formation of the two graben-bounding faults could be dated. This age together with the estimates of the dip slip along the faults resulted in the determination of the local slip rates. More recently several online publication came out (Arrowsmith, 2001c,b,a).

Mitchell (1996) applied the diffusion transport model to date highly bioturbated pelagic sediments across marine fault scarp crests. This study was based on several proposals that bioturbation may cause downslope creep which can hence be modelled with a simple analytic solution to the diffusion equation. The author used a modified diffusion equation which incorporates the mean sedimentation rate of an area. Although the application of the model in the marine environment is more complicated due to bottom currents and gravity processes transporting sediment and thus reducing deposition, the results suggested that morphologic dating may also be applicable to marine fault scarps, especially in relatively sediment-free areas, such as mid-ocean ridges.

Nash (1998) presented his study about the influence of scarp height on the accuracy of morphologic dating. Careful examination of terrace scarps hence indicated that the simple model is not appropriate for scarps higher than a few meters. The fit between observed and modelled is good for scarps less than five meters high but it gets worse with height. Additionally, the author observed that scarps get increasingly asymmetric with height, i. e., the basal concavity is more rounded than the crestal convexity. This suggests that the flux on higher scarps is not proportional to gradient, probably mainly due to a stronger erosion by water on higher scarps.

Two approaches both based on diffusion were applied and evaluated by Nivière et al. (1998) to show that morphologic dating is also suitable for slowly evolving scarps with a continuous vegetation cover in temperate climate. Both methods were applied to an abandoned Würmian strath terrace riser at the SE end of the upper Rhine valley in NE France. The authors used (1) the scarp degradation model based on the development of analytical solutions to the diffusion equation, here called D method (e. g., Andrews and Hanks, 1985), and (2) the Gaussian erosion model using the slope distribution along profile, here called SD method (Avouac, 1993). The local diffusivity was determined with an abandoned railway embankment of known age. Nivière et al. (1998) plotted the scarp slope as a function of scarp height for their profiles and matched a set of theoretical curves for various values of the degradation coefficient $\tau = Dt$ on their field data. The resulting values of τ indicated that the scarp is not isochronous along its strike because other parameters controlling D are the same. Next, forward modelling for different ages was used to find the best least-square fit between the observed and synthetic profile. The SD method was applied to find the bell-shaped curve of the erosion function with its variance yielding the diffusive age of a scarp. The estimated ages were younger than those of the D method; in addition, for some profiles a two-stage erosion function was obtained implying a more complex scarp evolution including perhaps a reactivation stage. The different age estimations can be explained by an early stage of scarp evolution when the scarp wedge above the mid-offset location is degraded. During this time the variance of the corresponding Gaussian bell decreases until the maximum slope begins to decrease and the profile derivative fits well to a Gaussian curve. After that stage the maximum scarp angle steadily decreases, and hence the profile width and the variance increase. Nivière et al. (1998) calculated a time correction depending on the diffusivity and the scarp offset which must be added using the SD method. Finally, two possible explanations for the observed two-stage erosion functions are given: (1) a lower profile reactivation due to e. g., incision, and (2) an upper profile reactivation due to e. g., landsliding. The variance of the largest Gaussian bell corresponds to the age of the old scarp while the variance of the smallest curve gives the age of the reactivation. However, the location of the reactivation must be away from the mid slope to be discernible in the scarp shape.

Hanks (1999) described quantitative modelling of scarplike landforms using diffusion-equation analysis. The author pointed out that applying the diffusion equation assumes, besides the other assumptions as, e. g., conservation of mass, that "erosional diffusivity" differs only slightly from "depositional diffusivity" which allows to assume a spatially constant diffusivity. Two ways of quantitative analysis of scarps were described and applied: (1) the simplest analytical solutions of the diffusion equation which were used for direct profile modelling, and (2) the slope-offset analysis of Bucknam and Anderson (1979) which

was slightly modified. In his paper, Hanks listed the uncertainties of the geomorphological dating method and described them in detail: among those, the uncertainty of using the diffusivity from one setting in another is the most difficult one to assess. Hence, this systematic error (or epistemic uncertainty) arises simply from a lack of understanding of geological processes and precise age estimates must come from one or more of the other dating methods (compare Sect. 1.2). Different estimates of the diffusivity D were reviewed and discussed in detail; all of them are also listed in Table 5.1. Finally, the author also touched nonlinear models, all of which are described above, and pointed out that only little work has been done on formulating and justifying height-dependent transport laws.

A more detailed description of the setting of the analysed scarps, the applied methods and their calibration of Nivière et al. (1998) is given in Nivière and Marquis (2000). Hence, the calibration of the diffusivity showed that there is no strong correlation of maximum scarp angle, i. e., state of scarp degradation, with orientation. Analysing the temporal representativeness of the diffusivity, it was additionally demonstrated that colder climates imply a decrease in D, probably due to permafrost, which indicates the amount of climatic forcing on the mass flux. In general, the match between synthetic and observed profiles was good for both, the D and the SD method. But some results of the D method showed that the crestal portion of the profile is less rounded than the bottom. This indicated that diffusion might not be the main process shaping the scarp which is related to an increased material coherency near the surface due to vegetation cover, i. e., diffusivity varies in space. Compared with their study from 1998, the authors additionally presented the results of numerical modelling of the evolution of a reactivated scarp as indicated above. For this purpose, Nivière and Marquis solved the diffusion equation using a finite difference scheme. Numerical modelling of composite signals and knowing the age of the present-day and the pre-existing scarp enabled to estimate (1) the incision rate along strike, and (2) the palaeowidth of the Rhine valley. Finally, the authors showed how the timing of the abandonment of these local terrace risers yielded information about climatic and tectonic forcing.

Linear and nonlinear transport models and their incorporation into the diffusion equation were discussed by Mattson and Bruhn (2001). The nonlinear transport model is the frictional sliding model of Andrews and Bucknam (1987) assuming a sediment flux being proportional to gravity and other driving forces and resisted by the intergranular friction of the soil. The authors presented analytical (for the linear model) and numerical (for both the linear and nonlinear model) solutions to each transport model, and considered three temporal rupture pattern for scarp generation: single-event, multiple-event, or constant slip rate. The calibration of both linear and nonlinear models using scarps of known ages was described and it was shown for the latter that (1) the diffusivity D is usually about half the value of D in the linear model, and that (2) there is no correlation between D and scarp height for scarps < 25 m. Although the fit between model and field profiles for the linear and nonlinear sediment transport models did not vary significantly, the authors gave guidelines which diffusion model should be used depending on above listed rupture pattern. Finally, Mattson and Bruhn applied the nonlinear solution to undated, multiple-event fault scarps to estimate slip rates and temporal pattern of faulting.

Carretier et al. (2002b) applied morphologic dating to relate the morphology of cumulative reverse fault scarps to the average deformation rate, and to analyse the interactions be-

tween thrusting and geomorphic processes. Their model involves diffusive erosion during the interseismic period, the gravitational collapse of the coseismic fault scarp just after formation, and the variation of the surface rupture location. The gravitational collapse is also modelled using the diffusion equation by increasing the diffusivity for slopes greater then a specified angle of repose. The authors showed that, although such a collapse is not a diffusive process, this numerical approach enables to form instantaneously a gravity-controlled face being consistent with field observations. The linear diffusion equation was solved by "forward time central space" finite difference method. The modelling results suggested that the parameters controlling the amount of frontal collapse, i. e., the magnitude of coseismic offsets, the dip of the fault near the surface, and the step distance between faults, influence the morphology of a scarp and its apparent degradation stage. Folding results in an overestimate of the morphologic age Dt; together with thrusting, it creates a convexity on the upper part of a scarp and increases its height. Finally, Carretier et al. (2002b) expected that nonlinear erosion effects remain within the uncertainties relative to erosion parameters that they estimated.

Carretier et al. (2002a) evaluated the ability of analytical linear diffusion models for scarp degradation including continuous or incremental uplift to date cumulative reverse fault scarps. To do so, the authors compared degradation coefficients ($\tau = Dt$, see above) predicted by two linear diffusion models with those of a more realistic numerical model which has already been partly introduced in Carretier et al. (2002b). The numerical model behaviour was examined by carrying out a parametrical study obtaining different morphologies for different "true" values of Dt. The "estimated" values from the analytical models are the results of inversions: Synthetic profiles were computed with the numerical model, the analytical models were used to calculate the degradation coefficient, and for each value the root-mean-square of the misfit between synthetic and modelled elevation profile was determined. In their calculations, the value for the diffusivity varied between 1 and 10 m^2/ka. Additionally, the location of the fault was involved in this inversion method. By plotting the "true" degradation coefficients versus offset, Carretier et al. (2002a) analysed the conditions for which some processes involved in cumulative reverse fault scarp evolution could be neglected, with an "acceptable" error in the determination of τ. Hence, it was shown that for cumulative reverse faulting without folding, neglecting fault dip and gravitational collapse mostly lead to valid estimates of the degradation coefficient. Concerning the dating of scarps, the results suggested that for reverse faults the fault dip is important and that for a given τ the reduced scarp slope (maximum slope - regional slope) varies according to it.

5.3 Additional models and studies incorporating the diffusion equation

A theoretical model was developed by Kenyon and Turcotte (1985) to simulate the progradation of a river delta where bulk-transport processes (e. g., creep and landsliding) dominate the deposition and movement of sediment on the delta front slope. The maximum slope is controlled by the depth of the receiving basin, the sediment supply to the delta, and the rate of sediment transport on the delta front slope. Hence, the diffusion equa-

tion was applied to model the subaqueous motion of creep which is mainly induced by bioturbation but also by pressure variations caused by the passage of waves. The authors obtained much higher transport coefficients than for subaerial hillslopes (> 24 m^2/ka), probably either because of accelerated creep processes in a subaqueous environment or because landsliding was not involved in the current studies concerning subaerial hillslopes. Differences in that rate between various deltas appeared to reflect differences in sediment composition and/or rate of sediment supply between those deltas.

Transport rates for granular soils in the Pacific coastal mountains of California, Oregon, and Washington were investigated by Reneau (1988). These rates can be used to estimate values for the diffusion coefficient if it is assumed that transport is proportional to the average contributing hillslope gradient. For the examined hillslopes within their humid climate, Reneau determined a diffusivity of 4.9 ± 3.7 m^2/ka.

McKean et al. (1993) examined the dependence of the soil-creep rate on slope gradient and quantified average soil transport rates over a period of $\sim$ 3500 years on a convex soil-mantled, clay-rich hillslope. The results of the applied mass-balance model that incorporates fluxes of both cosmogenic isotope ^{10}Be and soil supported the assumption that the soil creep rate is proportional to local slope gradient as used in most geomorphic models. The authors determined a diffusivity of 36 ± 5.5 m^2/ka for the East Bay region, California, USA, with a Mediterranean climate. The data indicated that the diffusivity may increase slightly and furthermore that the steady rate of production of soil by rock weathering may decrease in downslope direction implying that the slope is not in dynamic equilibrium. A comparable study was presented by Monaghan et al. (1992).

The post-depositional transport of pelagic sediments on young abyssal hills was approximated as a nonlinear diffusive process by Webb and Jordan (1993). Fitting of theoretical models to an observed slope distribution yielded an average value for the apparent diffusivity of $\overline{D} = 130 \pm 14$ m^2/ka. Further applications of diffusion models in this research field include, e. g., Mitchell (1995) who determined a median diffusivity of 40–110 m^2/ka for the transport of pelagic sediments on the Mid-Atlantic Ridge.

Rosenbloom and Anderson (1994) analysed a set of marine terraces along the central California coastline to assess geomorphic processes. A transient, two-dimensional finite difference model of landscape evolution with both hillslope and channel components was used to calibrate long-term rates to (1) construct large-scale landscape evolution models, and to (2) develop insight into the evolution of marine terraced landscape in general. Concerning hillslope process rules and the diffusion algorithm, the authors slightly modified the local hillslope diffusivity and defined a weathering-limited diffusivity which is dependent on the estimated depth of the layer involved in transport and the local regolith depth, and which brings the transport rate to zero as the regolith thickness vanishes. Rosenbloom and Anderson (1994) worked with a diffusivity of 10.0 m^2/ka. The inclusion of bedrock weathering and diffusive transport resulted in an asymmetric slope evolution.

In recent years, also moderate- to large-scale (1–1000 km) landscape evolution models employed diffusion to simulate the long-term (1–100 Ma) erosional denudation of slopes resulting from slow and/or rapid mass movement; some a briefly described below. According to Anderson (1994), the main difference between such large-scale and small-scale models is that at small scales the diffusion model describes well the processes operating

locally on hillslopes where the diffusivity can often be determined or measured in the field. But at large scales the processes are not necessarily diffusive, and the effective diffusivities necessary to ensure that the resulting model elevations remain reasonable are commonly many times those measured in the field.

A preliminary, 2-D finite difference model of topographic evolution of an arid, internally drained landscape including a weathering and an angle of repose algorithm was presented by Anderson and Humphrey (1990). The aim was to find model components within the modelling of basin evolution that are capable of predicting the sediment flux from the mountain front to an adjacent basin. The authors modelled the mass movement of regolith using the diffusion equation with the transport rate q increasing exponentially as a critical topographic slope of 34° is approached. Including a weathering rate which depends on the thickness of the regolith additionally showed that a shallow initial bedrock interface restricts the rate of crestal rounding. Thus, the symmetry of the pure diffusion case is broken producing a consistently higher curvature of the top of the scarp. The presented model was next upscaled to the scale of a mountain front and additional scale-dependent processes such as fluvial activity were included. Finally, a couple of large-scale problems, e. g., the altitudinal dependence of the weathering rate and the scaling of the diffusivity, were discussed.

A quantitative combined surface processes model was applied by Kooi and Beaumont (1994) to investigate the factors that control the evolution and retreat of a model escarpment on rifted margins. In their model, the long-term changes in topography resulted from simultaneous short- and long-range mass transport processes. The former was represented as linear downslope diffusion of material volume. To produce a realistic-looking topography, the starting diffusivity parameter values for bedrock and sediment were set to 0.5 m^2/a and 5 m^2/a, respectively. Note that these values again differ greatly from all values listed in Table 5.1. But such high values would confirm the previously often mentioned conclusion of an increasing diffusivity with increasing height. Fluvial transport modelled by advection and reaction represented long-range mass transport processes. Kooi and Beaumont (1994) also examined the influence of lithological contrasts with a diffusivity decreasing with depth for less erodible layers. The surface process model was again applied by Kooi and Beaumont (1996) to analyse landscape response times and to investigate the response of the model to tectonic forcing. The behaviour of the model was compared with landscape evolution envisaged in conceptual models considering the micro-, meso-, and macroscale.

To examine whether the topography of a particular landscape is in balance with current processes controlled by climate, Rinaldo et al. (1995) used a mathematical model of landscape evolution incorporating two erosion processes: fluvial processes, i. e., relatively rapid erosion by running water, and diffusive sediment transport, i. e., the slow downslope movement depending on the local surface slope. The authors suggested that extreme climatic fluctuations that cause accelerated threshold-limited erosion seem likely to occur and to leave very long-lived morphological evidence where slope-dependent processes are ineffective.

At the scale of the diffusive disturbance, diffusion becomes a roughening instead of a smoothing process. This was investigated by Jyotsna and Haff (1997) who distinguished

large-scale and small-scale processes in arid, lightly vegetated terrain. The former include roughening due to disturbances such as animal burrows, hoof prints of grazing animals, and small landslides whereas the latter involve diffusive processes such as rainsplash and creep that tend to erase the roughness elements. To produce diffusional roughening, the values of the horizontal distance x and of the time t (as used in the diffusion model) must be great instead of being arbitrarily small. For instance, the actual physical size (plan-view dimension) of a disturbance associated with the macroscopic effect is then represented by x. Additionally, different values for the diffusion constant D were chosen for the large- and the small-scale processes. Both diffusive processes can be superposed to operate simultaneously. Finally, by measuring the areal density of large-scale processes, i. e., of surface disturbances, on a slope, the ratio of small- to large-scale diffusivities can be estimated. Jyotsna and Haff (1997) concluded that if a hillslope is not densely covered with large-scale disturbances, mostly small-scale diffusion controls hillslope dynamics.

Kirkby (1997) showed in his report that it is feasible to extend relatively simple geomorphological process models up to basin or continental scales. Many aspects of stream processes which seem to dominate at large scales can be approximated as flux- or transport-limited processes. Thus, adequate geomorphological models can be used to examine the strongly interactive links between geophysical and geological processes and landforms at regional to continental scales.

A numerical landscape model that bridges the gap between orogenic-scale and landform-scale simulation was developed by Densmore (1998). His model joined tectonic displacement with several geomorphic processes based on the continuity equation, including bedrock landsliding, regolith production and transport, and fluvial sediment transport. The transport of weathered material was modelled as a linear diffusive transport. In his experiments that simulated the landscape evolution of semiarid to arid regions, the author worked with a diffusivity of 10 m^2/ka. As the diffusion equation ignores any potential for advective regolith transport (e. g., by shallow landsliding), the author followed Anderson and Humphrey (1990).

Roering (1999) presented evidence for nonlinear, diffusive sediment transport on large-scale steep and soil-mantled hillslopes and examined the mechanics of diffusive processes and how they influence landscape morphology. This is based on the observation that on many soil-covered hillslopes curvature seems to vary systematically: Slopes are typically convex near their divide and become increasingly steeper and planar downslope. Such a hillslope form is inconsistent with constant-curvature (i. e., parabolic) slope profiles as predicted by the linear diffusion. The author thus presented a diffusive transport law that depends nonlinearly on slope gradient and which suggests (1) that diffusive transport varies linearly with slope at low gradients, but (2) that material flux increases rapidly nonlinearly as slope approaches a critical value (approx. 51°). Roering (1999) tested and calibrated the proposed transport law using high-resolution topography data of five small watersheds within the central Oregon Coast Range, Oregon, USA. Assuming that the rate of sediment transport is not affected by soil depth, a diffusivity of 3.6±1.6 m^2/ka was determined. Roering et al. (2001) examined how nonlinear transport influences hillslope evolution and introduced a dimensionless parameter ψ_L which is defined as the ratio of nonlinear to linear components of sediment flux at the hillslope base. Steady state hillslopes with relatively constant curvature between the crest and channel are reflected by

low values of ψ_L. An increasing ψ_L corresponds to slope angles approaching the threshold angle. Hillslopes with narrow, highly convex hilltops and relatively planar sideslopes are characterized by high values of ψ_L. On steep slopes, further steepening is limited by rapid increases in transport rate near the critical gradient, i. e., transport rates increase rapidly for small increases in slope angle. Hence, hillslope relief and slope angle are not sensitive indicators of tectonic forcing and erosion rate. But the nonlinear model indicated that hilltop curvature varies proportionally with erosion rate. With increasing importance of nonlinear transport on hillslopes the equilibrium adjustment timescale decreases rapidly, i. e., the timescale for sediment flux and erosion rate to approach an equilibrium is more rapid than predicted by the linear transport model. Consequently, the signal of tectonic forcing may be quickly assimilated by hillslopes in steep, soil-mantled landscapes.

Linear and nonlinear transport relations in large-scale hillslope evolution models to simulate the long-term evolution of hillslope profiles found in small drainage basins in coastal British Columbia, Canada, were tested and calibrated by Martin (2000). The aim was to define transport equations for slow and rapid mass movements based on large field data compilations. For linear diffusion, diffusivity values of 0.2 m^2/ka and 100 m^2/ka were yielded for slow and rapid mass movements, respectively. However, the best fit to a plot of transport rate against gradient for a data set representing rapid, episodic mass movements (e. g., shallow landsliding) was provided by a hyperbolic tangent relation in which transport increases nonlinearly with gradient above some threshold gradient. Model runs included slope evolution using the determined linear diffusivities, a range of diffusivities from former studies (1–100 m^2/a), and using the nonlinear transport function of which the model parameters were obtained for resistant and nonresistant geology after examination of the field data. Martin (2000) additionally incorporated weathering into some model runs to ensure that transport rates at high gradients obtained in the model reflect natural conditions. The rate of hillslope change decreased when theoretical sediment transport rates exceeded sediment supply. Events producing an oversteepened gradient (e. g., tectonic forcing, glaciation, fluvial undercutting) are thus followed by a rapid hillslope change that eventually eliminates steep gradients and significantly reduces hillslope transport. Hence, landsliding appears to be a dominant factor in landscape change on slopes greater than about 30°.

Further noteworthy geomorphic models that investigated how tectonic activity, climate change, land use, and partly weathering affect large-scale landscape evolution and where hillslope erosion is simulated as a linear diffusive process include, e. g., Koons (1989), Flemings and Jordan (1989), Willgoose et al. (1991a,b,c), Braun and Sambridge (1997), and Tucker and Slingerland (1994, 1997). To simulate nearly planar hillslopes, several models are also based on the assumption that, on steep slopes, sediment transport increases nonlinearly with gradient. A majority of these models claim that sediment flux combines slow and rapid processes of mass movement, the latter mostly occurring above some gradient threshold, and involve, e. g., Kirkby (1984, 1985), Anderson (1994), Howard (1994a,b, 1997), and Martin and Church (1997). Combinations of linear and nonlinear diffusion equations were applied by, e. g., Avouac and Burov (1996).

Chapter 6

Geomorphological dating model

6.1 What is new?

If a scarp separates different geological deposits, the diffusivity D might be a function of position x. Or, if a scarp spans significant climatic fluctuations in its lifetime, D might be a function of time t. Generally, combinations of both cases are conceivable too. This study introduces a spatial variation in D based on observations of present-day scarps which often show asymmetric profiles, mostly with a crestal radius of curvature being smaller than the basal one. Such asymmetry might be due to slope wash processes and concentrated water runoff in small surface rills resulting in a retained sharper curvature of the crest between rills and gullies. It is furthermore suggested that surface runoff is stronger in lower parts of a profile. Avouac (1993) described that in arid and semi-arid regions sharper crests might also evolve because of eolian action on scarps with a sparse vegetation cover: Deflation removes finer particles from the crest resulting in the formation of a stone pavement more resistant to erosion. Scarp erosion by such surface rills smoothes the basal curvature as the rills tend to deposit small fans at the base of a scarp. Basal smoothening may also result from trapped eolian sediments (loess) that have been cemented within scarp colluvium. Andrews and Bucknam (1987) also noted that in arid climates scarps with heights >10 m tend to have systematically sharper curvatures at crest than at base. Mayer (1987) proposed that the erosional and depositional parts of the scarp might degrade at different rates which in turn might partially explain why higher scarps appear to have a larger diffusivity (see Chap. 5).

The simple diffusion equation with a constant diffusivity as presented previously can only model hillslopes showing a symmetric rounding of the crestal convexity and the basal concavity with time. To simulate the evolution of asymmetric slopes, a diffusivity which increases in downslope direction is assumed by applying a linear approach. The height-dependent diffusion coefficient is given by:

$$D(H) = D_0 + D'[H_{\max} - H(x,t)] = D_0 + D'\Delta H \tag{6.1}$$

where D_0 and D' are parameters of the linear approach, $H_{\max}$ is the maximum height of the initial scarp, and H is the height of a point at a given distance x at time t. Such a linear increase is based ont the simple assumption that a regular rain distribution results in a steady, i. e., linear, increase in the water flow downhill which in turn increases the value of the diffusivity. If a particle is eroded or deposited still depends in the end on the curvature (see Sect. 4.3). Figure 6.1 illustrates the modification for crestal diffusivities being smaller than basal ones.

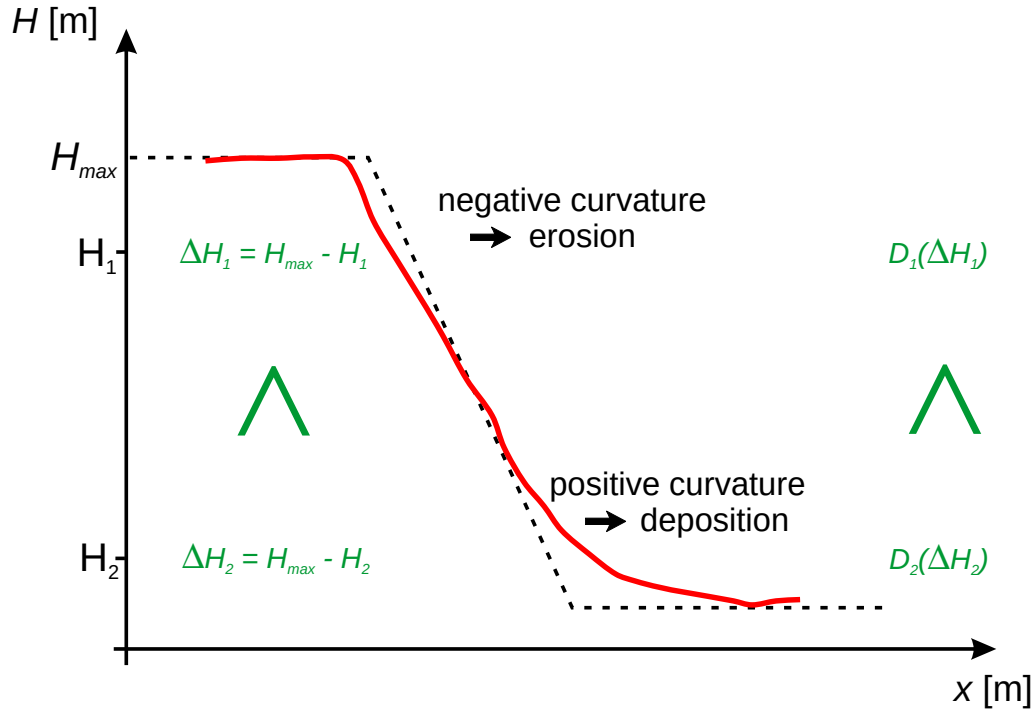

Figure 6.1. Increasing diffusivity in downslope direction. The red line and the dashed line display the observed profile and the initial profile for simulation, respectively.

Plugging equation (6.1) into the diffusion equation (4.6) and eliminating the parameter D_0 by introducing the rescaled variables

$$\tilde{t} \coloneqq tD_0, \qquad \tilde{D'} \coloneqq \frac{D'}{D_0}$$

yields the nonlinear diffusion equation

$$\frac{\partial H}{\partial \tilde{t}} = \frac{\partial}{\partial x}\left[(1 + \tilde{D'}\Delta H)\frac{\partial H}{\partial x}\right] \tag{6.2}$$

Above rescaling results in only one necessary adjustment of the rescaled parameter D' although originally two new parameters (D_0 and D') have been introduced. After each calculation run the values of $\tilde{t}$ (morphologic age) and $\tilde{D'}$ are known; $\tilde{t}$ is calculated by

multiplying the amount of iteration-steps with dt, $\tilde{D}'$ is determined directly. D should either be taken from literature or estimated individually from scarps of known age.

As

$$D = D_0 + D'\Delta H \quad \Rightarrow \quad D = D_0(1 + \frac{D'}{D_0}\Delta H) = D_0(1 + \tilde{D}'\Delta H) \quad \Rightarrow \quad D_0 = \frac{D}{1 + \tilde{D}'\Delta H}$$

and

$$\tilde{t} = tD_0 \qquad \Rightarrow \qquad t = \frac{\tilde{t}}{D_0},$$

the age in years t is hence calculated dividing the morphologic age $\tilde{t}$ by above determined value of D_0 (see also p. 79):

$$t = \tilde{t}\,\frac{1 + \tilde{D}'\Delta H}{D}. \tag{6.3}$$

Finally D' is determined with

$$\tilde{D}' = \frac{D'}{D_0} \qquad \Rightarrow \qquad D' = \tilde{D}' \cdot D_0$$

and D is again

$$D = D_0 + D'\Delta H.$$

As Chapter 8 will show, the fit between modelled and observed profile is improved by applying above modification.

6.2 Solution of the modified diffusion equation

The linear diffusion equation is a partial differential equation and has been solved for scarp boundary conditions by numerical (mainly finite-difference or finite-element) methods (e. g., Nash, 1980a, 1980b, 1981a, 1984; Carretier et al., 2002a) as well as by analytical methods (e. g., Colman and Watson, 1983; Mayer, 1984; Hanks et al., 1984; Andrews and Hanks, 1985; Pierce and Colman, 1986). Such an analytical solution is analogous to that for one-dimensional heat flow in a semi-infinite solid having a specific initial temperature distribution and a surface kept at zero temperature. If the initial configuration of the analogous scarp is specified with a fixed midpoint at the origin, the analytical solution

of the diffusion equation yields a model for scarp degradation which is for half the scarp, and where the other half behaves symmetrically. Furthermore, only changes in elevation in cross section are considered while effects of the length or curvature along the length of the scarp are assumed to be negligible. The upper and lower boundary are fixed, i. e., no overall lowering of the landscape and a constant base level are assumed. Carslaw and Jaeger (1959) presented such a general solution to equation (4.8) which has been applied by many studies. Following Hanks et al. (1984) the form of degraded scarps resembles the error function which is one fundamental analytical solution to the 1-D diffusion equation for steplike initial conditions (e. g., a newly formed fault scarp) and which is described in detail in their study. This solution is in analogy with the problem of thermal evolution within a slab with an initial step in temperature. Hence, the slope at the midpoint of the scarp, which is often the steepest slope, decays as the square root of time. The error function is closely connected with the cumulative probability function of a Gaussian distribution with the difference that the former is arranged to be antisymmetric about the origin with asymptotes of ± 1 as $\zeta \to \pm\infty$, while the latter is antisymmetric about the point (0, 0.5) with asymptotes 0 ($\zeta \to -\infty$) and 1 ($\zeta \to +\infty$). Several further approaches to the diffusion equation for various boundary and initial conditions are also presented by Crank (1979).

But in general, analytical solutions to nonlinear problems are available only for very special cases, and solutions must often be found by numerical methods. It is than frequently necessary to make assumptions, simplifications or to seek approximations in order to obtain such solutions. In the presented study, the diffusion equation is solved numerically which additionally facilitates computer calculation of it. To replace its derivation, a finite-difference approximation method was applied. The general way of proceeding is as follows and is described below in more detail (mostly following Marek and Götz, 1995, and Stüwe, 2000):

(1) Choice of lattice regarding the geometry and the boundary conditions (discretizations of the calculation area);

(2) setting up of approximation equations for each lattice point and for each time step;

(3) involving the boundary conditions, i. e., defining the starting conditions and the equations at the boundaries;

(4) repeated solution of the resulting system of equations.

Item (1): In simple words, the calculation area is covered with a lattice or grid. The exact solution is no more searched but an approximated solution at single discrete grid points. The finer the lattice is, the more exact is the numerical solution. In this study, a regular grid with N grid points and $N - 1$ gaps is used. Hence, the distance between two grid points Δx is for a grid of length L: $\Delta x = L/(N - 1)$. In the borderline case of an infinite fine lattice, the numerical solution tends towards the exact solution of the differential equation. But as with accuracy also the calculation time increases, it is necessary to reach a compromise between both quantities and to accept a finite approximations accuracy. In the presented study, with the discretization, the hillslope is represented as a large number of points separated by an equal horizontal distance.

Mathematically, the finite-difference method carries out a discretization of differentials (e. g., the spatial differential $\mathrm{d}H/\mathrm{d}x$), either by (1) forward differencing, (2) backward differencing, or (3) central differencing (Fig. 6.2). The calculation of the differential $\mathrm{d}H/\mathrm{d}x$ does not consider the limit $\Delta x \to 0$ but a Δx with finite value. In principle, the gradient of a function $f(x)$ at distance x_i is expressed mathematically by such a differential. The finite-difference method approximates this gradient by determining the height difference at two points with the finite distance Δx. Forward differencing of above differential gives

$$\frac{\mathrm{d}H}{\mathrm{d}x} \approx \frac{H_{i+1} - H_i}{x_{i+1} - x_i} = \frac{H_{i+1} - H_i}{\Delta x}. \tag{6.4}$$

The index i is the number of an discrete grid point with $i = 0, \ldots, N-1$. H_i is the height at the point with number i, H_{i+1} is the height of the next point of the grid, H_{i-1} is the height of the point before. Backward and central differencing are, respectively, of following left and right form:

$$\frac{\mathrm{d}H}{\mathrm{d}x} \approx \frac{H_i - H_{i-1}}{\Delta x} \tag{6.5}$$

and

$$\frac{\mathrm{d}H}{\mathrm{d}x} \approx \frac{H_{i+1} - H_{i-1}}{2\Delta x}. \tag{6.6}$$

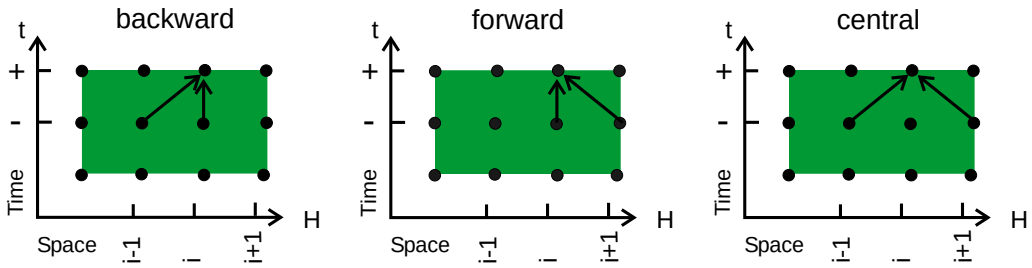

Figure 6.2. Schematic representation of different methods of discretization. The x-axis shows four points of an one-dimensional discrete spatial grid with assigned height values. The y-axis displays three time steps. The height at the third grid point i at time + is determined by either forward, backward, or central differencing from the height at time −. Modified after Stüwe (2000).

Temporal differentials are handled similar. To distinguish temporal from spatial differentials, the signs "+" and "−" (sometimes also "$j+1$" and "j") are used to denote the next and the last discrete time step, respectively:

$$\frac{\mathrm{d}H}{\mathrm{d}t} \approx \frac{H_i^+ - H_i^-}{\Delta t}. \tag{6.7}$$

Differentials of second order (e. g., $\mathrm{d}^2H/\mathrm{d}x^2$) are solved with the same proceeding as used above for the approximate solution of simple differentials by dividing the difference of the gradient at two different points with distance Δx:

$$\frac{\mathrm{d}^2H}{\mathrm{d}x^2} = \frac{\mathrm{d}\left(\frac{\mathrm{d}H}{\mathrm{d}x}\right)}{\mathrm{d}x} \approx \frac{\left(\frac{H_{i+1}-H_i}{\Delta x}\right) - \left(\frac{H_i-H_{i-1}}{\Delta x}\right)}{\Delta x} = \frac{H_{i+1} - 2H_i + H_{i-1}}{\Delta x^2}. \tag{6.8}$$

Item (2): When setting up the approximation equations, the differential quotients are replaced by difference quotients, thus the partial differential equations are transformed to algebraic equations. The diffusion equation is a differential equation with time and space differentials which requires a combination of different indices. The height at point i at the next time step can be denoted either as $H_{i,j+1}$ or as H_i^+. In this study, the latter denotation is applied. Solving differential equations with the finite-difference method distinguishes explicit, implicit and mixed methods which are illustrated in Figure 6.3 and described below.

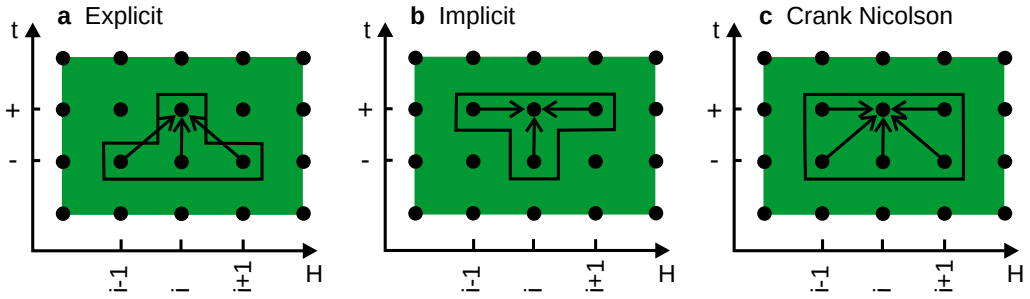

Figure 6.3. Differentiation schemata for explicit and implicit methods. The Crank-Nicolson method is a mixed method with an explicit and an implicit part. Modified after Stüwe (2000).

Explicit methods: If the initial values for a point of time (mostly $t = 0$) are known, the values for the next time step can be calculated directly without solving linear systems of equations, i. e., the new values are calculated with the values of the prior lap (Fig. 6.3a). The height at point i at the next time step H_i^+ is calculated from the three known heights at points $i-1$, i and $i+1$ of the last calculated time step. Applying this method to the linear diffusion equation with D independent of x gives:

$$\frac{\partial H}{\partial t} = D\frac{\partial^2 H}{\partial x^2} \approx \frac{H_i^+ - H_i^-}{\Delta t} = D\frac{H_{i+1}^- - 2H_i^- + H_{i-1}^-}{\Delta x^2} \tag{6.9}$$

Solving (6.9) for the height to be calculated, yields:

$$H_i^+ = H_i^- + R(H_{i+1}^- + 2H_i^- + H_{i-1}^-) \qquad \text{with} \qquad R = \frac{D\Delta t}{\Delta x^2}. \tag{6.10}$$

This method has the advantage that the simple algorithm is easy to calculate and to programme. But it is disadvantageous that the method is not stable for all possible temporal and spatial steps and that unstable numerical oscillations, i. e., physical absurd results, may occur. The value of the constant R in (6.10) is important for the stability and the accuracy of the approximation and is termed *Fourier cell number* or *mesh-ratio*; for the one-dimensional case R must be < 0.5 to apply the approximation. As the value of the diffusivity D is given, this condition restricts the choice of the spatial, Δx, or temporal, Δt, steps in the approximation. Regarding

equation (6.10) reveals that there is no solution at the points $i = 0$ and $i = N-1$ because there are no grid points "-1" and "N" with heights H_{-1} and H_N, respectively. Equation (6.10) is thus only solvable for grid points between $i = 1$ and $i = N-2$. To calculate the heights at the points $i = 0$ and $i = N-1$, the boundary conditions have to be known (see item (3)). Stability conditions and methods to estimate the accuracy are discussed in detail by, e. g., Anderson et al. (1984), Smith (1985), and Fletcher (1991).

Implicit methods: The discretization does not occur at time step t but at $t + \Delta t$, i. e., the new values are calculated with the forward calculated results of one time step in advance (Fig. 6.3b). The height H_i^+ at time step $t + \Delta t$ is not calculated using the known heights at time t. Instead, for each time step Δt a linear system of equations for the heights at time $t + \Delta t$ has to be solved. From these values H_i^- is calculated. Precondition is thus that all heights of the grid at a new time are calculated simultaneously. This is possible because of the known boundary conditions. Consequently, at the new time step only the heights at $N-2$ grid points must be calculated: A system of equations with $N-1$ equations can be set up with those $N-2$ unknowns. The implicit approximation of the diffusion equation (4.8) is then:

$$\frac{\partial H}{\partial t} = D\frac{\partial^2 H}{\partial x^2} \approx \frac{H_i^+ - H_i^-}{\Delta t} = D\frac{H_{i+1}^+ - 2H_i^+ + H_{i-1}^+}{\Delta x^2}. \tag{6.11}$$

Solving (6.11) with respect to the height to be calculated, results in:

$$H_i^- = H_i^+ - R(H_{i+1}^+ - 2H_i^+ + H_{i-1}^+) \qquad \text{with} \qquad R = \frac{D\Delta t}{\Delta x^2}. \tag{6.12}$$

The advantage of this scheme is that it is always stable and no oscillations occur independent of the chosen step size. The disadvantage is the necessity of solving a linear system of equations (see below).

Mixed methods: Such methods use explicit and implicit information and are just briefly mentioned for the sake of completeness. Mixed methods yield a high stability and accuracy. For instance, the Crank-Nicolson method is often used to solve differentials of second order as the diffusion equation (Fig. 6.3c):

$$\frac{H_i^+ - H_i^+}{\Delta t} = \frac{D}{2}\left(\frac{H_{i+1}^+ - 2H_i^+ + H_{i-1}^+}{\Delta x^2} + \frac{H_{i+1}^- - 2H_i^- + H_{i-1}^-}{\Delta x^2}\right). \tag{6.13}$$

Methods to implement equation (6.13), e. g., the Thomas algorithm, are described in most numeric books.

In this study an implicit method was used. But above solution (6.12) is only valid for a constant diffusivity D which is not the case in this study. Hence, the solution has to be

adapted to a variable D. For a diffusivity dependent on x, the diffusion equation has the form of equation (4.6)

$$\left.\frac{\partial H}{\partial t}\right|_i = \left.\frac{\partial}{\partial x}\left(D\frac{\partial H}{\partial x}\right)\right|_i .$$

In the presented case, instead of $(D_i - D_{i-1})$ and $(D_{i+1} - D_i)$, a mean of the diffusivity at $i + \frac{1}{2}$ and $i - \frac{1}{2}$ is taken. The fully implicit approximation for the diffusion equation with a variable diffusivity D dependent on x thus results in:

$$\frac{H_i^+ - H_i^-}{\Delta t} = \frac{D_{i+\frac{1}{2}}(H_{i+1}^+ - H_i^+) - D_{i-\frac{1}{2}}(H_i^+ - H_{i-1}^+)}{\Delta x^2} \tag{6.14}$$

which is finally solved with respect to the height to be calculated:

$$H_i^- = H_i^+ - \frac{\Delta t}{\Delta x^2}[D_{i+\frac{1}{2}}(H_{i+1}^+ - H_i^+) - D_{i-\frac{1}{2}}(H_i^+ - H_{i-1}^+)]. \tag{6.15}$$

Fully substituting above equation with

$$D_{i+\frac{1}{2}} = \frac{1}{2}(D_i + D_{i+1}) \tag{6.16}$$

and

$$D_{i-\frac{1}{2}} = \frac{1}{2}(D_i + D_{i-1}) \tag{6.17}$$

yields:

$$-R(D_i + D_{i-1})H_{i-1}^+ + (1 + R(D_{i+1} + 2D_i + D_{i-1}))H_i^+ - R(D_{i+1} + D_i)H_{i+1}^+ = H_i^- \tag{6.18}$$

with $R = \frac{\Delta t}{2\Delta x^2}$.

Item (3): Following boundary conditions can be distinguished:

(1) Dirichlet's boundary conditions: fixed preset values at the boundary (here fixed height values) which can be either temporally constant or variable;

(2) Neumann's boundary conditions: preset flux at the boundary (here preset material flux) which can be either temporally constant or variable;

(3) Newton's boundary conditions: preset coefficient of heat transmission and temperature of a surrounding fluid in the case of conductive heat flow; is a special case of (1) and is not relevant in the context of this work.

In the presented study, Dirichlet's boundary conditions with temporally constant height values were chosen (see also Section 4.3 and Section 8.3).

Item (4): If the implicit finite-difference approximation is applied, linear systems of equations for the individual lattice points have to be solved either by

direct methods with a fixed number of arithmetical operations; the solution generally includes rounding errors; in the ideal case of a solution without rounding error, the direct methods yield the exact solution; e. g., Gaussian algorithm, Gauss-Jordan method, or by

iterative methods with an initial approximation of the solution which is improved stepwise; the solution is never the exact solution, but always an approximation; e. g., Jacobi iteration, Gauss-Seidel iteration.

In this study, the Gaussian algorithm (or elimination) as a direct method was used to solve the system of equations. First, a system matrix $\hat{A}$ must be set up corresponding to:

$$a_i H_{i-1}^{+} + b_i H_i^{+} + c_i H_{i+1}^{+} = H_i^{-} \tag{6.19}$$

to yield

$$\hat{A} \cdot \vec{x} = \vec{d} \tag{6.20}$$

where the values of the tridiagonal matrix $\hat{A}$ and of the vector $\vec{d}$ are known and those of the vector $\vec{x}$ are unknown. To get these unknown values of $\vec{x}$, $\hat{A}$ must be inverted:

$$\vec{x} = \hat{A}^{-1} \cdot \vec{d}. \tag{6.21}$$

The solution of a system of equations does not depend on the arrangement of the equations; thus, any equivalent operations in a row are allowed when converting $\hat{A}$ (exchange of rows, multiplying a row by a constant, addition or substraction of multiples of rows to or from other rows, etc.). The aim is a stepwise elimination of all x_i from the equations $i+1$ up to N until there is only left a x_N in the N^{th} equation. This is achieved by determining the suitable multiplier and adding up the resulting and existing equations. Following (6.19), the general form of the given system of equations is:

$$b_0 x_0 + c_0 x_1 = d_0 \tag{6.22}$$

$$a_i x_{i-1} + b_i x_i + c_i x_{i+1} = d_i \tag{6.23}$$

$$a_{N-1} x_{N-2} + b_{N-1} x_{N-1} = d_{N-1} \tag{6.24}$$

with $i = 1, \ldots, N-2$ and d_i = starting values of x_i. Hence, in the presented case d_i corresponds to H_i^- and x_i to H_i^+. (6.22) and (6.24) express the boundary conditions.

The matrix $\hat{A}$ is transformed to an upper triangular matrix with zeros below the diagonal by forward elimination. This is followed by backward elimination calculating recursively x_i for $i = 1, \ldots, N-2$. The matrix is converted to a diagonal one and the solution can be read of. One finally find that:

$$c'_0 = \frac{c_0}{b_0}, \quad (6.25) \qquad c'_{i+1} = \frac{c_{i+1}}{b_{i+1} - a_{i+1}c'_i}, \quad (6.26)$$

$$d'_0 = \frac{d_0}{b_0} \quad (6.27) \qquad \text{and} \qquad d'_{i+1} = \frac{d_{i+1} - a_{i+1}d'_i}{b_{i+1} - a_{i+1}c'_i}, \quad (6.28)$$

and hence,

$$x_{N-1} = d'_{N-1} \quad (6.29)$$
$$x_i = d'_i - c'_i x_{i+1}. \quad (6.30)$$

Further details of the Gaussian algorithm can be looked up in several mathematics books.

If now $D = D(H)$ with $H = H(x,t)$, the diffusivity is actually dependent on x and t. Hence, a_i, b_i, and c_i in equation (6.19) must be newly determined with following valid diffusivities:

$$D_{i-1} = D_0 + D'[H_{\max} - H_{i-1}], \quad (6.31)$$
$$D_i = D_0 + D'[H_{\max} - H_i], \quad \text{and} \quad (6.32)$$
$$D_{i+1} = D_0 + D'[H_{\max} - H_{i+1}]. \quad (6.33)$$

Equation (6.18) is rewritten as:

$$\begin{aligned} &- R[2D_0 + D'(2H_{\max} - H_i - H_{i-1})]H_{i-1} \\ &\quad + [1 + R(4D_0 + D'(4H_{\max} - H_{i+1} - 2H_i - H_{i-1}))]H_i \\ &\quad - R[2D_0 + D'(2H_{\max} - H_{i+1} - H_i)]H_{i+1} = H_i, \end{aligned} \quad (6.34)$$

which results in:

$$a_i = -R[2D_0 + D'(2H_{\max} - H_i - H_{i-1})], \quad (6.35)$$
$$b_i = 1 + R[4D_0 + D'(4H_{\max} - H_{i+1} - 2H_i - H_{i-1})], \quad \text{and} \quad (6.36)$$
$$c_i = -R[2D_0 + D'(2H_{\max} - H_{i+1} - H_i)] \quad (6.37)$$

with $R = \frac{\Delta t}{2\Delta x^2}$. Implementing the previously described rescaling leads to:

$$a_i = -R[2 + \tilde{D}'(2H_{\max} - H_i - H_{i-1})], \tag{6.38}$$

$$b_i = 1 + R[4 + \tilde{D}'(4H_{\max} - H_{i+1} - 2H_i - H_{i-1})], \quad \text{and} \tag{6.39}$$

$$c_i = -R[2 + \tilde{D}'(2H_{\max} - H_{i+1} - H_i)] \tag{6.40}$$

From above defined abbreviations one can easily calculate the wanted heights H_i^+.

6.3 Calibration of the model (choice of D)

To estimate the true age of a scarp, the diffusion coefficient D must be known. Generally, the diffusivity D is given in units of [length^2/time] and expresses the volume of material that can move per unit time. D reflects the long-term transport efficiency as being a time-independent function of climate (and with that of vegetation cover) and microclimate (hillslope aspect), and of underlying slope material (Tucker and Bras, 1998). Furthermore, the diffusivity depends on the underlying slope material and reflects the effects of soil erosion, surface runoff and detachability of particles. Additionally, the effect of scarp height on the variability of the diffusion constant may be included. These factors make the diffusivity D thus highly site specific.

Climate and microclimate: The yearly number of hydration shrink-swell cycles and frost heave episodes is determined by climate. Additionally, the drainage density tends to decrease with a higher diffusivity under a humid climate and vice versa for an arid climate. Nivière and Marquis (2000) stated that D decreases in colder climates and that actually there are no published values of D for such environments. This decrease also implies a reduced D during glacial periods, probably on account of permafrost. Type and density of vegetation, which is again controlled by climate, hinder erosion and additionally determine the efficacy of wind toppling of trees as a downslope transfer mechanism. The effect of hillslope aspect is discussed, e. g., by Nash (1984) and Pierce and Colman (1986) who state that especially in semi-arid areas the diffusivity is smaller on north-facing scarps (compare p. 47 and p. 49).

Slope material: The susceptibility of the material to frost heaving is influenced by the size sorting and clay mineralogy of the underlying material. According to Nash (1984), the diffusivity increases with finer material comprising a scarp.

Effect of scarp height: Especially Colman and Watson (1983), Hanks et al. (1984) and Pierce and Colman (1986) studied this effect and explored the correlation between scarp height and different values of D. Pierce and Colman (1986) suggested that the assumption of linearity between scarp slope and sediment discharge is not valid on higher scarps where different processes occur (compare again p. 49). Hence, in nature the combined effect of the various hillslope processes is not linearly diffusive with a constant diffusivity and the effective diffusivity depends on the scale at which it is measured. In the case of such a dependence of D, the diffusion model does not strictly apply.

It is supposed that for scarps composed of the same material and degraded under approximately the same climatic conditions the value of D will be approximately equal. In the

model, it is additionally assumed that D does not directly change with time. But the previously described effects of climate on D actually indicate changes of D over time. The temporal independence is especially questionable for the dating of pre-Holocene scarps given the extent to which Holocene climate differed from that of the Pleistocene (compare Sect. 7.4) (Nash, 1986). But it is difficult to determine how significantly the diffusivity is affected by such climatic changes, although a strong effect may be inferred from the great variability of derived values of D from different climates listed in Table 5.1 on page 44. The crux is that over a period of time one actually measures or estimates an average value of D which should reflect the climatic history. Additionally, time affects the process of scarp degradation because the materials exposed to erosion may change (1) due to the possible exposure of lower layers with different D, and (2) due to sorting possibly changing the characteristics of the scarp sediments (Mayer, 1984).

The diffusion constant can also be regarded as the product of horizontal transport speed v and the thickness h_s of an erodible surface boundary layer:

$$D = vh_s. \tag{6.41}$$

h_s depends on the lithology (= type of soil), and so does the variability of the diffusion coefficient D (Beaumont et al., 1992; Stüwe, 2000). According to Kooi and Beaumont (1994), (6.41) also contains a climatic component: Regolith in which cohesion has been destroyed is produced by weathering being influenced by climate, and the thickness h_s of this regolith is involved in hillslope diffusive processes. Similarly, the velocity v is influenced by soil saturation and groundwater, both variables which again depend on climate. Following Burbank and Anderson (2001), D also reflects both the bulk density of the transported material ρ_b, and the efficiency of the transport process which in turn is reflected by the proportionality constant k: $D = k/\rho_b$. The density of material along the profile is assumed to be constant which is reasonable except for calcareous rock and tropical conditions (Carson and Kirkby, 1972). All such variations and complications, i. e., all effects of any specific erosional processes, materialize in the diffusivity constant D and the multitude of factors that contribute to the variability of scarp morphology thus affect its value.

However, D must in some way be estimated or determined, either empirically or analytically, from field data in order to solve for time, and this is the most serious limitation of the diffusion equation model. In the best case, the value of D for a particular material type in a particular climate should be derived from nearby scarps of various known ages which should be underlain by the same material, and which should have the same aspect as the scarp to be dated. To determine D analytically, two methods often applied in previous studies exist which both yield the value of the morphologic age Dt (compare also p. 40).

(1) For various values for the product Dt, a family of curves of maximum slope angle versus initial scarp height for a given initial scarp angle can be generated. By trial and error the curve representing the best fit to observed data points and the corresponding value of Dt is found (e. g., Nash, 1980b; Mayer, 1982; Hanks et al., 1984; Hanks and Andrews, 1989). This method results in a sample of D values for the dated scarp which can then be averaged to yield a mean diffusivity. But also a single D value can be used

to generate a series of synthetic maximum scarp angles for varying scarp heights and to find out the best fit between synthetic and observed profile (e. g., Nash, 1980b).

(2) Similar, for a given initial scarp angle, a single-parameter search can be performed by forward numerical modelling in which Dt is incremented to generate a series of synthetic profiles to find the best match to an observed profile of known age (e. g., Hanks et al., 1984; Andrews and Bucknam, 1987; Tapponnier et al., 1990; Avouac, 1993; Avouac and Peltzer, 1993; Arrowsmith et al., 1998; Nivière et al., 1998; Nivière and Marquis (2000); Carretier et al., 2002b). The best match is thus determined by calculating the root mean squared error (RMS) or as termed by Avouac (1993) the standard deviation (SD) of the misfit between observed and modelled profiles:

$$\mathrm{RMS} = \sqrt{\frac{1}{N_{\mathrm{obs}}} \sum_{i=1}^{N_{\mathrm{obs}}} \left[H_{\mathrm{modelled}}(x_i) - H_{\mathrm{observed}}(x_i)\right]^2} \tag{6.42}$$

where N_{obs} is the number of observations defining the profile, $H_{\mathrm{modelled}}(x_i)$ is the model elevation at distance x_i, and $H_{\mathrm{observed}}(x_i)$ is the observed elevation at x_i. The best fitting synthetic profile is defined by the distribution of RMS versus Dt which usually passes through a well defined minimum ($\mathrm{RMS}_{\mathrm{min}}$). For further explanations see Bevington and Robinson (1992) or Kirkby et al. (1993). Hanks and Andrews (1987) and Mattson and Bruhn (2001) only determined the fit between the upper half of an observed and of a synthetic profile and rejected the lower half as it may be modified by lateral sediment transport, sediment ponding in a graben, or, in the case of a fault scarp, by back rotation of the hanging wall into the fault.

Another method to determine D is to plot the relationship among initial and degraded slope angle, scarp offset, diffusivity and age of a scarp (e. g., Nash, 1981b, 1984, 1986). In rare cases of independently dated scarps, the rate coefficient can also be calculated directly. For a horizontal far-field slope, Colman and Watson (1983, note 11) inverted a derivation of a generalized analytical solution to the diffusion equation to estimate the diffusivity D using the present-day shape of a scarp of known age which was rearranged by Pierce and Colman (1986):

$$D = \left(\frac{h}{4\sqrt{t}\, \tan\alpha\, \mathrm{erf}^{-1}(\tan\theta / \tan\alpha)} \right)^2 \tag{6.43}$$

where h is the scarp height, t is the age of the scarp, α is the angle of repose (i. e., the initial angle), θ is the maximum slope angle, and erf^{-1} is the inverse error function. The error function is tabulated in the appendix of many textbooks on mathematics and engineering, and is of the form:

$$\mathrm{erf}[X] = \frac{2}{\sqrt{\pi}} \int_0^X e^{\eta^2} d\eta. \tag{6.44}$$

But often a scarp of known age is not available. Additionally, D must possibly be corrected for scarp height and exposure direction. As the diffusion constant D has already been found for slopes in a great variety of different areas (see Table 5.1, p. 44), the relationship between D and climate, aspect, and material might become so well established that D can be estimated directly from these parameters and previously published data (e. g., Hanks and Schwartz, 1987; Hanks and Andrews, 1989; Begin, 1993; Enzel et al.; Enzel et al., 1994; 1996). This was done in the presented study with an emphasize lying on the studies carried out by Nivière et al. (1998) and Nivière and Marquis (2000). The authors applied above equation (6.43) to determine D and additionally evaluated D from the amount of eroded material of a scarp of known age which is analogous to Dt. Nevertheless, it has always to be taken into account that different diffusion constants are associated with different models. But diffusivities were also estimated by fitting modelled profiles to observed ones of roughly known age.

Above statements and comparing the diffusion constants in Table 5.1 allow to draw some conclusions: High diffusivity values might either represent lithologies that intrinsically diffuse easily due to low or no cohesion, or that a cohesionless regolith is produced sufficiently rapidly by weathering to satisfy the continuous degradation with a high effective D (Kooi and Beaumont, 1994). A high diffusion constant might also be produced by a thick and moist soil cover but vegetation and other factors can in turn limit diffusion; low diffusivities represent poorly developed dry regolith. Concerning climate, areas in humid temperate climate with high precipitation rates have higher values of D and evolve faster than landscapes in arid regions.

6.4 Variation of initial slope angle α

As described above the diffusion equation model applies only after the scarp has reached its angle of repose which is in fact analogous to the initial geometry of a scarp at the starting point of a simulation run. The exact value of the angle of repose is unknown for the materials in most scarps but its range in nature is known (see Sect. 2.3, page 12). Hence, various angles can be used in the model to determine the influence of the initial geometry of a scarp on the resulting morphology. The most accurate way to determine the initial slope angle would be by assuming that the slope angles of subrecent scarps are equivalent to the angles of recent scarps formed in the same material and in the same area (Nash, 1984). But this is seldom practicable. The angle of repose, thus the initial morphology of a scarp, can also be estimated by trial-and-error calculations to determine the smallest deviation between the observed profile and the starting profile for simulation. But in this case again the age of the observed scarp must be known because the minimum standard deviation alone does not put any constraint on the initial scarp slope angle which should be determined independently (Avouac, 1993; Nivière and Marquis, 2000). This is also shown in Section 8.2.

The presented model and analysis is valid only for simple scarps with a simple initial geometry, i. e., scarps with horizontal crests and bases separated by a straight midslope at the angle of repose. Such scarps include fluvial cut-banks, marine and lacustrine wave-cut bluffs, but also some scarps produced by normal faulting. Undercutting of a terrace scarp

during its formation may not completely remove the older terrace level which results in an initial profile that consists of two or more subsidiary terrace scarps. Such scarps formed by the intersection of two or more terrace scarps may therefore show a more complex initial morphology. Fault scarps generally show an initial morphology which is more complex than that of simply formed fluvial cut-banks. The reason might, for instance, be either a splaying of the fault surface near the ground surface or a present fault scarp being the result of at least two separate faulting events. Both such more complex scarps should be rejected for morphologic dating using the presented model.

Colman and Watson (1983) also estimated repose angles for fault scarps in the western United States. These estimates were a few degrees lower than what one might expect for these materials. Therefore, Colman and Watson (1983) described the angle of repose more accurately as the angle at which the diffusion equation begins to apply to the degradation of the scarp and suggest to select an initial angle that minimizes the dependence of the diffusivity on the height which is achieved for initial angles $<30°$. This was also suggested by Hanks et al. (1984). Nash (1984) remarked that the midsection slope alone should not be used unquestioned to determine the relative ages of hillslopes as he observed that in the same study site younger and older terrace scarps may differ in their slope angle and that even scarps of the same age in the same area might have different midsection gradients. But nevertheless, the starting angle is thought to be related to the angle of repose and is thus best estimated studying underlying materials and field measurements of vegetated scarps at or near the repose angle.

According to Pierce and Colman (1986) who followed Rahn (1969), the initial angle is considered to be independent of orientation or height of a scarp. Vegetative cover might stabilize a scarp which results in a larger angle of repose, and thus a larger initial angle (Pierce and Colman, 1986). This fact was integrated by Nivière et al. (1998) and Nivière and Marquis (2000) who worked with an initial angle of 41°. The authors stated that additionally a heterogeneous granulometry of the scarp deposits contributes to maintain a steeper initial scarp. Begin (1993) stated that for scarps which degrade to much lower angles than the angle of repose, the calculated morphologic age is at any rate not very sensitive to the choice of the initial angle. Initial scarp angles ranging from 29° to 32° were used by Enzel et al. (1996) also to detect the sensitivity of the age estimation to that starting angle. Hence, the variability of Dt is only very small and the authors worked with an average initial angle of 30°.

Nevertheless, it was evaluated how variations in the initial scarp slope angle α influence the analysis by testing different values of α on profiles 6 (Turtmann valley, CH), 9 (Schwerfen), 20 (Blens) and 22 (digitized profile). The results are presented in Section 8.2.

6.5 Software

Initially the "GeomorphDating-Model" was written in the programming language C which served its purpose. To appeal to a broader spectrum of possible users, the model was rewritten in the programming language Java. On the one hand this made it more comfortable to create a graphical user interface (GUI) which is essential to reach more users. On the other hand this served the adaption of the program with regard to object-oriented

programming. Java is a programming language which is mostly independent of the platform and which is used more and more often to program different tools, web sites and applications. The development environment is available for free in the World Wide Web[1] and can be downloaded, e. g., for Unix, Linux and Windows. Below described software was developed with following versions: Java(TM) 2 Runtime Environment, Standard Edition (build 1.4.2-b28), and Java HotSpot(TM) Client VM (build 1.4.2-b28, mixed mode). The source code as well as a compiled version of the "GeomorphDating-Model" can be downloaded for non-commercial use from **ftp://ftp.geo.uni-bonn.de/pub/GD-Model**.

If a Java development environment is installed, the source code is compiled with

`javac MainGD.java`.

The compilation produces several classes saved in the same folder which contains the source code. To run the software, type

`java MainGD`.

6.5.1 Numerical dating model

The purpose of modelling is to gain an insight into the complexity of the various processes interacting to degrade a slope. Simplifications have been made when deciding which details must be preserved in the model in order to remain faithful enough to the real world to answer the specific questions being asked of it. This model does not treat every sand grain in the scarp.

The initial scarp profile is assumed to consist of a straight, inclined scarp face separated from a horizontal crest by a crestal convexity, and from a horizontal base by a basal concavity. The presented model is a digital approximation of an analog system where the initial profile shape is not a continuous line but discretized into equally spaced nodes with distance Δx; N is the total number of nodes. The nodes must be regularly spaced for stability of the numerical method. The model times do not elapse continuously, and based on the temporal duration and the density of spatial steps, a stable discrete time step width Δt is chosen. An increase in the number of data points comprising the scarp profile as well as a reduction of the time increment will both increase the time necessary for one simulation run.

In the case of a variable diffusivity, the previously explained modification of the diffusion equation is applied. The value of the parameter D_0 is fixed to 1.0 as described in Section 6.1. D' must be specified but is initially set to 0.0; the stepwise change of D' is defined by the initial choice of D_{alt}. By forward numerical modelling, a parameter search for the incremented D' is performed. After each step, the observed and the modelled profile are compared and the root mean square (RMS) of the misfit is determined using equation (6.42). D_{alt} is added to D' if the fit between both profiles increases, otherwise D_{alt} is subtracted. If 3 or more deviations are calculated, the RMS versus D' passes through a well defined minimum ($\mathrm{RMS}_{\min}$). A parabola fitting is carried out to find the absolut minimum value of RMS, and hence the best fit between the modelled and the observed profile. The corresponding values are used to simulate the best fitting synthetic profile

[1] http://java.sun.com

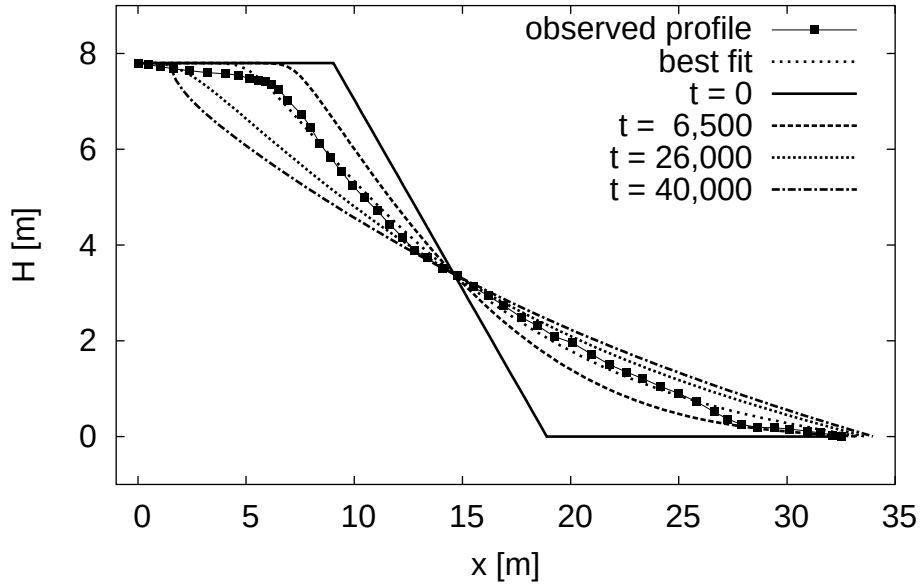

Figure 6.4. Different degradation stages of an exemplary profile including the best fit between observed and modelled profile as well as younger and older degradation stages.

reflecting the scarp age. Figure 6.4 illustrates the simulated evolution of an exemplary scarp beginning with the initial profile at $t = 0$, followed by an additional snapshot at $t = 6,500$ and the best fit which represents the present-day shape. Two further profiles ($t = 26,000$ and $t = 40,000$) allow to look into the future evolution of the scarp.

The absolute age t of a scarp in years results from the obtained value of the morphologic age $\tilde{t}$ and the variable diffusivity D. For this, the given value of D can be either specified before or after a completed simulation run and is assumed to be the value (1) at the top, (2) in the midpoint, or (3) at the base of the scarp yielding corresponding values for D_0, D' and t. The age is, for instance, calculated as follows:

$$t_{\text{top}} = \tilde{t}\,\frac{1+\tilde{D}'(H_{\max}-H_{\max})}{D}, \tag{6.45}$$

$$t_{\text{mid}} = \tilde{t}\,\frac{1+\tilde{D}'((H_{\max}-H_{\min})/2)}{D}, \qquad \text{and} \tag{6.46}$$

$$t_{\text{base}} = \tilde{t}\,\frac{1+\tilde{D}'(H_{\max}-H_{\min})}{D}, \tag{6.47}$$

with $H_{\max}$ as the maximum and $H_{\min}$ as the minimum height of the initial scarp.

The so-called midpoint which is displayed on the graphical output after an observed profile has been loaded is determined over the approximate total area beneath this observed profile. For that, the areas of single columns are added up. Each column has a width equal to the distance between two neighboring measurement points and a height equal to the median height between them. The resulting total area approximates that of a rectangle of which the height is the same as the maximum height of the observed profile. Dividing

the rectangle by its height yields the distance x which is analogous to the X-value of the midpoint. The H-value is calculated with

$$H = \frac{(X - x_1)h_2 + (x_2 - X)h_1}{x_2 - x_1} \tag{6.48}$$

where x_1 and h_1, and x_2 and h_2 are distance and height of the surveyed data point left and right of the midpoint, respectively.

The upper far-field slope is determined between the first (upper, left) observed x-/h-pair and the point where the slope seems to start which is set by the user. The user can also set the point where the slope seems to end which, together with the last (lower, right) observed x-/h-pair defines the lower far-field slope.

If an initial profile is generated by the software, the maximum and minimum height, i. e., the crestal and basal heights, are equal to the first and last observed height measurement, respectively. This should be taken into account if the crest is not even or if a bulge appears at the base. The program starts with a vertical profile of which the angle is decreased stepwise until the smallest starting deviation between both the initial and the observed profile is determined.

If the initial angle is changed, the best approximation to the entered angle according to the number of data points is determined. For a total number of nodes of, e. g., $N = 100$ (the recommended default), it is nearly never the exact angle which can be displayed. The degree of approximation is also dependent on the shape of the observed profile, for instance, on the maximum and minimum height. If the inaccuracy of the initial angle is too large, an increase in the number of data points mostly improves the approximation. In most cases, the approximation is sufficient for $N = 100$.

6.5.2 Usage

After initiating the program a screen as shown in Figure 6.5 appears. In the upper part of the GUI a drawing area appears on the left and a text area on the right side where the graphical simulation and hints to handle the program as well as numerical information during a simulation run are displayed, respectively. In the lower part are several buttons and checkboxes as well as two sliders to control the behaviour of the program. Input and result information appear in text fields with grey (not editable) or white (editable) background. If the program is initiated for the first time, two subfolders of the program folder called "./input" and "./result" are created to save input and result files, respectively. In addition, a folder "./result/output_files" is created for the files containing only the initial and resulting length- (x-) and height- (h-) values.

The most comfortable way for newbies of this program to watch a simulation run is to press DEFAULT. An observed (P16) and a corresponding initial profile for simulation are loaded and the parameters set. Furthermore a default name is given to save the result. But beforehand both default profiles must be downloaded[2] and it has to be considered

[2] ftp://ftp.geo.uni-bonn.de/pub/GD-Model

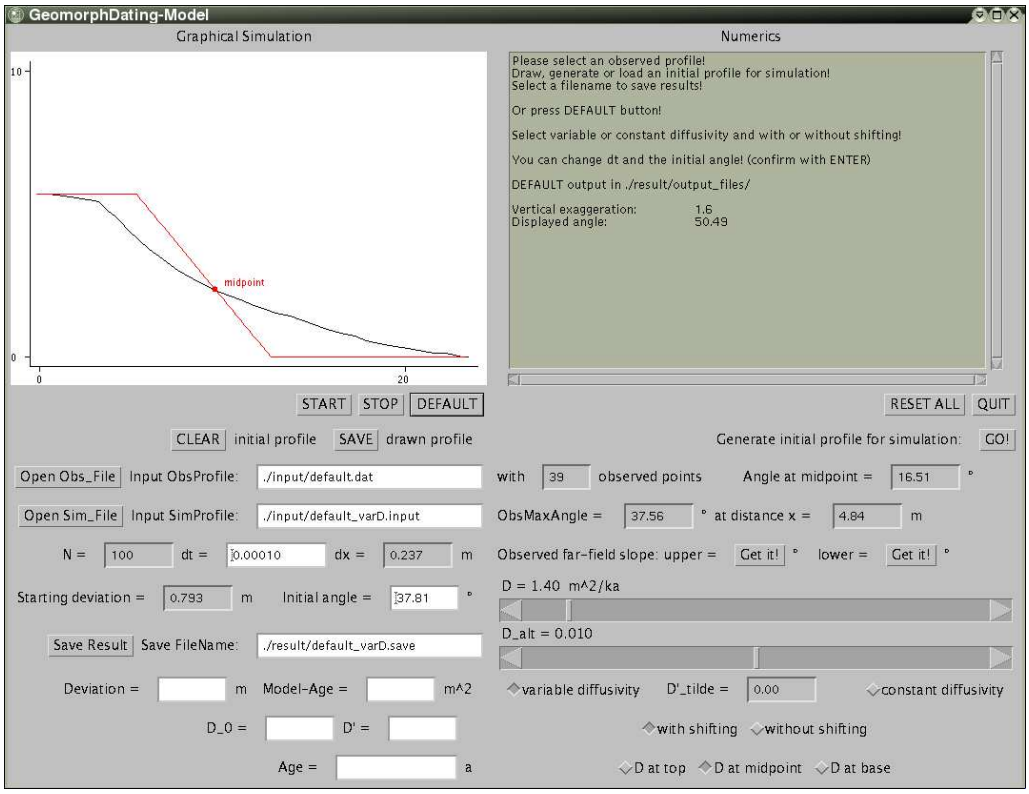

Figure 6.5. Screenshot of the dating software at the start of a simulation run with DEFAULT profiles loaded as input.

that the complete simulation run of this clear asymmetric profile takes some time! The general way of proceeding is described as follows.

At first, an observed profile has to be loaded by pressing Open Obs_File. The input files containing the observed data need the extension ".dat" and should be saved in the subfolder "./input". The data must consist of x- and h-values listed in two columns separated by tabstops and where the last line must not be empty. The values must not be available as absolute length- and height-measurements but with the smallest x-value and the lowest height value equal to zero and the profile running from the upper left to the lower right. The displayed midpoint is described in above Section 6.5.1. The number of surveyed data points as well as the value of the angle at the midpoint are shown in the grey fields on the right. The maximum observed slope angle and the distance x where it was determined are displayed in the fields beneath. The upper and lower far-field slope, i. e., the slope above and below the scarp, can be determined pressing the buttons Get it! right of the appropriate labels. The user is then required to click the point where the slope seems to start or to end for the upper and lower far-field slope, respectively.

Next an initial profile for the simulation must be added. There are three possibilities: the user can load an input file, generate an initial profile or construct one in the drawing area.

Load an input file

Initial input files can be loaded by pressing Open Sim_File. The input files containing the data need the extension ".input" and should be saved in the subfolder "./input". The data must consist of a list of parameters (N, dt, dx, angle, D_0, D', D_{alt}, D) labelled with the numerical mark followed by two columns with x- and h-values of the initial input profile separated by tabstops and where the last line must not be empty. The x- and h-values must be scaled to the corresponding observed profile. Loading initial profiles always shifts them on top of the observed profile intersecting its midpoint. After shifting, a question dialog pops up asking to adjust the data points and to elongate the profile if it is shorter in length than the observed one. After choosing YES, the user is informed about possible changes of N.

Generate an initial profile

After pressing GO!, a parameter panel pops up to define a couple of values needed for the simulation. Next, a filename must be chosen to save all values in an input file; the extension ".input" is attached automatically. This file contains the parameters (N, dt, dx, angle, D_0, D', D_{alt}, D) labelled with the numerical mark followed by two columns with x- and h-values of the generated profile separated by tabstops. A generated profile is always shifted on top of the observed profile intersecting its midpoint and matches the length according to the observed one. As such an initial profile has always the smallest starting deviation it is mostly necessary and also recommended to change the angle to a higher one which is in the order of magnitude of the angle of repose according to the underlying material (see p. 12).

Draw an initial profile

By clicking in the drawing area, the starting point, the upper and lower edge and the ending point of an initial profile can be set. Using more than these four points or drawing from right to left leads to error messages. The line between starting point and upper edge as well as the line between lower edge and ending point must be straight. To adjust the set points, the ovals can be dragged and dropped. After pressing SAVE, a parameter panel pops up to set a couple of parameters. The originally drawn profile and a shifted copy intersecting the midpoint are displayed. Both deviations between observed and drawn profile and between observed and shifted drawn profile are calculated and shown in a question dialog. If the user decides to shift the profile, another question dialog pops up asking to adjust the data points and to elongate the drawn profile if it is shorter in length than the observed one. Again both deviations (without and with adjustment and elongation) are calculated and displayed in this question panel. After choosing YES, the user is informed about possible changes of N. Finally, a file dialog opens to save the drawn profile. As described above all values are saved in a file given the extension

".input". It contains the parameters (N, dt, dx, angle, D_0, D', D_{alt}, D) labelled with the numerical mark followed by two columns with x- and h-values of the generated profile separated by tabstops.

Shifting profiles and their adjustment and elongation

After shifting an initial profile on top of an observed one, it often no longer reaches from the upper starting to the lower end point of the observed profile. For this reason, the user can decide whether to adjust the data points of the initial profile, i. e., take them away where they go beyond the length of the observed profile and attach these points on the opposite side. If this does not suffer or if the initial profile is too short in its total length, it is elongated in the upper and/or lower part.

Parameter panel

This panel pops up after pressing GO! to generate a profile or when saving a drawn profile. Following parameters are displayed and can be changed:

- N : total number of nodes or data points;
- dt : time step width Δt;
- D_{alt} : value for the stepwise change of D';
- D : diffusivity.

The value of dx and the slope angle are calculated after the profile was generated or saved. D_0 and D' are fixed values which are cannot be edited. All parameters are displayed in the relevant fields on the screen.

For each initial profile several values are shown in the middle left part of the GUI: the total number of data points N, the time step dt (corresponds to Δt), the distance between two data points dx (corresponds to Δx), the starting deviation between both profiles and the slope angle. The vertical exaggeration as well as the resulting displayed angle are given in the upper right text area.

Finally, filenames to save the result must be selected by pressing SAVE RESULT . In the case of a generated or drawn profile, these names are selected automatically and are similar to the relevant input-files; pressing this button enables the user to change these names manually. By default, one file with the initial extension "_varD.save" (because initially a variable diffusivity is set) is saved in the subfolder "./result" and contains all relevant data as the deviations of the stepwise change of D', the choice of parameters and the resulting age-values. Two files are saved in the subfolder "./result/output_files" and consist of the x- and h-values of both the modelled (columns one and two) and the observed (columns three and four) profile. One of these files contains the values before the simulation run, the other one after the simulation run. These filenames are put together of the result filename, the number of iteration-steps and the value of D', e. g., "*_varD.save.t000000.D_prime0.0".

The following possible changes work only if the simulation is not yet running. Pressing CLEAR after adding an starting profile, deletes the starting profile for simulation. The

observed profile is still displayed and a new initial profile can be chosen according to above possibilities. New values of dt and the angle can be typed in the relevant fields with white background. For details about the way how the change of an initial angle is carried out see above Subsection 6.5.1. On the right, D and D_{alt} can be changed using the sliders. Only new values of D can also be selected after a simulation run has completed. The user can choose variable or constant diffusivity and with or without shifting. Default settings are variable diffusivity and a simulation with shifting. With the choice of a constant diffusivity, above result file extension changes to "_constD.save". However, it is recommended that any file extensions containing information about the setting of either variable or constant diffusivity should be as follows: "_varD.input" or "_constD.input", and "_varD.save" or "_constD.save". Any other notations might lead to doubled or wrong naming. "with shifting" shifts the simulated profile to the observed one after each height alteration, i. e., after each iteration step, while "without shifting" means that there is no more shifting during a simulation run. The setting "with shifting" leads to an artificial improvement of the adjustment between both profiles and must be considered when comparing results.

After these preparations, the simulation is started by pressing START. A run can be paused (PAUSE) and stopped (STOP). After stopping it or after completing a simulation, pressing RESET resets the initial profile and its parameters to the starting values and settings.

The results of a simulation run are displayed in the white fields in the lower left part of the GUI. Additional information is given in the upper text area. The smallest deviation between observed and simulated profile [m] and the model-age [m^2] are shown as well as the determined values of D_0 and D'. The age is given in years. If the user selects a different location of D, D_0, D' and the age are newly calculated and displayed in the same fields. The same goes for changed values of D. All relevant information is also added to the result file.

RESET ALL clears the drawing area, resets all values and enables the user to choose a new observed profile. Pressing QUIT exits the "GeomorphDating-Model".

Chapter 7

Data base and field work

7.1 Data acquisition

To assess the "GeomorphDating-Model" and as an example of the utility of this approach for estimating scarp ages, the modified diffusion equation was applied to several data sets of terrace scarp morphology. The presented model is especially applicable to terrace scarps because their initial form and age can often be inferred and material eroded from the upper part of the scarp is deposited on the lower part in an essentially closed system. In addition, terrace scarps are transport-limited (see Chap. 3, p. 26) and integrate the long-term effects of slope processes.

The cross-section profiles were measured perpendicular to the strike of a scarp with a total station allowing a high estimated accuracy within a few percent for scarp heights and derived slope angles. The data consist of measurements of horizontal distance along a profile x and height h. Such observations permit a detailed assessment of the match between model and data although it is a little uncertain how the particular profiles represent the entire scarp along strike. In vertical view, the profiles run from an upper left edge (with $x = 0$ and $h =$ maximum height) to a lower right edge (with $x =$ maximum horizontal distance and $h = 0$). As far as possible, profiles were chosen without complicating factors such as channels at the base of and parallel to the scarp or cobbles and boulders to avoid minor local irregularities. Following Tapponnier et al. (1990), irregularities in the profiles often appear to be due to three-dimensional effects such as erosion by small gullies whose courses are not perpendicular to the scarp or deposition in small fans at the foot of the scarp. Generally, the uncertainty of such measurements is difficult to quantify but horizontal and vertical errors are estimated to be a 1–2 cm at most. But as the natural roughness of the topographic surface is probably the main cause of that uncertainty, measurement errors on levelled points are negligible (Nivière and Marquis, 2000). Local drainage patterns must be avoided as mass transport through both the upslope channels and their downslope fans are explicitly excluded by the diffusion equation (4.6). It is moreover important that the topmost soils of the scarps are not cemented and consequently have not inhibited scarp degradation. As far as possible, the transects were extended beyond the upper and lower edge of a scarp to distances where changes in the far-field slope angle were minimal. But the crest and toe was seldom really even which in fact restricts the

use of the diffusion equation to model the evolution of scarps. In addition it was often discovered, when analysing the field data, that the transects should have been extended even more far. But this was mostly not possible because of accessibility and availability. The influence of both the far-field slope and longer crests and toes is investigated in Section 8.3. The scarps must be relatively straight in plan view and must have been initially cut back to the angle of repose of the material of which they are composed. Additionally, the ridge line must be as straight as possible in plan view, i. e., flow lines should neither converge nor diverge downslope, because the influence of plan-view scarp morphology is not incorporated in the model.

Generally, the degree of preservation of a scarp limits the number of suitable scarps for this investigation. When selecting such scarps, it was one of the main preconditions to find slopes and scarps not or only little disturbed by any human-caused action. This was shown to be a very unreliable factor in the study areas mentioned in the following Section 7.2. The described "GeomorphDating-Model" is very susceptible to the distortion of the unspoilt shape of a scarp, for instance, caused by a farmer dumping a load of soil at the upper or lower edge of it. Climate and vegetation raise further difficulties: The temperate climate of Central Europe leads to a continuous vegetation cover on almost every land surface ranging from grassland to covering with mainly trees and bushes. It is doubtless that the type of cover influences the degradation of a scarp in considerable extent. Finally, it was necessary to survey at least a few scarps with known age to assess and evaluate the presented dating model. For this purpose literature was studied and searched specifically for suitable scarps. In the field those described scarps were often found to be unusable for examination mostly because of disturbances by man. Often such slopes did not even exist any more in the described shape due to the construction of streets or buildings. Fault scarps were not included in this investigation because field work revealed that determining such scarps within the working area was associated with even more problems than discovering appropriate terrace risers. Especially because the research areas are not such active tectonic regions as those regions of other studies investigating fault scarps described in Section 5.2. Fault scarps will only be formed where a fault breaks the surface, and it is on the one hand difficult to recognize and identify such scarps as real fault scarps, on the other hand they have to be young enough to be suitable for this dating method, i. e., they should be not older than Upper Pleistocene.

The profiles were recorded with a high precision total station which provides digital displays and angular readings with a built-in distancer so that vertical and horizontal angles as well as distance can be measured simultaneously. In its current form it is a telescope mounted to swivel both horizontally and vertically. All today's total stations have an electro-optical distancer and an electric gauge to measure off the angle. The encoded division of horizontal and vertical circle are screened electronically and displayed digitally. Horizontal distance, height difference and coordinates are calculated automatically and all measurements and additional information can be registered. The topographical profile surveys of this work were carried out with a **Leica** total station TCA1800. Technical details are listed in Table 7.1.

After selecting suitable scarps it is necessary to mark cross-sections perpendicular to the horizontal extension of a scarp, e. g., by putting up two ranging-rods (Fig. 7.1). For measuring, the total station is installed on a tripod at the upper or lower edge of the scarp

Table 7.1. Specifications of the Leica total station TCA1800.

Angle measurement	1", 0.3 mgon
Distance measurement	1mm + 2ppm
Measuring time	3 s
Built-in programs	Orientation and height transfer, Resection, Tie-distance, Stakeout
Range*	2.5 km
Magnification	30 x
Laser plummet	Located in alidade, turning with the instrument, accuracy 1.0 mm at 1.7 m

* circular prism, average atmospheric conditions

that shall be investigated. A helper with a circular prism fixed on a reflector pole paces out the marked line reducing the distances between neighboring measurement points in the area of highest curvature. The number of survey points per profile depends on the scarp height: A scarp of 10 m height and a horizontal distance along a profile of about 40 m was surveyed with at least 30 measurements to maintain accuracy. To reduce revising of the field data it is recommended to measure from the upper to the lower edge.

It is essential to note down the height of the total station (instrument height = IH) from ground to a given mark on the instrument as well as the height of the circular prism (prism height = PH). GPS (Global Positioning System) measurements of the total station position as well as of the beginning and the ending of the profile were also logged in the field. This simplifies the following data processing of the raw data.

The raw data have to be converted into data which is suitable for the presented dating tool. The data output format of **Leica** (called GSI data format) consists of sequences of numbers, arranged in columns and rows. Each surveyed point is represented in a row where single measurements are labelled with a characteristic index number. Table 7.2 lists the most important index numbers and their assigned values required for data conversion as well as the used abbreviations.

Table 7.2. Description of Leica GSI data format index numbers and used abbreviations.

Index	**Description**	**Abbreviation**
21	horizontal angle	HA
22	vertical angle	VA
31	oblique distance	OD
32	horizontal distance	HD
33	height difference (measured)	ΔH_m
88	instrument height	IH

The GSI file contains values of horizontal and vertical angles given in [gon] with five digits after the decimal point and distances and height differences given in [meters] with four

Figure 7.1. Data acquisition with a total station in the field. Profile 2 (Hausen). View to SE.

digits after the decimal point. The horizontal and vertical angle and the oblique distance are essential values. The horizontal distance HD and the measured height difference ΔH_m result from

$$HD = sin(VA)\,OD \qquad \text{and} \qquad \Delta H_m = cos(VA)\,OD$$

The real height difference ΔH is then defined as $\Delta H = IH - PH + \Delta H_m$.

As it was found difficult to find a useful description of data processing for the required use, this procedure is roughly described here using a calculation software like Microsoft Excel or OpenOffice.

After importing the raw data in a spreadsheet and deleting the unnecessary columns, the angle of refraction a_r is calculated. For this the starting point of a cross-section is defined as a fixed point. a_r is calculated for each surveyed point as

$$a_r = HA \text{ (of the surveyed point)} - HA \text{ (of the fixed starting point)}$$

If this result is < 0, then 400 must be added.

Next the angle of direction a_d has to be determined. This angle represents the clockwise angle from the grid north direction to the direction of the relevant point. To ascertain the angle of direction a_d, the location of the total station and the fixed starting point

are joined up and the deviation between this line and the geographical north direction is approximately determined. Often it is sufficient to estimate the deviation simply from a map, always assuming that the position of the total station and the profile distance are known. The best procedure is to measure the direction from the total station to the first point of the profile measurement with a compass. The angle of direction is added to the just calculated a_r; if the result is > 400 the deviation is subtracted from a_r. Up to now all values represent polar coordinates locating a position by angle and distance.

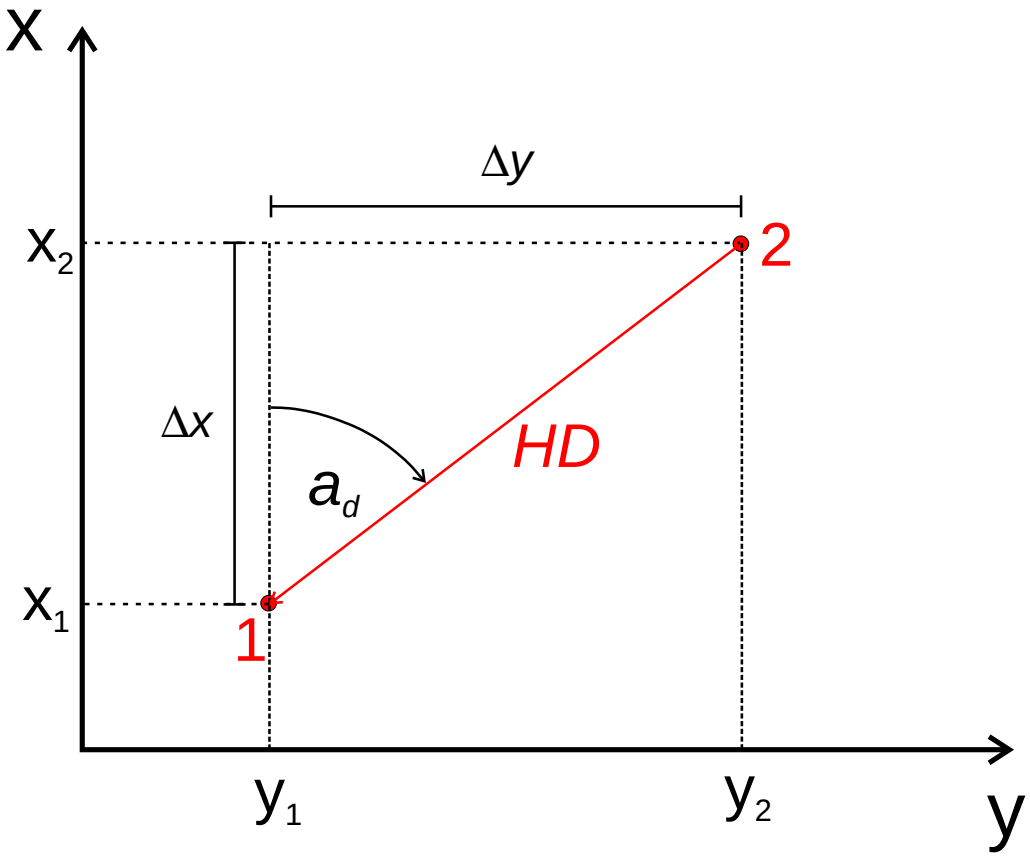

Figure 7.2. Conversion from polar to right-angled coordinates.

Figure 7.2 illustrates the conversion to coordinates of a plane coordinate system resulting from

$$\Delta y = sin(a_d)\, HD \qquad \text{and} \qquad \Delta x = cos(a_d)\, HD$$

Knowing the Y and X coordinates of the total station position, the coordinates of the surveyed points can be easily determined with

$$Y = Y_{\text{total station}} + \Delta y \qquad \text{and} \qquad X = X_{\text{total station}} + \Delta x$$

For the most part the surveyed three-dimensional profiles do not simply run from West to East. This raises the problem that cross-section profiles have height values but also two planar coordinates, X and Y. But as the model tool requires two-dimensional profiles, it is necessary to apply another tool called **transformation**. The tool is programmed in C; the

source code as well as the compiled tool can be downloaded for non-commercial use from **ftp://ftp.geo.uni-bonn.de/pub/GD-Model**. The input file requires four columns: X- and Y-coordinates, and relative and absolute height values. The transformation from 2-D data couples in 1-D data points is achieved by lying a regression line through all data points and determining its gradient. This also emphasizes the importance to measure a profile line as straight as possible to optimize the adjustment of the regression line to the point cloud. Next, the angle towards the x-axis is calculated and the regression line is rotated by this angle towards the x-axis yielding the required two-dimensional profiles. The result file again contains four columns: horizontal distances along the profile, i. e., the X-values, the Y-values and the unchanged relative and absolut height values. X- and Y-values do of course not correspond to the former real values anymore; in fact the Y-values can be neglected anyway. To display the cross section profiles within the model tool, the smallest X-value and the lowest height must finally each be equated with zero and the remaining values must be calculated in accordance. Both the resulting length- (x-) and height- (h-) values should be saved in a single file with the extension ".dat" (see alsoSection 6.5).

7.2 Surveyed scarps

As mentioned in Chapter 1, this work is project C 5 within the Research Training Group (GRK) 437 "Landform – a structured and variable boundary surface" at the University of Bonn. Its research areas are localized in low relief (Lower Rhine Embayment), in medium relief (Rhenish Massive) and in alpine environment (Valais, Switzerland) to cover an extended range of different landform structures. Profiles 1–5 and 9–20 were surveyed in low and medium relief in areas around Bonn, Germany; the locations are shown in Figure 7.3.

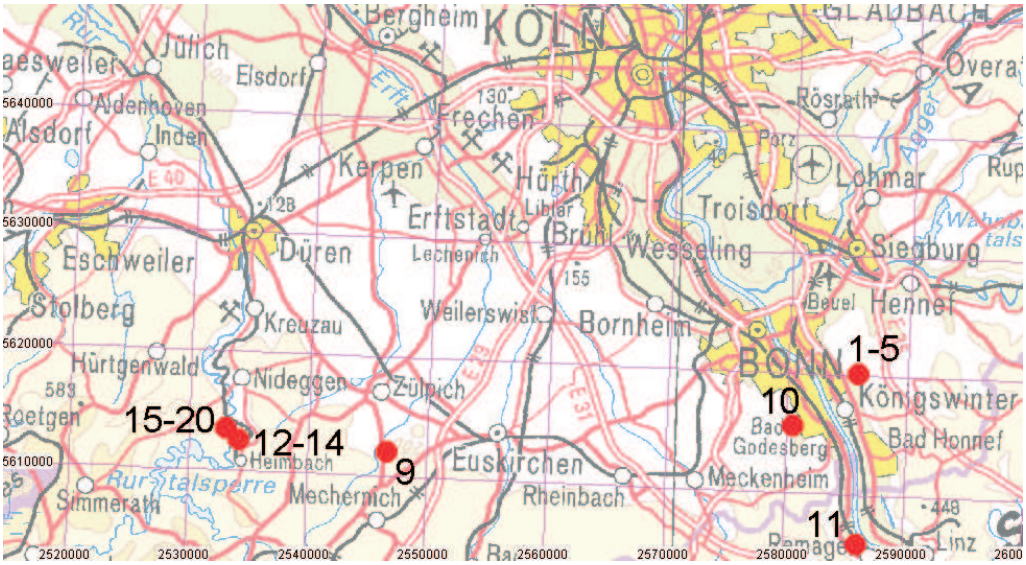

Figure 7.3. Red filled circles show location of profiles 1–5 and 9–20. German Gauß-Krüger coordinates.

Profiles 1–4, 13 and 14, 15–18 as well as profiles 19 and 20 are profiles measured along the length of the same scarp (see Fig. 9.1 on p. 136) while all other measurements are reflecting single scarps. Another three profiles (6–8) were logged in the Turtmann valley, Valais, Switzerland, which is part of the above mentioned alpine research area (Fig. 7.5). This Section describes location, geology and surficial deposits as well as geomorphology or rather shape of the investigated scarps. The sources about the deposits are given for each set of profiles as footnote. The slope angles were measured at the midpoint (see Subsect. 6.5.1). If an age or age-range of a scarp is known it is also given. All important profile data (together with the following digitized and provided profiles) are collected in Table 7.4 at the end of Section 7.3 on page 99. Appendix A from page 159 on shows plots of all investigated profiles. Except for profiles 29, 29a and 33 the plots are scaled on the same length-axis and take into account below described changes due to subdivisions and cut offs. In addition, Appendix B includes photographs of some scarps from page 165 on.

Profiles 1–5 (Frankenforst estate)[1]

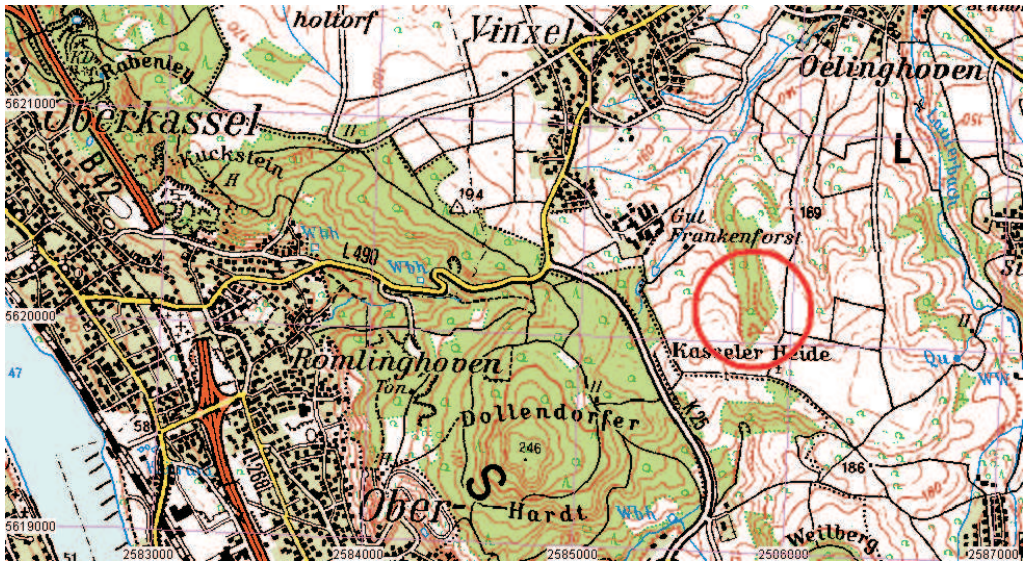

Figure 7.4. Red circle shows location of profiles 1–5 near Vinxel, Frankenforst estate. German Gauß-Krüger coordinates.

Profiles 1–5 were levelled southeast of the Frankenforst estate which is, including its surrounding, a research area of the University of Bonn (Figs. 7.4 and 9.1a). The research area is a typical loess covered low mountain range with altitudes between 130 m and 192 m a.s.l.; it is located 15 km southeast of Bonn. The geological set-up is composed of trachyte tuff of Oligocene age deposited on a Lower Devonian basement (mud-, silt- and sandstones). The tuff is superposed unconformably by up to 10 m thick Pleistocene aeolian deposits of often loamificated calcareous sand dust (Würmian loess and loess loam) or sandy gravel of the main or middle terrace. The Holocene river aggradation in the valley bottom consists of up to 10 m thick humic loamy sand, gravel and loam. Regarding the soil types, the investigated slopes are composed of 10 to 20 dm thick para-brown earths out of loess. Para-brown earths are soils without influence of ground water and damming

[1] Geological map of NRW, 1:25000, No. 5209 Siegburg; Soil map of NRW, 1:50000, No. L 5308 Bonn.

wetness in the upper floor. The soil is typically silty loam to loamy silt, partly slightly stony. In places the para-brown earths are strongly eroded and soils as rendzina are found: Loamy silt to silty loam, 0 to 8 dm thick, partly above calcareous loamy silt, 8 to more than 20 dm thick and above Pleistocene, partly above Devonian deposits. The soil type in the valley bottom is gley (ground water soil) out of Holocene fluvial depositions composed of silty, partly sandy, clayish or stony loam with a thickness of 3 to 20 dm.

The lowest scarp is profile 5 with a height of 5.7 m (altitude 157.2–162.9 m a.s.l.), a horizontal distance of 13.2 m, and a slope angle of 31°. This profile was levelled across a smaller scarp within the upper part of the entire main scarp. Profiles 1–4 were surveyed across that main scarp with a distance of approx. 50 m. The highest scarp is profile 1 with 14.3 m height difference (altitude 153.5–167.8 m a.s.l.), a horizontal distance of 68.2 m, and a slope angle of 14°. The age of these five scarps could not be limited reliable.

Profiles 6–8 (Turtmann valley, CH) [2]

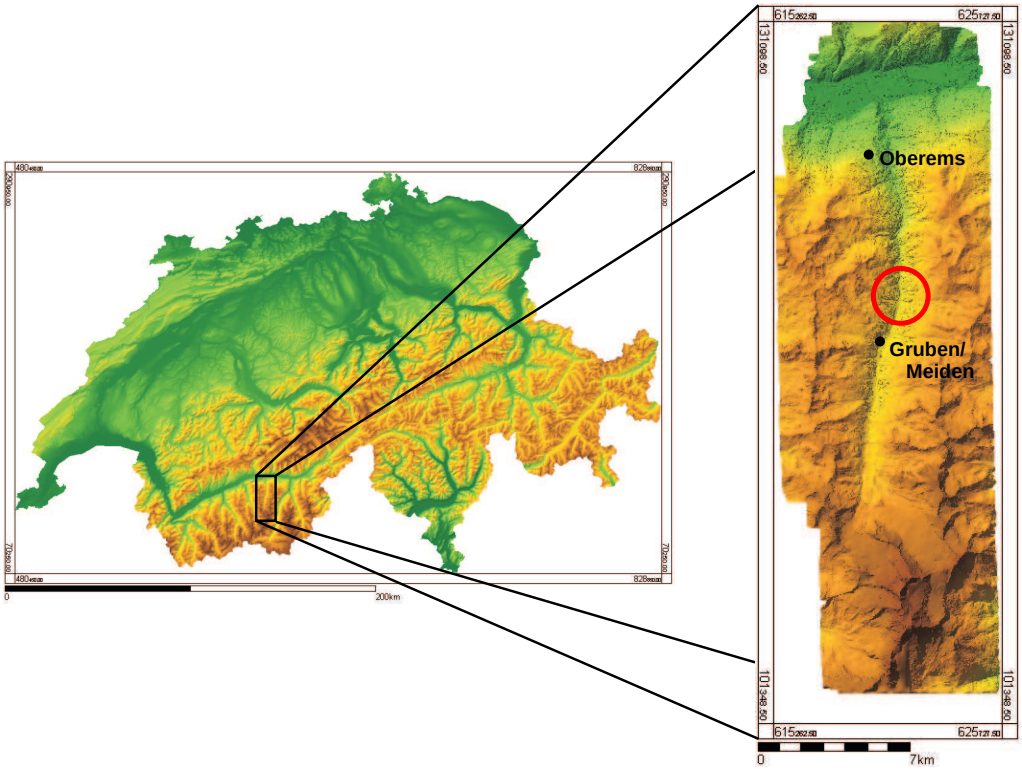

Figure 7.5. Red circle shows location of profiles 6–8 in the Turtmann valley, CH. Maps by courtesy of M. Nyenhuis (member of the Research Training Group 437, project C 7).

The Turtmann valley is located in the central Alps south of the Rhone valley in the Canton of Valais in Switzerland. It is approx. 15 km long, reaching from the village of Turtmann in the Rhone valley in the north (620 m a.s.l.) to the Turtmann glacier in the south (2260 m a.s.l.). The profiles were logged in the gentle middle part of the valley (Fig. 7.5 and Figs. B.1 and B.2).

[2] Geological atlas of Switzerland, 1:25000, No. 1308 St. Niklaus.

Penninic nappes form the geological basement and consist of mainly metamorphic rocks: two-mica gneiss and chlorite mica schists. The rocks are intensely folded and are interstratified by banded amphibolites and pegmatites. Situated above, partly slaty limestones, marble and sandstones with clayish layers (flysch) of Triassic to Tertiary age were deposited. The Quaternary glaciation of the Turtmann valley formed extensive morainic covers in the main valley and in upper hanging valleys. The bottom of the Turtmann valley is filled with glaciofluvial sand and gravel. Up to four terrace levels within this material in the gentle middle part of the valley reflect different glaciofluvial stages of the active Turtmann glacier. Mainly the older terraces are overprinted by talus cones on both sides of the valley. Due to a dam at the valley end and because most of the glacier runoff is taken away, glaciofluvial processes are limited to the a small area right in front of the Turtmann glacier.

All three profiles were measured in an altitude around 1800 m a.s.l. with 12.6 m (profile 6), 7.2 m (profile 7) and 6.7 m (profile 8) height difference, 26.2 m, 24.7 m and 18.6 m horizontal distance, and 41°, 9°and 36° slope angle, respectively. Because profile 7 was surveyed over two terrace risers, it was separated into two single profiles 7a and 7b with overlapping data points at the toe and the crest, respectively. Profile 7a is 4.9 m high and 17.5 m long; profile 7b is 2.4 m high and 9.3 m long. The slope of profile 7a is 29°, and of profile 7b 24°. The age of the terraces must be younger than 14,000 years after the Quaternary glaciation of the entire valley has ceased (see below).

Profile 9 (Schwerfen)[3]

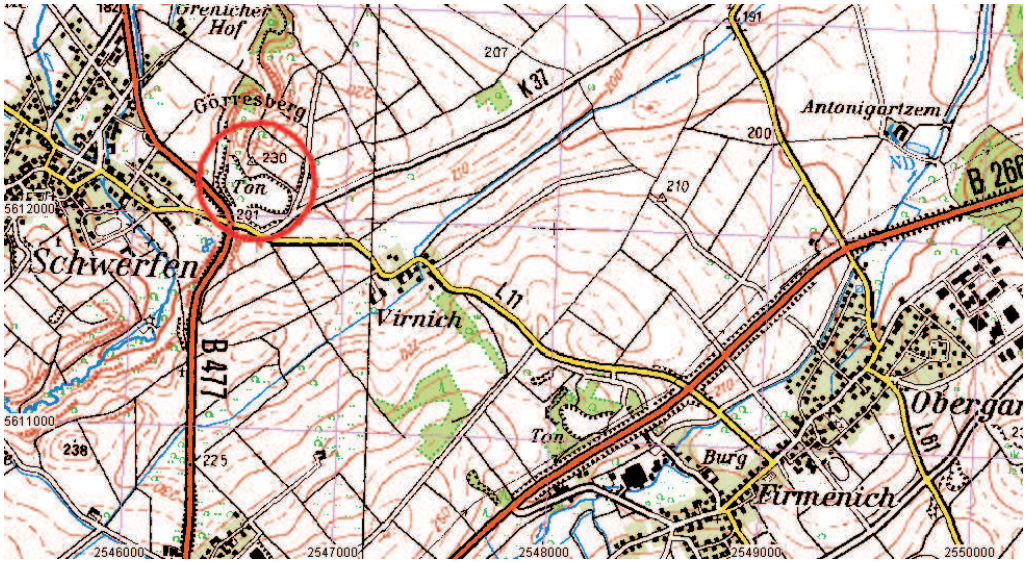

Figure 7.6. Red circle shows location of profile 9 near Schwerfen. German Gauß-Krüger coordinates.

Profile 9 was surveyed at the edge of an abandoned clay and loam sand pit east of Schwerfen (Figs. 7.6 and B.3). The geological subsoil consists of up to 10 m thick white quartzous gravel with siliceous oolites and lydites of lower Pliocene age. In higher parts, this day stone is overlain by Pleistocene sandy gravel, mostly loamy, of the main terrace. The

[3]Geological map of NRW, 1:25000, No. 5305 Zülpich; Soil map of NRW, 1:50000, No. L 5304 Zülpich.

soil type is braunerde, partly with similigley, in some places podsol braunerde, out of gravelly solifluction (soil flow) formations. Braunerde represents, like para-brown earth, soil without influence of ground water and damming wetness in the upper floor. The soil is 3 to 7 dm thick and consists of loamy gravel to gravelly loamy silt, partly sandy. It is often found with a fragmentary overburden of redeposited loess loam of Holocene or Pleistocene age.

This profile is 13.4 m high (altitude 205.7–219.1 m a.s.l.) and 24.8 m long. The slope angle comes to 35°. The scarp was formed artificially during active mining. As the pit was closed in 1976, it is assumed that the scarp is at least 28 years old (personal communication, archives of the City of Schwerfen).

Profile 10 (Bad Godesberg) [4]

Figure 7.7. Red circle shows location of profile 10 near Bad Godesberg. German Gauß-Krüger coordinates.

The profile is surveyed across a scarp SE of the Godesberger creek at the south-western end of Bad Godesberg (Fig. 7.7). The geological set-up consists of up to 20 dm thick aeolian deposits (loess) of calcareous silt, superficially mostly decalcified and loamificated, on a lower Devonian basement ("Siegener Beds"). In the valley bottom, sandy silt and silty sand, mostly humic and often with gravel underground, represent typical fluvial depositions of Holocene age. The soil is composed of 10 to 20 dm thick para-brown earth out of loess which is described in detail on page 91 (profiles 1–5). In the valley bottom the soil consists of gley out of Holocene fluvial depositions also mentioned previously.

The profile was surveyed between 107.4 m and 116.0 m a.s.l. (scarp height 8.6 m). The horizontal distance is 26.6 m; the slope angle is 36°. According to Bibus (1980), the peneplanation on both sides of the Godesberger creek can be merged to an upper Middle terrace, although due to a lack of sediments only with reservations.

[4] Geological map of NRW, 1:25000, No. 5308 Bonn - Bad Godesberg; Soil map of NRW, 1:50000, No. L 5308 Bonn.

Approximately 500,000 years ago, the Rhenish Massive became an area of fast uplift for more than 300,000 years where erosion was stronger than accumulation causing the development of the narrow valley of the Middle Rhine (Schirmer, 1994). Thome (1998) states that this change in valley development is connected with the first large glacial (Günz or Menapian complex), i. e., the narrow valley started to evolve more than 800 ka ago.

Generally, periods of strong vertical erosion coincide with periods of uplift which are followed by phases of aggradation. The Middle terraces in the Rhine area were deposited between the Elster and the Saale glacial, during the upper Middle Pleistocene between about 330 ka and 127 ka ago and after the deposition of the higher Main terraces (Ehlers, 1994). This corresponds to Thome (1998) who describes strong vertical erosion at the end of the Main terrace age (Cromer complex) and during the Elster glacial, and high aggradation rates at the latest until the first half of the Elster glacial (upper Middle terraces) and from the end of the Elster glacial period until the maximum of the Saale glacial (lower Middle terraces). The incision of the Rhine during the Elster glacial was the deepest vertical erosion and reached today's base of the Quaternary. Fränzle (1969) and Siegburg (1987) state that the floor of the Godesberger valley corresponds to the valley bottom of the Rhine during the Saale glacial. According to Schreiner (1992) and Benda (1995), up to four Middle terraces can be distinguished in the Rhine valley. Especially along the steep faces of the narrow Rhine valley they are characterized by narrow strip-like planations. Average distances between different terrace levels are 10–30 m but may also be less (Schirmer, 1994). Bibus (1980) claims that the planations of the upper Middle terrace are located approx. 140 m a.s.l. which is more than 20 m higher than the surveyed profile 10. This implies that the scarp might rather belong to the younger middle or lower Middle terrace with an age ranging between about 127 ka and 300 ka (Grabert, 1998).

Profile 11 (Remagen) [5]

This profile was levelled northwest of the Apollinaris monastery in Remagen within the narrow part of the lower Middle Rhine valley (Fig. 7.8). The geological set-up is made up of superficial loamificated schlierenlike banded slates and quartzite sandstones of lower Devonian age belonging to the middle "Siegener" stage. Superimposed Pleistocene sands are partly cemented calcareously. This carbonate is supplied by the uppermost deposits of loess loam and loess. The soil type is a 10 to 20 dm thick para-brown earth and secondary a braunerde consisting of loam and silt described on page 91 (profiles 1–5) and page 94 (profile 9), respectively.

The height of the profile comes to only 4.4 m (altitude 133.6–138.0 m a.s.l.) with a horizontal distance of 12.8 m and a slope angle of 4° at the midpoint. As the profile as a whole appears as two scarps, it was separated into two single profiles 11a and 11b with overlapping data points at the toe and the crest, respectively. Height and length of profile 11a are 2.7 m and 7.6 m, and of profile 11b 1.8 m and 6.4 m. Profile 11a has a slope angle of 39°, and profile 11b one of 20°. The surveyed scarp is assigned to the so-called Apollinaris terrace mentioned byJungbluth (1918). This terrace level is developed only locally and corresponds probably to the middle Middle terrace (Fränzle, 1969; Meyer and Stets, 1996). This roughly limits the scarp age to 330–127 ka (Ehlers, 1994).

[5] Geological map of NRW, 1:25000, No. 5409 Linz; General map of the soil type assemblages of Rhineland-Palatinate 1:250000.

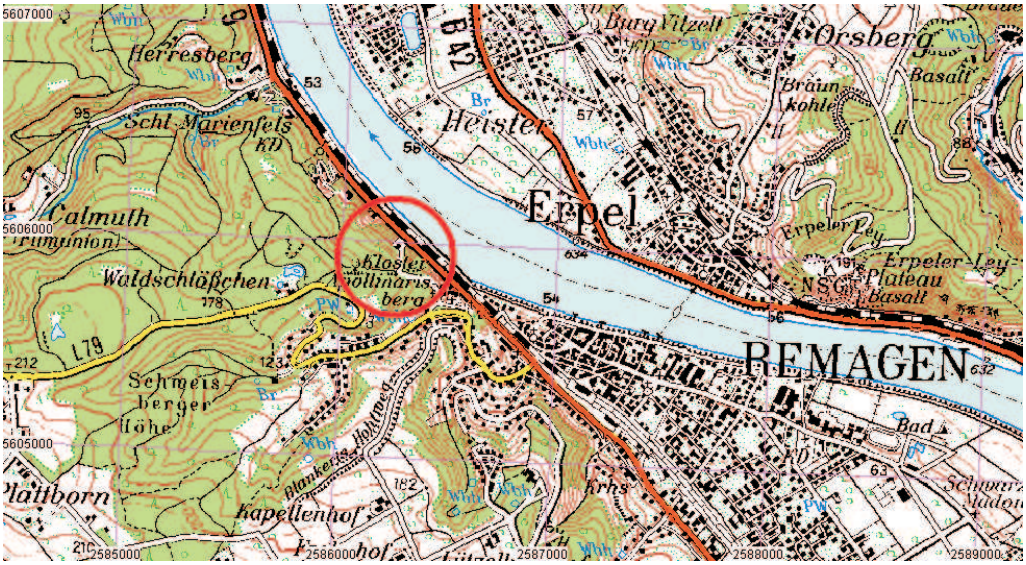

Figure 7.8. Red circle shows location of profile 11 near Remagen. German Gauß-Krüger coordinates.

Profiles 12–20 (Hausen and Blens) [6]

Profiles 12–14 were surveyed southwest of Hausen and profiles 15–20 southwest of Blens near the mouth of the Odenbach into the Rur (Figs. 7.9, 9.1b–d, B.4, B.5, B.6 and B.7). Both villages are located along the river Rur in the northern part of the Eifel. The geological underground is composed of up to 800 m thick lower Devonian sandy clay schist with interposed finely granular greywacke sandstone ("Koblenz Beds"). In the case of profiles 12 to 14 near Hausen the underground is superposed by Pleistocene gravel and pebble of the upper terrace group. On loamificated plains of erosion of the river Rur, these fluvial aggradations show pebbles in places. At both locations Pleistocene partly loesslike slope wash and layers of slope-wash alluvium are found as talus deposits. In the lower most valley bottom Pleistocene loam, gravel and pebble are deposited. In coombs loam and debris as products of soil separation in layers are formed. Regarding the soil types, the investigated slopes near Hausen (P12–P14) consist of partly podzolic braunerde out of slope loam. The soil is 3 to 8 dm thick and is composed of gravelly silty to silty-sandy loam, in parts stony. Above Pleistocene terrace gravel and concerning profiles 15 to 20 near Blens, the soil type is braunerde, partly colluvium or para-brown earth, in some places similigleyed or gleyed, out of loess containing slope loam. The soil is 10 to more than 20 dm thick and is composed of silty loam, partly very sandy or calcareous. Near Blens in some upper parts of the profiles the soil type is a partly similigleyed braunerde out of Palaeozoic rocks, partly of Quaternary talus deposits or covering detritus. It is often overburdened with a thin layer of slope loam of Holocene or Pleistocene age. The soil consists of stony silty loam, in parts gritty soil or clayish, and is 3 to 7 dm thick. The soil type in the valley bottom near Blens is gley (ground water soil) out of loamy fluvial depositions and composed of silty loam, partly gravelly, clayish or with turfy moulder and in some places peaty, with a thickness of 6 to more than 20 dm.

[6] Geological map of NRW, 1:25000, No. 5304 Nideggen; Soil map of NRW, 1:50000, No. L 5304 Zülpich.

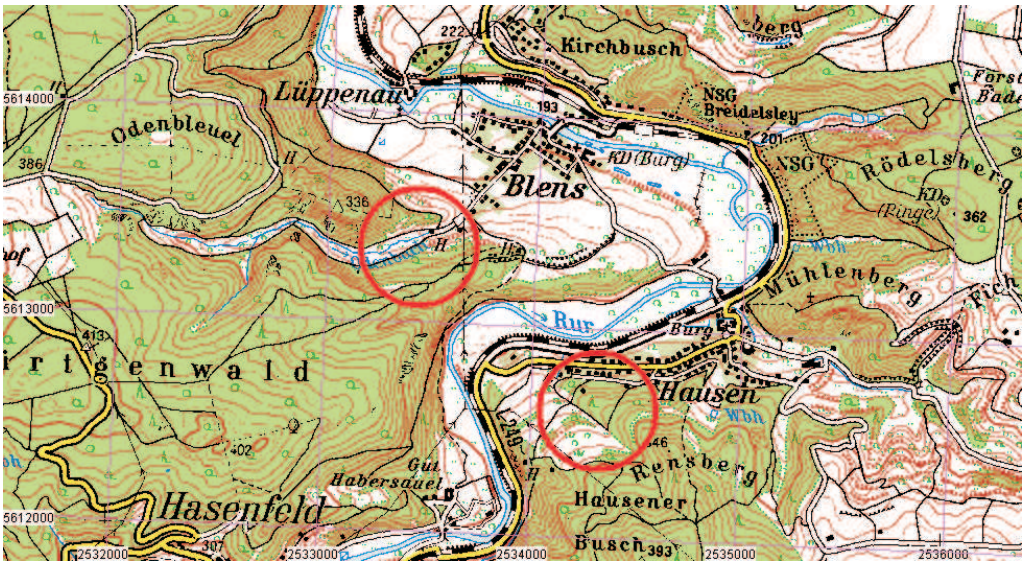

Figure 7.9. Red circle shows location of profiles 12–20 near Hausen and Blens. German Gauß-Krüger coordinates.

The profiles surveyed near Hausen are only 4.8 m (profile 12), 3.3 m (profile 13) and 3.5 m (profile 14) high, and 15.9 m, 11.2 m and 12.2 m long, respectively. The slope angles come to 18°, 27° and 23°. Profile 12 was levelled in an altitude of about 230 m a.s.l.; profiles 13 and 14 levelled across the same scarp range between 195 m and 199 m a.s.l. Following Quaas (1917) who studied the terraces of the Rur intensively, these scarps probably belong to the youngest or middle terrace of Pleistocene age (terrace group I or II) and correspond to the Lower or Middle terrace of the Rhine. Hence, the age must be younger than 70 ka or 127 ka (Grabert, 1998). If the age of these scarps is equal to the older Lower terrace of the Rhine, the age can be limited to 70–18 ka. As profile 12 is approx. 30 m higher than profiles 13 and 14, it might also belong to terrace group III, i. e., it might be somewhat older. Profiles 15–20 near Blens were levelled across two smaller scarps one lying on top of the other. Their heights vary between 5.6 m and 7.8 m, their horizontal distances between 20.6 m and 35.0 m, and their slope angles between 12° and 34°. The altitudes range between 195 m and 226.5 m a.s.l. As the Odenbach is situated on the Middle terrace of the Rur (Quaas, 1917), the age must be younger than that one which corresponds to the Middle terrace of the Rhine. The investigated scarps must thus be younger than 127 ka. Profiles 19 and 20 were levelled across the lower of both scarps, and should consequently be even somewhat younger.

7.3 Digitized profiles from literature

In addition to above described scarps, eight profiles that were surveyed by Nivière and Marquis (2000) were digitized and dissected to assess a possible improvement of the modified approach in comparison to conventional diffusion equation models using a constant diffusivity (see Section 5.2). Nivière and Marquis (2000) levelled profiles at the SE end of the Upper Rhine graben north of Basel (CH) in the hollow of Sierentz. This hollow

consists of a sequence of five step-like strath terraces with their tops between 200 m and 320 m a.s.l. The profiles were measured along the most prominent and continuous abandoned terrace riser limiting the western side of the Rhine flood plain with a height ranging between 7 m and 17 m and increasing northwards. 21 cross-strike topographic profiles at locations roughly 350 m apart were measured. The deposited material consists of alternating, not cemented coarse sands and gravels of fluvial origin; Nivière and Marquis (2000) described the deposit as a cohesionless sedimentary pile. Following the authors, the terrace has to be younger than 80 ka due to the Würmian alluvial sediment infill of the hollow of Sierentz and older than 2 ka because of the presence of Roman settlements in the plain below the scarp. From palaeoclimatic studies, Nivière and Marquis (2000) inferred major climate changes in Alpine Europe during the Pleistocene and showed that, owing to regional evidence, the Würmian climate alternated between glacial and interglacial periods. The recent climate is described as semi-continental with warm and rainy summers and cold winters. According to Nivière and Marquis (2000) the terraces in the hollow of Sierentz were covered by forests in the past and the present-day forest is close to that of the Holocene. Generally, the profiles show an upper concave erosional part and a lower convex depositional part.

The profiles were scanned and digitized using the C-tool "digitize" by Prof. Dr. St. Hergarten who is a member of the Geodynamics working-group at the University of Bonn. This tool scales the scanned data points according to a before created reference file and outputs them to a new file. Table 7.3 lists profiles 21 to 28 and their corresponding denotations in the work of Nivière and Marquis (2000). Simple type profiles are profiles formed during single incisive periods; two-stage type profiles appear to have older crests than bases. They were partially reactivated during either a new incisive episode (reactivated base) or a landsliding event (reactivated crest). Forward modelling of the scarp morphology yielded an age for the simple scarps of 19±2 ka and of approx. 33 ka for the two-stage scarps that were reactivated 15 ka ago (Nivière et al., 1998; Nivière and Marquis, 2000).

Table 7.3. Denotations of profiles in this work and of corresponding profiles in the work by Nivière and Marquis (2000).

This work	**N. & M. (2000)**	**Type**
Profile 21	Profile 5	simple
Profile 22	Profile 9	simple
Profile 23	Profile 14	simple
Profile 24	Profile 17	simple
Profile 25	Profile 2	two-stage
Profile 26	Profile 4	two-stage
Profile 27	Profile 18	two-stage
Profile 28	Profile 20	two-stage

Additionally, Bertrand Nivière, one of above mentioned authors, made a set of five further profiles (29–33) available that were also levelled in the southern Rhine graben in the area of Basel and Mulhouse. The investigated scarp corresponds to a terrace riser of the Rhine with similar deposited material as described above for profiles 21 to 28. It was formed in the Weichsel Glacial Period limiting the age between 15 ka and 80 ka but B. Nivière assumes the scarp to be around 50 ka old (personal communication). The height data points of these profiles were measured only about every meter due to lithology. Because of a bulge at the basal part of profile 29, it was cut off and saved as profile 29a which was then used for modelling. The same was done with profile 33 (saved as profile 33a).

Table 7.4. Important data of all profiles investigated in this work. The slope angle is measured at the midpoint.

Profile	height [m a.s.l.] min.	max.	Δh [m]	x[m]	Deposits	slope angle	approx. age [ka]
1	153.5	167.8	14.3	68.2	loess loam or sandy gravel	14	?
2	157.6	169.8	12.2	55.8	loess loam or sandy gravel	15	?
3	159.3	173.1	13.8	63.3	loess loam or sandy gravel	14	?
4	163.1	174.3	11.2	54.5	loess loam or sandy gravel	12	?
5	157.2	162.9	5.7	13.2	loess loam or sandy gravel	31	?
6	1802.6	1815.2	12.6	26.2	sand and gravel	41	<14
7	1797.0	1804.2	7.2	24.7	sand and gravel	9	<14
7a	1799.3	1804.2	4.9	17.5	sand and gravel	29	<14
7b	1797.0	1799.4	2.4	9.3	sand and gravel	24	<14
8	1795.4	1802.1	6.7	18.6	sand and gravel	36	<14
9	205.7	219.1	13.4	24.8	sandy gravel	35	>0.028
10	107.4	116.0	8.6	26.6	sand and gravel	36	127–300
11	133.6	138.0	4.4	12.8	sand and loess loam	4	127–330
11a	135.3	138.0	2.7	7.6	sand and loess loam	39	127–330
11b	133.6	135.4	1.8	6.4	sand and loess loam	20	127–330

continued on next page

continued from previous page

Profile	height [m a.s.l.] min.	max.	Δh [m]	x[m]	Deposits	slope angle	approx. age [ka]
12	227.0	231.8	4.8	15.9	gravel and pebble	18	70–127
13	194.7	198.0	3.3	11.2	gravel and pebble	27	18–70
14	195.5	199.0	3.5	12.2	gravel and pebble	23	18–70
15	198.7	204.5	5.8	20.6	gravel and pebble	34	<127
16	196.0	201.7	5.7	23.4	gravel and pebble	17	<127
17	195.0	200.6	5.6	22.4	gravel and pebble	15	<127
18	219.6	226.5	6.9	29.7	gravel and pebble	20	<127
19	212.1	219.7	7.6	35.0	gravel and pebble	14	<127
20	210.7	218.5	7.8	32.5	gravel and pebble	12	<127
21	–	–	10.2	34.1	sand and gravel	32	19±2
22	–	–	12.1	42.9	sand and gravel	37	19±2
23	–	–	11.8	39.7	sand and gravel	35	19±2
24	–	–	9.1	29.3	sand and gravel	30	19±2
25	–	–	11.1	30.1	sand and gravel	24	33
26	–	–	11.3	34.8	sand and gravel	30	33
27	–	–	11.4	29.5	sand and gravel	24	33
28	–	–	10.8	29.8	sand and gravel	34	33
29	–	–	5.2	93.3	sand and gravel	20	50
29a	–	–	5.2	76.3	sand and gravel	21	50
30	–	–	4.5	49.4	sand and gravel	20	50
31	–	–	5.0	61.2	sand and gravel	23	50
32	–	–	3.7	49.6	sand and gravel	14	50
33	–	–	3.8	89.5	sand and gravel	13	50
33a	–	–	3.8	54.5	sand and gravel	20	50

7.4 Local climate record

As indicated in Chapter 2, climate is a major factor in weathering, soil-forming processes and geomorphic processes, e. g., periglacial processes being more active in a denudational sense than temperate ones. The importance of the climate record of the surveyed localities is thereupon obvious and shall be outlined briefly. Most important in the context of this work is the present climate and the climate since the Quaternary as these are the periods of stronger erosion than deposition. The Quaternary is the youngest and shortest system of geological history and goes back only 1.65 to 2.4 Ma before present, depending on the method of delimitation. On a geobotanic basis, the Quaternary in the region of the Lower and Middle Rhine is determined to begin 2 Ma BP (Brunnacker, 1978). Generally, the

Quaternary is subdivided into the Pleistocene and the Holocene which covers the time from 10 ka BP until now. Table 7.5 shows the geological timescale for the Quaternary.

After sub-tropic to warm humid conditions in the Tertiary, the northern hemisphere experienced extreme climatic fluctuations in the Pleistocene: glacial episodes of around 80–100 ka duration alternated with 10–20 ka lasting interglacial periods (Benda, 1995). The mean annual temperature during the interglacial periods was with 8–11°C comparable to present temperatures. In Central Europe deciduous forests were widespread. With regard to terrace formation, the rivers incised during the warm intervals into the deposits that accumulated during the cold intervals, i. e., the terracing took place in the interglacials (Wirth, 1978). During the glacial intervals in Europe, huge ice-sheets reached from Scandinavia far into the south with the southernmost glacier advance in the Saalian glacial which ended near Düsseldorf (Grabert, 1998). Additionally, glaciers spread from the Alps in northern direction. Central Europe with its low mountain ranges was surrounded by glaciers and represented a region of periglacial climate with temperatures 10–15°C below today. With the onset of each glacial interval, the climate became cold, but initially remained fairly humid in Western Europe giving rise to intense gelifluction. During each of the glacial maxima, the climate grew colder and dryer.

Table 7.5. Geological timescale for the Quaternary. Modified after Ehlers (1994), Grabert (1998), Thome (1998) and Murawski and Meyer (1998).

age (Ma)	**Series**	**Stage Central Europe**	**Stage NW Europe**	**Glacial/ Interglacial**
	Holocene			
0.010	Pleistocene	Würm	Weichsel	Glacial
> 0.070		Riss/Würm	Eem	Interglacial
0.127		Riss	Saale	Glacial
0.250		Mindel/Riss	Holstein	Interglacial
0.330		Mindel	Elster	Glacial
0.500		Günz/Mindel	Cromer complex	Interglacial
> 0.700		Günz	Menap complex	Glacial
0.900		Donau/Günz	Waal complex	Interglacial
> 1.300		Donau	Eburon complex	Glacial
1.600		Biber/Donau	Tegelen complex	Interglacial
> 2.200		Biber	Pre-Tegelen complex (Brüggen)	Glacial
2.400				

The Upper Pleistocene ranges from the start of the Eemian interglacial (approx. 127 ka BP) to the end of the Weichselian glacial (approx. 10 ka BP) (Benda, 1995). This last glacial period started with a transitional mostly colder period with a total duration of approx. 70 ka. During the warmer episodes of the glacial epoch, in the interstadials with a temporary retreat of the ice, the temperature varied between +2°C and +6°C,

and pine and birch trees spread out. During the colder periods mostly deforestation took place and the glaciers spread significantly. Following Schreiner (1992), the last glacial maximum at about 18 ka BP lowered the mean annual temperature to approx. -4°C to -7°C. This temperature decrease of 8–10°C below present temperatures in the mid-latitude continental interiors caused the greatest latitudinal shift of climatic zones of the northern hemisphere (Ahnert, 1996). One last time most of nonglaciated Europe north of the Alps became a periglacial region. Warm air and moisture from the south were blocked by the Alpine ice cap; pack ice and lower sea level blocked the northward flow of the warming Gulf Stream. Powerful global westerly winds occurred, as well as easterly winds pouring down off the edges of the Scandinavian ice sheets (Bloom, 1991). There were no forests in Europe and permafrost was widespread. It is assumed that total precipitation was reduced to about 80 per cent of today's values. Frost-churned residual soils and the gelifluction deposits of the wetter phase were mantled by thick loess deposits.

While the Upper Pleistocene is characterized by a intense terrace formation, the Holocene is the age of erosion. Consequently, in the context of this study the climate of Central Europe during the last 10,000 years is of biggest importance. The ice margins retreated as the climate became warmer and more humid; simultaneously the sea-level rose and the permafrost ceased. The temperature increased from a mean July temperature of ca. +3°C to ca. +18°C nowadays (Grabert, 1998). According to Bloom (1991), a late-glacial tundra environment changed to birch and pine forest with cold and rather dry climate approx. 8,500 years ago. An ice-free Northern Europe can be dated back 8,000 years BP (Grabert, 1998). The climate of the northern middle European lowlands was warm-humid, and from 7,500 years on first farmers inhabited the area around Bonn (Welp and Plümer, 1999). About 5,000 years ago, the climate became maritime and moist. The average temperature was perhaps 2°C warmer than today. Northwestern Europe was covered with heavy deciduous forests and peat bogs were widespread on uplands and lowlands. About 3,000 years BP, the degeneration of the forests began, perhaps owing to a slightly cooler, drier climate but more likely owing to the beginning of Neolithic agriculture. Clearance and cultivation of crops by Man has strongly affected subsequent morphogenesis in Western Europe. Although intervals with lower and higher temperatures alternated after the climate optimum in the Atlanticum (5,500–2,500 BC), Welp and Plümer (1999) state that the average temperature did not vary more than ±1°C since the end of the last glacial (15°C). The forests had there biggest extension with more than 90% of the area in the 7^{th} century in a cool and rainy climate. During the early Middle Ages (mainly from 1,000 BC on) agriculture was intensified due to an accelerated population growth. In the middle of the 14^{th} century the climate worsened with frequent extreme heavy rainfall. In the 16^{th} century the beginning of a "small glacial" is provable which lasted into the 19^{th} century. This change together with intense agriculture caused a period of excessive erosion. Afforestation and increased use of grassland reduced the soil erosion again (Welp and Plümer, 1999). Until today the erosion rates of the Middle Ages have not been reached again.

Today, Western and Central Europe are part of the temperate humid climate. This environment is characterized by (1) evenly-distributed rainfall which occurs mainly as prolonged falls of low intensity, (2) more rainfall than potential evapotranspiration during most months of the year, and (3) temperatures in winter that freeze only a shallow top

layer of the soil (Young, 1975). All profiles except profiles 6–8 were measured in very similar climatic regions. If not quoted different the following climate data (except those for profiles 6–8) are taken from the "Climate Atlas of North Rhine-Westphalia" (Deutscher Wetterdienst, 1989). The average annual temperature varies between +9°C and +10°C with mean January temperatures between 0°C and +5°C, in higher altitudes also between -5°C and 0°C, and mean July temperatures ranging from +15°C to +20°C. The long-standing average annual precipitation is 500–750 mm/a.

Locations of profiles 10 and 11 (Bad Godesberg and Remagen) are more or less in the Rhine valley. Due to its protected position between the surrounding low mountain ranges, the climate is influenced more continentally: Early spring, more stable weather conditions with less precipitation and warmer climate in summer, long-lasting autumn, and relatively cold and dry winter (Meyer and Stets, 1996). Temperatures in January range from 0°C to +3°C and in July from 16°C to 18°C. Precipitation occurs mainly in summer and varies between 500 and 700 mm/a. Pfeffer (1997) describes this as a "wintermild continental climate". The climate in the region where profiles 12–20 (Hausen and Blens) were levelled is an "oceanic hilly country climate" with mild January temperatures between -1°C and +2°C, July temperatures between 16°C and 18°C, and precipitation ranging from 700–900 mm/a (Pfeffer, 1997).

Profiles 6–8 were surveyed in the alpine environment of the Turtmann valley, Switzerland. According to Schreiner (1992), the main lateglacial alpine glaciers melted in not more than 2,000 years from around 14,000 a BP. Today it is a strongly continental influenced region: relatively low precipitation together with rather high temperatures. These climate data are taken from Burga (1998). Average January temperatures vary from -5°C to -10°C decreasing to -15°C in higher altitudes. The range for the average July temperatures is between +15°C and +20°C; for higher areas it is between +10°C and +15°C. The long-standing average precipitation depends again on the height: 1000–2000 mm/a and for higher altitudes above 2000 mm/a. Van Tatenhove and Dikau (1990) state a precipitation of 600–900 mm/a for an altitude of 2000 m a.s.l.

Due to above stated characteristics of temperate humid climate, the intensity of geomorphological processes is only moderate. The soil in humid temperate zones is permanently moist in depth, and chemical weathering is predominant. The depth of freezing is insufficient for solifluction, and woodland vegetation hinders strong rainsplash and surface wash under natural conditions. Suffice is to say at this point that climatic changes are obviously more frequent than significant changes in the evolution of landforms due to new climatic conditions. It is therefore not appropriate to assume that every recognized climatic fluctuation causes a significant change in geomorphic processes. For a rather comprehensive review of the Quaternary, see e. g., Schreiner (1992), Ehlers (1994), Benda (1995) and Thome (1998).

Chapter 8

Results

8.1 Analysis of investigated slopes

The scarps to be examined and dated including observed, digitized and provided profiles were analysed to discover any conspicuous or common features although they are from quite different sites. Only those profiles are considered here that were finally taken for modelling, i. e., profiles 7, 11, 29 and 33 are excluded but instead profiles 7a, 7b, 11a, 11b, 29a and 33a are analysed (see Sect. 7.2). Figure 8.1 illustrates the frequency distribution of all slope angles measured at the midpoint.

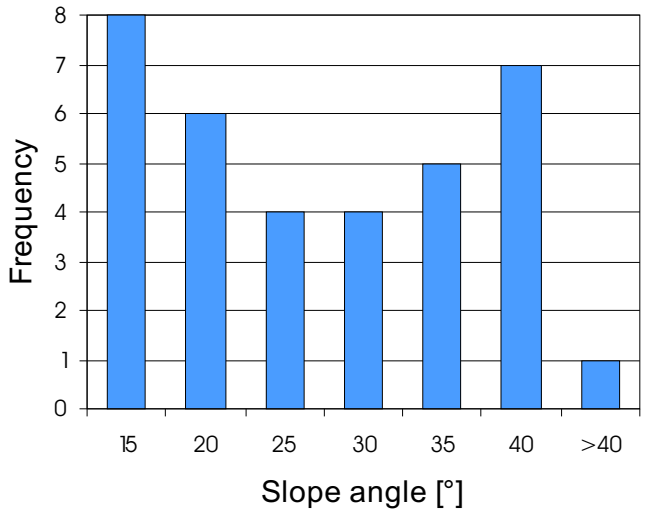

Figure 8.1. Distribution of all examined profiles 1–33a with respect to the slope angles measured at the midpoint.

The midpoint slope angles of all analysed profiles vary between approx. 12° and 41°. Among those, the levelled profiles span the whole slope range and the height range 1.8 m–14.3 m. All digitized profiles have angles between 25.6° and 38.0° and heights between 9.1 m and 12.1 m. The slopes of the provided profiles vary between 14.5° and 23°, their

heights range from 3.7 m–5.2 m. This documents how narrow the slope and height ranges of the digitized and provided data are which were each levelled across the same scarps and that the levelled data spans a wider range in both sizes. The scattering is also illustrated in Figures 8.2 and 8.3 where the scarp slope and the reduced scarp slope are plotted as a function of scarp height, respectively. Hanks and Andrews (1987, 1989) described the effect of far-field slope in detail and introduced the reduced scarp slope into the field of geomorphological dating as the maximum scarp slope minus the far-field slope. It was actually suggested for a set of profiles presumed to be coeval and of various heights. This reduction was proposed because in diffusion mathematics the effect of the far-field slope is included in solutions to the linear diffusion equation with a constant diffusivity. Applying the diffusion equation to scarp degradation thus implies that it is rather $tan\theta - b$ than $tan\theta$ alone which counts into age determination. Here again θ is the maximum slope angle, b is the far-field slope.

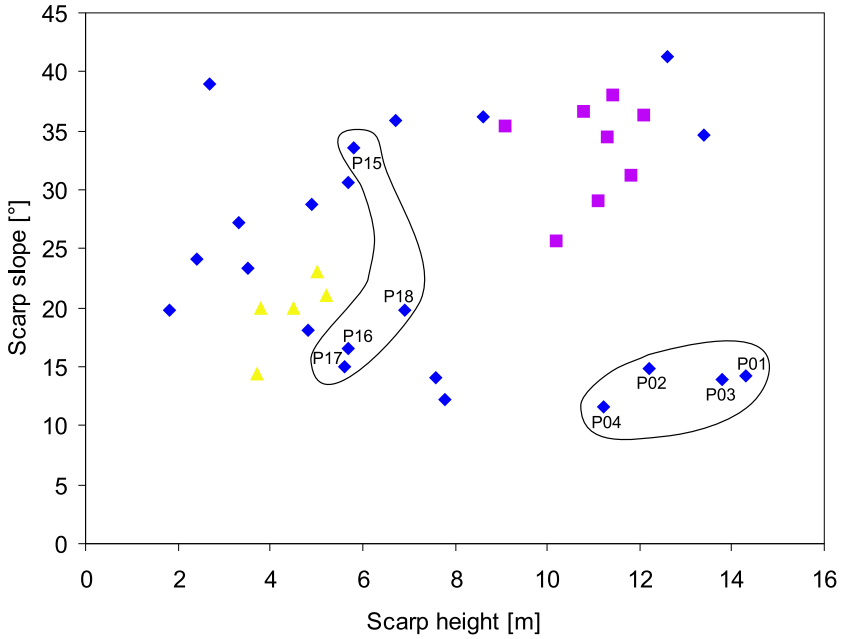

Figure 8.2. Scarp height plotted against scarp slope of all surveyed (diamonds), digitized (squares) and provided (triangles) profiles. For details see text.

Both Figures 8.2 and 8.3 show that only P01–P04 that were also surveyed across the same scarp scatter less; this is also indicated by their quite similar cross-sections (see Fig. 9.1a, p. 136). Profiles 15–18 were also levelled across the same scarp but disperse again stronger. Profile 15 might be seen as an outlier as this profile additionally shows a topographic kink at a x-distance of approx. 10 m in the cross-section (see Fig. A.3, p. 161) but for this conclusion the data base is actually too small. Both Figures also illustrate that the range of products Dt, for which various curves of maximum scarp slope versus initial scarp height can be generated and that include all data used in this work, is not narrowly limited (see also p. 74).

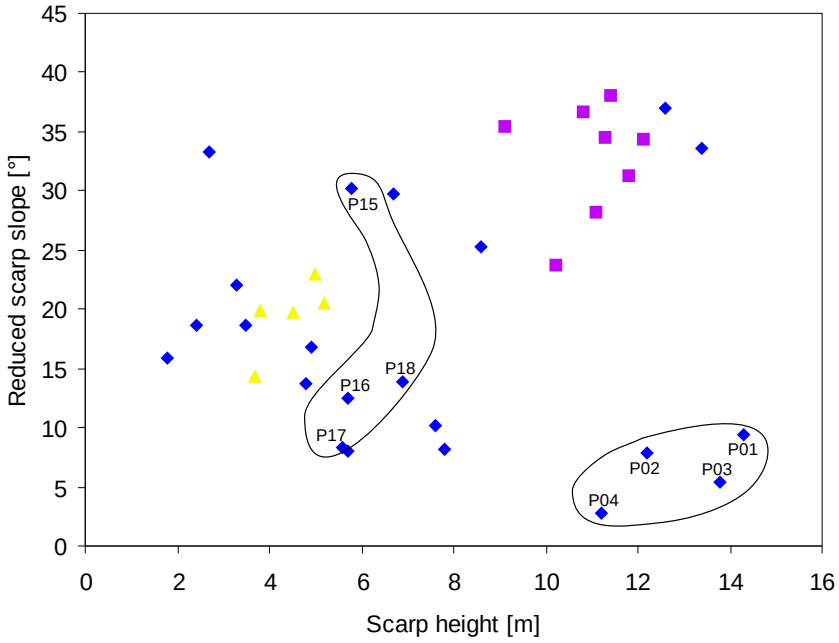

Figure 8.3. Scarp height plotted against reduced scarp slope, i. e., maximum scarp slope minus far-field slope, of all surveyed (diamonds), digitized (squares) and provided (triangles) profiles. For details see text.

8.2 Influence and calibration of initial slope

Table 8.1 lists assumed initial angles at which diffusive erosion starts of the most recent studies on geomorphological dating (see also Sect. 6.4). The span ranges from 29° to 41° and brings up the question, how big the influence of the initial angle on model results is and which the appropriate starting angle for the presented model is.

Four different profiles were used to investigate this influence: P06 (Turtmann valley, CH) was chosen because it is the steepest levelled profile although its environment differs from the other profiles concerning climate, altitude, etc. P09 (Schwerfen) is the youngest and P20 (Blens) is the most gentle and additionally a strong asymmetric profile. P22 as one of the digitized profiles was selected to compare these results to those of Nivière and Marquis (2000). The initial slope analysis was carried out with both constant and variable diffusivity, each with shifting, to recognize any differences. The examined values of initial scarp slope angles span the range from 30° to 50°; following parameter values for the model runs were used: $N = 100, dt = 0.0001, D_0 = 1.00, \tilde{D}' = 0.00, D_{alt} = 0.01, D = 1.4$. In Figures 8.4 to 8.7, which show the influence of the initial slope angle for model runs with a constant diffusivity, the value of Dt equals again the degradation coefficient τ or the model-age, i. e., diffusivity times scarp age. Figures 8.8 to 8.11 show the influence of the starting angle using variable diffusivity; the x-axis also displays the value of Dt.

Figures 8.4a to 8.7a illustrate that enlarging α in model runs with constant diffusivity shifts the curves towards higher degradation coefficients Dt, i. e., the age of a scarp increases

Table 8.1. Initial angles for simulation runs as used in most recent studies. Sources in literature are given.

Initial angle	Source
29°–32°	Enzel et al. (1994)
30°	Enzel et al. (1996)
30°	Carretier et al. (2002a)
31°	Avouac and Peltzer (1993)
31°	Begin (1993)
32°	Avouac (1993)
35°	Carretier et al. (2002b)
35°	Arrowsmith et al. (1998)
40°	Mattson and Bruhn (2001)
41°	Nivière and Marquis (2000)

with increasing initial angle. The minimum standard deviations (SD_{min}) of profiles 6 and 9 (Figs. 8.4a and 8.5a) show a decrease followed by an increase with larger α, i. e., the fit between observed and synthetic profiles decreases. Profile 20 (Fig. 8.6a) has minimum standard deviations lying very closely together; SD_{min} of profile 22 (Fig. 8.7a) decreases at first to remain unaffected by changes in α.

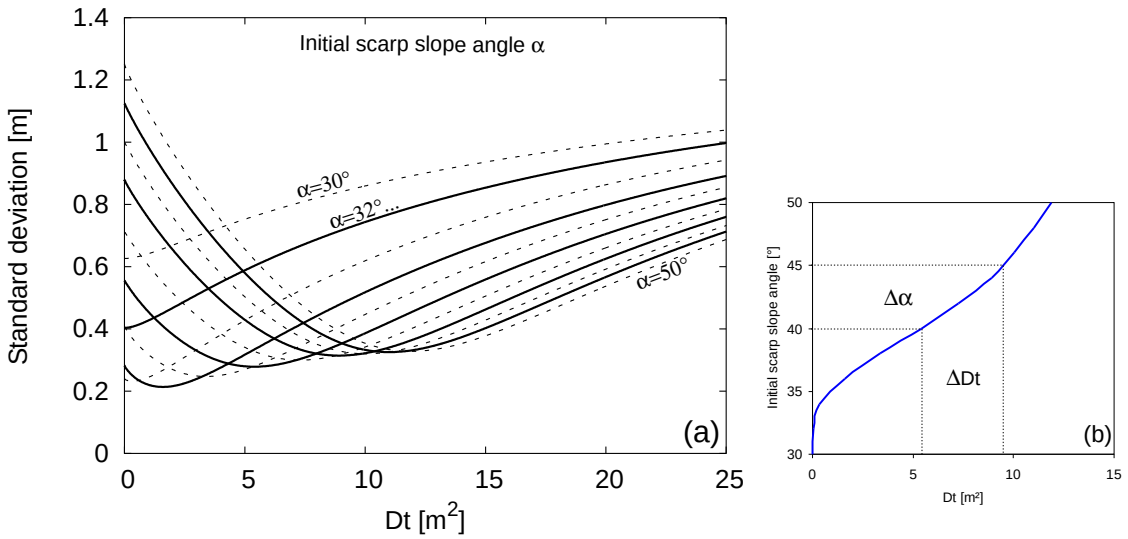

Figure 8.4. Sensitivity of Dt of P06 to initial scarp slope angle α with constant D. (a) Standard deviation plotted vs. Dt assuming different values of the initial scarp slope ranging from 30°–50° as denoted above. (b) Plot of optimum value of Dt as a function of initial scarp slope.

The error ΔDt results from an error $\Delta\alpha$ on the starting scarp slope angle and is for each profile modelled with a constant diffusivity shown in Figures 8.4b to 8.7b. Each example illustrates that an uncertainty on α results in different relative variations of Dt. While

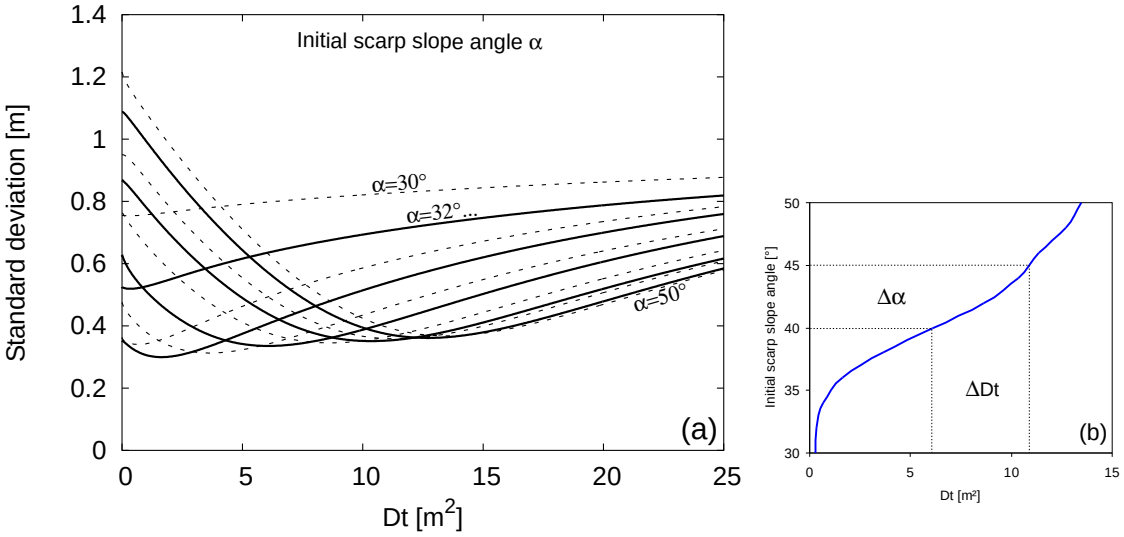

Figure 8.5. Sensitivity of Dt of P09 to initial scarp slope angle α with constant D. (a) Standard deviation plotted vs. Dt assuming different values of the initial scarp slope ranging from 30°–50° as denoted above. (b) Plot of optimum value of Dt as a function of initial scarp slope.

these variations are only little for initial angles <34°, they increase with increasing α for P06 and P09 (Figs. 8.4b and 8.5b). For profiles 20 and 22 (Figs. 8.6b and 8.7b) the variations of Dt are clearly much smaller with increasing α. As Dt is diffusivity times scarp age, these variations are the same for the relative errors on the scarp age.

In the case of model runs with a variable diffusivity, Figures 8.8a to 8.11a illustrate that the general influence of the initial angle is partly comparable to previously described simulations with a constant D: Higher angles α shift the curves towards increasing values of Dt for nearly all examined profiles. Concerning the match between modelled and observed profiles, P06 and P09 show a general decrease in SD_{min} for small α. After a minimum value of SD_{min} with $\alpha = 36°$, the minimum standard deviations increase and the fit between observed and modelled profile decreases (Figs. 8.8a and 8.9a). For both profiles 6 and 9, the curves for $\alpha < 34°$ and $\alpha < 36°$, respectively, initially seem to shift towards decreasing values of Dt, together with decreasing SD_{min}. But examining the results in detail reveals that in fact for P06 the model-age at SD_{min} increases from 0.003 m^2 (30°) to 0.116 m^2 (32°). The curve with an initial angle of $\alpha = 34°$illustrates this again more clearly (Fig. 8.8a). Only P09 shows a slight decrease from 0.023 m^2 (30°) to 0.015 m^2 (32°) and 0.016 m^2 (34°) at SD_{min}. After reaching the minimum value of SD_{min}, both plots show that the curves again shift towards higher degradation coefficients. For the strong asymmetric profile 20 there are remarkable differences between simulation runs with constant and variable diffusivity. Figure 8.10a shows that the curves also shift to higher Dt-values when enlarging α. The standard deviations still lie quite closely together and both, the ranges of Dt and of SD_{min}, are more narrow than for P06, P09 and P22. But compared to Figure 8.6a, each curve shows a clear minimum value of SD_{min}. This difference is also illustrated in Figure 8.12. The values of SD_{min} of profile 22 again first decrease slightly to remain nearly unchanged with higher starting angles (Fig. 8.11a).

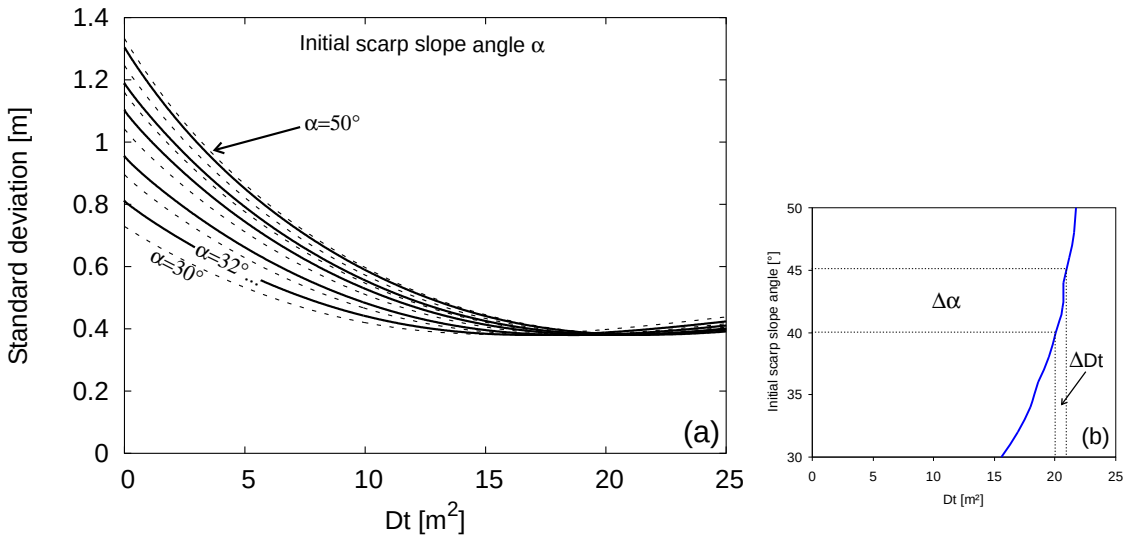

Figure 8.6. Sensitivity of Dt of P20 to initial scarp slope angle α with constant D. (a) Standard deviation plotted vs. Dt assuming different values of the initial scarp slope ranging from 30°–50° as denoted above. (b) Plot of optimum value of Dt as a function of initial scarp slope. Note the different scaling of the x-axis.

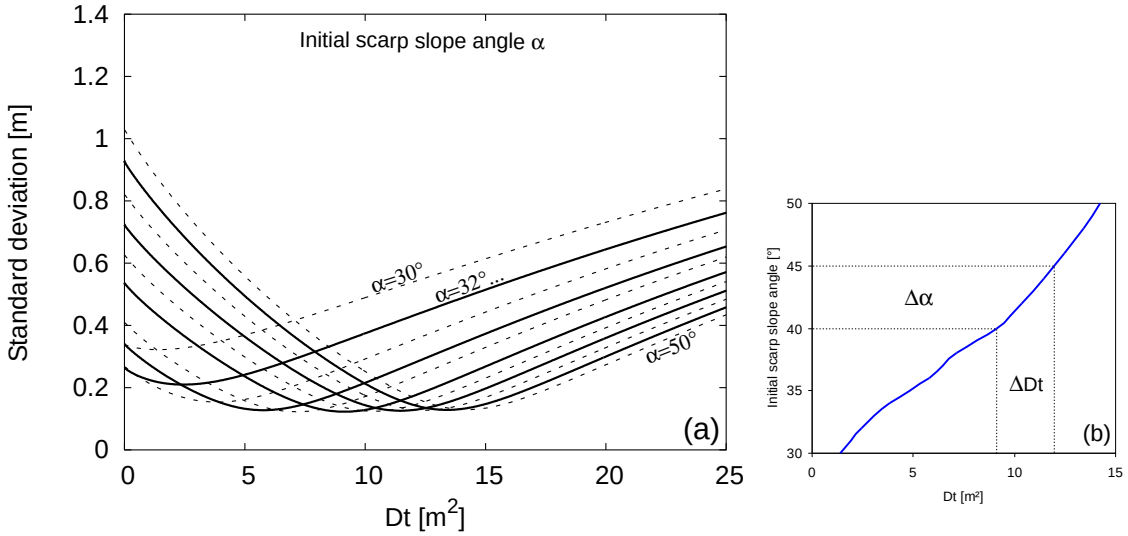

Figure 8.7. Sensitivity of Dt of P22 to initial scarp slope angle α with constant D. (a) Standard deviation plotted vs. Dt assuming different values of the initial scarp slope ranging from 30°–50° as denoted above. (b) Plot of optimum value of Dt as a function of initial scarp slope.

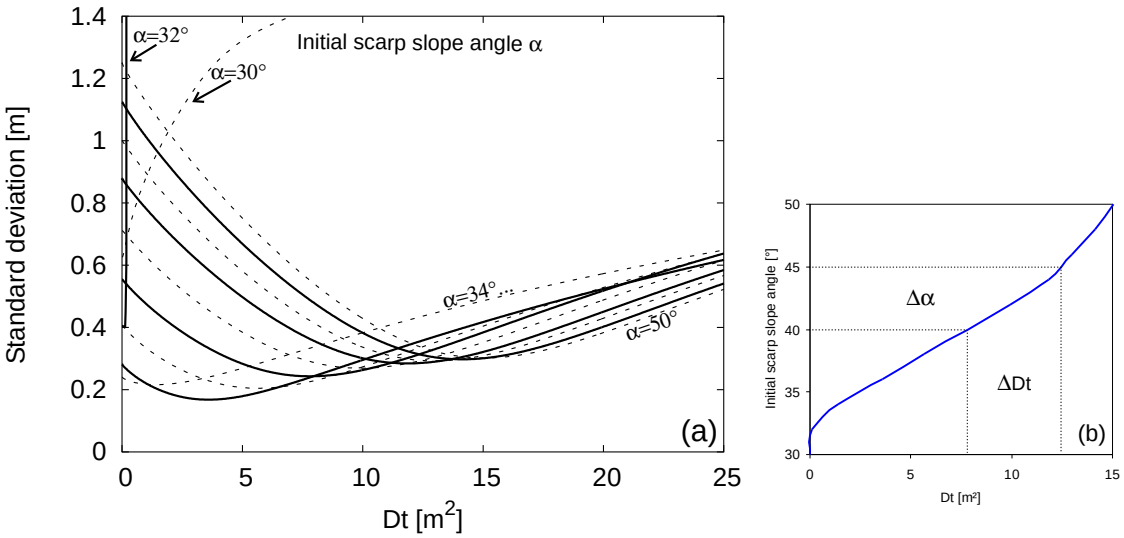

Figure 8.8. Sensitivity of Dt of P06 to initial scarp slope angle α with variable D. (a) Standard deviation plotted vs. Dt assuming different values of the initial scarp slope ranging from 30°–50° as denoted above. (b) Plot of optimum value of Dt as a function of initial scarp slope.

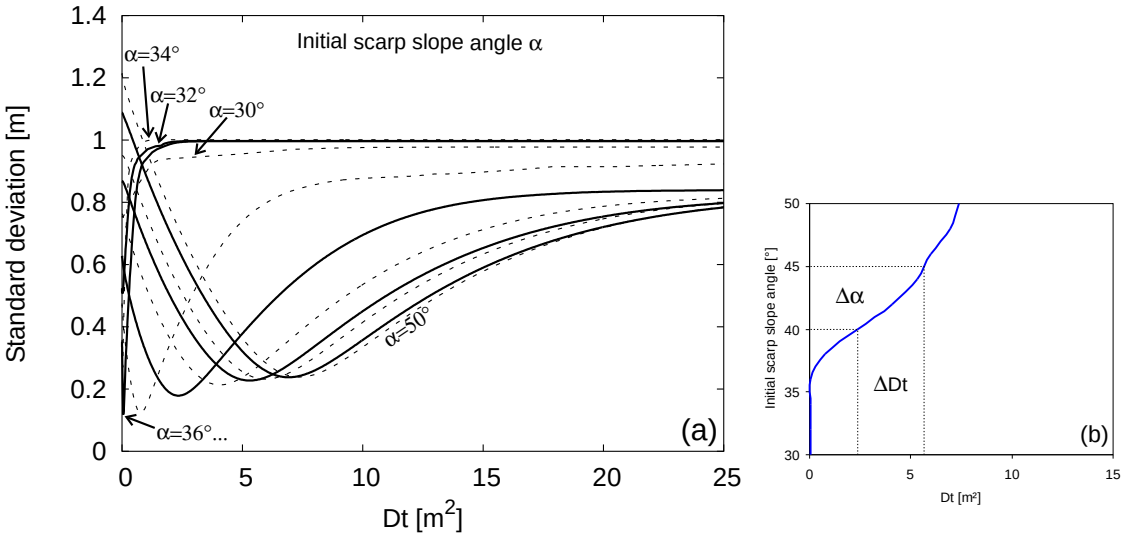

Figure 8.9. Sensitivity of Dt of P09 to initial scarp slope angle α with variable D. (a) Standard deviation plotted vs. Dt assuming different values of the initial scarp slope ranging from 30°–50° as denoted above. (b) Plot of optimum value of Dt as a function of initial scarp slope.

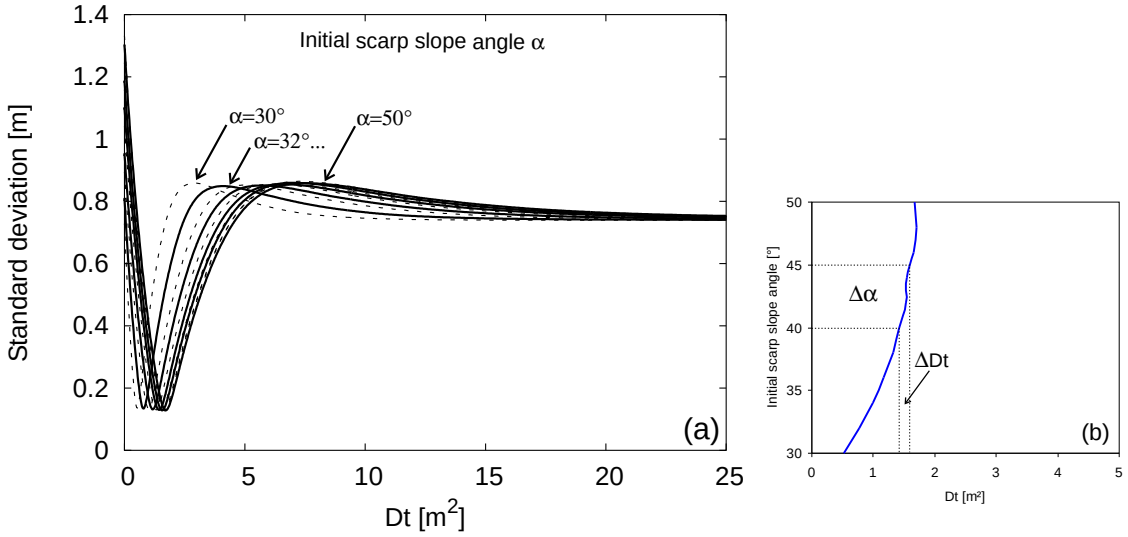

Figure 8.10. Sensitivity of Dt of P20 to initial scarp slope angle α with variable D. (a) Standard deviation plotted vs. Dt assuming different values of the initial scarp slope ranging from 30°–50° as denoted above. (b) Plot of optimum value of Dt as a function of initial scarp slope. Note the different scaling of the x-axis.

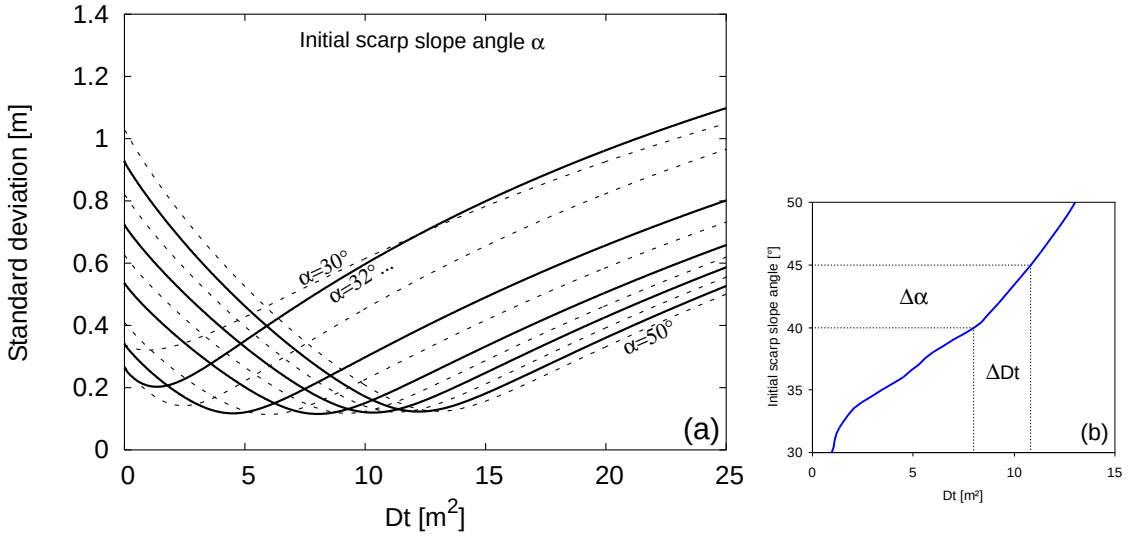

Figure 8.11. Sensitivity of Dt of P22 to initial scarp slope angle α with variable D. (a) Standard deviation plotted vs. Dt assuming different values of the initial scarp slope ranging from 30°–50° as denoted above. (b) Plot of optimum value of Dt as a function of initial scarp slope.

Figures 8.8b to 8.11b again reveal that uncertainties on α result in different relative variations of Dt. For P06 and P09, these variations are only little for initial angles <32° and <36°, respectively (Figs. 8.8b and 8.9b), and increase with larger α. In the case of profile 9, the error ΔDt decreases slightly using a variable diffusivity for modelling. Especially for P20 (Fig. 8.10b) the variations in Dt resulting from $\Delta\alpha$ are again much smaller than those for P06, P09 and P22; the range of ΔDt is comparable to model runs with constant D. For profile 22, the range of the error ΔDt remains the same for simulations with constant and variable diffusivity but again the order of magnitude has varied. As above these variations are in all cases the same for the relative errors on the scarp age.

Comparing all values of Dt in Figures 8.4b to 8.11b reveals that the range of Dt-values decreases from model runs with constant diffusivity to those runs with variable diffusivity for profiles 9, 20 and 22; only the model-ages of P06 increase. The most remarkable decrease is found for P20: The range of Dt decreases for $\alpha = 30°$–$50°$ from 15.6–21.7 m^2 to 0.5–1.7 m^2 which corresponds to a relative decrease of 93.3%. For profiles 9 and 22 this relative decrease is 52.5% and 13.3%, respectively. The relative increase of the range of Dt-values for P06 is 37.8%. Consequently, assuming equal ages implies that the value of D must be lower in model runs with variable diffusivity for P09, P20 and P22; for P06 it must be higher.

Table 8.2. Improvement of fit between observed and modelled profiles using constant and variable diffusivities for initial angles of 36° and 38°. The last column displays the mean improvement for initial angles spanning the whole range 30°–50°. The Table shows the best fit reflected by SD_{min} given in [m].

	constant D	**variable** D	**improvement of fit**	**initial angle** [°]	**mean improvement**
P06	0.213	0.168	0.045	36	0.026
	0.247	0.204	0.043	38	
P09	0.299	0.116	0.183	36	0.113
	0.313	0.124	0.189	38	
P20	0.380	0.131	0.249	36	0.250
	0.380	0.130	0.250	38	
	0.381	0.127	0.254	50	
P22	0.127	0.117	0.010	36	0.007
	0.122	0.114	0.008	38	

Together with mostly lower values of Dt, the values of the minimum standard deviations decrease in model runs with a variable diffusivity (Table 8.2). The results imply that assuming an initial angle between 36° and 38° seems reasonable for the presented range of different scarp shapes. This choice additionally takes into account various underlying materials (see Tables 2.2 and 7.4) and a possible stabilization of a slope due to vegetation roots or a combination of different grain sizes. Profile 6 and 9 show the biggest improvement for a starting angle of 36°; the mean improvement averaged over the whole

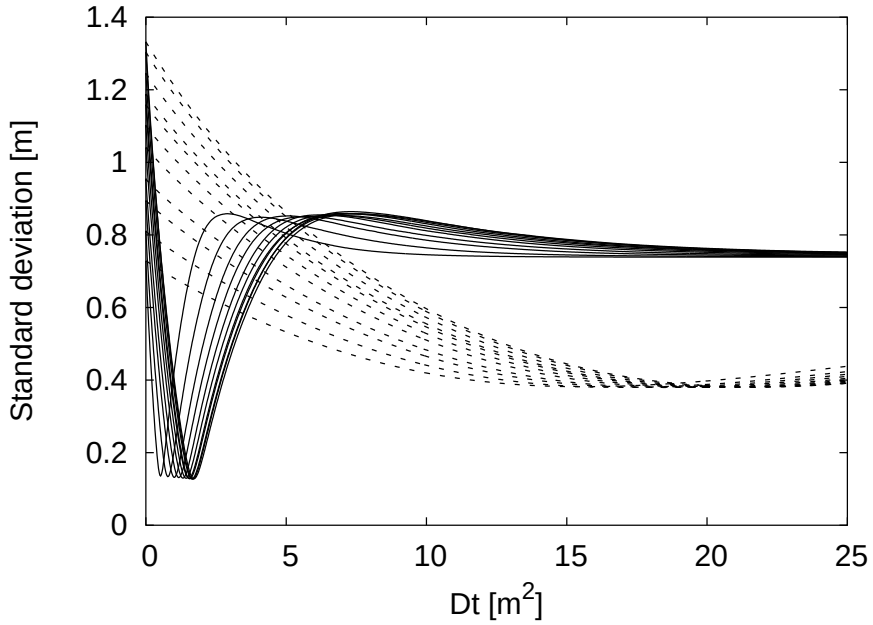

Figure 8.12. Improvement of fit of P20 for various initial angles with constant (broken line) and variable (solid line) diffusivity. For a constant and a variable D, the angles are from top to bottom and from left to right, respectively, 30°, 32°, ... , 50°.

range of angles (30°–50°) is 0.026 m and 0.113 m, respectively. The smallest deviation between the strong asymmetric observed and with variable D modelled P20 is derived with an initial angle of 50°. The mean improvement spanning the whole range of starting angles is 0.250 m. For P20, it is noticeable that the differences in SD_{min} are very small between low and high α for each model run with both constant and variable D (see again Fig. 8.12). The best fit of profile 22 improves mostly with an initial angle of 38°; the mean improvement is only 0.007 m.

8.3 Influence of far-field slope and boundary conditions

The influence of the far-field slope and the boundary conditions was again studied with profiles 6, 9, 20 and 22 for the same reasons as above. As described in Section 4.3 the influence of the model boundary conditions on the pattern of scarp degradation is reduced by giving the scarp a long crest and base. For this reason, all four profiles were lengthened for approx. 15 m at both the crest and the base (Fig. 8.13) so that the regional far-field slope equals ±0°. This analysis was carried out with variable diffusivities and with shifting for each profile: initial angles were set to 36° and 38°. The parameter values used for these simulation runs were again: $N = 100, dt = 0.0001, D_0 = 1.00, \tilde{D}' = 0.00, D_{alt} = 0.01, D = 1.4$. The x-axes again display the degradation coefficient Dt.

Figure 8.14 illustrates that the general tendencies of the elongated profiles 6, 9, 20 and 22 for increasing initial angles α spanning the same range as above (30°–50°) are similar as

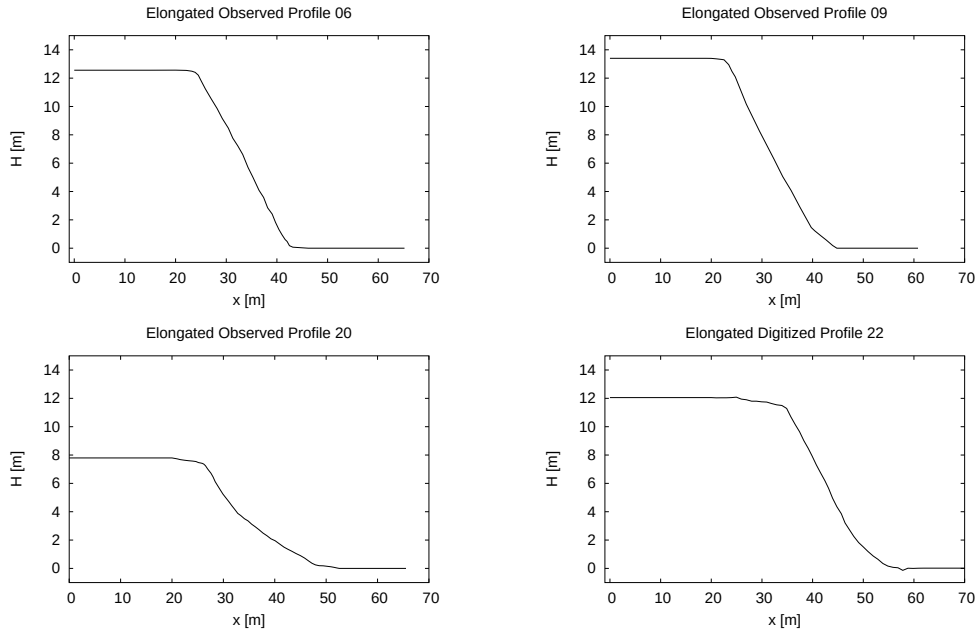

Figure 8.13. Artificially elongated P06, P09, P20 and P22 to investigate the influence of the far-field slope and the boundary conditions which are set to constant elevations at both the crest and the base.

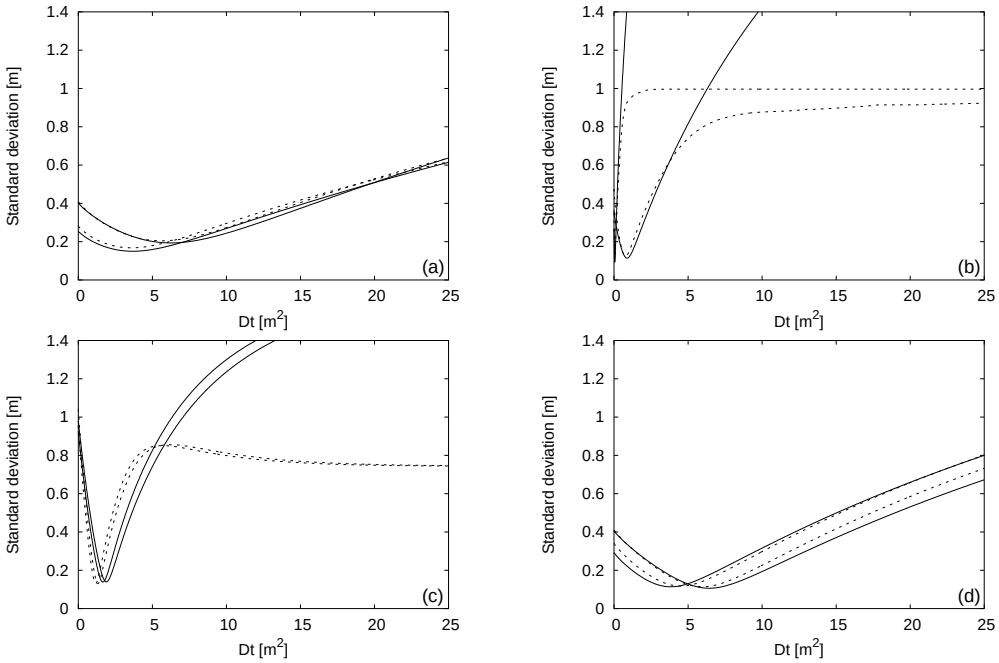

Figure 8.14. Sensitivity of Dt to original (broken line) and elongated (solid line) P06 (a), P09 (b), P20 (c) and P22 (d) with variable D. For both line types each left $\mathrm{SD}_{\min}$ displays $\alpha = 36°$ and the right one $\alpha = 38°$.

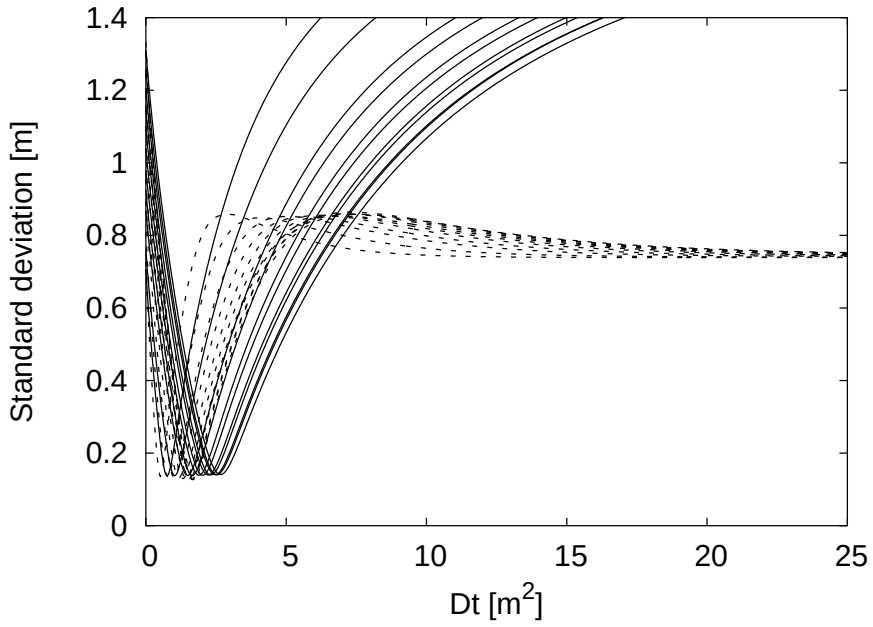

Figure 8.15. Slightly reduced fit of modelled P20 for various initial angles to the observed original (broken line) and elongated (solid line) profile. For both line types, the angles are from left to right 30°, 32°, ... , 50°.

previously described in Section 8.2: All curves shift towards higher degradation coefficients Dt when enlarging α. The match between observed and modelled profiles using starting angles between 30° and 50° slighty increases for P06, P09 and P22 and decreases for P20 compared to model runs with the original profiles. Table 8.3 shows the results for initial angles of 36° and 38°. For the whole range, the fit of profiles 6 and 9 increases at first followed by a decrease after an absolut minimum of the standard deviation with $\alpha = 36°$ has been reached. The values of $\mathrm{SD}_{\mathrm{min}}$ of profile 22 also decrease at first to remain nearly unaffected by changes in α. The curves of the strong asymmetric profile 20 show again clear minimum standard deviations lying closely together for the whole range of initial angles (see also Fig. 8.15), i. e., again the range of Dt is quite narrow and the values of $\mathrm{SD}_{\mathrm{min}}$ are only slightly affected when enlarging α.

Relative uncertainties of Dt (ΔDt) and hence of the age also depend in the same way on variations on α ($\Delta\alpha$) as described above (Fig. 8.16). For all profiles 6, 9, 20 and 22 the curves are similar to those in Figures 8.8b to 8.11b although they are more "undulating" in simulation runs with elongated profiles. For the elongated profile 6 there is no modelling with variable D possible for $\alpha = 30°$ because the deviation between observed and initial profile is already the minimum value and no smaller deviation is yielded after the simulation has started. The variations ΔDt should in all cases be again the same for the relative errors on the scarp age. Comparing all values of Dt with those of the last Section, shows that they all increase relatively compared to simulation runs with the original profiles. For P06 (8.4%), P09 (3.0%) and P22 (0.9%) these changes are quite small. The values of Dt increase most with profile 20 with a relative increase of 46.8%. Hence, the elongation of a profile seems to have no great influence on D assuming equal ages for most profiles. But it might be important when investigating strong asymmetric profiles.

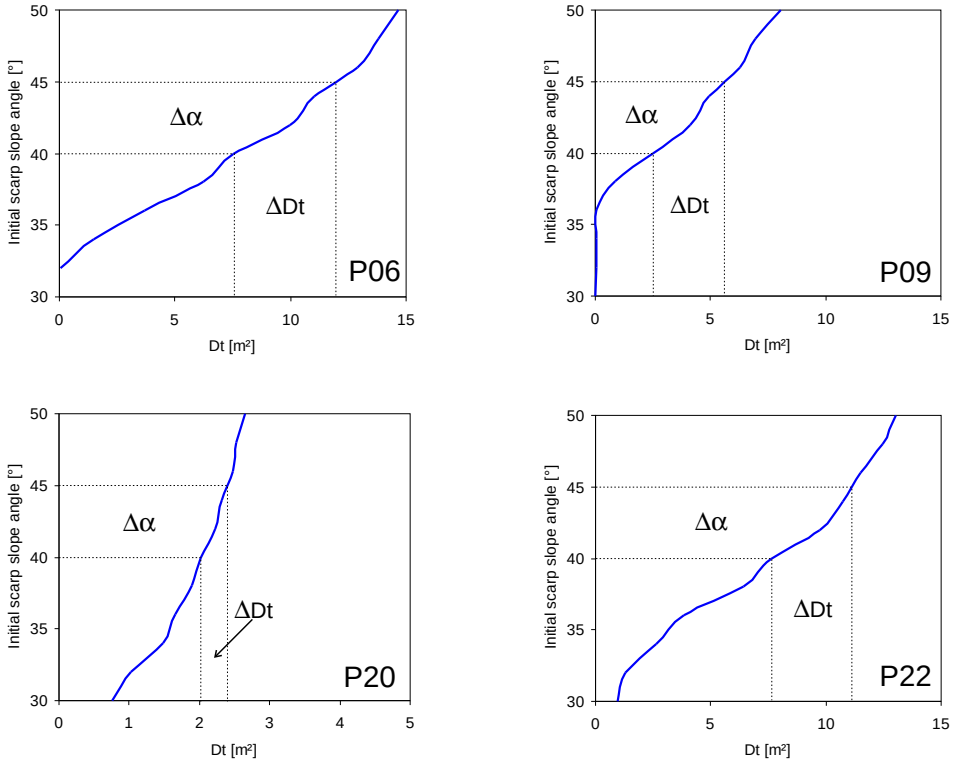

Figure 8.16. Plots of optimum value of Dt as a function of initial scarp slope for elongated P06, P09, P20 and P22. Note the different scaling of the x-axis of P20.

Table 8.3. Improvement of fit between observed and modelled profiles using variable diffusivities, initial angles of 36° and 38° and elongated crests and bases to reduce the influence of boundary conditions. The last column displays the mean improvement for initial angles spanning the whole range (30°–50°). The Table shows the best fit reflected by SD_{min} given in [m]. Note that for P20 the fit decreases slightly.

	original profile	**elongated profile**	**improvement of fit**	**initial angle [°]**	**mean improvement**
P06	0.168	0.150	0.018	36	0.021
	0.204	0.193	0.011	38	
P09	0.116	0.092	0.024	36	0.048
	0.124	0.114	0.010	38	
P20	0.131	0.138	-0.007	36	-0.009
	0.130	0.139	-0.009	38	
	0.127	0.141	-0.014	50	
P22	0.117	0.113	0.004	36	0.010
	0.114	0.106	0.008	38	

The values of SD_{min} of the lengthened profiles 6, 9 and 22 decrease compared to the SD_{min} values of model runs with the original profiles (Table 8.3). Comparing SD_{min} of P06 and P09 reveals that the fit improved mostly again for an initial angle of 36° with a mean spanning 30°–50° of 0.021 m and 0.048 m, respectively. Figure 8.17 illustrates exemplary the improved fit of profile 9 within the range of $\alpha = 30°$–$50°$. As stated above, the misfit between observed and modelled P20 increases with a longer crest and base. The reduction of fit is most for $\alpha = 50°$; the averaged "improvement" is -0.009. The improvement for profile 22 is also again highest with a starting angle of 38° with a small mean value of 0.010 m. For P06 and P22, the mean improvements working with elongated observed profiles and spanning the range $\alpha = 36°$–$50°$ are in the same order of magnitude as the mean improvements between model results using constant and variable diffusivities. The improvement is about half for P09. Up to now, the most remarkable improvement of fit between observed and modelled profiles is achieved between model results with constant and variable D for the strong asymmetric profile 20 (0.250 m; see Table 8.2).

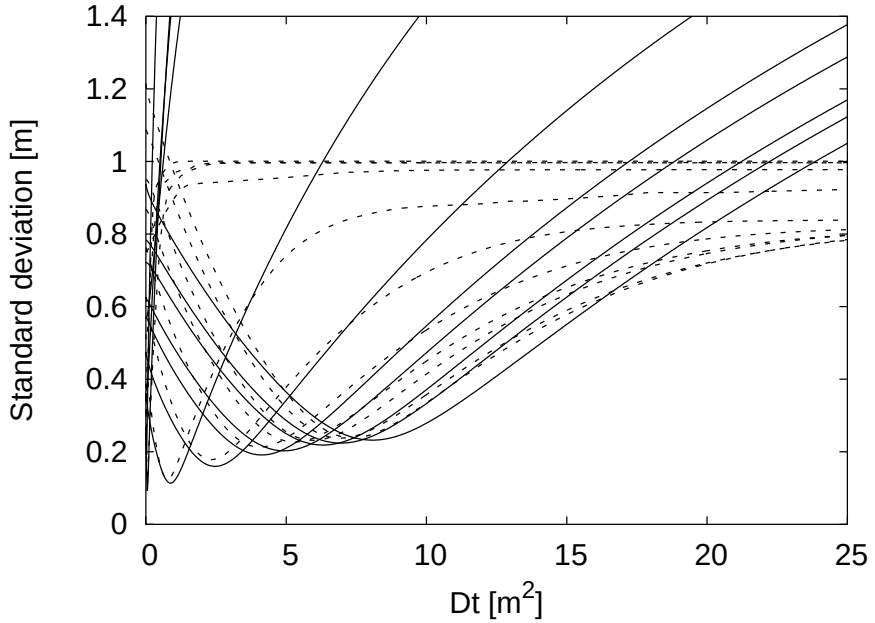

Figure 8.17. Slightly improved fit of modelled P09 for various initial angles to the observed original (broken line) and elongated (solid line) profile. For the original profile the lines are denoted as in Fig. 8.9; for the elongated profile the angles are from left to right 30°, 32°, . . . , 50°.

8.4 Influence of node spacing and time step width

Both parameters, the number of data points N, which determines the node spacing Δx, and the size of Δt, which is the width of a time step dt, are included in R with $R = \Delta t / 2\Delta x^2$. As this factor is involved in the applied solution of the diffusion equation (see Section 6.2), this Section investigates the influence of different values for N and dt on modelling results and age determination.

Table 8.4. The influence of different node spacings investigated for P20. N = number of data points of the initial profile, dx = node spacing [m], $\mathrm{SD_{min}}$ = minimum standard deviation [m], $\tilde{t}$ = model-age [m^2]. The age is calculated using $D = 1.4$ m^2/ka. For details see text.

	dx [m]	**starting $\mathbf{SD_{min}}$ [m]**	**final $\mathbf{SD_{min}}$ [m]**	**$\tilde{\mathbf{t}}$ [m^2]**	**age [a]**	**initial angle [°]**
$N = 50$	0.644	0.974	0.130	1.086	17,085	36
		1.032	0.128	1.173	17,688	38
$N = 100$	0.329	0.955	0.131	1.173	16,825	36
		1.041	0.130	1.321	17,652	38
$N = 200$	0.164	0.960	0.131	1.193	16,870	36
		1.031	0.131	1.365	17,509	38
$N = 500$	0.065	0.963	0.132	1.237	16,859	36
		1.031	0.131	1.382	17,498	38

Table 8.4 shows the effect of tighter node spacing on the resulting model profile and indicates that the results are not strongly dependent on the degree of spatial discretization. For these simulation runs carried out with P20, all other parameters were set to the following values: $dt = 0.0001, D_0 = 1.00, \tilde{D}' = 0.00, D_{alt} = 0.01, D = 1.4$. For both initial angles of 36° and 38°, the final values of $\mathrm{SD_{min}}$ and of $\tilde{t}$, i. e., of the resulting ages, do not differ significantly: (1) For $\alpha = 36°$, the mean standard deviation is $\mathrm{SD_{min}} = 0.131 + 0.001/-0.001$ m and the mean value of $\tilde{t}$ is 1.172 +0.065/-0.086 m^2. The corresponding mean age determined with $D = 1.4$ m^2/ka is 16,910 +175/-85 years. (2) For $\alpha = 38°$, the mean standard deviation is $\mathrm{SD_{min}} = 0.130 + 0.001/-0.002$ m and the mean value of $\tilde{t}$ is 1.310 +0.072/-0.137 m^2. Using $D = 1.4$ m^2/ka yields a corresponding mean age of 17,587 +101/-89 years. The recommended value for N is 100. This value can be increased to achieve a better approximation of the initial angle (see Section 6.5). But it has to be kept in mind that a larger amount of data points also increases the calculation time.

Varying values of dt, i. e., of the time step width Δt, do also not show great effects on model results Table 8.5). Simulations runs using again profile 20 were carried out with all remaining parameters set to: $N = 100, D_0 = 1.00, \tilde{D}' = 0.00, D_{alt} = 0.01, D = 1.4$. Again for both starting angles (36° and 38°), there is no significant difference in $\mathrm{SD_{min}}$. $\tilde{D}'$ and $\tilde{t}$ are, respectively, smaller and larger for $dt = 0.1$ than for the other values of dt. But the resulting ages determined with both parameters and with, e. g., $D = 1.4$ m^2/ka, are in the same order of magnitude. (1) For $\alpha = 36°$, the mean standard deviation is $\mathrm{SD_{min}} = 0.133 + 0.007/-0.002$ m. The mean value of $\tilde{t}$ is 1.697 +1.603/-0.524 m^2. Using $D = 1.4$ m^2/ka yields a corresponding mean age of 16,893 +246/-70 years. (2) For $\alpha = 38°$, the mean standard deviation is $\mathrm{SD_{min}} = 0.132 + 0.008/-0.002$ m and the mean value of $\tilde{t}$ is 1.883 +1.817/-0.562 m^2. The corresponding mean age determined with $D = 1.4$ m^2/ka is 17,696 +132/-46 years. It is recommended to choose a value of $dt = 0.0001$ which was also used in the remaining calculations. Furthermore it is advised to retain the values of $D_0 = 1.00, \tilde{D}' = 0.00$, and $D_{alt} = 0.01$ for simulation runs.

Table 8.5. The influence of different values of dt investigated for P20. SD_{min} = minimum standard deviation [m], $\tilde{t}$ = model-age [m^2]. The age is calculated using $D = 1.4$ m^2/ka. Starting deviations are for $\alpha = 36°$ and $\alpha = 38°$ 0.955 m and 1.041 m, respectively. For details see text.

	final SD_{min} [m]	**$\tilde{D}'$**	**$\tilde{t}$ [m^2]**	**age [a]**	**initial angle [°]**
$dt = 0.1$	0.140	1.609	3.300	17,139	36
	0.140	1.474	3.700	17,828	38
$dt = 0.01$	0.132	3.384	1.660	16,831	36
	0.130	3.393	1.740	17,684	38
$dt = 0.001$	0.131	4.870	1.180	16,846	36
	0.130	4.510	1.331	17,668	38
$dt = 0.0001$	0.131	4.894	1.173	16,825	36
	0.130	4.542	1.321	17,652	38
$dt = 0.00001$	0.131	4.895	1.173	16,823	36
	0.130	4.542	1.321	17,650	38

8.5 Calibration of the model

One of the biggest influences on the age determination is given by the choice of the diffusivity D. The calibration of the diffusivity was carried out again with both constant and variable diffusivities and with shifting for each profile. The parameters for these simulation runs were set as in Sections 8.2 and 8.3: $N = 100, dt = 0.0001, D_0 = 1.00, \tilde{D}' = 0.00, D_{alt} = 0.01$. For all runs an initial angle of $\alpha = 38°$ was selected. The most promising calibration was thought to be achieved using the data of Nivière et al. (1998) and Nivière and Marquis (2000) which are digitized and provided profiles with rather reliable age approximations that were dated geomorphologically and a determined value of the diffusivity $D = 1.4$ m^2/ka. As their investigation was carried out under very similar climatic conditions, it was assumed that this value of D is also valid for the research areas of the presented work.

A first model run was carried out with constant diffusivity and with shifting. Consequently, the results should at least yield correct age ranges for the digitized and provided profiles 21–33a of known ages. But model results revealed that the age determination scattered significantly and yielded much younger ages than expected; this is illustrated for the sets P21–P24 and P25–P28 in Figure 8.18. The mean of the calculated ages of the three sets P21–P24, P25–P28 and P29a–P33a with assumed ages of 19 ka, 33 ka and 50 ka yielded results of 3.1 ka, 1.4 ka and 4.4 ka, respectively (Table 8.6). Hence, the value of $D = 1.4$ m^2/ka appears to be too high for the presented model when applying constant diffusivity.

Simulation runs were next carried out for the same profiles with a variable diffusivity, also with shifting. Assuming initially the same value for D=1.4 m^2/ka at the midpoint of the scarp, yielded a similar scattering of determined ages (Fig. 8.19). The averaged

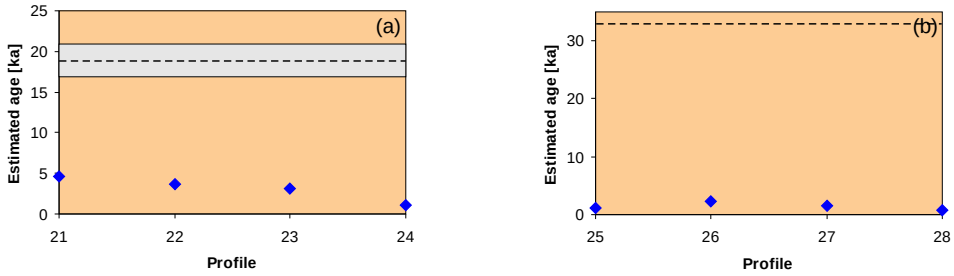

Figure 8.18. Age scatter of (a) P21–P24 and (b) P25–P28 with constant D=1.4 m^2/ka. The broken line displays the known age of the scarp; in (a) the shaded area is the tolerance.

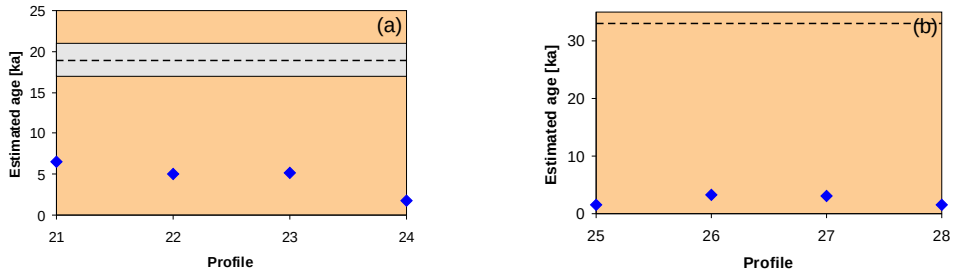

Figure 8.19. Age scatter of (a) P21–P24 and (b) P25–P28 with variable D; D=1.4 m^2/ka is set at the midpoint. The broken line displays the known age of the scarp; in (a) the shaded area is the tolerance.

age determinations of the three sets of profiles with the most reliable known ages are each higher than with a constant D (Table 8.6). The ages for D set at the crest or base did not yield better results. Table 8.6 reveals that the determined ages are still significantly younger than the assumed ages of the scarps. The Table also shows that there is no consistency in the relation between D and the age concerning the relative differences between determined and assumed ages. Applying the value of D =1.4 m^2/ka at the midpoint yields for set P21–P24 an age which is about one fourth of the assumed age; for set P25–P28, the calculated age is more than tenfold too small; and for set P29a–P33a, the determined age should be approximately sevenfold higher. Furthermore, set P25–P28 shows that D in this case decreases downslope instead of increasing as initially suggested. Comparing each single result with the according shape of a profile shows that this is valid for all profiles where the crest is rounder than the base and which is in agreement with the applied modification. As above, the value of D = 1.4 m^2/ka determined by Nivière and Marquis (2000) for a similar climatic environment seems to be again too high for the presented model when applying variable diffusivity.

Next, it was proven if the model could be calibrated taking the profiles with known approximate ages and finding the suitable diffusivity which yields these ages. Table 8.7 shows the calibration results of simulation runs with constant diffusivity: For instance, the set P21–P24 yields a mean diffusivity of 0.2 m^2/ka with a mean of the corresponding ages of 19.0 ka. Taking this value of D = 0.2 m^2/ka and calculating each age of a profile with it,

Table 8.6. Mean age determinations for the sets of profiles with known ages calculated with constant and variable diffusivity ($D = 1.4$ m^2/ka). In model runs with variable D it was assumed that this is the value at the top, the midpoint or the base yielding different ages because the values of D_0 and D' differ for each setting too.

Profiles	approx. age [ka]	calc. age [ka] with const. D	var. D	
P21–P24	19±2	3.1	top	3.4
			mid	4.6
			base	5.9
P25–P28	33	1.4	top	4.2
			mid	2.4
			base	0.5
P29a–P33a	50	4.4	top	5.0
			mid	6.6
			base	8.2

gives a mean of 22.0 ka for the whole set. This was done for all three sets. Table 8.7 also reveals that the range of determined diffusivities lies between 0.06 m^2/ka and 0.2 m^2/ka. The calculated mean is $D = 0.12 + 0.08/ - 0.06$ m^2/ka.

Table 8.7. Mean determinations of D [m^2/ka] for the sets of profiles with known ages modelled with constant diffusivity.

Profiles	approx. age [ka]	mean deter. D	mean deter. age [ka]	mean calc. age [ka]
P21–P24	19±2	0.20	19.0	22.0
P25–P28	33	0.06	33.1	33.2
P29a–P33a	50	0.10	50.2	62.1

The model was next calibrated for the use with a variable diffusivity D. Table 8.8 shows that D, for instance, set at the midpoint, ranges between 0.10 m^2/ka and 0.36 m^2/ka with a calculated mean of $D = 0.21 + 0.15/ - 0.11$ m^2/ka. The last column of Table 8.8 lists again the calculated mean ages for each set of profiles.

All in all it is finally to say that the determined diffusivities are much smaller than other D-values under similar climatic conditions (compare Table 5.1 on p. 44). It is hence questionable how reliable the estimated ages, presented in the following Section, are.

Table 8.8. The mean determinations of D [m^2/ka] for the sets of profiles with known ages modelled with variable diffusivity and assuming that this is the value at the top, the midpoint or the base. Each assumption yields different ages because the values of D_0 and D' differ for each setting too.

Profiles	approx. age [ka]	mean deter. D		mean deter. age [ka]		mean calc. age [ka]	
P21–P24	19±2	top	0.25	top	18.6	top	18.9
		mid	0.36	mid	18.3	top	18.0
		base	0.43	base	19.1	top	19.1
P25–P28	33	top	0.18	top	33.3	top	32.9
		mid	0.10	mid	32.2	top	33.0
		base	0.02	base	32.6	top	33.8
P29a–P33a	19±2	top	0.14	top	50.8	top	50.1
		mid	0.18	mid	50.4	top	51.5
		base	0.23	base	50.1	top	50.1

8.6 Scarp modelling and age determination

The next step is to combine scarp modelling with dating: All profiles 1–33a were simulated with the "GeomorphDating-Model" applying a variable diffusivity and including the shifting of the synthetic profiles after each calculation step. The parameter values were set as follows: $N = 100, dt = 0.0001, D_0 = 1.00, \tilde{D'} = 0.00, D_{alt} = 0.01$. As determined in above Section 8.5, the scarp ages were estimated applying a value for the diffusivity of $D = 0.21 + 0.15/ - 0.11$ m^2/ka. At first, all initial profiles were generated by the model, i. e., the starting profile showed the smallest starting deviation between synthetic and observed profile. The initial angle was then set to α =38°.

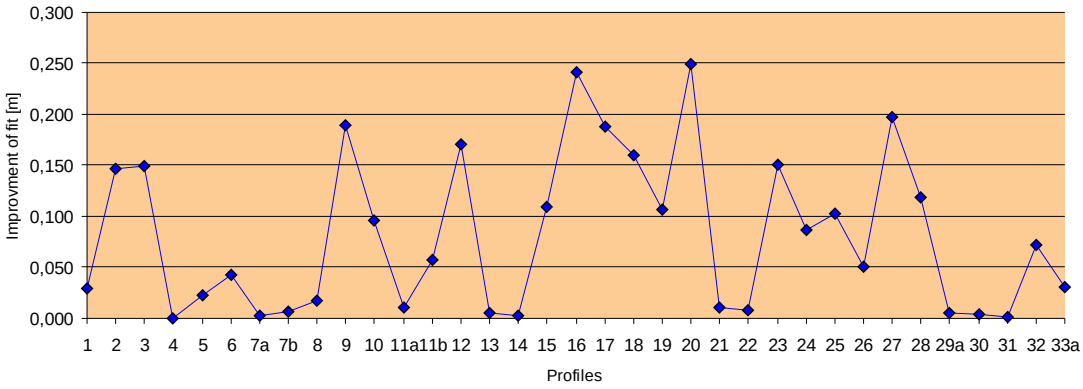

Figure 8.20. Improved fit of all profiles 1–33a using a variable D and compared to modelling with a constant D. D was set to 0.21 +0.15/-0.11 m^2/ka.

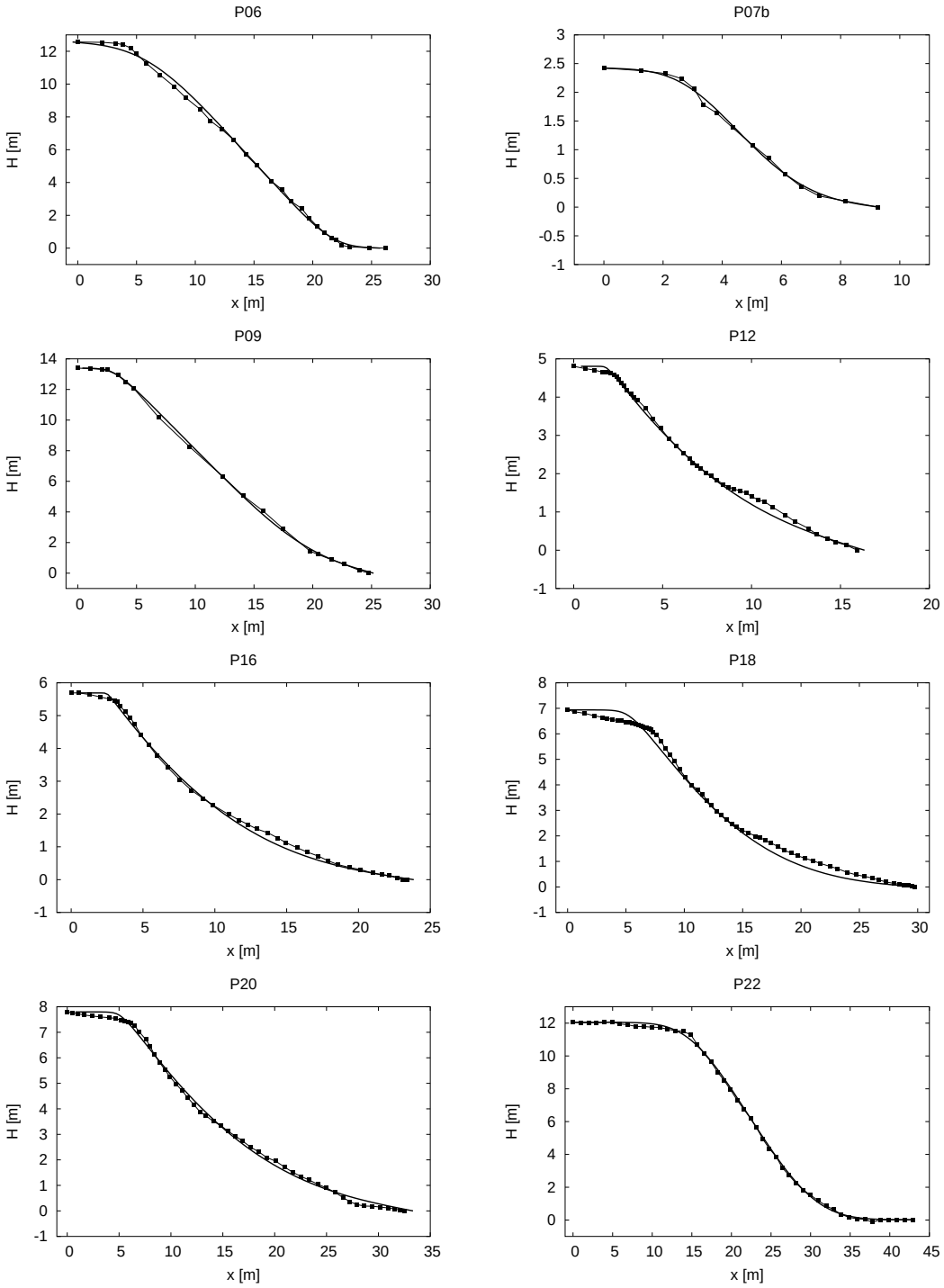

Figure 8.21. Model results of P06, P07b, P09, P12, P16, P18, P20 and P22 simulated with variable D. The observed profiles are displayed as connected squares, each square is a measured point. The solid lines are the modelled profiles with the smallest deviation. Note the different scalings of both axes.

All synthetic profiles show a better fit to the observed ones if using a variable instead of a constant diffusivity. (Fig. 8.20). The mean SD_{min} for profiles modelled with constant D and variable D is 0.201 m and 0.118 m, respectively. The average improvement is 0.083 m which is within the range of typical misfit between observed and modelled profiles (Avouac, 1993). The fit has most improved for P20 as a strong asymmetric profile. Analysing the results illustrated in Figure 8.20 reveals that the improvement is in fact highest for such asymmetric profiles. A selection of model results as cross-section profiles is shown in Figure 8.21. The remaining model results are collected in Appendix C from page 169 on. The Figures reveal that the maximum misfit almost always occurs (1) where the topography is quite rough and this cannot be eliminated by modelling, and (2) where the upper and lower far-field slope is $> 0°$which occurs very often. Upper and lower roundings or sharper edges as well as most of the intermediate part of profiles are matched very closely. Both types of profiles are included in the modelling with either sharp crests and rounded bases or vice versa. Table 8.9 lists the resulting age estimates applying the above determined value of the diffusivity of $D = 0.21 + 0.15/ - 0.11$ m^2/ka and shows that only some of these estimated ages are within an acceptable range of the approximated ages. An acceptable range was chosen to be roughly ±10–15% of the approximated age based on the introductory words about other dating methods (see Sect. 1.2 on p. 2). For the determination of the approximated ages of the surveyed scarps P1–P20, see also Section 7.2. The results indicate that in fact the calibration of the model did not succeed which limited the further investigation significantly and which is further discussed in the following Chapter 9.

Table 8.9. Age results of P1–P33a applying the determined $D = 0.21 + 0.15/ - 0.11$ m^2/ka.

Profile	approx. age [ka]	Estimated age [a] applying D = 0.10 m²/ka	D = 0.21 m²/ka	D = 0.36 m²/ka
1	?	1,439,586	625,517	399,885
2	?	1,041,615	496,007	289,338
3	?	1,769,175	842,464	491,438
4	?	1,414,140	673,400	392,817
5	?	28,230	13,443	7,842
6	<14	37,581	17,896	10,439
7a	<14	44,385	21,136	12,329
7b	<14	12,729	6,061	3,536
8	<14	30,974	14,750	8,604
9	>0.028	49,686	23,660	13,802
10	127–300	81,647	38,879	22,680
11a	127–300	1,702	810	473
11b	127–300	9,474	4,511	2,632

continued on next page

continued from previous page

Profile	approx. age [ka]	Estimated age [a] applying $D = 0.10\ m^2/ka$	$D = 0.21\ m^2/ka$	$D = 0.36\ m^2/ka$
12	70–127	81,414	38,769	22,615
13	18–70	25,392	12,092	7,053
14	18–70	31,604	15,050	8,779
15	<127	36,968	17,604	10,269
16	<127	131,187	62,470	36,441
17	<127	79,272	37,749	22,020
18	<127	130,365	62,079	36,213
19	<127	308,939	147,114	85,817
20	<127	247,128	117,680	68,647
21	19±2	91,310	43,481	25,364
22	19±2	70,876	33,750	19,688
23	19±2	71,525	34,060	19,868
24	19±2	24,963	11,887	6,934
25	33	22,857	10,884	6,349
26	33	44,832	21,349	12,453
27	33	41,807	19,908	11,613
28	33	22,415	10,674	6,226
29a	50	132,518	63,104	36,811
30	50	81,422	38,773	22,617
31	50	69,707	33,194	19,363
32	50	107,920	51,390	29,978
33a	50	71,915	34,245	19,976

If the calibration would have succeeded and a dating would have been possible, it was additionally planned to define confidence intervals for the age determination which are determined graphically following, e. g., Avouac (1993); Avouac and Peltzer (1993), Arrowsmith et al. (1998), and Carretier et al. (2002b). For completeness, this procedure is briefly explained at this point for following researchers on this topic. Such confidence intervals are estimated by relating the range of acceptable fitting to the RMS values lower than $SD_{min} + 5$ cm (Fig. 8.22). According to Avouac (1993), it appears that for profiles across scarps formed in sandy to cobbly deposits the minimum standard deviation is in the order of 10 cm which can consequently be regarded as the typical misfit between observed and modelled profiles. Consequently, the choice of acceptable standard deviations within 5 cm is considered to be representative of such typical misfits if one half of this size is taken to be a measure of significance. The reasons for these misfits are mainly the roughness of the topographic surface and the inadequacy of the applied model or the idealized initial shape and not measurement errors. The latter produce systematic mis-

fits, so that unrealistic uncertainties on the model parameters are provided by a standard least squares inversion that assumes normally distributed misfits (Avouac, 1993). Above confidence intervals on Dt do not depend on the distribution and number of surveyed data points. According to Avouac (1993), such intervals provide an objective and quantitative evaluation of the precision with which the degradation coefficient is determined although a statistical meaning cannot be assigned to them. As Arrowsmith et al. (1998), the author agrees and would have also adapted this criterion. Avouac (1993) additionally pointed out that the assessment of ΔDt, of the uncertainty of the minimum Dt, may be improved if values are compared which were obtained from different profiles surveyed across different similarly oriented scarps of the same age or across the same scarp. Carretier et al. (2002b) also retained this criterion to estimate objectively how precise morphological ages are determined if topographic levelling with a precision of approx. 5 cm is taken into account. The observed profiles of this study have been levelled with a high precision total station which is accurate to less than 5 cm. This would have justified the adaption of the value $\mathrm{SD}_{\mathrm{min}}$+5 cm to define such confidence intervals for estimating morphological ages. Carretier et al. (2002b) determined the morphologic age by $\frac{\Delta Dt_{\mathrm{min}}+\Delta Dt_{\mathrm{max}}}{2}$ and its uncertainty δDt by $\Delta Dt_{\mathrm{max}} - Dt$.

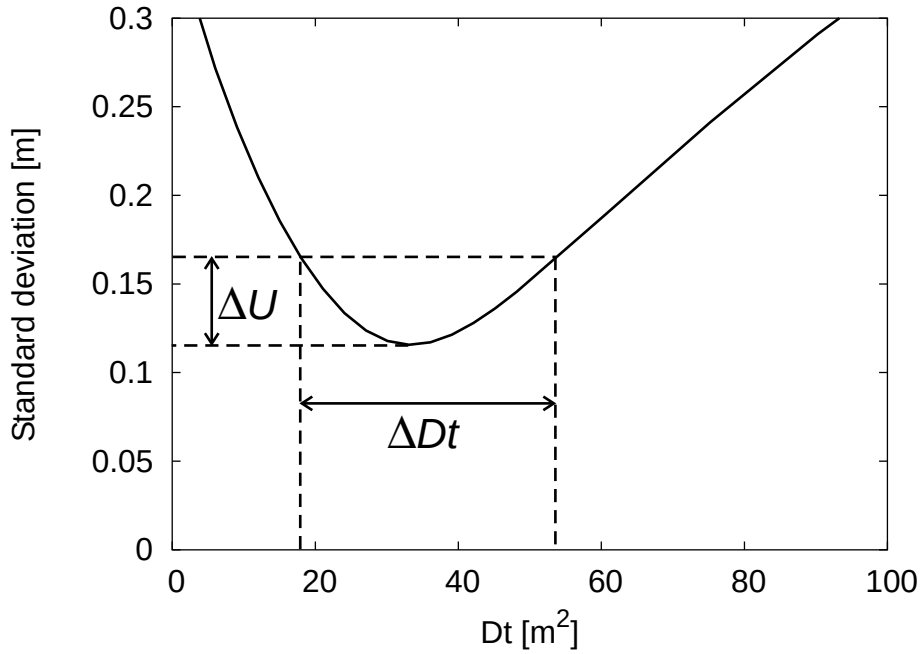

Figure 8.22. Graphical determination of accepted degradation coefficients Dt within a confidence interval ΔDt of $\mathrm{SD}_{\mathrm{min}}$ + 5 cm (ΔU). The curve was produced with P09 modelled with variable D and shifting; the initial angle was 36°. Adapted from Avouac (1993).

Chapter 9

Discussion

9.1 Evaluation of the modified diffusion-type dating model

Validating and evaluating the presented model and relating its behaviour to natural scarps, must address on the one hand to the values and meaning of the model parameters which should be, as far as possible in this case, related to and confirmed by those measured in other studies. On the other hand, model results and model behaviour should be compared with observations and tested against natural conditions. General restrictions of geomorphological dating as correct site and scarp selection are discussed in Section 9.2. It is to say at this point that two problems bedevil all attempts to evaluate models of hillslope evolution: (1) convergence and equi-finality, i. e., there is no certainty that the forms were produced in the manner proposed under the model, and (2) inheritance, i. e., it cannot be assumed that the same processes have acted throughout the period of time over which the hillslope has reached its present form.

9.1.1 Model behaviour

As the results of Section 8.2 have shown the minimization of the standard deviation does not put any constraint on the initial slope angle. Consequently, it must be determined independently. This was also discussed by Avouac (1993) and Nivière and Marquis (2000) who showed that enlarging the initial angle α shifts the curve to higher degradation coefficients but that the minimum value of the standard deviation between synthetic and observed profile remained the same; this was for the most part confirmed in the presented study. The fact that steeper initial angles result in higher values of Dt is one hint that a correct solution of the diffusion equation was applied: the higher a starting angle is, the more time does a scarp need to degrade to recent angles. Taking into account the slope heights and angles as well as the underlying materials, it was assumed that initial angles between 36° and 38° seem to be reasonable values.

In this study, hillslopes are assumed not to be isolated from the surrounding landscape and therefore to be open systems. Material is added constantly to the system and the upper boundary elevation remains the same. At the lower boundary, material is removed

which also results in an unchanged elevation. It was examined how and if the boundary conditions influence the modelling by elongating some profiles such that the upper and lower far-field slopes are ±0°. The results of Section 8.3 indicate that with starting angles of 36° or 38° the influence is positive in most cases (P06, P09, P22), i. e., the fit between observed and modelled profiles improves. But this does not seem to be valid for strong asymmetric profiles (P20). It is important to emphasize at this point that especially upper far-field slopes ±0° seldom represent natural conditions. The mean upper and lower far-field slope of all natural scarps examined in this study is 0.3° and 6.4°, respectively. For profiles 15-18 levelled across the same scarp the averaged upper and lower regional slope is 5.0° and 0.2°, respectively. Due to this inconsistency an artificial elongation of the observed profiles was not carried out although the match between observed and modelled profiles improved in most cases. But to verify the statement that the influence of upper and lower boundary conditions is only little for strong asymmetric profiles, the modelling should be carried out with a larger number of such strong asymmetric profiles. This study did not investigate hillslopes assumed to be closed systems or if model results are affected by other boundary conditions, e. g., variable elevation.

The influence of node spacing and width of time steps was also examined. As Section 8.4 showed, both parameters do not significantly affect the model results which proves that the correct solution is implemented in the model.

9.1.2 Age determination and improvement of fit

As already indicated in Section 8.6, the resulting age determinations show that it was not possible to calibrate the model properly. On the one hand, the range of acceptable age estimates is for most profiles too large to present the "GeomorphDating-Model" as a reliable dating tool. On the other hand, at least the profiles levelled across the same scarps (P1–P4, P13 and P14, P15–P18, and P19 and P20) should yield similar values of Dt and, using the same diffusivity, of the scarp age. Table 8.9 showed that this did not succeed for any set. In addition, even a relative dating seems to be impossible as, e. g., model runs with P15–P18 should result in higher Dt-values than model runs with P19 and P20 as the former are older than the latter (see p. 97).

But it has to be remarked that the determined values of Dt are significantly smaller in the presented study where there are comparative values. This is the case with the digitized profiles of this work taken from Nivière and Marquis (2000) which should consequently yield similar values of Dt. Smaller Dt-values result in smaller diffusivities D to yield equal ages. Compared to the determined diffusivity of Nivière and Marquis (2000) which is 1.4 m^2/ka, the value of D in this study is with a mean of 0.2 m^2/ka almost tenfold smaller which might be due to different lithology and vegetation cover stabilizing a slope (see Sect. 9.2). On the other hand, reviewing existing diffusivity estimates from former studies (Table 5.1 on p. 44) would imply higher values of D in the investigated temperate regions as D appears to decrease with increasing arid environments. However, the assumption of similar D-values in similar climatic regions could not be confirmed. The presented diffusivity estimate contributes to the often discussed large range of D-values.

Several reasons might be responsible for the failed calibration and as other studies have already reported, geomorphological dating should be generally handled very carefully. Several authors mentioned, e. g., the high dependence on site selection and the difficulties in finding the adequate diffusion coefficient. These items are discussed separately in Section 9.2. The question whether the applied modification is the proper way to describe the geomorphological processes acting upon a scarp is also discussed separately in Subsection 9.1.3. However such limitations are, and with the initial assumption that the diffusion equation including a height-dependent D is a valid description of scarp degradation, it would be unreasonable to compare simulated hillslopes with a single natural hillslope. This work tried to calibrate the model with a few scarps with roughly known ages to apply it to various scarps of different ages and shapes. The highly site-specific usage of this dating method and of the value of D could not be eliminated and is still one of the biggest constraints of the model. It is anyway necessary to derive some representative against which to test model predictions concerning geomorphological dating through forward modelling. This is especially important as this fairly young research field is growing and more modified models are to be tested. In addition, any ages derived from such models of scarp degradation should either incorporate or define the uncertainties involved in obtaining an age estimate.

Regarding the simulated profiles without any dating assessment reveals at least that the predicted hillslopes bear qualitative resemblance to actual hillslopes. Those profiles which have a rounder crest than base yield a negative $\tilde{D}'$ and, hence, D', i. e., the diffusivity decreases downslope for P01–P04, P06, P10, P11a, P21, P25-P28, P29a and P31. Such a shape indicates an upper reactivation of a scarp due to a new incisive period. This was also discussed by Nivière and Marquis (2000) who detected a couple of reactivated profiles. The authors proved that scarps consisting of a composite signal were probably reactivated either in the lower part due to new incisive episodes or in the upper part because of landsliding. The composite signal was determined by using the slope distribution method proposed by Avouac (1993) (see Sect. 5.2, p. 52). This method was not carried out in the presented study but the digitized profiles 25–28 are four of such two-stage profiles taken from Nivière and Marquis (2000). Hence, the results imply that such a decreasing diffusivity in downslope direction might also be an indicator for a reactivated scarp with the crest being more rounded and consequently older than the base.

Even with an improved fit between observed and modelled profiles, it is questionable whether such a relative little improvement justifies the introduction of a modified diffusion equation throwing up new problems although the old problems with the linear approach have not been solved sufficiently. However, applying the geomorphological dating model to simulate the evolution of scarps and to date them by forward modelling averages several thousands of years of erosion, and, as stated by Nivière and Marquis (2000), one must always bear in mind that the profiles shown are only a snapshot of this erosional process. Because all dating techniques may be subject to considerable error, reliability should be assessed by stratigraphic consistency between results of different dating methods or of the same method. More than one age determination is required to establish reliable age control. In doing so, numerical ages from one or more of the initially mentioned physico-chemical methods (see Sect. 1.2) are preferred although they may have large, non-analytical errors. But relative-dating and correlation methods are important because they

can provide age control in the absence of numerical techniques, or they can be used to evaluate the numerical ages. To provide dating control and to evaluate the reliability of specific age estimates, surficial geological studies and local time-calibrated stratigraphies are both vital in the study of geomorphological dating. The introduced height-dependent diffusivity of this work can thereby be seen as another part of the jigsaw in the discussion of nonlinear models for scarp dating.

9.1.3 Modelling of hillslope processes

Mathematical models as the one presented here are limited by the accuracy with which an equation describes the functioning of a particular process. Beyond the multitude of possible processes are questions of scale, persistence, ecological processes like continuing changes of vegetation, and climatic changes with a variety of durations and effects on landforms. In addition, many processes depend on feedback and thresholds. Simulating the evolution of hillslopes or scarps by applying a diffusive-type model relies on a highly simplified representation of the geomorphic processes acting upon a slope. The process types controlling material transport downslope are still not well understood and their rates often not known (Arrowsmith et al., 1998). Nash (1986) already noted that the diffusion model should probably be rejected for scarps formed by the degradation of slope wash as such overland flow erosion is not accurately described by the diffusion equation. The advective aspects of hillslope evolution (such as slope wash) are included in the diffusion equation (see Sect. 4.3) but according to Tucker and Bras (1998), it does not consider variations in flow depth as one moves progressively away from the drainage divide. Hence, it is an important limitation to assume that runoff is uniform across a scarp. The presented modified diffusion equation incorporates this item in a very simple way: an increasing water amount downslope leads to an increased diffusivity downslope. As already mentioned, it finally depends on the curvature of the slope if material is eroded or deposited. According to Tucker and Bras (1998), the closest natural analog for the use of the diffusion equation would be a semi-arid, low- to moderate relief landscape with predominantly Hortonian overland flow (spatially uniform runoff generation), sparse vegetation, and loose surface soils.

One of the decisive factors for the modification of the linear diffusion equation was the observation that the crest of a profile is often less rounded than the base. This was also detected by Nivière and Marquis (2000) whose studies were a main connecting thread of this work. The authors questioned whether it is diffusion that mainly controls the evolution of the shape of a scarp and related this to the vegetation cover which increases the surficial material coherency, i. e., diffusion varies in space. Consequently, the crestal erosion may be occurring in discrete stages rather than as a continuum. This would result in profiles with a smaller crestal curvature while the bases are always rounded. The degree of rounding at the top depends on the last removal of crestal material.

Each modified diffusive-type model has to be calibrated with different values of D as they span a very wide range (see Table 5.1). Several studies already introduced modifications of the linear diffusion equation (see Sect. 5.2) trying to improve the modelling and hence the dating which is directly coupled to the model results. They are all based on field observations and ample evidence which suggest that realistic models of landform evolution

must be nonlinear. Often a nonlinear mass transport is included in such nonlinear models as the value of D seems to be strongly scale dependent on large dimension scales (Hanks, 1999). A dependence of the diffusivity on the height as the total scarp offset, was suggested by Pierce and Colman (1986) and others. But for processes modelled by the linear diffusion equation, the diffusivity D should not change with scarp height. This is not to be mixed up with the presented modification: The presented idea was that D depends on the height but always in the same way no matter if a scarp is, say, <10 m or >25 m. In fact, the problem of dependency of D on scarp height is still poorly understood. Scarps higher than 25 m often exhibit hummocky topography which indicates that degradation might be controlled by nondiffusive processes such as slumping and creep, or by sapping due to an elevated water table on the upthrown side of a fault scarp. Such scarps will appear to have a greater diffusivity than is predicted by the diffusion modelling because sediment transport will be more rapid. The transition from diffusive to nondiffusive processes will probably vary regionally due to climate and aggregate properties of the sediments.

There is no doubt that there appears to exist some kind of relation between both the height and D. And nonlinear mass transport which has already been involved in geomorphological dating is a function of slope and not of height. The introduction of a height-dependent diffusivity and the failure of calibration now questions whether such a linear modification still reflects the geomorphological processes acting upon a slope in a proper way. Or is the diffusion equation in general an adequate description of slowly acting scarp degradation in temperate humid climate? In most former studies it has been proven that the linear diffusion equation adequately describes such processes if the scarp is located in an arid or semi-arid region. The diffusion equation includes the diffusive (such as creep and rainsplash) as well as the advective (such as slope wash) aspects of hillslope evolution. The presented approach is based on the simple assumption that the amount of water of steady rainfall increases downslope which in turn increases D, hence the runoff-dominated erosion plays an important role. But in the progress of sediment down a single slope there may be periods of storage, short-term as between rainstorms, and somewhat longer in colluvial deposits. During such rainstorms, the effectiveness of surface wash is increased in at least four ways: raindrops are larger, infiltration capacity is more likely to be exceeded (Hortonian runoff), the water table is more likely to rise to the surface (saturation runoff), and rate of transport increases more than linearly with volume of flow. Furthermore, one has always to be aware of spatial variability in sediment sources and transport even on small scale slopes, i. e., various processes operate in different relative proportions on different scarps. According to Horton (1945), an unchanneled hillslope represents a "belt of no erosion" within which overland flow strength is below a threshold necessary for erosion (see also Fig. 2.2). Such potential thresholds for channel initiation include runoff generation, overland flow shear stress, and landsliding. Several models have explored that concept of a runoff erosion threshold, e. g., Willgoose et al. (1991a), Howard (1994b), Kirkby (1994), Rinaldo et al. (1995), and Tucker and Slingerland (1997). Tucker and Bras (1998) demonstrated that the existence of such a runoff-erosion threshold leads to greater curvature of the hillslope forms which are then solely controlled by creep transport, and that valley formation begins where (1) the threshold is exceeded, e. g., in landscapes with a robust vegetation cover (Dietrich et al., 1993; Kirkby, 1994; Howard, 1996), and (2) there is sufficient erosive power that diffusive processes do not inhibit incision.

Summarizing the previous considerations it is indeed a difficult task to optimize and calibrate a model which includes numerous processes in more or less only one equation with only one parameter left to average the rate of all these such single processes.

9.2 Limitations of geomorphological dating

This Section shall describe and discuss known and new constraints on the use of geomorphological dating. What are the main sources of error? What, e. g., unrecognized factors unrelated to time, additionally influence the scarp morphology? And how sensitive is such a model by which scarp degradation is estimated to these errors?

(1) Calibration of D: One of the biggest difficulties is the calibration of the diffusivity D as the most significant variable in the model which finally determines the age. The choice of D should incorporate (a) episodes with different climate together with (b) certain slope deposits. While climate might, for instance, lead to an increased D, soil development and vegetation may progressively stabilize slopes which causes D to decrease through time.

(a) Calibrating D assumes that it is constant through time, but climatic fluctuations have been dramatically during the past 100 ka due to glacial cycles. This may have caused diffusivity to fluctuate too. In order to calibrate the model properly, the selected value of D must average and reflect such dramatic climatic changes including rainfall, vegetation cover, sun-facing azimuth, annual freeze-thaw cycles, etc. This is particularly important for scarps with an assumed age >10 ka, i. e., for pre-Holocene scarps when the climate was significantly different from the present climate. Nivière and Marquis (2000) investigated the temporal representativeness of D suggesting that it decreases during colder climates from (in their study) 1.4 m^2/ka to a value of only 0.5 m^2/ka. On the other side, a wetter climate seems to increase D which is indicated by the numerous values of D which have already been determined (see Table 5.1). Fundamental climatic fluctuations can only be surly excluded if morphologic dating is limited to scarps younger than 10 ka. But even in very similar climates and regions, the value of D appears to differ too much to apply diffusivities which were determined at one specific site.

(b) As pointed out in Section 6.3, different diffusivities D have to be used for different materials, i. e., in principle higher values of D for scarps formed in cohesionless and erodible lithologies.

In Section 8.5 it was tested if the model can be calibrated accurately. The results revealed that no diffusivity could be determined which fits all investigated profiles. As pointed out above, the match between observed and synthetic profile could be improved applying the modified diffusion equation. But a correct value of D can, if at all, possibly only be ensured and validated by masses of field data of scarps with known ages which again limits the easy applicability of this dating method. This study confirms once again that values of D must indeed be determined for each specific site.

(2) Measurement errors: Different levelling techniques must be carefully calibrated to yield some kind of standardized profiles. Already small variations in the measurement of the scarp height, slope and above all of the upper and lower curvature result in relative large variations of the inferred value of the morphologic age Dt. At what point does the surveyor mark the "start" of the profile, particularly if the far-field slope is unequal 0° which is true for most cases (see Sect. 8.3)? Some of such measurement errors should be eliminated when levelling profiles with a high precision total station as carried out in this study although it is questionable if such a levelling technique is not unnecessarily too accurate for the presented dating model and what can be achieved by it.

(3) Type of scarp: Not all kinds of scarps are suitable for this dating model. Terrace risers as those scarps investigated in this study can be seen as relative simple scarps mostly with a simple evolutionary history. Such terrace scarps include abandoned fluvial cutbanks as well as abandoned wave-cut bluffs where eroded material is not removed by fluvial or wave undercutting but accumulates at the scarp base. This must not be mixed up with a lower boundary condition where material leaves the system to retain a constant elevation (see above Section 9.1): Material still accumulates below the scarp but leaves the system as soon as there is a slope at the lower boundary. A simple development may also be valid for single fault scarps, either produced by normal or reverse faulting. But including such fault scarps in the analysis would have complicated the simple development in the case of repeated faulting or splaying faults resulting in composite scarps and multiple scarps, respectively, with complex initial morphologies and with again seldom equally inclined crest and base. Although it has to be kept in mind that terrace risers can evolve in a more complicated way too. Such reactivated scarps were already discussed above.

(4) Scarp shape: Next to the evolutionary history it might be important how high or steep a slope is. The morphology of a scarp is highly dependent on the underlying material, and coeval scarps in different lithologies have different scarp shapes. Scarps formed in cemented deposits will have steeper initial angles and will thereafter always be steeper than scarps of the same age formed in unconsolidated materials. Consequently, those steeper scarps will appear younger. Bull (1984) pointed out that diffusivity-type modelling is only appropriate for scarps whose maximum slopes are less than 35°. And Hanks et al. (1984) showed that angles as low as 4° still comply with the diffusion model. Although it should be remarked that certain low slope angles might cause degradation to halt, and that such slopes may be stable and unchanged for very long time periods (Begin, 1993). Applying the model to these slopes is not valid and results in too young age estimates. In this study, scarps with slopes ranging between 12° and 41° were investigated and as in most other studies concerning geomorphological dating, a limitation based on the scarp slope angle could not be recognized. There are no remarkable differences in modelling scarps with certain maximum slopes.

(5) Site selection: The problems in field data lie in finding field situations that satisfy the conditions of the model: Highly variable scarp morphology results in also highly variable morphology-derived age estimates and probably only a sufficient sample size constraints this factor. But how many profiles then do represent the entire structure of a scarp? Hanks et al. (1984) on the other side remarked that even a large set of profiles cannot be blindly averaged to obtain the "representative" profile. Regarding profiles 1–4, 12 and 13, 15–18, and 19 and 20 reveals that there is a remarkable similarity for profiles levelled

across the same scarp (Fig. 9.1). The positions along the strike of each scarp were selected arbitrary but in an approx. distance of at least 30 m. Hence, the general shape of a scarp appears to be determinable even by single profiles without the need of large sample sizes. But other questions might arise, e. g., in Figure 9.1c, why is P18 bigger than P15–P17 although measured in a smaller distance to the mouth of the Odenbach into the Rur? It is hence necessary to consider not only a scarp but also its geologic setting and environment. This discussion only emphasizes that site selection is indeed a very important item no matter how many profiles are levelled across the same scarp.

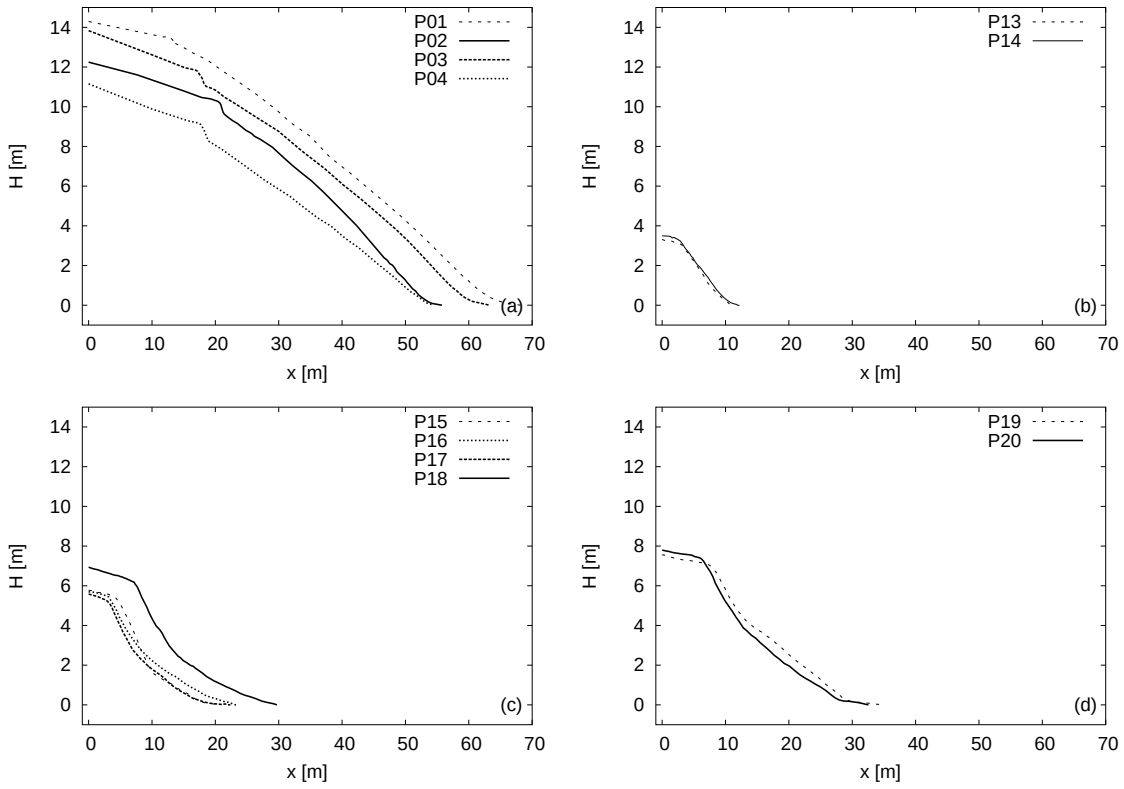

Figure 9.1. Comparison of observed profiles levelled across the same scarps. (a) P01–P04, Frankenforst, (b) P13 and P14, Hausen, (c) P15–P18, Blens, and (d) P19 and P20, Blens. The Figure illustrates the resemblance of each suite of profiles.

Further limiting factors concerning the site selection are the locations of the profiles themselves: Scarp faces notched by gullies or channels and profiles displaying local irregularities of small fans deposited at the base of scarps, or of trapped eolian sediments are unsuitable and should be avoided (Nash, 1980b; Hanks and Andrews, 1989; Burbank and Anderson, 2001). In addition and particularly in the regions studied in this work, it has to be ensured that the shape of a scarp is not disturbed by Man. It is essential to take account of the impact of human activity on the landscape which has been increasing at an accelerating rate, especially since the Industrial Revolution and the introduction of modern farming techniques. Human agency can influence natural landscape by creating new landforms and more important by altering the rate of geomorphic processes. Agriculture, lumbering and

the construction of settlements can all cause dramatic changes in land use which in turn may greatly change the susceptibility of the landsurface to erosion. Some studies proved this by comparing pre- and post-Man rates or simply rates of natural and accelerated erosion (Young and Saunders, 1986). The increase in atmospheric pollutants during the last century has increased the amounts of precipitated solute concentrations which in turn could affect rates of weathering. A doubling of weathering rates due to anthropogenic alteration of Earth-atmosphere hydrochemistry is suggested by Selby (2000). But the major impact of Man is the increase of erosion rates by surface wash and its consequences for river sediment loads and total denudation. Following Young and Saunders (1986) this increase is due to (1) clearance of natural forests and its replacement by non-intensive agricultural use accelerating denudation 1.5–3 times, (2) a change to intensive agriculture with adequate soil conservation accelerating denudation up to 5–10 times, and (3) a change to agriculture with poor soil conservation including overgrazed pastures with denudation rates to be accelerated by 4–16 times on steep slopes and by around 10 times on gentle slopes. So the impact of Man might not only influence the shape of a scarp but at last also the value of the diffusivity which is thought to average *all* erosive activity on a slope. And this influence is particularly difficult to assess, especially if different scarps from different regions are to be examined.

Chapter 10

Conclusions and outlook

To determine the age of slopes and the timing of the events that are responsible for the forms of hillslopes as they exist at the present time from their present-day morphology is not simple. Many researchers who worked in the field of geomorphological dating demonstrated the potential of the diffusion equation model for estimating the ages of many scarps (e. g., Colman and Watson, 1983; Nash, 1986; Arrowsmith et al., 1996, 1998; Hanks, 1999; Nivière and Marquis, 2000). But all of them also emphasized more or less strongly the difficulties and limitations of this dating method and that it should be used with considerable care. In the presented study, these difficulties and limitations were found to be present in a way that at this point of time, the model does not seem to be an alternative to efforts to provide age dating by other more accurate dating techniques. As Chapter 8 has shown, the absolute dating in years is mostly arbitrary. The method works with some scarps, with others not. Many authors pointed out that several profiles of one and the same scarp should be measured to achieve reliable results. This could not be confirmed in the presented study. In fact, already one and same scarp yielded profiles which differed considerably.

However, a reliable dating technique should, in the opinion of the author, be a method without such enormous elements of uncertainty. The value of D determines the age of an examined scarp, and this is hence even the most serious limitation of the model. Regarding Table 5.1 on page 44 already reveals the range of diffusivity values even in similar climates. In this study only terrace risers were investigated which might be seen as an additional limitation in comparison with other related studies which mainly carried out geomorphological dating of fault scarps. The reason for this confinement was to ensure that only simple scarps were included in the examination which was thought to ensure a possible calibration. Most terrace risers appear to have a less complicated evolution history than fault scarps. This is especially valid for the research areas with their relative low degree of tectonic activity. Hence, recognizable fault scarps are seldom produced by a single event but are rather the result of continuous movements.

Concerning dating, it is in most cases anyway necessary to use several dating methods because of the limited range of a given technique, the presence of appropriate materials, and the need to check the reliability of any given dating technique by using another method. The results of this study showed that although geomorphological dating might

be a valuable tool for determining the age of certain landforms, it is not appropriate for all hillslopes and must be used with much caution, especially if modified slightly. In this case, the inadequate calibration and too many limitations constrain a possible wider application of the proposed geomorphological dating.

As an outlook, the effects of climate, material and form on the diffusivity D should be determined more exactly. More rounding rates must be found for dated transport-limited scarps under various climatic conditions, with a variety of underlying material but also, e. g., aspects. Mainly the geomorphological processes must be better understood to evaluate other modifications or different transport laws and should be the subject of more thorough investigation, both observationally and analytically. The presented model could be tested with various fault scarps, i. e., with normal and reverse, single event and cumulative fault scarps. Although the calibration is still questionable. Following researchers on this topic might formulate other modifications which also improve the fit between asymmetric observed and synthetic profiles, e. g., exponential instead of linear increase of D or height-dependent transport laws. As the model was limited to one dimension, it could be investigated if an extension in two dimensions improves the model. Finally, the scarps in the presented study were not examined with regard to reactivation as described by Nivière and Marquis (2000). An investigation especially of the strong asymmetric profiles might be interesting and could be used to verify the mentioned supposition that diffusivities decreasing downslope imply scarps that were reactivated in the upper part of the slope.

Acknowledgements

I wish to thank Prof. Dr. St. Hergarten who supervised this study and who is thanked for his helping support, many discussions and his patience in explaining me a part of the world of geophysics. Thanks to Prof. Dr. H.-J. Neugebauer for the pleasant working conditions and several conservations. This work has benefited from discussions with and help of many colleagues within the Geodynamics Working Group. Thoughtful reviews and critical comments by several members of the Research Training Group (GRK) 437 including lectures and other scholarship holders supported the success of this study. Thanks to Prof. Dr. R. Dikau, Prof. Dr. N. Froitzheim and Prof. Dr. L. Plümer for participating in my examining board.

I am grateful to C. Karny, I. Roer, I. Wolf and R. Elias for their support in field work and data acquisition. Thanks to Bertrand Nivière for providing profile data and to Mrs. Reibold from the City of Schwerfen for her detection work.

Special thanks to R. Elias who supported me throughout the whole PhD thesis and who often helped me to keep on going. The same goes for my parents and especially for my mum who always believed in me. I owe both of you a lot! And last but not least thanks to all my friends who were really good listeners.

This study is related to the project C 5 of the Research Training Group (GRK) 437 "Landform – a structured and variable boundary surface" at the University of Bonn and was financially supported by the German Research Foundation (DFG).

References

AG Boden (1994) Bodenkundliche Kartieranleitung. E. Schweizerbart'sche Verlagsbuchhandlung (Nägele u. Obermiller), Stuttgart, 4th edn. 392 pp.

Ahnert F (ed.) (1964) Quantitative Models of Slope Development as a Function of Waste Cover Thickness. Paper presented at the meeting of the IGU Commission on Slope Evolution.

Ahnert F (1966) Zur Rolle der elektronischen Rechenmaschine und des mathematischen Modells in der Geomorphologie. Geogr. Z. 54: 118–133.

Ahnert F (1970a) Brief description of a comprehensive three-dimensional process-response model of landform development. Z. Geomorph. Suppl. 24: 11–22.

Ahnert F (1970b) A comparison of theoretical slope models with slopes in the field. Z. Geomorph. Suppl. 9: 88–101.

Ahnert F (1970c) Functional relationships between denudation, relief and uplift in large mid-latitude drainage basins. Am. J. Sci. 268: 243–263.

Ahnert F (1971) A general and comprehensive theoretical model of slope profile development. Univ. Maryland Occasional Papers in Geography 1: 95 pp.

Ahnert F (1973) COSLOP 2 – A comprehensive model program for simulating slope profiles. Geocom Programs 8: 99–122.

Ahnert F (1976) Brief description of a comprehensive three-dimensional process-response model of landform development. Z. Geomorph. Suppl. 25: 29–49.

Ahnert F (1987) Process-Response Models of Denudation at Different Spatial Scales. Catena Suppl. 10: 31–50.

Ahnert F (1996) Einfhrung in die Geomorphologie. Eugen Ulmer Verlag, Stuttgart. 440 pp.

Anderson DA, Tannehill JC, Pletcher RH (1984) Computational fluid mechanics and heat transfer. Series in computational methods in mechanics and thermal sciences. McGraw Hill, New York. 599 pp.

Anderson RS (1994) Evolution of the Santa Cruz Mountains, California, through tectonic growth and geomorphic decay. J. Geophys. Res. 99 (B10): 20,161–20,174.

Anderson RS, Humphrey NF (1990) Interaction of weathering and transport processes in the evolution of arid landscapes. In: Cross TA (ed.), Quantitative Dynamic Stratigraphy, pp. 349–361. Prentice Hall, Englewood Cliffs, N. J., USA.

Anderson TC (1977) Compound faceted spurs and recurrent movement in the Wasatch Fault zone, north central Utah. Brigham Young Univ. Geol. Stud. 24: 83–101.

Andrews DJ, Bucknam RC (1987) Fitting Degradation of Shoreline Scarps by a Nonlinear Diffusion Model. J. Geophys. Res. 92 (B12): 12,857–12,867.

Andrews DJ, Hanks TC (1985) Scarp degraded by linear diffusion: Inverse solution for age. J. Geophys. Res. 90 (B12): 10,193–10,208.

Armstrong A (1976) A three-dimensional simulation of slope forms. Z. Geomorph. Suppl. 25: 20–28.

Arrowsmith JR (1995) Coupled tectonic deformation and geomorphic degradation along the San Andreas Fault System. Ph.D. thesis, Stanford Univ., Stanford, California, USA. 356 pp.

Arrowsmith JR (2001a) Application of a Hillslope Development Model to Scarps Along the San Andreas Fault, Carrizo Plain, California. Online, Dept. of Geology, Arizona State University, Tempe, AZ. Cited 07 March 2001. Available from: <http://activetectonics.la. asu.edu/carrizo/application_full.html>.

Arrowsmith JR (2001b) Diffusion modeling references. Online, GLG 362/598 Geomorphology Course Documents, Dept. of Geology, Arizona State University, Tempe, AZ. Cited 31 May 2001. Available from: <http://www.public.asu.edu/~arrows/geomorph/diffuse/references.html>.

Arrowsmith JR (2001c) Simulation of hillslope processes using Microsoft Excel. Online, GLG 362/598 Geomorphology Course Documents, Dept. of Geology, Arizona State University, Tempe, AZ. Cited 31 May 2001. Available from: <http://www.public.asu.edu/~arrows/geomorph/diffuse/index.html>.

Arrowsmith JR, Pollard DD, Hilley G, Rhodes DD (1995) Morphologic dating of scarps along the San Andreas fault, Carrizo Plain, California and progressive deformation along the Big Bend. EOS, Transactions of the American Geophysical Union 76 (46): F575.

Arrowsmith JR, Pollard DD, Rhodes DD (1996) Hillslope development in areas of active tectonics. J. Geophys. Res. 101 (B3): 6,255–6,275.

Arrowsmith JR, Rhodes DD, Pollard DD (1998) Morphologic dating of scarps formed by repeated slip events along the San Adreas Fault, Carrizo Plain, California. J. Geophys. Res. 103 (B5): 10,141–10,160.

Avouac JP (1993) Analysis of Scarp Profiles: Evaluation of Errors in Morphologic Dating. J. Geophys. Res. 98 (B4): 6,745–6,754.

Avouac JP, Burov EB (1996) Erosion as a driving mechanism of intracontinental mountain growth. J. Geophys. Res. 101 (B8): 17,747–17,769.

Avouac JP, Dobremez JF, Bourjot L (1994) Paleoclimatic interpretation of a topographic profile across middle Holocene regressive shorelines of Longmu Co. (western Tibet). Palaeo–3 120: 93–104.

Avouac JP, Peltzer G (1993) Active Tectonics in Southern Xinjiang, China: Analysis of Terrace Riser and Normal Fault Scarp Degradation Along the Hotan-Qira Fault System. J. Geophys. Res. 98 (B12): 21,773–21,807.

Bakker JP, Le Heux JWN (1946) Projective-Geometric Treatment of O. Lehmann's Theory of the Transformation of Steep Mountain Slopes. K. Nederl. Akad. Wetens. Series B 49: 533–547.

Band LE (1985) Simulation of slope development and the magnitude and frequency of overland flow erosion in an abandoned hydraulic gold mine. In: Woldenberg MJ (ed.), Models in Geomorphology, pp. 191–211. Allen and Unwin, Boston, and Chichester.

Beaumont C, Fullsack P, Hamilton J (1992) Erosional control of active compressional orogens. In: McClay KR (ed.), Thrust Tectonics, pp. 1–18. Chapman and Hall, New York.

Begin ZB (1987) ERFUS 6: a FORTRAN program for calculating the response of alluvial channels to base level lowering. Comput. Geosci. 13: 389–398.

Begin ZB (1988) Application of a diffusion-erosion model to alluvial channels which degrade due to base-level lowering. Earth Surface Processes and Landforms 13: 487–500.

Begin ZB (1993) Application of quantitative morphologic dating to paleo-seismicity of the northwestern Negev, Israel. Isr. J. Earth Sci. 41 (2–4): 95–103.

Begin ZB, Meyer DF, Schumm SA (1981) Development of longitudinal profiles of alluvial channels in response to base-level lowering. Earth Surface Processes and Landforms 6: 49–68.

Benda L (1995) Das Quartär Deutschlands. Gebrüder Borntraeger, Berlin, Stuttgart.

Bevington PR, Robinson DK (1992) Data Reduction and Error Analysis for the Physical Sciences. McGraw-Hill, New York, 2nd edn. 328 pp.

Bibus E (1980) Zur Relief-, Boden- und Sedimententwicklung am unteren Mittelrhein. Ser. D Vol. 1, Frankfurter Geowiss. Arb., Frankfurt.

Black TA, Montgomery DR (1991) Sediment transport by burrowing animals, Marin County, California. Earth Surface Processes and Landforms 16: 163–172.

Bloom AL (1991) Geomorphology: A Systematic Analysis of Late Cenozoic Landforms. Prentice Hall, Englewood Cliffs, N.J., USA. 532 pp.

Bowman D, Gerson R (1986) Morphology of the latest Quaternary surface faulting in the Gulf of Elat region. Tectonophysics 128: 97–119.

Braun J, Sambridge M (1997) Modeling landscape evolution on geological time scales; a new method based on irregular spatial distribution. Basin Res. 9: 27–52.

Bremer H (1989) Allgmeine Geomorphologie. Gebrüder Borntraeger, Berlin, Stuttgart.

Brunnacker K (1978) Neuere Ergebnisse über das Quartär am Mittel- und Niederrhein. In: Reiche E (ed.), Das Rheinische Schiefergebirge und die Niederrheinische Bucht im Jungtertiär und Quartär, vol. 28 of *Fortschritte in der Geologie von Rheinland und Westfalen*, pp. 111–122. Geologisches Landesamt Nordrhein-Westfalen, Krefeld.

Brunsden D (ed.) (1971) Slopes form and process, vol. Special Publ. No. 3. Institute of British Geographers.

Brunsden D, Kesel RH (1973) Slope development on a Mississippi River Bluff in Historic Time. J. Geol. 81: 576–598.

Brunsden D, Prior DB (1984) Slope Instability. John Wiley & Sons Ltd., New York.

Bryan K (1922) Erosion and sedimentation in the Papago Country. U.S. Geol. Surv. Bull. 730-B: 19–90.

Bucknam RC, Anderson RE (1979) Estimation of fault-scarp ages from a scarp-height-slope-angle relationship. Geology 7: 11–14.

Bull WB (1984) Tectonic Geomorphology. Journal of Geological Education 32: 311–324.

Burbank DW, Anderson RS (2001) Tectonic Geomorphology. Blackwell Science.

Burga CA (1998) Vegetation und Klima der Schweiz seit dem jngeren Eiszeitalter. Ott, Thun.

Carretier S, Lucazeau F, Ritz JF, Philip H (2002a) Comparison of morphological dating models for cumulative reverse fault scarps. J. Geophys. Res. 107 (B10).

Carretier S, Ritz JF, Jackson J, Bayasgalan A (2002b) Morphologic dating of cumulative reverse fault scarp: examples from the Gurvan Bogd fault system, Mongolia. Geophys. J. Int 148: 256–277.

Carslaw HS, Jaeger JC (1959) Conduction of Heat in Solids. Oxford University Press, Oxford, 2nd edn. 510 pp.

Carson MA (1977) Angles of repose, angles of shearing resistance and angles of talus slopes. Earth Surface Processes 2: 363–380.

Carson MA, Kirkby MJ (1972) Hillslope Form and Process. Cambridge University Press, Cambridge. 475 pp.

Carter CA, Chorley RJ (1961) Early slope development in an expanding stream system. Geol. Mag. 98: 117–130.

Carter G, Nobes MJ (1980) The application of erosion slowness theory to hillslope formation. Earth Surface Processes and Landforms 5: 131–141.

Chase CG (1992) Fluvial land sculpting and the fractal dimension of topography. Geomorphology 5: 39–57.

Colman SM (1983) Progressive changes in the morphology of fluvial terraces and scarps along the Rappahannock River, Virginia. Earth Surface Processes and Landforms 8: 201–212.

Colman SM (1987) Limits and constraints of the diffusion equation in modeling geological processes of scarp degradation. In: Crone AJ, Omdahl EM (eds.), Proceedings of Conference XXXIX–Directions in Paleoseismology, U.S. Geol. Surv. Open File Rep., 87-0673, pp. 311–316.

Colman SM, Watson K (1983) Ages estimated from a diffusion-equation model for scarp degradation. Science 221: 263–265.

Crank J (1979) The mathematics of diffusion. Oxford Science Publication. Clarendon Press, Oxford, 2nd edn..

Crittenden R, Muhs DR (1986) Cliff height and slope-angle relationships in a chronosequence of Quaternary marine terraces, San Clemente Island, California. Z. Geomorph. 30: 291–301.

Culling WEH (1960) Analytical theory of erosion. J. Geol. 68: 336–344.

Culling WEH (1963) Soil creep and the development of hillside slopes. J. Geol. 71: 127–161.

Culling WEH (1965) Theory of erosion on soil-covered slopes. J. Geol. 73: 230–254.

Dalrymple JB, Blong RJ, Conacher AJ (1968) A hypothetical nine-unit landsurface model. Z. Geomorph. Suppl. 12: 60–76.

Davis WM (1899) The geographical cycle. Geogr. J. 14: 481–504.

Densmore A (1998) Landsliding and the evolution of normal-fault-bounded moutains. J. Geophys. Res. 103 (B7): 15,203–15,219.

Deutscher Wetterdienst (1989) Klima-Atlas von Nordrhein-Westfalen. Bibliothek d. DWD, Offenbach.

Dietrich WE, Wilson CJ, Montgomery DR, McKean J (1993) Analysis of erosion thresholds, channel networks, and landscape morphology using a digital terrain model. J. Geol. 101: 259–278.

Dikau R (1989) The application of a digital relief model to landform analysis in geomorphology. In: Raper J (ed.), Three dimensional applications in Geographical Information Systems, chap. 5, pp. 51–77. Taylor & Francis, London, New York, Philadelphia.

Dikau R, Schmidt J (1999) Georeliefklassifikation. In: Schneider-Sliwa R, Schaub D, Gerold G (eds.), Angewandte Landschaftsökologie - Grundlagen und Methoden, pp. 217–244. Springer-Verlag, Berlin, Heidelberg, New York.

Dunkerley DL (1980) The Study of the Evolution of Slope Form over long periods of time: A review of Methodologies and some new Observational Data from Papua New Guinea. Z. Geomorph. 24: 52–67.

Dunne T (1978) Field studies of hillslope flow processes. In: Kirkby MJ (ed.), Hillslope Hydrology, pp. 227–293. John Wiley & Sons Ltd., New York.

Ehlers J (1994) Allgemeine und historische Quartärgeologie. Ferdinand Enke Verlag, Stuttgart.

Ellison WD (1947) Soil Erosion Studies. Agric. Engng. 28: 145–146, 197–201, 245–248, 297–300, 349–351, 402–405, and 442–444.

Enzel Y, Amit R, Bruce J, Harrison J, Porat N (1994) Morphologic dating of fault scarps and terrace risers in the southern Arava, Israel: Comparison to other age-dating techniques and implications for paleoseismicity. Isr. J. Earth Sci. 43 (2): 91–103.

Enzel Y, Amit R, Porat N, Zilbermann E, Harrison BJ (1996) Estimating the ages of fault scarps in the Arava, Israel. Tectonophysics 253 (3–4): 305–317.

Exner FM (1922) Zur physikalischen Auffassung der Gefällskurve von Flüssen. Sitzber. Akad. Wiss. Wien., math.-naturw. Kl., Abt. IIa 131.

Fair TJ (1947) Slope Form and Development in the Interior of Natal. Geo. Soc. S. Africa Trans. 50: 105–120.

Fisher O (1866) On the disintegration of a chalk cliff. Geol. Mag. 3: 354–356.

Flemings PB, Jordan RE (1989) A synthetic stratigraphic model of foreland basin development. J. Geophys. Res. 94 (B4): 3,851–3,866.

Fletcher CAJ (1991) Computational techniques for fluid dynamics 1st Fundamental and general techniques. Springer series in computational physics. Springer-Verlag, Berlin, Heidelberg, New York, 2nd edn. 401 pp.

Fränzle O (1969) Geomorphologie der Umgebung von Bonn, vol. 29 of *Arbeiten zur Rheinischen Landeskunde*. Geographisches Institut der Universität Bonn, Ferd. Dümmlers Verlag Bonn.

Freeze RA (1987) Modelling interrelationsships between climate, hydrology, and hydrogeology and the development of slopes. In: Anderson MG, Richards KS (eds.), Slope Stability: Geotechnical Engineering and Geomorphology, pp. 381–403. John Wiley & Sons Ltd., New York.

Gilbert GK (1877) Geology of the Henry Mountains. Tech. rep., U.S. Geogr. and Geol. Surv..

Gilbert GK (1909) The convexity of hilltops. J. Geol. 17: 344–350.

Gossmann H (1976) Slope modelling with changing boundary conditions-effects of climate and lithology. Z. Geomorph. 25: 72–88.

Grabert H (1998) Abriß der Geologie von Nordrhein-Westfalen. E. Schweizerbart'sche Verlagsbuchhandlung (Nägele u. Obermiller), Stuttgart.

Hack JT (1960) Interpretation of erosional topography in humid temperate regions. Am. J. Sci. 258A: 80–97.

Hamblin WK (1976) Patterns of displacement along the Wasatch Fault. Geology 4: 619–622.

Hanks TC (1999) The age of scarp-like landforms from diffusion-equation analysis. In: Sowers JM, Noller JS, Lettis WR (eds.), Quaternary Geochronology: Methods and Applications, no. 4 in AGU Ref. Shelf. AGU, Washington, D. C..

Hanks TC, Andrews DJ (1987) Far-field slopes and the nature of general diffusion models of scarplike landforms in weakly consolidated terrains. In: Crone AJ, Omdahl EM (eds.), Proceedings of Conference XXXIX–Directions in Paleoseismology, U.S. Geol. Surv. Open File Rep., 87-0673, pp. 339–357.

Hanks TC, Andrews J (1989) Effect of far-field slope on morphologic dating of scarplike landforms. J. Geophys. Res. 94 (B1): 565–573.

Hanks TC, Bucknam RC, Lajoie KR, Wallace RE (1984) Modification of wave-cut and faulting-controlled landforms. J. Geophys. Res. 89 (B7): 5,771–5,790.

Hanks TC, Schwartz DP (1987) Morphologic dating of the pre-1983 fault scarp on the Lost River fault at Doublepring Pass Road, Custer County, Idaho. Bull. Seismol. Soc. Am. 77: 837–846.

Hanks TC, Wallace RE (1985) Morphological analysis of the Lake Lahontan shoreline and beachfront fault scarps, Persching County, Nevada. Bull. Seismol. Soc. Am. 75: 835–846.

Heimsath AM, Dietrich WE, Nishiizumi K, Finkel RC (1997) The soil production function and landscape equilibrium. Nature 388: 358–361.

Hirano M (1968) A mathematical model of slope development: An approach to the analytical theory of erosional topography. J. Geosci., Osaka City Univ. 11: 13–52.

Hirano M (1972) Quantitative morphometry of fault scarp with reference to the Hira Mountains, central Japan. Japanese Jour. Geol. and Geogr. 42: 85–100.

Hirano M (1975) Simulation of development process of interfluvial slopes with reference to graded form. J. Geol. 83: 113–123.

Hirano M (1976) Mathematical model and the concept of equilibrium in connection with slope shear ratio. Z. Geomorph. Suppl. 25: 50–71.

Horton RE (1945) Erosional development of streams and their drainage basins; hydrophysical approach to quantitative morphology. Geol. Soc. Am. Bull. 56: 275–370.

Howard AD (1988) Equilibrium models in geomorphology. In: Anderson MG (ed.), Modelling Geomorphological Systems, pp. 49–72. John Wiley & Sons Ltd., New York.

Howard AD (1994a) Badlands. In: Abrahams AD, Parsons AJ (eds.), Geomorphogy of Desert Environments, pp. 213–242. Chapman and Hall, New York.

Howard AD (1994b) A detachment-limited model for drainage basin evolution. Water Resour. Res. 30(7): 2,261–2,285.

Howard AD (1996) Thresholds and bistable states in landform evolution models. EOS, Transactions of the American Geophysical Union 76 (46): S136.

Howard AD (1997) Badland morphology and evolution: Interpretation using a simulation model. Earth Surface Processes and Landforms 22: 211–227.

Howard AD, Dietrich WD, Seidl MA (1994) Modelling fluvial erosion on regional or continental scales. J. Geophys. Res. 99 (B7): 13,971–13,987.

Humphrey NF, Heller PL (1995) Natural oscillations in coupled geomorphic systems: An alternative origin for cyclic sedimentation. Geology 23: 499–502.

Imeson AC, Kwaad FJPM (1976) Some effects of burrowing animals on slope processes in the Luxembourg Ardennes Part 2: The erosion of animal mounds by splash under forest. Geografiska Annaler 58A: 317–328.

Johnson AM, Pollard DD (1977) Part of the field notes of Grove Karl Gilbert for the period 20 June 1875 – 24 November 1876 taken during his study of the Henry Mountains and areas to the west. Unpublished manuscript of the School of Earth Sciences, Stanford University, Stanford, California, USA.

Jungbluth FA (1918) Die Terrassen des Rheins von Andernach bis Bonn. Verh. naturhist. Ver. Rheinld. Westf., 73. Jahrgang, Bonn.

Jyotsna R, Haff PK (1997) Microtopography as an indicator of modern hillslope diffusivity in arid terrain. Geology 25 (8): 695–698.

Kenyon PM, Turcotte DL (1985) Morphology of a delta prograding by bulk sediment transport. Geol. Soc. Am. Bull. 96: 1,457–1,465.

King LC (1953) Canons of landscape evolution. Geol. Soc. Am. Bull. 64: 721–752.

Kirkby MJ (1967) Measurement and theory of soil creep. J. Geol. 75: 359–378.

Kirkby MJ (1971) Hillslope process-response models based on the continuity equation. In: Brunsden D (ed.), Slopes form and process, vol. 3, pp. 15–30. Inst. Br. Geog. Spec. Pub..

Kirkby MJ (1976) Deterministic continuous slope models. Z. Geomorph. Suppl. 25: 1–19.

Kirkby MJ (1984) Modelling cliff development in South-Wales: Savigear re-viewed. Z. Geomorph. 28: 405–426.

Kirkby MJ (1985) A model for the evolution of regolith mantled slopes. In: Woldenberg MJ (ed.), Models in Geomorphology, pp. 213–237. Allen and Unwin, Boston, and Chichester.

Kirkby MJ (1986) A two-dimensional simulation model for slope and stream evolution. In: Abrahams AD (ed.), Hillslope Processes, pp. 203–222. Allen and Unwin, Boston, and London.

Kirkby MJ (1987) General Models of Long-Term Slope Evolution Through Mass Movement. In: Anderson MG, Richards KS (eds.), Slope Stability, pp. 359–379. John Wiley & Sons Ltd., New York.

Kirkby MJ (1994) Thresholds and instability in stream head hollows: a model of magnitude and frequency for wash processes. In: Kirkby MJ (ed.), Process Models and Theoretical Geomorphology, pp. 295–314. John Wiley & Sons Ltd., New York.

Kirkby MJ (1997) Tectonics in geomorphological models. In: Stoddart DR (ed.), Process and Form in Geomorphology, pp. 121–144. Routledge, London, New York.

Kirkby MJ, Naden PS, Burt TP, Butcher DP (1993) Computer Simulation in Physical Geography. John Wiley & Sons Ltd., New York. 227 pp.

Kooi H, Beaumont C (1994) Escarpment evolution on high-elevation rifted margins: Insights derived from a surface processes model that combines diffusion, advection, and reaction. J. Geophys. Res. 99 (B6): 12,191–12,209.

Kooi H, Beaumont C (1996) Large-scale geomorphology: Classical concepts reconciled and integrated with contemporary ideas via a surface process model. J. Geophys. Res. 101 (B2): 3,361–3,386.

Koons PO (1989) The topographic evolution of collisional mountain belts: A numerical look at the Southern Alps, New Zealand. Am. J. Sci. 289: 1,041–1,069.

Lawson AC (1915) The epigene profiles of the desert. Univ. California Pubn. Bull. Dept. Geol. 9: 23–48.

Lehmann O (1933) Morphologische Theorie der Verwitterung von Steinschlagwänden. Vierteljahresschrift Naturforsch. Ges. Zurich 78: 83–126.

Looman H (1956) Observations about some Differential Equations concerning Recession of Mountain Slopes I and II. K. Nederl. Akad. Wetens. Series B: 259–271 and 272–284.

Luke JC (1972) Mathematical models for landform evolution. J. Geophys. Res. 77 (14): 2,460–2,464.

Luke JC (1976) A note on the use of characteristics in slope evolution models. Z. Geomorph. Suppl. 25: 114–119.

Machette MN (1982) Quaternary and Pliocene faults in the La Jenica and southern part of the Albuquerque-Belen basins, New Mexico: Evidence of fault history from fault-scarp morphology and Quaternary geology. In: Field Conference Guidebook New Mexico Geological Society, vol. 33, pp. 161–170.

Machette MN (1989) Slope-morphometric dating. In: Forman SL (ed.), Dating methods applicable to Quaternary geologic studies in the Western United States: Utah Geological and Mineral Survey Miscellaneous Publication 89-7, vol. 89–7, pp. 30–42. Utah Geol. and Min. Surv..

Marek R, Götz W (1995) Numerische Lösung von partiellen Differentialgleichungen mit finiten Differenzen. Moreno-Verlag, Buchloe.

Martin Y (2000) Modelling hillslope evolution: linear and nonlinear transport relations. Geomorphology 34: 1–21.

Martin Y, Church M (1997) Diffusion in landscape development models: on the nature of basic transport relations. Earth Surface Processes and Landforms 22: 273–279.

Matmon A, Zilberman E, Enzel Y (2000) Determination of escarpment age using morphologic analysis: An example from the Galilee, northern Israel. Geol. Soc. Am. Bull. 112 (12): 1,864–1,876.

Mattson A, Bruhn RL (2001) Fault slip rates and initiation age based on diffusion equation modeling: Wasatch Fault Zone and eastern Great Basin. J. Geophys. Res. 106 (B7): 13,739–13,750.

Mayer L (1982) Quantitative Tectonic Geomorphology with Applications to Neotectonics of Northwestern Arizona. Ph.D. thesis, University of Arizona, Tucson.

Mayer L (1984) Dating Quaternary fault scarps formed in alluvium using morphologic parameters. Quat. Res. 22: 300–313.

Mayer L (1987) Sources of error in morphologic dating of fault scarps. In: Crone AJ, Omdahl EM (eds.), Proceedings of Conference XXXIX–Directions in Paleoseismology, U.S. Geol. Surv. Open File Rep., 87-0673, pp. 302–310.

McKean JA, Dietrich WE, Finkel RC, Southon JR, Caffee MW (1993) Quantification of soil production and downslope creep rates from cosmogenic ^{10}Be accumulations on a hillslope profile. Geology 21: 343–346.

Meyer W, Stets J (1996) Das Rheintal zwischen Bingen und Bonn. No. 89 in Sammlung Geologischer Führer. Gebrüder Borntraeger, Berlin, Stuttgart.

Miayzaki T (1993) Water flow in soils. Marcel Dekker, Inc., New York.

Mills HH (1978) Hillslope Evolution on the Pennington Formation, Central Tennessee: an Illustration of Dynamic Equilibrium. J. Tennessee Acad. Sci. 53: 150–153.

Mitchell JK (1976) Fundamentals of soil behaviour. John Wiley & Sons Ltd., New York. 422 pp.

Mitchell NC (1995) Diffusion transport model for pelagic sediments on the Mid-Atlantic Ridge. J. Geophys. Res. 100 (B10): 19,991–20,009.

Mitchell NC (1996) Creep in pelagic sediments and potential for morphologic dating of marine fault scarps. Geophys. Res. Lett. 23 (5): 483–486.

Moeyersons J (1975) An experimental study of pluvial processes on granite gruss. Catena 2: 289–308.

Moglen GE, Bras RL (1994) Simulation of observed topography using a physically-based basin evolution model. R. M. Parsons Laboratory, Hydrology and Water Resources Report 340, MIT, Cambridge, MA.

Monaghan MC, McKean J, Dietrich W, Klein J (1992) ^{10}Be chronometry of bedrock-to-soil conversion rates. Earth Planet. Sci. Lett. 111: 483–492.

Murawski H, Meyer W (1998) Geologisches Wrterbuch. Ferdinand Enke Verlag, Stuttgart.

Nash DB (1980a) Forms of bluffs degraded for different lengths of time in Emmet County, Michigan, U.S.A. Earth Surface Processes 5: 331–345.

Nash DB (1980b) Morphologic dating of degraded normal fault scarps. J. Geol. 88: 353–360.

Nash DB (1981a) Fault: A FORTRAN program for modeling the degradation of active normal fault scarp. Computers & Geosciences 7 (3): 249–266.

Nash DB (1981b) Fault scarp morphology: Indicator of paleoseismic chronology. Final Tech. Rep. Contract Number 14-08-0001-19109, U.S. Geological Survey.

Nash DB (1984) Morphologic dating of fluvial terrace scarps and fault scarps near West Yellowstone, Montana. Geol. Soc. Am. Bull. 95: 1,413–1,424.

Nash DB (1986) Morphologic Dating and Modeling Degradation of Fault Scarps. In: [panel chairman] REW (ed.), Active Tectonics: Impact on Society, pp. 181–194. Natl. Acad. Press, Washington, D.C..

Nash DB (1987a) A comparative review of limit equilibrium methods of stability analysis. In: Anderson MG, Richards K (eds.), Slope stability, pp. 325–338. John Wiley & Sons Ltd., New York.

Nash DB (1987b) Reevaluation of the linear-diffusion model for morphologic dating of scarps. In: Crone AJ, Omdahl EM (eds.), Proceedings of Conference XXXIX–Directions in Paleoseismology, U.S. Geol. Surv. Open File Rep., 87-0673, pp. 325–338.

Nash DB (1998) Influence of scarp height on the accuracy of morphologic dating. In: Geol. Soc. Am., 1998 annual meeting, abstracts with programs, vol. 30 of 7, p. 329. Geol. Soc. Am. (GSA), Boulder, USA.

Nivière B, Marquis G (2000) Evolution of terrace risers along the upper Rhine graben inferred from morphologic dating methods: evidence of climatic and tectonic forcing. Geophys. J. Int 141: 577–594.

Nivière B, Marquis G, Maurin JC (1998) Morphologic dating of slowly evolving scarps using a diffusive analogue. Geophys. Res. Lett. 25 (13): 2,325–2,328.

Noller JS, Sowers JM, Lettis WR (2000) Quaternary geochronology: methods and applications. AGU Reference Shelf 4, American Geophysical Union, Washington.

Ohmori H (1983) A three-dimensional model for the erosional development of mountain on the basis of relief structure. Trans. Jpn. Geomorph. Un. 4(1): 107–120.

Ohmori H (1984) Change in the Earth's surface altitude with absolute time simulated from the relations between mean altitude and dispersion, and between dispersion and denudation rate. Bull. Dept. Geogr. Univ. Tokyo 16: 5–22.

Ollier CD, Tuddenham WG (1962) Slope Development at Coober Pedy, South Australia. J. Geol. Soc. Australia 9: 91–105.

Pain CF (1986) Scarp Retreat and Slope Development near Picton, New South Wales, Australia. Catena 13: 227–239.

Parsons AJ (1976) An example of the application of deductive models to field measurement of hillslope form. Z. Geomorph. Suppl. 25: 145–153.

Parsons AJ (1988) Hillslope Form. Routledge, London, New York. 212 pp.

Pavich MJ, Leo GW, Obermeier SF, Estabrook JR (1989) Investigations of the characteristics, origin, and residence time of the upland residual mantle of the Piedmont of Fairfax County, Virginia. Professional Paper 1352, U.S. Geological Survey.

Pearthree PA, Calvo SS (1987) The Santa Rita fault zone: evidence for large magnitude earthquakes with very long recurrence intervals, Basin and Range province of southeastern Arizona. Bull. Seismol. Soc. Am. 77: 97–116.

Penck A, Brückner E (1909) Die Alpen im Eiszeitalter. Tauchnitz, Leipzig. 1,199 pp.

Penck W (1924) Die morphologische Analyse. Engelhorn, Stuttgart. 283 pp.

Penck W (1953) Morphological Analysis of Land Forms, H. Czech and K. C. Boswell, translators. Macmillian, London. 429 pp.

Pfeffer KH (1997) Ein Mittelgebirge mit großer naturgeographischer Vielfalt. In: Erdmann C, Pfeffer KH (eds.), Eifel, pp. 1–66. Gebrüder Borntraeger, Berlin, Stuttgart.

Pierce KL (1986) Dating Methods. In: Robert E. Wallace (panel chairman); Geophysics Study Committee; Geophysics Research Forum; Commission on Physical Sciences, Mathematics, and Resources; National Research Council (ed.), Active Tectonics: Impact on Society, pp. 195–214. National Academic Press, Washington DC, USA.

Pierce KL, Colman SM (1986) Effect of height and orientation (microclimate) on geomorphic degradation rate and processes, late glacial terrace scarps in central Idaho. Geol. Soc. Am. Bull. 97: 869–885.

Pierce KL, Colman SM (1987) Effect of height and orientation (microclimate) on degradation rates of Idaho terrace scarps. In: Crone AJ, Omdahl EM (eds.), Proceedings of Conference XXXIX–Directions in Paleoseismology, U.S. Geol. Surv. Open File Rep., 87-0673, pp. 317–324.

Pollack HN (1968) On the interpretation of state vectors and local tranformation operators. State Geol. Surv. of Kansas Computer Contrib. 22: 43–46.

Quaas A (1917) Das Rurtal. Ein Beitrag zur Geomorphologie der Nordeifel. Verh. Naturhist. Ver. Rheinl. u. Westf. 72: 179–308.

Rahn PH (1969) The relationship between natural forested slopes and angles of repose for sand and gravel. Geol. Soc. Am. Bull. 80: 2,123–2,128.

Reneau SL (1988) Depositional and erosional history of hollows: Application to landslide location and frequency, long-term erosion rates, and the effects of climatic change. Ph.D. thesis, Berkeley, University of California, USA. 328 pp.

Rey J (1991) Geologische Altersbestimmung. Ferdinand Enke Verlag, Stuttgart.

Rigon R, Rinaldo A, Rodriguez-Iturbe I (1994) On landscape self-organization. J. Geophys. Res. 99 (B6): 11,971–11,993.

Rinaldo A, Dietrich WE, Rigon R, Vogel G, Rodriguez-Iturbe I (1995) Geomorphological signatures of varying climate. Nature 374: 632–634.

Roering J (1999) Evidence for nonlinear, diffusive sediment transport on hillslopes and implications for landscape morphology. Water Resour. Res. 35 (3): 853–870.

Roering JJ, Kirchner JW, Dietrich WE (2001) Hillslope evolution by nonlinear, slope-dependent transport: Steady state morphology and equilibrium adjustment timescales. J. Geophys. Res. 106 (B8): 16,499–16,513.

Rohdenburg H (1989) Landschaftsökologie - Geomorphologie. Catena-Verlag, Cremlingen-Destedt.

Rosenbloom NA (1992) Calibration of coupled channel and hillslope processes in a marine terraced landscape, Santa Cruz, California. Master's thesis, Univ. of Calif., Santa Cruz.

Rosenbloom NA, Anderson RS (1994) Hillslope and channel evolution in the marine terraced landscape, Santa Cruz, California. J. Geophys. Res. 99 (B7): 14,013–14,030.

Savigear RAG (1952) Some Observations on Slope Development in South Wales. Inst. Br. Geogr. Trans. 18: 31–51.

Scheidegger AE (1961) Mathematical Models of Slope Development. Geol. Soc. Am. Bull. 72: 37–50.

Scheidegger AE (1991) Theoretical Geomorphology. Springer-Verlag, Berlin, Heidelberg, New York, 3rd edn..

Schirmer W (1994) Der Mittelrhein im Blickpunkt der Rheingeschichte. In: von Koenigswald W, Meyer W (eds.), Erdgeschichte im Rheinland, pp. 179–189. Pfeil-Verlag.

Schreiner A (1992) Einführung in die Quartärgeologie. E. Schweizerbart'sche Verlagsbuchhandlung (Nägele u. Obermiller), Stuttgart.

Schumm SA (1956) The role of creep and rainwash on the retreat of badland slopes. Am. J. Sci. 254: 693–706.

Schumm SA (1967) Rates of surficial creep on hillslopes in western Colorado. Science 155: 560–561.

Schumm SA, Mosely MP, Weaver WE (1987) Experimental Fluvial Geomorphology. John Wiley & Sons Ltd., New York. 413 pp.

Selby MJ (2000) Hillslope Materials and Processes. Oxford University Press, Oxford and New York, 2nd edn..

Sherman BJ (1987) The relationship of height to geomorphic degradation rates of terrace scarps in Idaho and Wyoming. Master's thesis, University of Cincinnati, Cincinnati, USA.

Siegburg W (1987) Talasymmetrien der Umgebung von Bonn. Dech. 140: 204–217.

Smith GD (1985) Numerical solutions of partial differential equations: finite difference methods. Oxford Applied Mathematics and Computing Science Series. Clarendon Press, Oxford, 3rd edn. 337 pp.

Souchez R (1963) Evolution des Versants et Theorie de la Plasticite. Rev. Belg. de Geog. 87: 10–94.

Souchez R (1966) Slow Mass Movement and Slope Evolution in Coherent and Homogeneous Rocks. Bull. Soc. Belg. de Geol. 74: 189–213.

Sterr H (1985) Rates of change and degradation of hillslopes formed in unconsolidated materials: a morphometric approach to date Quaternary fault scarps in western Utah, USA. Z. Geomorph. 29 (3): 315–333.

Stow DAV (1986) Deep clastic seas. In: Reading HG (ed.), Sedimentary environments and facies, pp. 399–444. Blackwell Sci. Publ., Oxford, UK.

Stüwe K (2000) Einführung in die Geodynamik der Lithosphäre. Springer-Verlag, Berlin, Heidelberg, New York.

Summerfield MA (1996) Global Geomorphology. Longman, Singapore, 2nd edn..

Tapponnier P, Meyer B, Avouac JP, Peltzer G, Gaudemer Y, Shunmin G, Hongfa X, Kelun Y, Zhitai C, Shuahua C, Huagang D (1990) Active thrusting and folding in the Qilian Shan, and decoupling between upper crust and mantle in northeastern Tibet. Earth Planet. Sci. Lett. 97: 382–403.

Terzaghi K (1950) Mechanism of landslides. In: Paige S (ed.), Application of Geology to Engineering Practice, pp. 83–123. Geol. Soc. of Am., Boulder, Colo., USA.

Thome KN (1998) Einführung in das Quartär. Springer-Verlag, Berlin, Heidelberg, New York.

Tödten H (1976a) Ein Analogmodell fr den Feststofftransport bei der Hangerosion. Ph.D. thesis, T.U. Aachen. 122 pp.

Tödten H (1976b) A mathematical model to describe surface erosion caused by overland flow. Z. Geomorph. Suppl. 25: 89–105.

Tricart J, Cailleux A (1972) Introduction to Climatic Geomorphology. Longman, London. 295 pp.

Trofimov AM, Moskovkin VM (1984) Diffusion models of slope development. Earth Surface Processes and Landforms 9: 435–453.

Tucker GE (1998) Process-Response Models of River Basin Evolution. online, Dept. of Civil and Environmental Enginneering, Massachusetts Institute of Technology, U.S.A. Cited 02 April 2001. Available from: <http://www.mit.edu/people/gtucker/pubs.html> or <http://platte.mit.edu/ gtucker/ cnr98notes.pdf>.

Tucker GE, Bras RL (1998) Hillslope processes, drainage density, and landscape morphology. Water Resour. Res. 34(10): 2,751–2,764.

Tucker GE, Slingerland RL (1994) Erosional dynamics, flexural isostasy, and long-lived escarpments: a numerical modeling study. J. Geophys. Res. 99 (B6): 12,229–12,243.

Tucker GE, Slingerland RL (1997) Drainage basin response to climate change. Water Resour. Res. 33 (8): 2,031–2,047.

van Dijk W, Le Heux JWN (1952) Theory of Parallel Rectilinear Slope Recession I and II. K. Nederl. Akad. Wetens. Proc. Series B 55: 115–122 and 123–129.

Van Tatenhove F, Dikau R (1990) Past and present permafrost distribution in the Turtmanntal, Wallis, Swiss Alps. Arctic and Alpine Research 22: 302–316.

Wallace RE (1977) Profiles and ages of young fault scarps, north-central Nevada. Geol. Soc. Am. Bull. 88: 1,267–1,281.

Wallace RE (1980) Degradation of the Hebgen Lake Fault scarps of 1959. Geology 8: 225–229.

Webb HF, Jordan TH (1993) Quantifying the distribution and tranport of pelagic sediments on young abyssal hills. Geophys. Res. Lett. 20: 2,203–2,206.

Welch DM (1970) Slope Analysis and Evolution of Protected Lacustrine Bluffs. Ph.D. thesis, Univ. of Western Ontario.

Welp G, Plümer G (1999) Bodennutzung und Bodenerosion seit dem Mittelalter am Beispiel von Landschaften des Bonner Raumes. Vortrag anläßlich der 51. Hochschultagung der Landwirtschaftlichen Fakultät der Universität Bonn.

Willgoose GR (1994a) A physical explanation for an observed area-slope-elevation relationship for catchments with declining relief. Water Resour. Res. 30: 151–159.

Willgoose GR (1994b) A statistic for testing the elevation characteristics of landscape simulation models. J. Geophys. Res. 99 (B7): 13,987–13,996.

Willgoose GR, Bras RL, Rodriguez-Iturbe I (1991a) A Coupled Channel Network Growth and Hillslope Evolution Model, 1. Theory. Water Resour. Res. 27 (7): 1,671–1,684.

Willgoose GR, Bras RL, Rodriguez-Iturbe I (1991b) A Coupled Channel Network Growth and Hillslope Evolution Model, 2. Nondimensionalization and Applications. Water Resour. Res. 27 (7): 1,685–1,696.

Willgoose GR, Bras RL, Rodriguez-Iturbe I (1991c) Results from a new model of river basin evolution. Earth Surface Processes and Landforms 16: 237–254.

Wirth W (1978) Zum Problem der Genese und der Einstufung pleistozäner Flußterrassen im Bereich des Rheinischen Schiefergebirges. In: Reiche E (ed.), Das Rheinische Schiefergebirge und die Niederrheinische Bucht im Jungtertiär und Quartär, vol. 28 of *Fortschritte in der Geologie von Rheinland und Westfalen*, pp. 65–83. Geologisches Landesamt Nordrhein-Westfalen, Krefeld.

Wischmeier WH (1978) Predicting rainfall erosion losses - a guide to conservation planning. U.S. Department of Agriculture Handbook 537.

Wischmeier WH, Smith DD (1962) Soil loss estimation as a tool in soil and water management planning. Intern. Assoc. of Scientific Hydrology, Publication 59.

Wood A (1942) The Development of Hillside Slopes. Proc. Geol. Ass. 53: 128–140.

Young A (1963) Deductive models of slope evolution. Nachri. Akad. Wiss. Gttingen Math. Phys. Klasse 2 5: 45–66.

Young A (1975) Slopes. Longman, London and New York. 288 pp.

Young A, Saunders I (1986) Rates of surface processes and denudation. In: Abrahams AD (ed.), Hillslope Processes, pp. 3–27. Allen and Unwin, Boston, and New York.

Appendix A

Profiles 1–33a

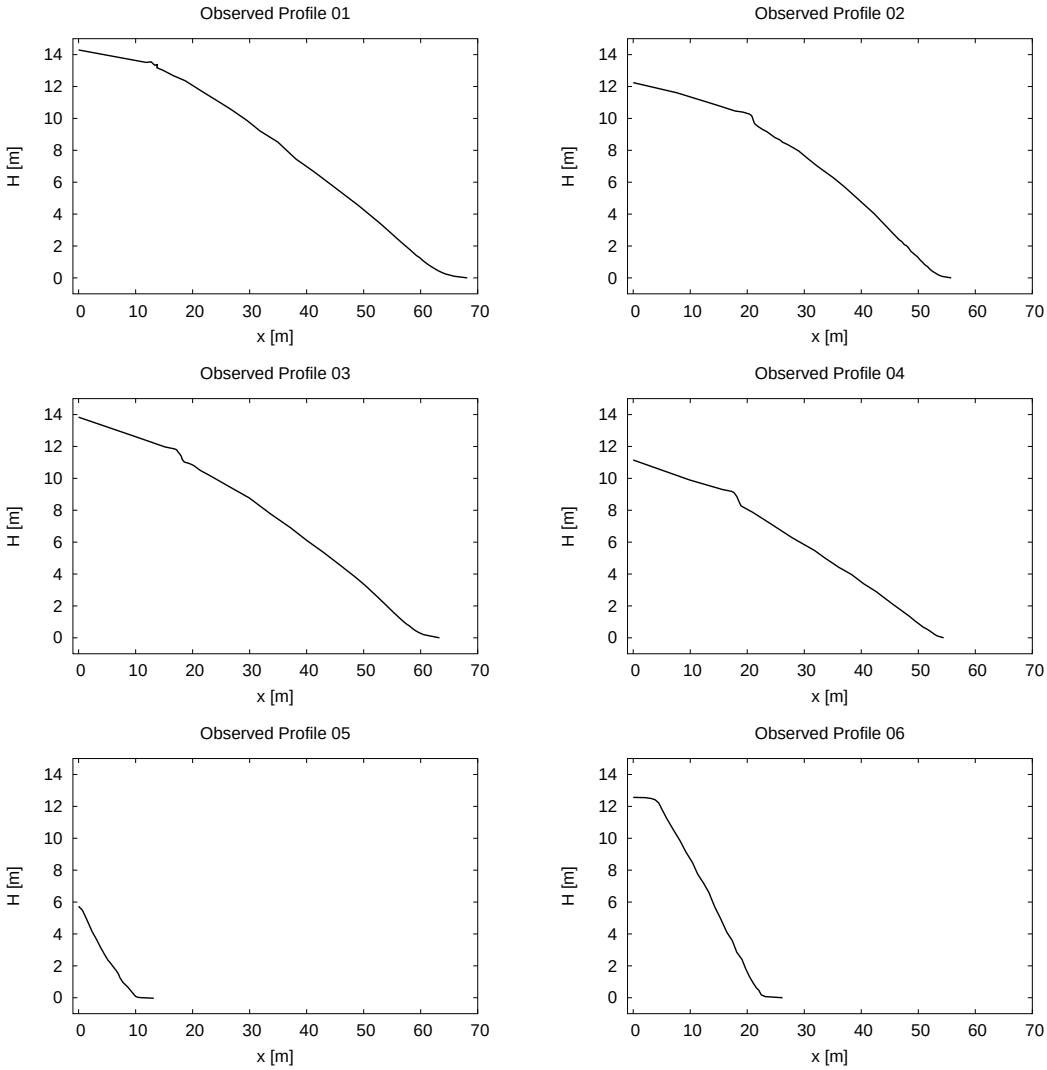

Figure A.1. Observed profiles 1–6.

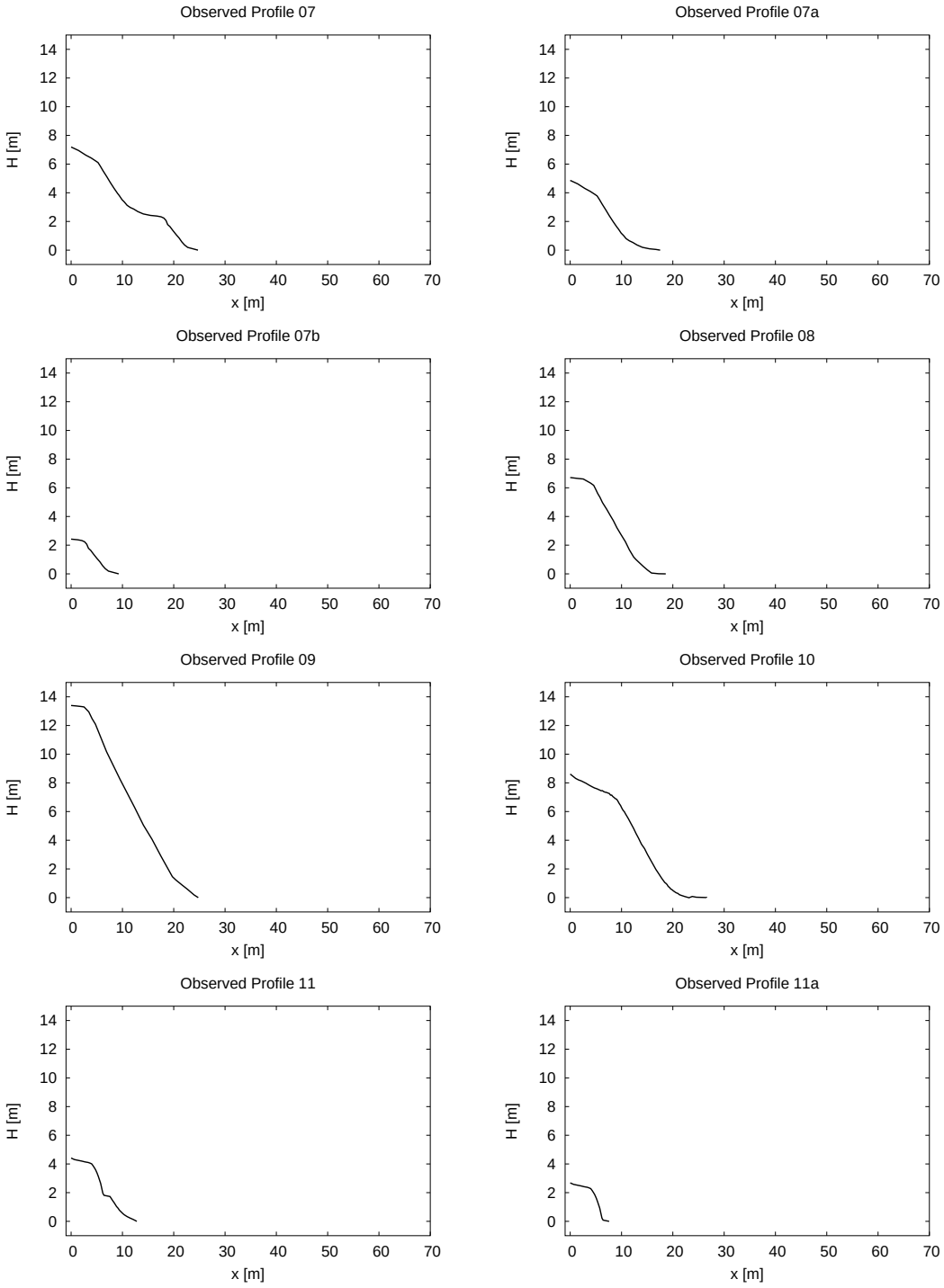

Figure A.2. Observed profiles 7–11a. Note that P07 and P11 were subdivided into P07a and P07b, and P11a and P11b (see next Figure A.3), respectively.

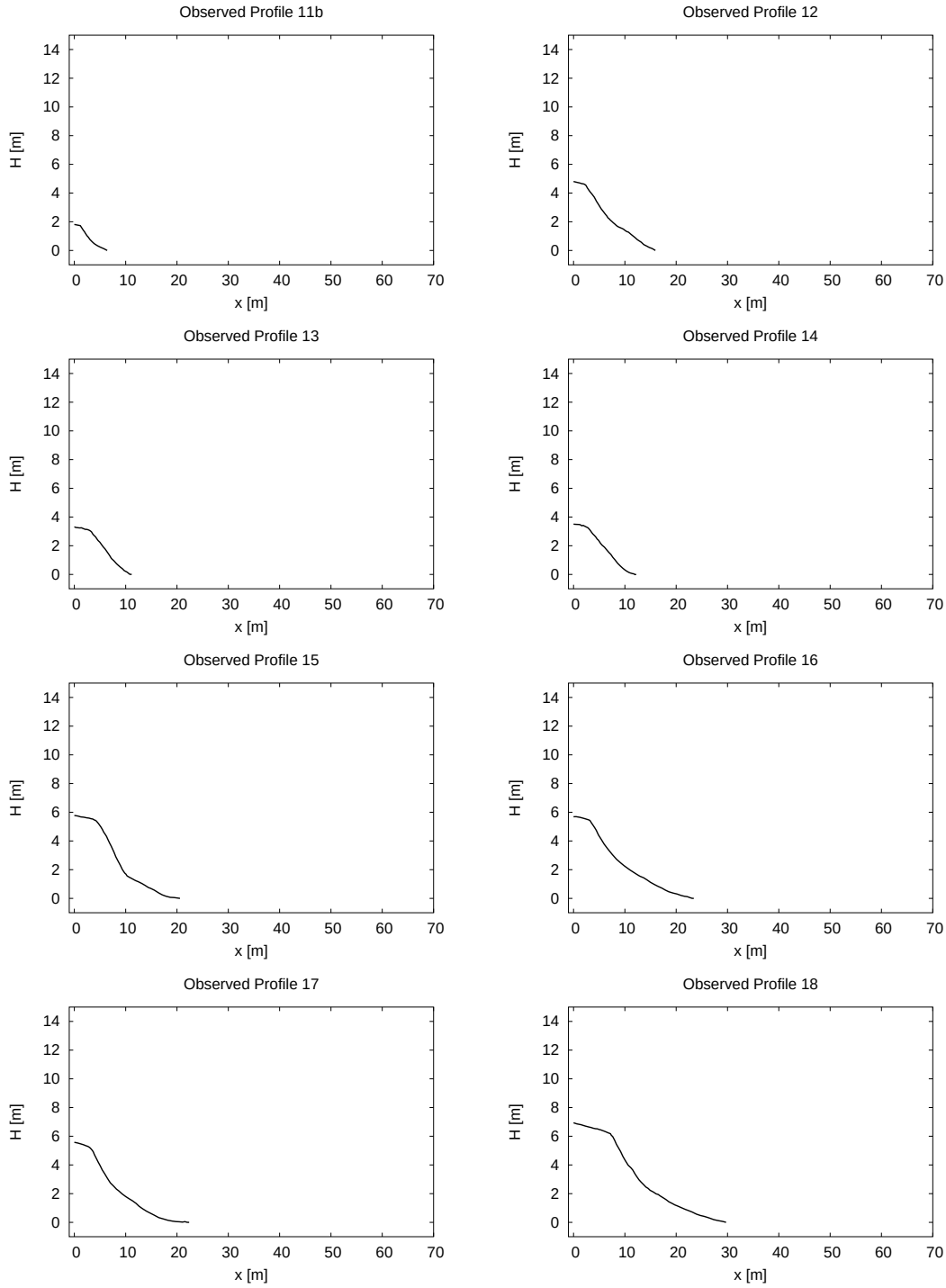

Figure A.3. Observed profiles 11b–18.

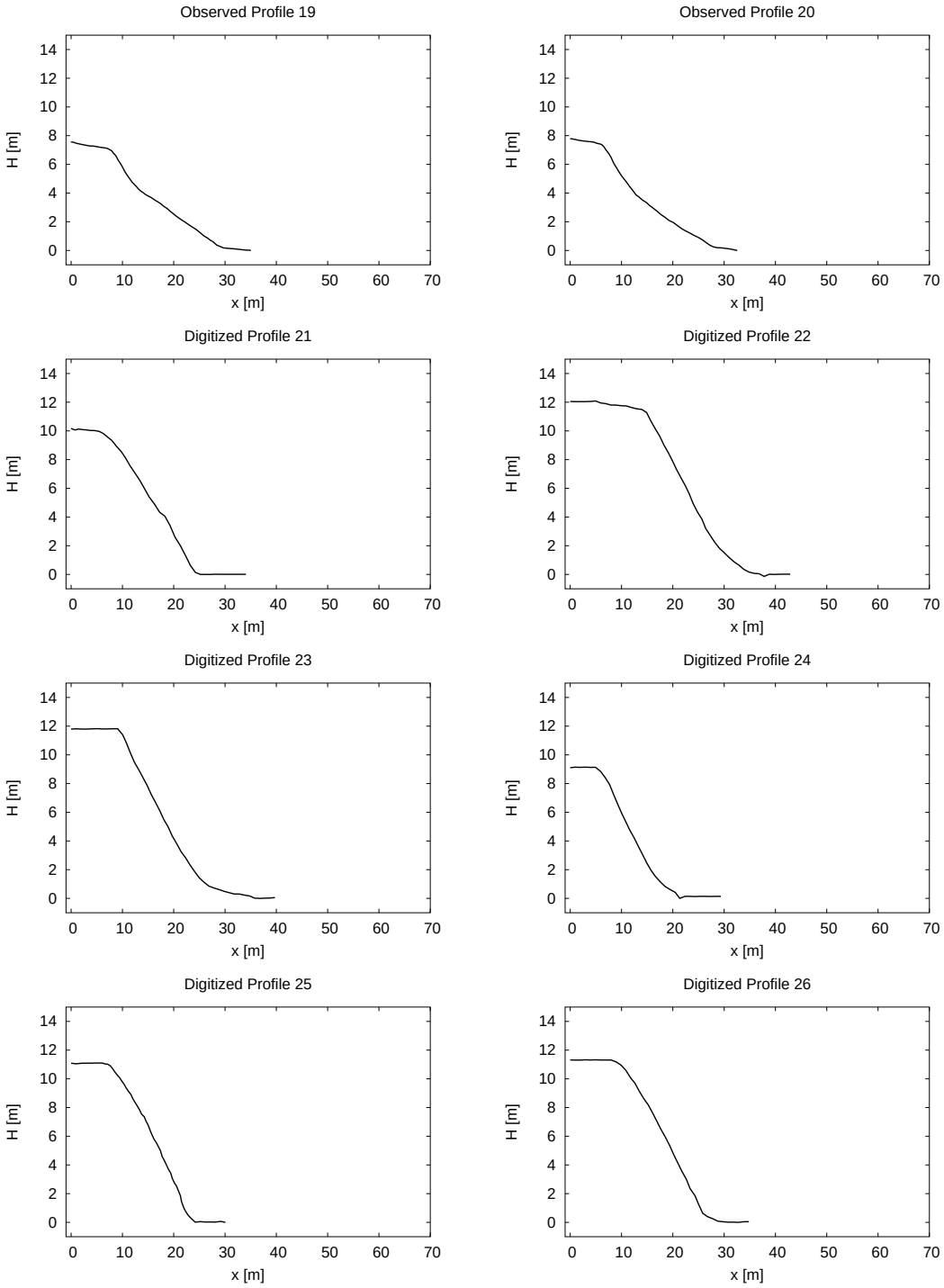

Figure A.4. Observed profiles 19 and 20 and digitized profiles 21–26.

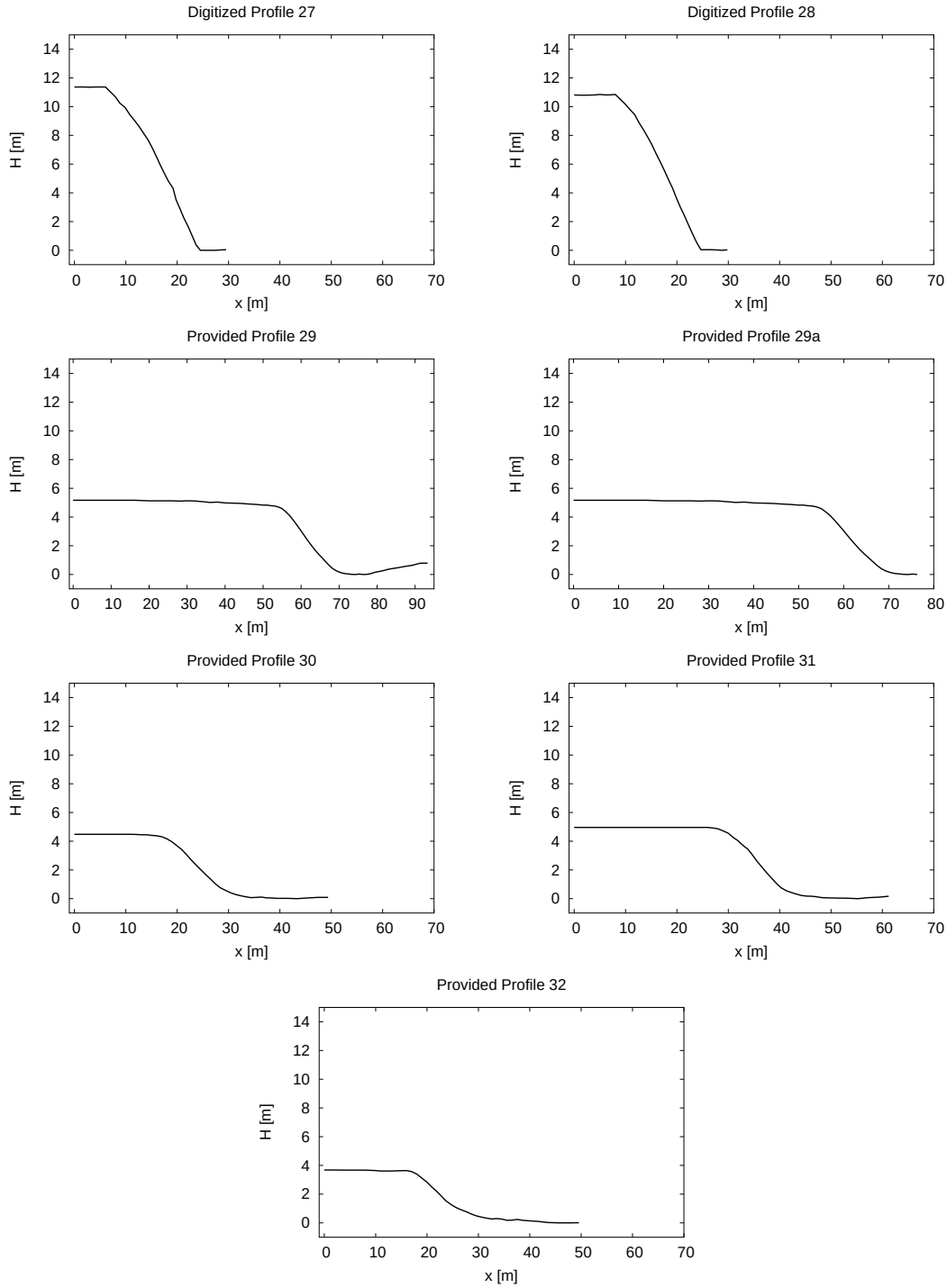

Figure A.5. Digitized profiles 27 and 28 and provided profiles 29–32. Note that profile 29 was cut off at distance x where the bulge appears (profile 29a), and that the x-axes of profiles 29 and 29a are scaled differently.

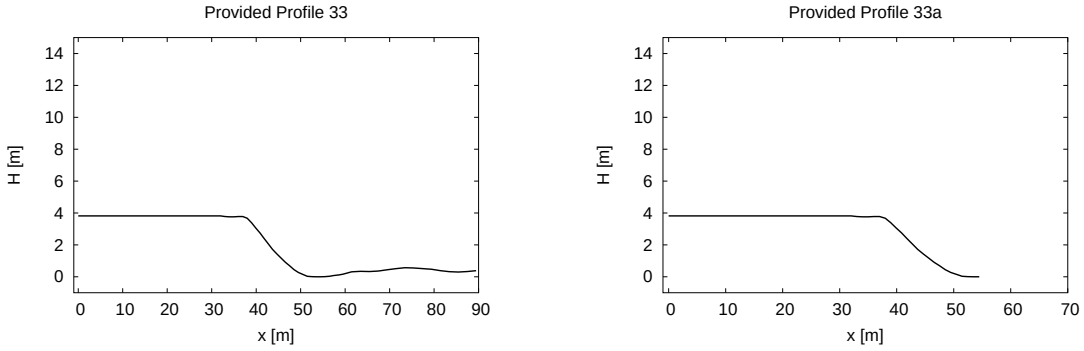

Figure A.6. Provided profile 33a. Note that profile 33 was cut off at distance x where the bulge appears (profile 33a), and that the x-axes of profiles 33 and 33a are scaled differently.

Appendix B

Photographs of selected scarps

Figure B.1. Photograph of profile 6 (Turtmann valley, CH). View to N.

Figure B.2. Photograph of profile 7b (Turtmann valley, CH). View to S.

Figure B.3. Photograph of profile 9 (Schwerfen). View to NW.

Figure B.4. Photograph of profiles 12 and 13 (Hausen). P12 was measured in the front, P13 in the back. View to E.

Figure B.5. Photograph of the scarp across which profiles 15–20 (Blens) were levelled. P15–P18 were measured across the upper, P19 and P20 across the lower scarp, each from the back to the front. View to W.

Figure B.6. Photograph of profile 15 (Blens). View to WNW.

Figure B.7. Photograph of profile 17 (Blens). View to ESE.

Appendix C

Model results

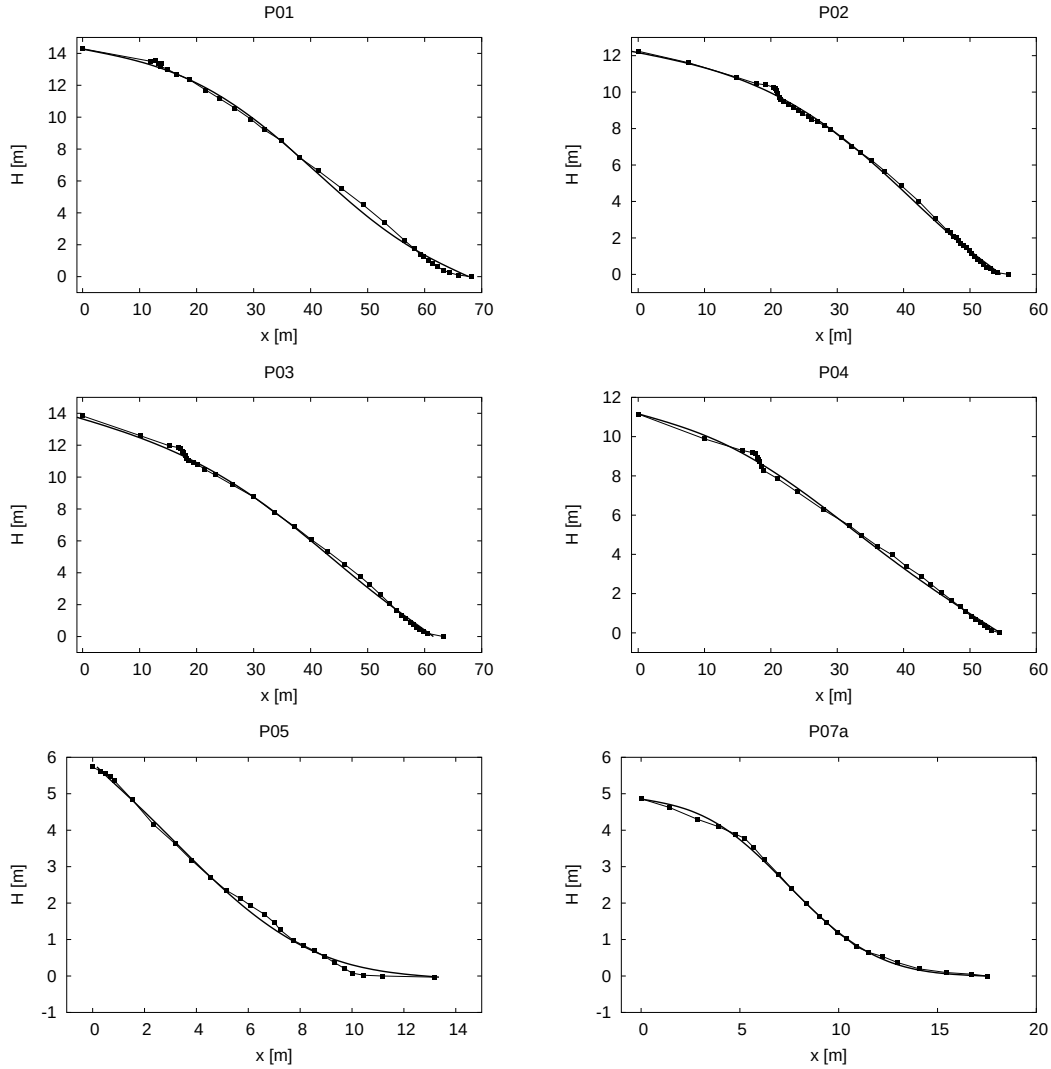

Figure C.1. Model results of P01–P05 and P07a. The observed profiles are displayed as connected squares, each square is a measured point. The solid lines are the modelled profiles with the smallest deviation. Note the different scalings of the both axes.

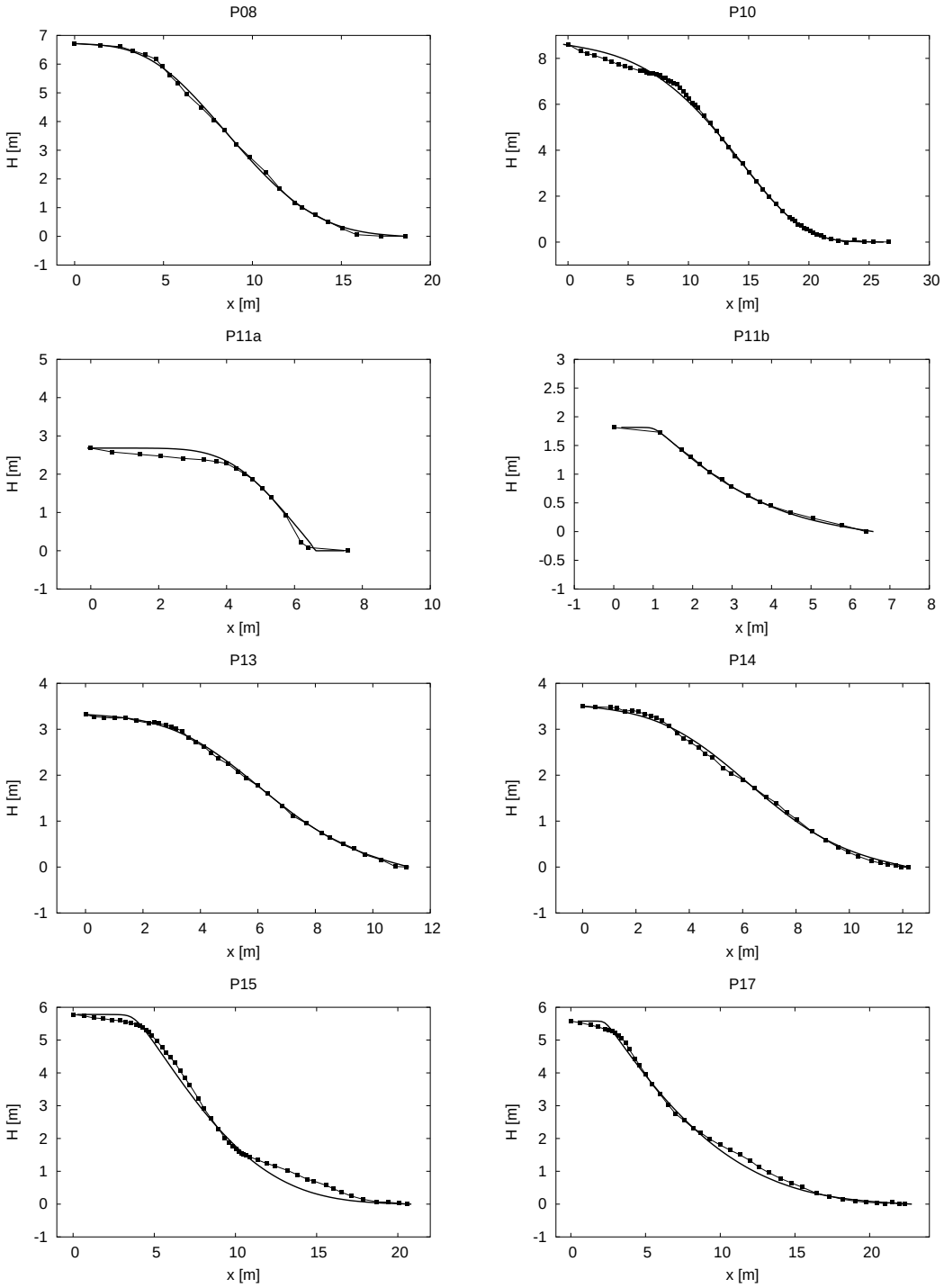

Figure C.2. Model results of P08, P10–P11b, P13–P15 and P17. The observed profiles are displayed as connected squares, each square is a measured point. The solid lines are the modelled profiles with the smallest deviation. Note the different scalings of the both axes.

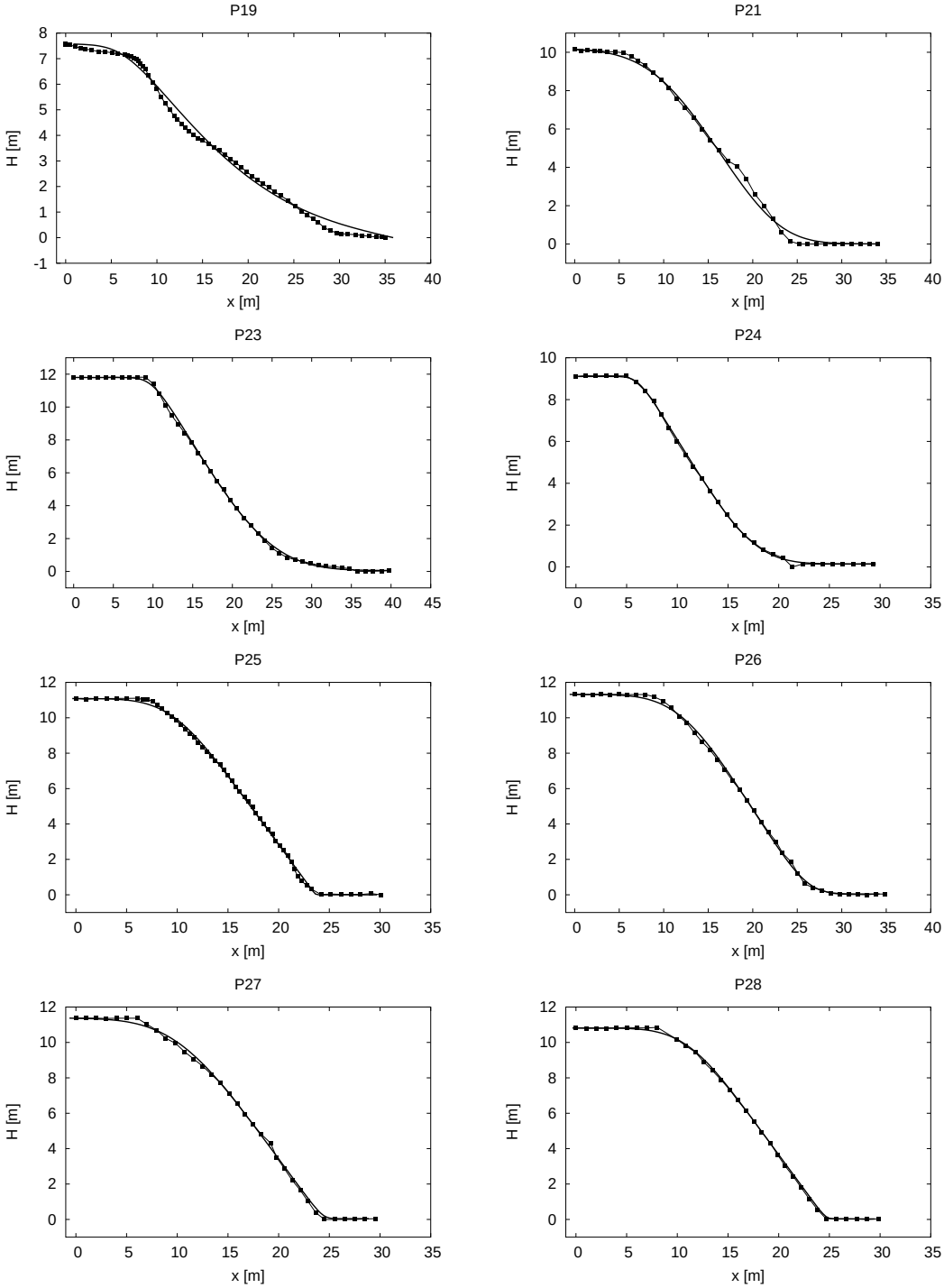

Figure C.3. Model results of P19, P21 and P23–P28. The observed profiles are displayed as connected squares, each square is a measured point. The solid lines are the modelled profiles with the smallest deviation. Note the different scalings of the both axes.

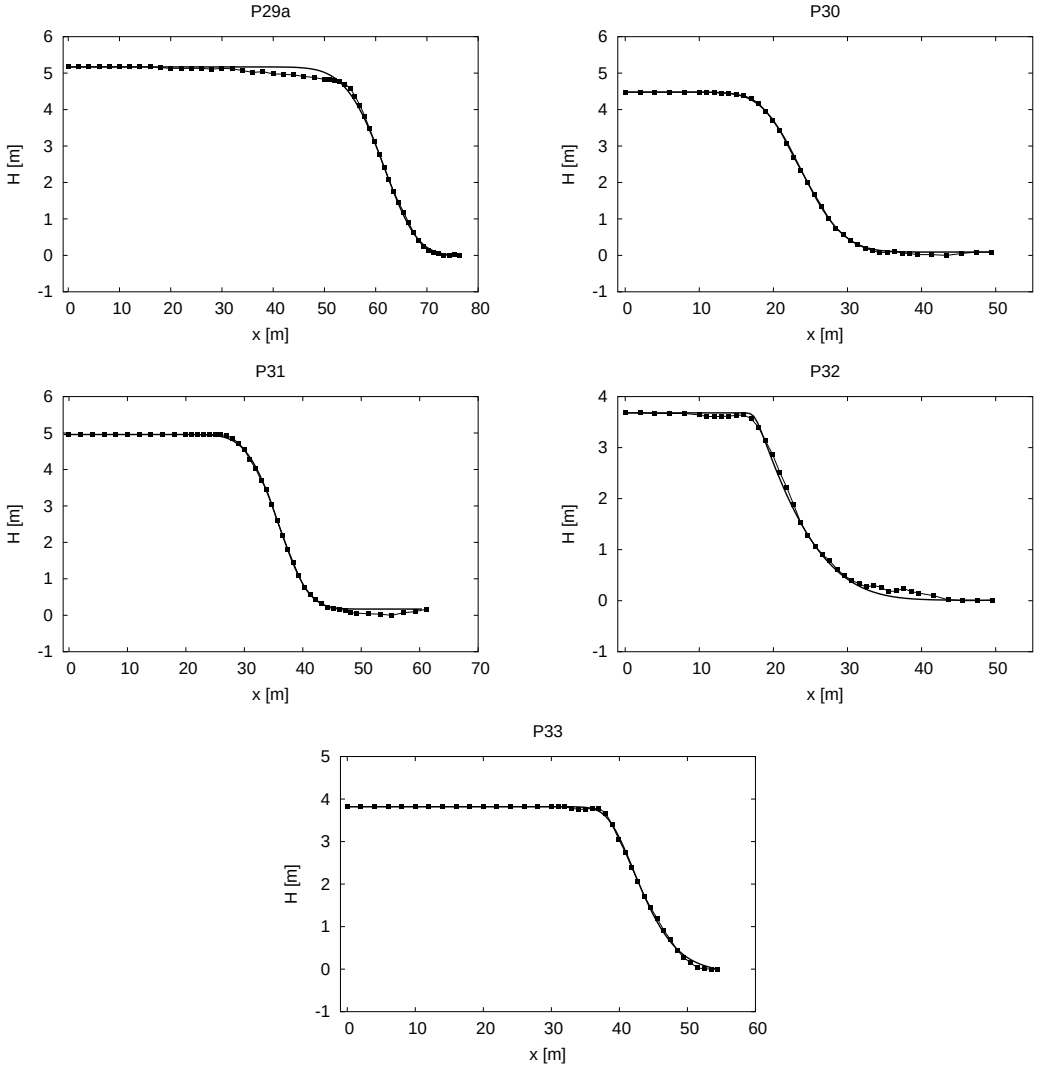

Figure C.4. Model result of P29a–P33a. The observed profile is displayed as connected squares, each square is a measured point. The solid line is the modelled profile with the smallest deviation. Note the different scalings of the both axes.

Index